



Al Mohamad, Zakriya Ali E. (2016) *Quantitative assessment of the biochemical composition of equine cartilage using 7T ultra-high field magnetic resonance imaging (MRI) techniques*. PhD thesis.

<http://theses.gla.ac.uk/8227/>

Copyright and moral rights for this work are retained by the author

A copy can be downloaded for personal non-commercial research or study, without prior permission or charge

This work cannot be reproduced or quoted extensively from without first obtaining permission in writing from the author

The content must not be changed in any way or sold commercially in any format or medium without the formal permission of the author

When referring to this work, full bibliographic details including the author, title, awarding institution and date of the thesis must be given

Enlighten:Theses
<http://theses.gla.ac.uk/>
theses@gla.ac.uk

Quantitative assessment of the biochemical composition of equine cartilage using 7T ultra-high field magnetic resonance imaging (MRI) techniques

Zakriya Ali E. Al Mohamad 0914037

BVet Med

Submitted in fulfilment of the requirement for the
Degree of Doctor in Philosophy

School of Veterinary Medicine

College of Medical, Veterinary and Life Science
(MVLS)

University of Glasgow

November 2016

Abstract

Equine fetlock region disease is responsible for significant morbidity and mortality. Diagnosis of sesamoidean ligament, cartilage and subchondral bone injury has been obtained by clinical MRI. Low-field MRI provides images helpful in the investigation of MCPJ/MTPJ region pathology in horses in the clinical setting but the greater resolution of high and ultra-field MR images has the potential to aid interpretation through a better understanding of MRI anatomy. Quantitative MRI could provide a non-invasive technique to determine tissue biochemical properties associated with the early onset of articular cartilage degenerative conditions such as osteoarthritis. So far, ultra-high field MRI has not been used in equine research and practice. However, recently 3T MRI has been introduced in equine hospitals in Europe and the US.

The general objectives of this project, which utilised cadaver limbs, was to improve understanding of the MRI anatomy of the equine MCPJ/MTPJ region and to evaluate the use of MRI for the non-invasive, quantitative assessment of articular cartilage from the same region. The first specific objective was to describe the appearance of the normal anatomy of the equine MCPJ/MTPJ region, especially the SDFT & DDFT and DSLs, using high field (1.5T) and ultra high field (7T) MRI and to compare the images obtained with the two systems. The second objective was to determine the accuracy and precision of articular cartilage thickness measurements using 1.5T and 7T MRI and comparing the measurements with those made from histological sections of the MCPJ/MTPJ. The third objective was to measure T1 & T2 MRI sequence relaxation times for normal horse articular cartilage pre and post gadolinium contrast (dGEMRIC) administration and to determine their correlation with GAG concentration, including a description of topographical variation. The fourth objective was to compare sodium concentration in normal equine MCPJ/MTPJ articular cartilage measured using 7T MR imaging with a dual tuned quadrature $^{23}\text{Na}/^1\text{H}$ coil with the biochemical properties (sodium concentration determined by flame photometry and GAG concentration). The final objective was to evaluate MR sodium imaging for the assessment of enzymatically degraded equine cartilage.

The findings demonstrated that 7T MRI produces high resolution images, which enable better evaluation of the hard and soft tissues of the equine MCPJ/MTPJ region than images from lower field MR systems and which permit accurate and precise articular cartilage thickness measurements to be made. Moreover, it was found that the dGEMRIC technique appears to provide a feasible quantitative tool for evaluating the articular cartilage properties. However, the quantitative parameters determined by the dGEMRIC method cannot fully characterise the biochemical properties of the cartilage. Moreover, delayed gadolinium-enhanced (dGEMRIC) techniques are time consuming, requiring relatively long incubation and scanning times. The measurement of T2 time is a very complex method. The work described in the last chapters demonstrated that sodium MRI was significantly correlated with the biochemical properties of the equine articular cartilage. Therefore the sodium MRI technique showed promise in imaging articular cartilage and providing useful information on the biochemical properties of the cartilage.

Acknowledgements

In the name of Allah the most beneficent, the most merciful, "Those truly fear Allah, among His Servants, who have knowledge" Holy Quran verse (35:28).

There are many people who deserve thanks for their huge and varied contribution to this PhD thesis, as completion of this PhD was not possible without the guidance and support of several people. I would like to first of all thank Dr. John Marshall, my first supervisor for the patient guidance and encouragement he has provided throughout my time as his PhD student. I have been extremely lucky to have a supervisor who has inspired and cared so much about my work as well as responding to any questions or queries I had so rapidly. Similarly I would like to acknowledge Dr. Lance Voute, my second supervisor, for his valuable support, guidance and encouragement he has provided throughout. I would like also to thank Prof Sandy Love for his continuous support. Additionally gratitude goes to Dr. William Holmes who provided me with extremely helpful information as well as technical support regarding MRI properties and for his part in performing the MRI scanning. I would like to give sincere thanks to Mr. Jim Mullin for his effort in designing the MRI sample setup and for the hours dedicated to scanning our samples.

I would like to thank the faculty staff members especially the Dean of the College of Veterinary Medicine and Animal research, Dr. Adel Ail-Shek Moubarak, Prof. Ramadan O. Ramadan, Dr. Mohamad R. Addin-Bey, Dr Saeed Al Ramadan, Dr. Abdurahman Al Angary, Dr. Abdurahman Al Hidar and Prof. Mohamad K. Sayid-Zabady at King Faisal University who gave me this opportunity to study abroad in order to get this degree. Many special thanks to the Cultural Bureau, Royal Embassy of Saudi Arabia in London, not only for providing the funding which allowed me to under take this research, but also for the continued technical guidance and support.

I must express my gratitude to my parents, who spent their time looking after me, for their continuous support and encouragement until they passed away. I must express my gratitude to my wife Zinab, who has been a constant inspiration and support as well as looking after my children Nawar, Al Zahra and Danyah, who experienced all of the up and downs throughout my research time as well as my brothers, sisters,

nephews, niece and cousins in Saudi Arabia who expressed their emotional help and support throughout this period. I give my deepest thank to my all brothers and sisters in-law especially, Hosain and Mohamad Al-Turki for their continuous emotional support.

Completing this study would have been all of the more difficult were it not for the support and friendship provided by Dr. Mohamad Al Mousa as well Dr. and Faraj Al Rished for his statistical support and advice. Similarly great gratitude goes to Dr. Ahmed Khweir and Mr. Abdullah Al Hasan for their valuable efforts and guidance.

Declaration

I hereby declare that this thesis represents my own work that has been done after registration for the degree of PhD in Veterinary Clinical Studies at the School of Veterinary Medicine. And has not included in previously included in any other thesis submitted to this institution.

Signature _____

Printed Name Zakriya A. Al Mohamad

Contents

Abstract	i
Acknowledgements	iii
Declaration	v
Contents	vi
List of Figures	xiii
List of Tables.....	xxiv
List of Abbreviations	xxvi
Definitions	xxviii
Chapter 1 Literature Review.....	1
1.1. Research Proposal.....	1
1.2. Introduction	1
1.3. Overview of Diagnostic Imaging in Equine Practice	2
1.4. Magnetic Resonance Imaging.....	3
1.4.1. Principles of MRI	3
1.4.2. How the MRI Image is Created	3
1.4.3. Relaxation Time	4
1.4.3.1. T2 Relaxation Time (T2 Mapping)	5
1.4.4. Image Acquisition.....	6
1.5. MRI Equipment (Magnet, Coils).....	6
1.5.1. Magnet.....	6
1.5.1.1. Types of Magnets	7
1.5.2. Radio Frequency Coils	7
1.5.2.1. Types of MRI Coils.....	8
1.5.2.1.1 Volume Coils.....	8
1.5.2.1.2 Surface Coils	8
1.5.2.1.3 Dual Tuned ²³ Na/ ¹ H Coils	9
1.6. Quantitative MRI Studies	9
1.6.1. Sodium MRI	10
1.6.2. MRI Contrast Media (dGEMRIC) Study	11
1.7. MRI In Equine Orthopaedics	13
1.7.1. The Foot.....	13

1.7.2. The Fetlock	13
1.8. Cadaver Studies.....	14
1.9. Articular Cartilage Morphology.....	15
1.10. Articular Cartilage Zones.....	15
1.10.1. Superficial (Tangential) Zone	15
1.10.2. Middle (Transitional) Zone.....	16
1.10.3. Calcified Zone	16
1.11. Articular Cartilage Physiology	16
1.12. Physiologic MRI of Articular Cartilage	17
1.13. Protocols For Articular Cartilage Measurements	17
1.14. Normal Appearance of The Articular Cartilage	18
1.15. Technical Factors Affecting MRI of Articular Cartilage Measurements	19
1.16. Sodium Content in The Biological Tissues	19
1.17. Osteoarthritis	20
1.17.1. Pathophysiology.....	20
1.17.2. Diagnostic Imaging.....	21
1.17.3. Classification.....	22
1.17.4. Osteoarthritis in The Horse.....	22
1.18. Hypotheses.....	23
Chapter 2 High- And Ultra-high Field Magnetic Resonance Anatomy Of The MCIII/MTIII Region Of The Horse.....	24
2.1. Introduction	24
2.2. Aims And Objectives	26
2.3. Materials And Methods.....	27
2.3.1. Limbs Collection.....	27
2.3.2. MRI Imaging.....	27
2.3.3. Data Analysis	28
2.4. Results.....	28
2.4.1. The Appearance of The Articular Cartilage, Synovial Fluid and Bone In T1- Weighted 7T and 1.5T MR Images of The MCPJ/MTPJ Region.....	28
2.4.2. The appearance of the articular cartilage, synovial fluid and bone in T2-weighted 7T and 1.5T MR images of the metacarpo/metatarsophalangeal region.....	34
2.4.3. The appearance of the soft tissues in T1- and T2-weighted 7T and 1.5T MR images of the metacarpo/metatarsophalangeal region	39

2.4.4. Appearance of the distal sesamoidean ligaments in T1-weighted 7T and 1.5T MR images	45
2.4.4.1. Distal Sesamoidean Ligaments	45
2.4.4.2. Cruciate Sesamoidean Ligaments	45
2.4.4.3. Oblique Sesamoidean Ligaments	45
2.4.4.4. Straight Sesamoidean Ligaments	46
2.4.4.5. Intersesamoidean ligament	46
2.5. Discussion	49
2.6. Conclusion	52

Chapter 3 Accuracy and Precision of Articular Cartilage Thickness

Measurement Using Ultra-High 7T and 1.5T High-Field Magnetic Resonance

Imaging (MRI)	53
3.1. Introduction	53
3.2. Aims And Objectives	54
3.3. Materials And Methods	55
3.3.1. Sample Collection	55
3.3.2. MRI Study	55
3.3.2.1. T1-weighted Image Analysis – Measurement of Cartilage Thickness from MR Images	56
3.3.3. Cartilage Sample Collection And Processing	58
3.3.4. Histology	58
3.3.5. Measurement of articular cartilage thickness from histological sections	58
3.3.6. Statistical Analysis	59
3.4. Results	60
3.4.1. MRI And Histological Measurements	60
3.4.1.1. T1-weighted 7T MRI Measurements	60
3.4.1.2. T1-weighted 1.5T MRI Measurements	62
3.4.1.3. Histological Measurements	63
3.4.2. Correlation Between T1-weighted (7T/1.5T) MRI and Histological Measurements	65
3.5. Accuracy and Precision of 7T and 1.5T T1-weighted Measurements of the Articular Cartilage Thickness Compared with Histological Measurements	68
3.6. Discussion	69
3.6.1. Measurement Variation	70
3.6.2. Difference in Thickness Mean	70

3.6.3. Correlation Between MRI vs. Histology	71
3.6.4. Accuracy And Precision Of The Articular Cartilage Thickness.....	71
3.7. Limitations Of The Study.....	72
3.8. Future Study.....	73
3.9. Conclusion	73
Chapter 4 A Comparison of Quantitative MR Imaging Techniques of the Normal Equine Fetlock Joint to Assess Articular Cartilage: Transverse Relaxation Time (T2-time), T1 signal intensity and dGEMRIC Study.....	75
4.1. Introduction.....	75
4.2. T2 relaxation Time Mapping.....	75
4.3. Delayed Gadolinium Enhanced Contrast MRI of Articular Cartilage (dGEMRIC).....	76
4.4. Aims and Objectives.....	78
4.5. Materials and Methods	79
4.5.1. Samples Collection and Preparation	79
4.5.2. MRI imaging (T1, T2 Relaxation Time Images and GdDTPA ²⁻ Enhanced Measurements).....	80
4.6. MRI Data Analysis.....	82
4.6.1. T1- Weighted Image Analysis (Signal Intensity)	82
4.6.2. T2-Relaxation Time Analysis.....	82
4.7. Biochemical Study (Cartilage Collection)	83
4.7.1. Water Content (Dry Weight)	84
4.7.2. Proteoglycan Assay.....	85
4.7.3. Statistical Analysis	86
4.8. Results.....	86
4.8.1. Biochemical Evaluation	86
4.8.1.1. sGAG Content.....	86
4.8.1.2. Percentage Water	91
4.9. MRI Image Evaluation	94
4.9.1. T2 relaxation Time Analysis of Equine Cartilage	94
4.9.2. T1-weighted Pre and Post dGEMRIC Analysis (Signal Intensity).....	97
4.10. Correlation between MRI parameters and the biochemical properties of equine cartilage.....	101
4.10.1. Correlation of T1 signal intensity post (dGEMRIC) with GAG Content.....	101
4.10.2. Correlation between water % and T2 relaxation time (ms).....	102
4.11. Discussion.....	102

4.11.1. Analysing the effect of contrast agent on MRI parameters..... 103

4.11.2. Topographical variation in the cartilage biochemistry 104

4.11.3. Correlation between MR imaging parameters and biochemical features of the equine cartilage..... 105

4.12. Conclusion 106

Chapter 5 *In Vitro* Quantitative Sodium MRI of Equine MC3/MT3 Articular

Cartilage 107

5.1. Introduction 107

5.2. Sodium MRI 108

5.3. Aims and Objectives 109

5.4. Materials and Methods 110

5.4.1. Samples Collection and Preparation 110

5.4.2. Agarose Phantom Preparation 110

5.4.3. Sodium Phantom Preparation 111

5.4.4. Sodium MR Imaging Technique 112

5.4.5. T1-weighted Hydrogen Images 112

5.4.6. Sodium Image Analysis 112

5.4.7. Collection of Articular Cartilage Samples for GAG and Flame Photometer Assays 113

5.4.8. Proteoglycan Assay..... 114

5.4.9. Sodium Concentration Measurement Using Flame Photometer Method..... 114

5.5. Statistical Analysis 115

5.6. Results..... 116

5.6.1. Agarose T2 Time Mapping 116

5.6.2. Sodium MRI Standard Curve..... 117

5.6.3. Sodium MRI Analysis vs. GAG 117

5.6.3.1. Sodium MRI Analysis 117

5.6.3.2. Proteoglycan Assay 118

5.6.4. Sodium MRI vs. Sodium (Flame Photometer)..... 119

5.6.4.1. Sodium MRI 119

5.6.4.2. Sodium content (Flame Photometer) 120

5.6.5. Correlation 121

5.6.5.1. Correlation Between Sodium MRI and GAG Content..... 121

5.6.5.2. Correlation Between Sodium MRI vs. Sodium (Flame Photometer) Content..... 124

5.7. Discussion..... 126

5.7.1. Sodium MRI Map and Topographical Variation in Cartilage.....	127
5.7.2. Topographical Variation in Cartilage Glycosaminoglycans	128
5.7.3. Relationship Between Quantification of Sodium by MRI and Flame Photometer.....	129
5.8. Conclusion	130
Chapter 6 Sodium MRI Evaluation of Equine Cartilage (Enzymatic Degradation)	131
6.1. Introduction	131
6.2. Aims and Objectives.....	132
6.3. Materials And Methods.....	133
6.3.1. Sample Collection And Preparation.....	133
6.3.2. Sample Enzymatic Degradation (Trypsin Enzyme).....	134
6.3.3. Sodium MRI and MRI Data Acquisition.....	135
6.3.4. Sodium MRI T1-Signal Intensity	135
6.3.5. Articular Cartilage Slice Collection for GAG and Flame Photometer Analysis....	137
6.3.6. GAG Assay (Glycosaminoglycans).....	138
6.3.7. Flame Photometer.....	138
6.4. Statistical Analysis	138
6.5. Results.....	139
6.5.1. Sodium Content (MRI) vs. GAG Content.....	139
6.5.1.1. Overall Sodium Content (MRI) Degraded Samples and Control Samples	139
6.5.1.2. Sodium Content (MRI) of Cartilage Samples Degraded by Different Trypsin Concentration	140
6.5.1.3. Overall GAG Content	142
6.5.1.4. GAG Content of Samples Degraded with Different Trypsin Concentration	143
6.5.2. Sodium Content (MRI) vs. Sodium Content (Flame Photometer).....	145
6.5.2.1. Overall Sodium Content Measured by Flame Photometer	145
6.5.2.2. Sodium Content (flame photometer) of Samples Degraded with Different Trypsin Concentration.....	146
6.5.3. Correlation	148
6.5.4. Correlation Between Sodium MRI vs. Sodium Flame Photometer Results	148
6.5.5. Correlation between sodium MRI vs. GAG content	151
6.6. Discussion.....	151
6.6.1. Sodium MRI Data Analysis.....	152
6.6.2. Exploring the Effect of Trypsin Enzymatic Degradation on the Equine Cartilage sodium (MRI) content.....	152

6.6.3. Exploring the Effect of Trypsin Enzymatic Degradation on the Equine Cartilage PG Content	153
6.6.4. Exploring the Effect of Trypsin Enzymatic Degradation on the Equine Cartilage sodium content.....	153
6.6.5. Exploring the Correlations Between Sodium MRI, GAG Content and Flame Photometry	154
6.7. Limitations of the study.....	155
6.8. Conclusion	155
Chapter 7 Overall Discussion and Conclusion	156
7.1. Overall Discussion.....	156
7.2. Overall Conclusion	160
7.3. Limitations of The Study	160
7.4. Future Work.....	161
Appendix A.....	163
List of references	164

List of Figures

Figure 1-1: Mid sagittal plane T1 7T (A), (B) T2-weighted and (C) Sodium MR images of the metacarpophalangeal region of a horse. Images obtained from a dorsal plane through the midpoint of the metacarpophalangeal articulation. The trabecular bone of distal MCIII and proximal P1 produces a punctate pattern of mixed signal intensity due to low intensity trabecular bone interspersed by high intensity bone marrow. It has low to intermediate signal intensity on T1 images (A) and low on T2 MR images (B). Articular cartilage has an intermediate signal intensity in T1 MR images (A) and high to intermediate on T2 MRI (B). 4

Figure 2-2: Dorsal plane 7T (A) and 1.5T (B) T1-weighted MR images of the metacarpophalangeal region. Images obtained from a dorsal plane through the midpoint of the metacarpophalangeal articulation and were matched as closely as possible but differences remain due to limb positioning and slice thickness. There is an increase in the thickness of the subchondral bone of the distal condyles of MCIII and proximal P1 midway between sagittal ridge/ sagittal groove and the abaxial margin (A & B, yellow arrowhead) in comparison to the remaining condyle. This feature reflects bone adaptation to exercise. The trabecular bone of distal MCIII and proximal P1 produces a punctate pattern of mixed signal intensity due to low intensity trabecular bone interspersed by high intensity bone marrow; the trabecular bone structure is only resolved in the 7T images (A). The periosteal and endosteal surfaces at the site of attachment of lateral and medial collateral ligaments of the metacarpophalangeal articulation to distal MCIII are smooth; the collateral ligaments are only clearly defined in 7T images compared to 1.5T images (A & B, white arrow). 33

Figure 2-3 Sagittal plane 7T (A, C) & 1.5T (B, D) T2-weighted MR images of the metatarsophalangeal joint. A & B were obtained in the mid-sagittal plane (through the sagittal ridge of distal MTIII); C & D in a parasagittal plane through a proximal sesamoid bone. The increased signal intensity of the synovial fluid compared to the surrounding tissues outlines the limits of the joint cavity, which extends further proximally in the parasagittal plane than the mid-sagittal plane. In the 7T images articular cartilage of distal MTIII and P1 is not readily differentiated from synovial fluid due their similar (intermediate) intensity (white arrows facing each other in C & D).

The boundary between cartilage and subchondral bone is indistinct in some regions in the 7T images due to the similar signal intensity of the tissues but is not visible in the 1.5T images because of their lower resolution.....36

Figure 2-4: Transverse plane 7T (A) & 1.5T (B) T2-weighted MR images of the metacarpo/metatarsophalangeal joint obtained through the metacarpo-sesamoidean articulation. The trabecular bone is of heterogeneous signal intensity as the result of a pattern of high intensity foci and low intensity streaks on an intermediate intensity background (white arrow in A & B). The palmar annular ligament of the fetlock (thick white arrow) and superficial and deep digital flexor tendons (blue arrow) are of low signal intensity and cannot be readily distinguished as separate structures in either image, although the high signal intensity of synovial fluid within the digital flexor tendon sheath delineates the dorsal border of the deep digital flexor tendon. Similarly the dorsal and lateral digital extensor tendons are of low signal intensity and not readily visualized as discrete structures (white arrowhead).38

Figure 2-5: Transverse plane 7T (A & B) & 1.5T (C & D) MR images of the metacarpophalangeal joint obtained through the distal portion of the metacarpo-sesamoidean articulation. A & C are T1-weighted, B & D T2-weighted images. The superficial collateral ligaments (thin yellow arrows) and deep (thin white arrows) of the metacarpophalangeal joint are of low signal intensity in both MRI sequences (white arrowheads). In the T1-weighted images (A & C) there is sufficient contrast with the surrounding tissues to be able to distinguish the ligaments but it is only in the 7T T1-weighted image (A) that the margins of the ligament can be clearly visualized. The digital vessels (white arrows) and nerves (black arrows) are visualized as intermediate-high signal intensity structures surrounded by a narrow low signal intensity zone, which are most clearly visualized in the 7T T1-weighted image (A)...42

Figure 2-6: Sagittal plane 7T (A & B) & 1.5T (D & E) MR images of the metacarpophalangeal joint; transverse plane 7T MR image (C) obtained through the distal portion of the metacarpo-sesamoidean articulation. Of the sagittal plane images, A, B & E are parasagittal, including a proximal sesamoid bone, and D is mid-sagittal. A, C & D are T1-weighted, B & E T2-weighted images. The superficial digital flexor tendon (while arrow) and deep digital flexor tendons (white arrowhead) are of low signal intensity and are visible in all images. The boundary between the tendons

is indistinct in the T2-weighted images and the striated pattern reflecting the fascicular structure of the tendons can only be seen clearly in the 7T T1-weighted sagittal plane image (A). The pattern is faintly visible in the 1.5T T1-weighted sagittal plane image (D) and not in the T2-weighted images. In the 7T T1-weighted transverse plane image (C&F), the fascicular structure is visualized as a fine speckled pattern (thin white arrows).....44

Figure 2-7: 7T T1-weighted MR images of the metacarpophalangeal region obtained in the dorsal (A, B & D), sagittal (E), transverse oblique (C) and transverse (F) planes. A & D are through the dorsal portion of the proximal sesamoid bones, B through the palmar portion of the metacarpophalangeal articulation, E is mid-sagittal, C & F transverse through the distal portion of the metacarpo-sesamoidean articulation, although slight distolateral to proximomedial obliquity has been used in C to highlight the intersesamoidean ligament. The cruciate, oblique and straight distal sesamoidean and the intersesamoidean ligaments are highlighted in the images. The ligaments are of intermediate to high signal intensity and have a coarse striated pattern reflecting their fascicular structure. The proximal portions of the cruciate distal sesamoidean ligaments are visualized in A (yellow arrowhead) but their orientation takes them dorsal to the image slice distally (so that they are overlaid by the oblique distal sesamoidean ligaments); in B the more dorsal image plane allows the entire ligament to be visualized (yellow arrowheads), clearly showing the cross-shaped configuration of the ligament. The oblique and straight distal sesamoidean ligaments are visualized in D (yellow arrows and white arrow respectively), which show the anatomical arrangement of axial straight ligament and adjacent, abaxial, oblique ligaments and the differing fibre directions of the ligaments. The signal intensity of the straight distal sesamoidean ligament is greater than the oblique (high compared to intermediate). The intersesamoidean ligament is highlighted in E (yellow arrowhead) and F (yellow arrow) but is more distinct in F where the image plane is parallel to the fibre direction.48

Figure 3-1: Sagittal plane T1-weighted images of left fore metacarpophalangeal joint acquired using the 7T MR system, illustrating the sites at which cartilage thickness was measured. (A) Through the lateral proximal sesamoid bone, (B) through the mid-sagittal ridge and (C) through the medial proximal sesamoid bone. Sagittal plane

images were used for all measurements. The MCIII/MTIII condyle and proximal P1 was divided into dorsal and palmar halves. Cartilage thickness was measured from the interface between low signal intensity subchondral bone and high signal intensity cartilage, and high signal intensity cartilage and medium signal intensity joint space using the measurement tool. Measurements were performed at three sites on both the dorsal and palmar halves and each measurement was repeated in triplicate. Each proximal sesamoid bone was divided into proximal and distal halves. Cartilage thickness was measured from the interface between low signal intensity subchondral bone and high signal intensity cartilage, and high signal intensity cartilage and medium signal intensity joint space using the measurement tool. Measurements were performed at three sites on both the proximal and distal halves and each measurement was repeated in triplicate. For each measured site the mean and standard deviation of the triplicate measurements was calculated.57

Figure 3-2: Photomicrograph of haematoxylin & eosin section from sample prepared from proximal P1 magnified 100 times. The dashed white line at the cartilage-bone interface was used to eliminate the effect irregularity of this boundary on cartilage thickness measurements. The three black double-headed arrows represent the three measurements of cartilage thickness made for each sample.59

Figure 3-4: Box plot of articular cartilage thickness measurements made from T1-weighted 7T MR images: anatomical location and site. MC3 = metacarpal/metatarsal condyle; P1 = proximal phalanx; sesamoid = proximal sesamoid bone.61

Figure 3-5: Box plot of articular cartilage thickness measurements made from T1-weighted 1.5T MR images: anatomical location. MC3 = metacarpal/metatarsal condyles; P1 = proximal phalanx; lateral/medial sesamoid = lateral/medial proximal sesamoid bone.....62

Figure 3-6: Box plot of articular cartilage thickness measurements made from T1-weighted 7T MR images: anatomical location and site. MC3 = metacarpal/metatarsal condyle; P1 = proximal phalanx; sesamoid = proximal sesamoid bone.63

Figure 3-7: Box plot of articular cartilage thickness measurements made from histological measurements: anatomical location. MC3 = metacarpal/metatarsal condyles; P1 = proximal phalanx; lateral/medial sesamoid = lateral/medial proximal sesamoid bone.....64

- Figure 3-8: Box plot of articular cartilage thickness measurements made from histological measurements: anatomical location and site. MC3 = metacarpal/metatarsal condyle; P1 = proximal phalanx; sesamoid = proximal sesamoid bone..... 65
- Figure 3-9: Scatter plot of 7T MRI articular cartilage thickness measurement means against histological articular cartilage thickness measurement means. There was moderate positive correlation of T1-weighted 7T MRI cartilage thickness measurements and histology cartilage thickness measurements for MCIII/MTIII, P1 and lateral & medial PSBs ($P<0.05$) correlation coefficient ($r=0.472$)..... 66
- Figure 3-10: Scatter plot of 1.5T MRI cartilage thickness measurements against histological cartilage thickness measurements. There was moderate positive correlation of T1-weighted 1.5T MRI cartilage thickness measurements and histology cartilage thickness measurements of MCIII/MTIII, P1 and lateral & medial PSBs ($P<0.05$) correlation coefficient ($r=0.414$)..... 67
- Figure 3-11: Scatter plot of T1-weighted 7T MRI cartilage measurements against T1 1.5T MRI cartilage measurements. There was moderate positive correlation between 7T MRI cartilage measurements and T1-weighted 1.5 T MRI cartilage measurements of the MCIII/MTIII, P1 and lateral & medial PSBs ($P<0.05$) correlation coefficient ($r=0.426$)..... 67
- Figure 4-1: This image represents cartilage samples preparation. 4 semi-circular cartilage and bone sections were taken (5mm width, 3cm height) of equine MC3 bone, and were labeled 1-4 from lateral to the medial aspect of the bone. Subsequently, kept in a container filled with isotonic solution (normal saline) for MRI and biochemical study. 79
- Figure 4-2: A dual tuned quadrature $^{23}\text{Na}/^1\text{H}$ coil designed by PulseTeq Limited Chobham, Surrey, UK, for this project. 81
- Figure 4-3: A plastic container containing metacarpal condyle fixed at the bottom with fixing MRI-friendly material to avoid signal alteration of the plastic container as well as fixing the samples in order to get the same slice parameters in each MRI scans. 81
- Figure 4-4: T2-weighted (relaxation time) image MRI analysis. By using a geometry tool, a straight line was drawn between the dorsal and palmar end points of the semi-circular cartilage sample, in which a 90° angle was created from the centre of the

straight line. From this centre 4 lines were drawn two from dorsal (A&B) and the others from palmar aspect (C&D) of the cartilage sample ROIs. Then, the track tool was used to manually track the cartilage ends, making sure that this tracking tool included the cartilage area only. The value obtained represented the average T1 signal intensity within the ROIs. The geometry afterward was overlaid onto the corresponding post or pre contrast imaging sample to make sure that the two pre and post contrast imaging sets ROIs were similar to each other in their slice position. 83

Figure 4-5: This diagram represents cartilage collection for biochemical assay study. Four cylindrical disks were harvested using 4mm biopsy punches and labelled A and B from the dorsal site and C and D from the palmar site. Samples were removed at specific regions and totally separated from the subchondral bone using a surgical scalpel making sure that full thickness of cartilage was carefully removed. These were then used to determine water and proteoglycan content. 84

Figure 4-6: This figure shows the scatter plot of the standard curve, used to measure the concentration of cartilage glycosaminoglycans, acquired from 5 standards with different concentrations measured by 650nm filter using a spectrophotometer. 85

Figure 4-7: Box plot shows the mean sGAG content ($\mu\text{g}/\text{mg}/\text{dw}$) over dorsal and palmar sites of the equine metacarpal-tarsal articular cartilage. The dorsal cartilage punches had higher GAG content ($44.34 \pm 10.64 \mu\text{g}/\text{mg}/\text{dw}$) than palmar punches ($34.56 \mu\text{g}/\text{mg}/\text{dw} \pm 8.19 \mu\text{g}/\text{mg}/\text{dw}$) ($P < 0.05$)..... 87

Figure 4-8: Box plot shows the mean of sGAG content ($\mu\text{g}/\text{mg}/\text{dw}$) of lateral and medial aspects of the equine metacarpal-tarsal articular cartilage. No significant difference was observed between lateral sites ($39.05 \mu\text{g}/\text{mg}/\text{dw} \pm 10.25 \mu\text{g}/\text{mg}/\text{dw}$), medial site ($39.85 \mu\text{g}/\text{mg}/\text{dw} \pm 11.11 \mu\text{g}/\text{mg}/\text{dw}$) ($P = 0.69$)..... 87

Figure 4-9: Box plot shows the mean of sGAG content ($\mu\text{g}/\text{mg}/\text{dw}$) of different punch locations of the equine metacarpal-tarsal articular cartilage. A is most dorsal, B dorsal & C palmer and D most palmar sites of the articular surface of the metacarpal-tarsal articular cartilage. A punch had higher sGAGS content $44.94 \pm 9.66 \mu\text{g}/\text{mg}/\text{dw}$ than B punch ($43.74 \mu\text{g}/\text{mg}/\text{dw} \pm 11.68 \mu\text{g}/\text{mg}/\text{dw}$), C punch ($32.75 \mu\text{g}/\text{mg}/\text{dw} \pm 6.02 \mu\text{g}/\text{mg}/\text{dw}$) and punch D ($36.37 \mu\text{g}/\text{mg}/\text{dw} \pm 9.68 \mu\text{g}/\text{mg}/\text{dw}$) ($P < 0.05$)..... 88

Figure 4-11: Box plot showing the water content (%) of lateral and medial aspects of the equine metacarpal-tarsal articular cartilage. Lateral site $72.46\% \pm 4.71\%$ and

medial sites $72.73\% \pm 3.88\%$ with no significant difference was found between these sites ($P=0.744$)..... 92

Figure 4-12: Box plot showing the water content (%)of different punch location as (A, B, C & D) of the equine metacarpal-tarsal articular cartilage. There was no significant difference found between them..... 92

Figure 4-14: Box plot showing the T2 relaxation time (ms) in lateral and medial aspects of the equine cartilage. There was no significant difference between medial ($30.23 \text{ ms} \pm 4.22 \text{ ms}$) and lateral sites ($31.29 \text{ ms} \pm 4.51 \text{ ms}$) ($P=0.20$)..... 95

Figure 4-15: Box plot showing the T2 relaxation time (ms) of different punch location as (A, B, C & D) of the equine metacarpal-tarsal articular cartilage. There was no significant difference found between them..... 95

Figure 4-16: Box plot showing the T1-signal intensity post dGEMRIC incubation of dorsal and palmar aspects of the equine cartilage. There was no significant difference between palmar ($1.91 \times 10^6 \pm 0.49 \times 10^6$) and dorsal aspects ($1.85 \times 10^6 \pm 0.48 \times 10^6$).. 98

Figure 4-17: Box plot showing the T1-signal intensity post dGEMRIC incubation of lateral and medial aspects of the equine cartilage. There was no significant difference between medial ($1.9 \times 10^6 \pm 0.51 \times 10^6$) and lateral sites ($1.85 \times 10^6 \pm 0.47 \times 10^6$)..... 99

Figure 4-18: Box plot showing the T1 signal intensity of different punch location as (A, B, C &D) of the equine metacarpal-tarsal articular cartilage. No significant difference was found between them. 99

Figure 4-20: Scatter plot of the percentage water content of the equine cartilage vs. T2 relaxation time (ms).. There was no significant correlation found between the water content and T2 relaxation time of the equine cartilage ($P=0.92$). 102

Figure 5-1: T2-time mapping image analysis. Using the geometry tool, a triangular track tool was used to draw a triangular ROI (ms) in each agarose phantom. Then 4mm line was plotted. The track tool was used to manually draw the ROI around the cartilage, making sure that only the cartilage area was included. The value obtained from this image represent the T2-weight time map. 111

Figure 5-2: Sodium MR image analysis. Using the geometry tool, a straight line was drawn between the two end points of the semi-circular blocks. Then, a perpendicular line was plotted from the centre of the straight line. From this centre line two other 4mm lines were drawn to represent the central palmar and the central dorsal ROIs.

To ensure that only the cartilage area was included, the track tool was used to manually draw around the cartilage (A). Afterwards, a triangular track tool was used to draw triangular area ROIs, to measure sodium signal in each phantom. The value obtained represents the average sodium signal intensity within the ROI (A&B)..... 113

Figure 5-3: Standard curve, used to measuring the concentration of cartilage sodium, acquired from 5 standards with different concentrations measured by flame photometer ($r=1$)..... 115

Figure 5-4: Standard curve scatter plot of the agarose T2-time (ms) and agar concentration (%) ($r=-0.917$). The agarose concentration for Na study phantom was calculated using this standard curve equation. 116

Figure 5-5: Standard curve used to determine the amount of cartilage sodium, acquired from 6 standards with different concentration measured using 7T sodium MR images ($r=0.867$)..... 117

Figure 5-6 Box plot describing the sodium content determined by MRI at three articular surface sites. There was no significant difference observed between sites. 118

Figure 5-7: Box plot describing the GAG content at different punch locations. A= dorsal, B= middle and C= palmar. The middle site of the articular surface had a significantly greater GAG content than palmar sites ($P=0.036$). 119

Figure 5-8: Box plot describing the distribution of sodium content MRI in the articular cartilage samples. The middle site had the greatest sodium content $343.34 \text{ mM} \pm 170.04 \text{ mM}$. There was no significant difference between sites ($P= 0.203$). 120

Figure 5-9: Box plot describing the distribution of sodium content determined using flame photometry for the dorsal, middle and palmer sample sites. Significantly greater sodium content was observed in the middle site compared with other sites ($P=0.006$), whereas no significant difference was observed between dorsal and palmar sites. 121

Figure 5-10: A scatter plot of sodium MRI content (mM/l) and glycosaminoglycan content ($\mu\text{g}/\text{mg}$ dry weight). Pearson correlation plot for all data points. A moderate positive correlation was observed between sodium MRI content and glycosaminoglycan content ($P=<0.004$, $r= 0.38$)..... 123

Figure 5-11: Scatter plot of sodium MRI content (mM/l) and glycosaminoglycan content ($\mu\text{g}/\text{mg}$ dry weight). Pearson correlation plot for all data points. When only

dorsal site data points are analysed, there was no significant correlation between sodium MRI content and glycosaminoglycan content (purple circles). When only middle data points are analysed, there was a statistically significant positive correlation between sodium MRI content and GAG content (black stars). When only the palmar data points were analysed there was a strong positive correlation observed between sodium MRI content and glycosaminoglycan content (red squares)..... 123

Figure 5-12: Scatter plot of all data points for sodium MRI content mM/l vs. sodium content (flame photometer) per mg dry weight. When all the data points were analysed, sodium MRI content has a statistically moderate positive correlation with sodium content (flame photometer) ($P=0.001$, $r=0.451$). 125

Figure 5-13: Scatter plot of sodium MRI contents mM/l vs. sodium content (flame photometer) per mg dry weight. When only dorsal site data points are analysed, there was weak correlation between sodium MRI content vs. sodium content (flame photometer) (purple circles). When only middle data points are analysed, there was a statistically significant positive correlation of sodium MRI content vs. sodium content (flame photometer) ($P=0.001$, $r=0.71$) (green circles). When only the palmar data points were analysed there was weak positive correlation was observed between: Sodium MRI content vs. sodium content (flame photometer) (red circles)..... 126

Figure 6-2: Demonstration of the articular cartilage digestion process. The top slice degraded with 10 µg/ml trypsin, middle one degraded with 50 µg/ml and last slice degraded with 100 µg/ml trypsin solution. Only the dorsal aspect aspects were immersed in the enzymatic solution (trypsin) for 30 min, while the palmer aspect in each slice covered by surgical gauze soaked with normal saline to avoid dryness of the articular cartilage surface, as they were used as a control. 134

Figure 6-3: A sagittal sodium MR image of equine MCIII and its articular cartilage. (A) T1-weighted MRI; (B) Sodium MRI; (C) sodium image merged with T1-weighted image and (D) sodium MRI of the phantoms containing different concentration of sodium. Sodium MRI analysis using geometry tool, a straight line was drawn between the two end points of the semi-circular slices a 90° angle plotted from the center of the central line. Two 4mm lines were plotted from the central point to represent two dorsal RIOs (digested part) and other two palmar (control) RIOs. The track tool was

used to manually draw around the articular cartilage, making sure that only the cartilage area was included. The values obtained show the average sodium signal intensity within the RIO.	136
Figure 6-4: Diagrammatic presentation of the biochemical assays preparation. Four 4mm biopsy punches were harvested and separated from the MCIII subchondral bone using scalpel; making sure the full thickness of the cartilage was included. Half of these punches were used for GAG assay and the other half went for flame photometer technique. Peeling of the cartilage was due to sample collection and occurred after MRI.	137
Figure 6-5: Difference in mean sodium (MRI) concentration in articular cartilage samples degraded trypsin solution and its control group. There was significant difference in sodium content determined by MRI between degraded and control samples ($P<0.01$).....	139
Figure 6-6: Difference in mean sodium (MRI) concentration in articular cartilage samples degraded trypsin solution (10 $\mu\text{g/ml}$) and its control group. There was significant difference in sodium content (MRI) between degraded and control samples ($P=0.049$).....	141
Figure 6-7: Difference in mean sodium (MRI) concentration in articular cartilage samples degraded trypsin solution (50 $\mu\text{g/ml}$) and the control group. There was a significant difference in sodium content (MRI) between degraded and control samples ($P=0.031$).....	141
Figure 6-8: Difference in mean sodium (MRI) concentration in articular cartilage samples degraded trypsin solution (100 $\mu\text{g/ml}$) and the control group. There was a significant difference in sodium content (MRI) between degraded and control samples ($P<0.01$).....	142
Figure 6-9 Difference in overall mean GAG content of the articular cartilage samples degraded in trypsin solution and the control group. There was a significant difference in overall GAG content between degraded and control samples ($P<0.01$).....	143
Figure 6-10: Difference in mean GAG content of the articular cartilage samples degraded with (10 $\mu\text{g/ml}$) trypsin solution and the control group. There was a significant difference in GAG content between degraded and control samples ($P<0.01$).....	144

Figure 6-11: Difference in GAG content mean of the articular cartilage samples degraded with 50 µg/ml trypsin solution and its control group. There was a significant difference in GAG content between degraded and control samples ($P<0.01$).	144
Figure 6-12: Difference in GAG content mean of the articular cartilage samples degraded with 100 µg/ml trypsin solution and its control group. There was a significant difference in GAG content between degraded and control samples ($P=0.001$).	145
Figure 6-13: Box plot describing the sodium content of all articular cartilage samples degraded with trypsin solution and control. There sodium content was significantly lower in degraded than control samples ($P=0.001$).	146
Figure 6-14: Box plot describing the difference in sodium content (flame photometer) of the articular cartilage samples degraded with 10 µg/ml trypsin solution and its control group. There was no significant difference in sodium content (flame photometer) between degraded and control samples ($P=0.702$).	147
Figure 6-15: Box plot describing the difference in sodium content (flame photometer) content mean of the articular cartilage samples degraded with 50 µg/ml trypsin solution and its control group. There was significant difference in sodium content (flame photometer) between degraded and control samples ($P=0.034$).	147
Figure 6-16: Box plot describing the difference in mean sodium content (flame photometer) of the articular cartilage samples degraded with 100 µg/ml trypsin solution and the control group. There was significant difference in sodium content (flame photometer) between degraded and control samples ($P<0.01$).	148
Figure 6-17: Sodium content treated (MRI) mM/L vs. sodium content treated (flame photometer) per mg dw. When sodium MRI results and sodium results measured by flame photometer of the same correspondent punches were analysed there was strong positive relation ship between them ($P=<0.01$, $r=0.670$).	149
Figure 6-18: Sodium content (MRI) control mM per litre vs. sodium content control (flame photometer control) per mg dry weight. When sodium MRI results (control) and sodium results measured by flame photometer (control) of the same correspond punches were analysed there was strong positive relationship between them ($P=<0.01$, $r=0.702$).	150

List of Tables

Table 2-2: Comparison of anatomical structures in 7T&1.5T MR images. Structures were classified as ‘seen’ or ‘indistinct’ as previously described (Dyson et al. 2003; Smith et al. 2011).....	49
Table 3-2: Correlation coefficient (r value) of T1 7T MRI, 1.5T MRI and histology cartilage thickness measurements.....	66
Table 3-3: Mean of articular cartilage thickness (mm) measured using T1 7T MRI, 1.5T MRI and histology.	68
Table 3-4: Accuracy and precision (STDEV) of the 7T and 1.5T MRI cartilage thickness measurements to the histological measurements.	69
Table 4-1: Mean and standard deviation of all variables (sGAG (mg), T1 signal intensity, T2 relaxation time (ms) and T1 dGEMRIC).....	88
Table 4-2: Paired Student’s T-test of topographical difference in cartilage GAG content $\mu\text{g}/\text{mg}/\text{dw}$	89
Table 4-3: ANOVA Post hoc t-test of sGAG content ($\mu\text{g}/\text{mg}/\text{dw}$) in different punch locations: Multiple comparisons dependent variable: sGAG content per mg Tukey HSD.	89
Table 4-5: Paired Student’s T-test of topographical difference in cartilage water content %.....	93
Table 4-6: Mean and standard deviation of water % vs. punch location (A, B, C, and D).	93
Table 4-7: ANOVA Post hoc t-test of water content % in different punch locations: Multiple comparisons dependent variable: water content % per mg/dw Tukey HSD.	93
Table 4-8: Paired Student’s T-test of topographical difference in cartilage T2 relaxation time (ms).	96
Table 4-9: Mean and standard deviation of T2 relaxation time (ms) vs. punch location (A, B, C, and D).....	96
Table 4-11: Paired student’s T-test of topographical difference in cartilage T1 signal intensity pre and post dGEMRIC.....	100
Table 4-12: Mean and standard deviation of T1 signal intensity (pre & post) vs. punch location (A, B, C, and D).	100
Table 5-1: MRI Technical Information.	111

Table 5-2: Table describing the sodium MRI protocol information.	112
Table 5-3 Pearson rank correlation test between sodium MRI content vs. GAG content all the data set.	122
Table 5-4: Pearson rank correlation test between sodium MRI content vs. GAG content for all cartilage punches.	122
Table 5-5: Pearson rank correlation test between sodium MRI content vs. sodium content (flame photometer).	124
Table 5-6 Pearson rank correlation test between sodium MRI content vs. sodium content (flame photometer) for different punch locations.	125
Table 6-1: This table shows the technical information for the Na MRI protocol.	135

List of Abbreviations

1.5T MRI= 1.5T Magnetic Resonance Imaging System

^1H = Hydrogen Atom

^{23}Na = Sodium Atom

2D= Two Dimension

3D= Three Dimension

7T MRI= 7T Magnetic Resonance Imaging System

CDI= Cartilage Degeneration Index

CS4= Chondroitin 4-Sulphate

CS6= Chondroitin 6-Sulphate

CT= Computed Tomography

DESS= Double-Echo Steady State

DDFT= Deep Digital Flexor Tendon

DSL= Distal Sesamoidean Ligament

dGEMRIC= Delayed Gadolinium Enhanced Magnetic Resonance Imaging

Dis= Distal

FCD= Fixed Charge Density

FLASH= Fast Low Angle Shot Sequence

GaDTPA²= Gadolinium Ethoxybenzyl Diethylenetriamine Pentaacetic Acid

GAGs= Glycosaminoglycans

GRE= Gradient Echo Sequences

Lat= Lateral

MC3= Metacarpal/Metatarsal Bone

MCIII/MTIII= Metacarpal/Metatarsal Bone

MCPJ/MTPJ= Metacarpo/Metatarsophalangeal Joint

Med= Medial

Mid= Middle

mm= Millimetre

mM=Millimole

μ M= Micrometre

NEX= Number of Excitation Averaged

OA= Osteoarthritis

P value= Probability Value

Pal= Palmar

PBS= Phosphate-Buffered Saline

PG= Proteoglycan

Pro= Proximal

R value= Correlation Coefficient Value

RF= Radio Frequency

Sag= Sagittal

SDFT= Superficial Digital Flexor Tendon

SE= Spin Echo

SNR= Signal to Noise Ratio

SPSS= Statistical Package for the Social Sciences

T1 sequence= T1- Weighted MR Images

T2 sequence= T2- Weighted MR Images

Tr= Repetition Time

Tran= Transverse

Definitions

Osteoarthritis (OA), it is determined by the American College of Rheumatology as a "heterogeneous group of conditions that lead to joint symptoms and signs which are associated with the defective integrity of articular cartilage, in addition to related changes in the underlying bone at the joint margins" (Arnett et al. 1988).

B0 Bo (B zero) is the symbol used to represent the constant (main) magnetic field of the MRI system. It is usually expressed in units of Tesla (10,000 gauss or about 20,000 times the magnetic field of the earth).

B1 is the symbol used to represent the radio frequency field of the MRI system. The B1 field is produced by the radio frequency coil at the Larmor frequency.

Chapter 1 Literature Review

1.1. Research Proposal

Musculoskeletal pain and injuries are the most common cause of performance loss in equestrian activities, which then may lead to loss of a large number of athletic horses. Magnetic resonance imaging (MRI) techniques have been used to investigate the pathological injuries that affect the performance of athletic horses, such as osteoarthritis. Recently, MRI has been used to study articular cartilage structure and degeneration in both *in vitro* and *in vivo* studies using proton and sodium MRI approaches. For example, the sensitive technique of ^{23}Na MRI has been used to detect noninvasively the loss of proteoglycans in diseased cartilage (Zbýň et al. 2012). Several experimental MRI techniques have been aimed at detection of early cartilage pathological degeneration (Shapiro et al. 2002a). No published studies however describe the use of ultra-high field MRI to produce high resolution images of normal equine musculoskeletal tissues or to investigate equine orthopaedic disease. Investigation of the correlation between ultra-high field MR imaging and histopathology, in particular, would help to validate this non-invasive technique. The project aims to use ultra high field (7T) MRI to study anatomical and functional aspects of the equine orthopaedic disease. The findings of this project may also be of benefit in the development of novel methods for teaching equine surgery and anatomy.

1.2. Introduction

The first MRI scan was performed in the early 1970s (Rothschild et al. 1990). Since the early 1980s, magnetic resonance imaging (MRI) has been used in human medicine but the first scan on a live horse was not performed until the 1990s (Bolas 2011). This modality has become widely accepted as a gold standard for neurological and orthopaedic diagnostic imaging. MR imaging has been used extensively in human medicine for assessment and diagnosis of osteoarthritis.

Recent studies have assessed the use of MRI in the horse (Murray et al. 2005). MRI has been widely used in the diagnosis of equine foot pain. Equine feet frequently undergo MRI due to the high incidence of foot disease and the relative difficulty of imaging the soft tissues of the equine foot compared with the more proximal limb. The use of MRI has been proven clinically helpful by providing diagnostic information that is not available from radiography, ultrasonography and any other investigative techniques (Dyson et al. 2005; Gutierrez-Nibeyro et al. 2009).

1.3. Overview of Diagnostic Imaging in Equine Practice

Digital radiography using either computed radiography or direct digital radiography has become the most commonly used diagnostic imaging technique in routine equine practice. It has a large number of advantages such as no need for ordinary radiography cassettes, film, processing chemicals, and viewing boxes. The digital image is transferred directly to a computer and presented on a computer screen for viewing. Moreover, experts can adjust, magnify, increase and decrease the contrast and brightness without the need for repeated imaging. A disadvantage of digital radiography in practice is the high cost of equipment and maintenance. The presence of hoof capsule makes assessment of soft tissues within the foot especially difficult because of the restrictions it imposes on ultrasonography, the most commonly used imaging modality for the diagnosis of soft tissue pathology (Bischofberger et al. 2006). MRI has been used for several years for the investigation of carpal and proximal metacarpal pain in equine practice because it provides information about both soft and osseous tissues that is superior to other imaging modalities (Brokken et al. 2007). MRI can provide detailed anatomical information about both soft and osseous tissue and has become a valuable method for equine lameness diagnosis (Werpy 2004). However, it is very important to understand how tissue and structures are represented in the MR images to be able to interpret the images accurately. An understanding of normal anatomic variation is also important (Murray et al. 2006; Smith et al. 2011).

1.4. Magnetic Resonance Imaging

1.4.1. Principles of MRI

MRI has a number of features that are not available in other diagnostic imaging modalities, such as conventional radiography, scintigraphy, computed tomography (CT), and ultrasonography, due to properties related to the physics of generation of MRI signals and production of the image.

- I. MRI can form images that have a completely different appearance depending on the sequence and the magnetic field strength of MRI scanner.

- II. The images produced by MRI scanner are usually suboptimal in some respect due to physical attributes of the tissues (tissue environment of the proton). So, changing any aspect, such as decreasing the slice thickness, should be done with understanding of the trade-offs and how would they affect the resulting image.

- III. MRI poses hazards related to the magnetic and electrical current effect on common tools, patient table, and surgical implants.

1.4.2. How the MRI Image is Created

In 1976 Damadian and colleagues published the first report of MRI of a living animal that used an MRI scanner in which the magnetic field was only uniform over a small body region (Damadian et al. 1976). Passing an electric current through the coils creating a strong magnetic field creates the MR images. While this is happening, other coils in the magnet send and receive radio waves. The magnetic field triggers protons in the body to align themselves. Once aligned, radio waves are absorbed by the protons, which are stimulated to spin. Energy is released after "exciting" the molecules, which in turn emit energy signals that are picked up by the coil (Fig 1.1). This information is then sent to a computer, which processes all the signals to generate an image.

The final product is a 3D image representation of the area being examined (Podadera et al. 2010; Bolas 2011). Figure 1 shows examples of MR images of the metacarpophalangeal joint region of a horse.

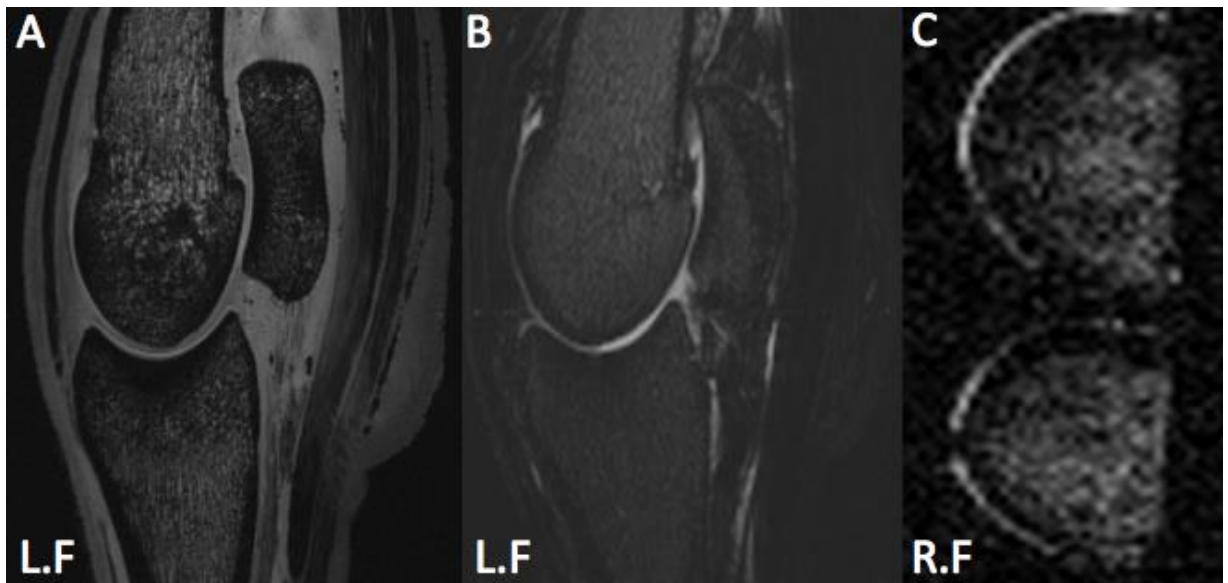


Figure 1-1: Mid sagittal plane T1 7T (A), (B) T2-weighted and (C) Sodium MR images of the metacarpophalangeal region of a horse. Images obtained from a dorsal plane through the midpoint of the metacarpophalangeal articulation. The trabecular bone of distal MCIII and proximal P1 produces a punctate pattern of mixed signal intensity due to low intensity trabecular bone interspersed by high intensity bone marrow. It has low to intermediate signal intensity on T1 images (A) and low on T2 MR images (B). Articular cartilage has an intermediate signal intensity in T1 MR images (A) and high to intermediate on T2 MRI (B).

1.4.3. Relaxation Time

T1 relaxation (spin-lattice relaxation) is also known as "longitudinal" relaxation. It indicates the time required for a substance to become magnetized after first being placed in a magnetic field or, alternatively, the time required to regain longitudinal magnetization following a RF pulse. T1 is determined by thermal interactions between the resonating protons, other protons, and other magnetic nuclei in the magnetic environment or "lattice". The interactions between resonating protons and other protons allow the energy absorbed by the protons during resonance to be spread to other nuclei in the lattice. The time of T1 relaxation in biological tissue is generally in the range of 10-1000 ms.

It is shorter in fat and longer in fluid. Therefore, it has been used to distinguish fat and fluids in images by applying pulses in quick succession. Water nuclei have no chance to recover while fat nuclei do more frequently and generate a strong signal (Bolas 2011). The T1 weighted sequence is commonly used for evaluation of contrast enhancement features which are associated with infections, inflammation or neoplasia such as keratoma (Gambarota et al. 2008), as well as investigation of anatomical structures such as metacarpophalangeal region in horses (Smith et al. 2011).

1.4.3.1. T2 Relaxation Time (T2 Mapping)

The T2 relaxation time mapping technique is focused on looking at the spin-spin time of the nuclei; which relates to the speed by which the nuclei lose their phase coherence in the transverse plane following radio frequency (RF) plane excitation and which results in decay of the T2 magnetisation (Choi & Gold 2011; Matzat et al. 2013). T2 mapping has been used as a non-invasive technique to characterise the structure and organization of hyaline articular cartilage and cartilage repair tissue (Goodwin 2001). Several studies have suggested that T2 MRI studies are beneficial for the diagnosis of the onset of OA due to T2 imaging being sensitive to the water content of the cartilage as T2 relaxation time found to be very sensitive to the integrity of the collagen network.

Several bovine articular cartilage studies have shown the ability and sensitivity of MRI T2 mapping in identifying changes in the articular cartilage, including collagen content (Nieminen et al. 2000; Nissi et al. 2004). A research group found that *in vivo* T2 transverse relaxation time was increased in patients that had severe osteoarthritis in contrast with healthy people (Mosher et al. 2000; Li et al. 2007). Furthermore, it has been found that T2 relaxation time is correlated with the loss of proteoglycans (PG) (Wayne et al. 2003). In 2001, Nieminen et al. concluded that T2 mapping could be used to evaluate the structure of collagen network fibres and is sensitive to PG content. However, T2 relaxation mapping technique has a number of limitations which reduces its usage in the routine clinical practice (Surowiec et al. 2014), despite the optimistic results obtained in many clinical studies (Nishii et al. 2008). The major

limitations are the long scan time required and susceptibility to magic angle artefact (Keenan et al. 2011).

1.4.4. Image Acquisition

The MRI scan must be good enough to allow diagnosis. Therefore, scan selection and quality are extremely important but must be balanced with the total scan time. The time a horse is under general anaesthesia needs to be minimized, thus scan sequence selection and planes that modify the diagnostic procedure are very important. Scan sequence should be chosen in advance of imaging as part of a standard protocol for any region in the body or the type of the problem, or might be selected dependent on the incomplete findings. The scan should be acquired in at least three planes: sagittal, dorsal and transverse. 3D rather than 2D imaging increases the ability to reconstruct the images and provide more anatomical details (Bolas 2011).

1.5. MRI Equipment (Magnet, Coils)

1.5.1. Magnet

The quality of the final MR image is influenced by the strength of the MR magnet. If the magnetic field is high, such as 3T and 7T, the MR image will be high-resolution due to the increased (SNR) signal-to-noise ratio which can be converted into increased spatial resolution resulting in a high-resolution MR image (Banerjee et al. 2008). Technically it is possible to get images at the earth's magnetic field (0.05mT) but to get an acceptable image in a reasonable time requires at least 0.2T (Bolas 2011). Nowadays, a 1.5T magnet is used most often in human medicine with higher field 3T systems gaining acceptance. MRI units of field strength greater than 3T are useful for research purposes but have yet to be used in human hospitals. Old MRI magnets required a high electrical current, which flowed through a coil of copper wires that were cooled by air or water flow. This technology was discarded because of the cost of cooling the system. Newer MRI systems are cooled by liquid helium instead of water or air. The diameter of conventional human MRI magnets, which are usually in the form of a cylindrical tube, is about 60-70 cm diameter internally and around 2-3 meters externally.

1.5.1.1. Types of Magnets

I. Open magnet

The open magnet MRI system does not use a tube design, it is U shape magnet in which the patient lie between two magnets bores and it is usually produces power from 0.2-0.3 Tesla such as low field standing MRI magnet.

II. Cylindrical short bore magnet

This type of MRI magnet is designed as a tube-like magnet, in which the patient lies down on the automated table that goes inside the MRI bore such as 1.5T MRI unit.

1.5.2. Radio Frequency Coils

Radio-frequency (RF) coils are an essential element in magnetic resonance (MR) imaging. They constitute the key hardware element for the transmission of RF signal pulses to the patient tissues and provide the means of collecting returning RF signal information from the body. Transmitter RF coils should be able to handle high power and generate a uniform radio frequency field for the whole scanned tissue; because RF coils serve as the intermediate interface between the body and the MRI system, their performance characteristics are very important determinants of image quality. Image quality is measured by the signal-to-noise ratio (SNR), signal homogeneity and spatial resolution. Coils demonstrate a wide range of functional characteristics ranging from large volume general use head coils to small phased-array surface coils for niche applications (Welker et al. 2001; Bolas 2011). RF coils play an important role in obtaining the maximum SNR during MR image acquisition. They are responsible for the B_1 field, which rotates the net magnetization in a pulse sequence, detects the transverse magnetization and processes it in the XY plane (Bolas 2011).

Radio frequency coils are typically classified into two main types: volume and surface coils (Gibby 2000). Surface coils are the most widely used in MRI as they are a convenient and effective way of acquiring a higher signal to noise ratio (SNR) than volume coils. However, the advantages of these coils in small animal practice are not as great as has been seen in human applications. The volume coil provides homogeneous transmission and reception over a large anatomical body region (Kneeland & Hyde 1989).

Recently, there has been an increase in interest in advanced RF coil design leading to a proliferation in the number of coils available to the imaging professional. These coils display a huge range of high functional characteristics varying from large volume general use surface head coil to small phased-array surface coils that have been used in specific clinical applications e.g. imaging of brain and skull base (Welker et al. 2001).

1.5.2.1. Types of MRI Coils

RF transmit coils are used in MRI to transmit electromagnetic waves creating the oscillating B1 magnetic field needed in order to excite the nuclear spins of the scanned body atoms. Receive coils detect the weak signal emitted by the spins as they change their orientation into B0 field (Axel & Hayes 1985). Radio frequency coils can be used to excite the nuclear spins or to receive the resulting magnetic signals or do both within the same coil. However, separate coils are preferred as this minimizes the inductive coupling that can occur between coils (Gibby 2000; Fishbein et al. 2005). They are mainly classified into two major types: surface coils, which are placed adjacent to the imaged tissue of interest; and volume coils which placed surround to the imaged object (Fishbein et al. 2005).

1.5.2.1.1 Volume Coils

This type of coil provides homogeneous transmission and reception over large scanned body regions, which are circumscribed by the coil. It has been used widely in neurological studies as they have lower signal-to-noise ratio compared with surface coils (Asher et al. 2010). Volume coils provide a clear larger sensitive volume but a reduced SNR compared to the smaller surface coils (Steidle et al. 2004).

1.5.2.1.2 Surface Coils

These types of coils are designed to work efficiently over a limited body region of interest. They provide high SNR reception over a small geometric area, which is immediately adjacent to the coil so that they are known as "local coils," (Kulkarni et al. 1986; Asher et al. 2010). However, the improved SNR, which is achieved at the cost of the RF reception, declines considerably beyond the area interest. Thus, they create an inherently inhomogeneous reception shape.

Examples are phased-array knee coils, which are commonly used in human medicine (Asher et al. 2010), and dual tuned ^{23}Na / ^1H coils which can be used to estimate sodium concentration in the living tissues (Gibby 2000).

1.5.2.1.3 Dual Tuned ^{23}Na / ^1H Coils

Dual tuned sodium and hydrogen channelled surface coils are one kind of surface coil that is widely used in MRI studies (Reddy et al. 1997). The availability of high and ultra-high field MRI systems with multinuclear capability, sufficient signal-to-noise ratio and a high spatial resolution and the performance of dedicated sodium MRI coils (Trattnig, et al. 2010), has led to interest in the so-called X-nuclei (other than ^1H hydrogen nucleus) imaging such as sodium (Trattnig et al. 2010) or phosphorus MRI techniques (Bogner et al. 2009). The increased interest in sodium MRI in particular stems from the theoretical knowledge that sodium is another tissue component that plays a very essential role in the body electrolyte homeostasis (Cannon et al. 1986). It is known that changes in sodium concentrations can provide information on the tissue health status in the body and may therefore be useful in the assessment of pathology in diseases such as osteoarthritis (OA) (Wheaton et al. 2004a), and monitoring of response to therapy (Nagel et al. 2013).

1.6. Quantitative MRI Studies

MRI is a valuable technique for clinical assessment of the health status of cartilage and soft tissues. Recently, advanced quantitative MRI techniques have been described for detecting early degenerative changes of the equine articular cartilage (Carstens et al. 2013). Studies have focused on the quantitative MRI techniques that are sensitive to the collagen network as well as glycosaminoglycan content of the articular cartilage, as these components are very important in articular cartilage health, functional status and the pathological changes that occur. Examples of these techniques are delayed gadolinium enhanced MRI and T2 time mapping (Bashir et al. 1996; Matzat et al. 2013).

1.6.1. Sodium MRI

Mankin et al. (1981) & Borthakur et al. (1999) in their studies found that loss of proteoglycans and change in collagen occurred in articular cartilage in the early stages of osteoarthritis and can be identified accurately by histology. In the early stages of osteoarthritis loss of proteoglycans is the predominant change in matrix composition (Mankin et al. 1981; Borthakur et al. 2000) – a non-invasive but sensitive technique for detecting this change would be advantageous. Several experimental MRI techniques have been reported aimed at the early detection of cartilage degeneration (Shapiro et al. 2002b). The strategies that have been used can be classified as proton and sodium MRI techniques. Conventional proton MRI technique studies, such as T1 and T2 weighted imaging, have been shown to be inconclusive in detecting early changes in osteoarthritis. Recent studies have shown that it is possible to measure proteoglycan changes in articular cartilage, both *in vivo* and *in vitro*, by delayed gadolinium (Gd)-enhanced MRI of cartilage (dGEMRIC). However, this technique has the disadvantage of requiring joint manipulation, as well as intravenous injection of the contrast agent (Akella et al. 2001). Sodium concentration in the articular cartilage has been found to correlate well with the glycosaminoglycan (GAG) concentration, which can therefore be used as a marker of articular cartilage health status (Madelin et al. 2012; Zbýň et al. 2012). Sodium (^{23}Na) MRI advanced imaging techniques, which use a dual tuned ^{23}Na / ^1H coil, can provide information non-invasively about tissue physiology and metabolism at the cellular level and has been used as a gold standard method in the development and testing of drugs for osteoarthritis treatment (Newbould et al. 2012).

Moreover, non-invasive sodium MRI can provide valuable qualitative and quantitative complementary information of the scanned tissue (Madelin & Regatte 2013; Madelin et al. 2014).

It has been found that OA is associated with proteoglycan loss from articular cartilage, as a result of which there are changes in the size and arrangement of collagen fibres and an increase in the water content of the cartilage resulting in increase in the rate of production and degeneration of matrix macro-molecules. Thus, resulting in incomplete breakdown in the PG matrix.

Then, the negatively charged sulphated and carboxylate groups within the complex PG molecules attract free floating Na positive ions within the extracellular matrix, thus attracting water molecules to accumulate in the extracellular matrix to maintain osmotic pressure. Several Na MRI studies found that the loss of PG is associated with the changes of sodium concentration and these changes may be detected by Na MRI (Brossmann et al. 1997; Reddy et al. 1998; Wheaton et al. 2004a; Borthakur et al. 2006; Madelin & Regatte 2013). However, the impact of sodium (^{23}Na) MRI has been minimized by technical difficulties, which arise from the inherent biological and MR properties of the ^{23}Na nucleus, hardware and software requirements (Staroswiecki et al. 2010).

1.6.2. MRI Contrast Media (dGEMRIC) Study

There has been increasing interest in the last decade in developing functional MRI techniques (Madelin & Regatte 2013) in order to detect and assess biochemical changes in the articular cartilage. These techniques include $T_{1\rho}$ mapping (Regatte et al. 2003), T2 mapping (Mosher & Dardzinski 2004) and delayed gadolinium-enhanced MRI of the cartilage (dGEMRIC) contrast studies (Bashir et al. 1996). The latter, which relies on the negatively charged contrast agent gadopentetate dimeglumine²⁻ (Gd-DTPA^{2-}), is now well established in human and small animal MRI, being used in neurology, oncology and to investigate osteoarthritis pathology. Few studies however have reported the use of this technique in equine medicine (Saveraid & Judy 2012; Carstens et al. 2013). For OA changes of the cartilage, gadolinium is injected either intravenously or intra-articularly before MRI scanning allowing considerable time for it to distribute through the joint region.

This technique relies on the negative charge conferred to cartilage by proteoglycans. Thus the gadolinium, and other negatively charged molecules, are excluded from healthy cartilage matrix (Maroudas 1970; Wiener et al. 2007).

When proteoglycans are lost from the cartilage matrix the negative charge density of the cartilage decreases, allowing the negatively charged gadolinium to infiltrate the cartilage. As a result, the gadolinium distributes and accumulates in inverse relationship to the proteoglycans of the cartilage matrix.

So, areas of cartilage with low PG content would accumulate a high amount of gadolinium in the cartilage matrix (Wucherer et al. 2012; Carstens et al. 2013; Matzat et al. 2013). This accumulation of the contrast medium can be measured on T1-weighted MR images by assessing signal intensity changes (Wucherer et al. 2012) or technically by merging pre and post contrast images. Gadolinium mainly shortens T1 time allowing this quantitative MRI technique to be used clinically to compare proteoglycan content in the cartilage matrix of healthy and pathological cartilage.

dGEMRIC MRI has a number of disadvantages, such as the time that must be allowed for distribution into the joint because of the repulsion from the negatively charged glycosaminoglycans (GAGs) (Aime & Caravan 2009), which make it challenging to perform on the routine basis clinically (Watanabe et al. 2009). In theory, dGEMRIC MRI is a specific method for assessing the GAG content of the cartilage (Bashir et al. 1996; Bashir et al. 1997). There are however several factors that might affect its ability to measure PG content in the cartilage using post-contrast T1 time, e.g. unknown plasma concentration of the contrast medium, variation in contrast agent diffusion as well as variation in pre-contrast T1 time and relaxivity of the contrast medium depending cartilage health state (Burstein & Gray 2006; Tiderius et al. 2006). However, despite these limitations dGEMRIC is believed to represent a generally reliable technique for monitoring GAG content in the degenerative cartilage which is associated with OA (Bashir et al. 1996; Bashir et al. 1997; Bashir et al. 1999), and is considered superior to standard MRI scanning protocols (Gold et al. 2009).

1.7. MRI In Equine Orthopaedics

1.7.1. The Foot

Foot pain is believed to be the most common cause of equine lameness that can usually easily be localised to the limb by investigation and nerve block. There are some limitations of the methods that are usually used in equine clinical practice to diagnose foot pain. Radiography is limited to the assessment of the mineralised tissues and some small pathological changes could be easily missed (Butler et al. 2008). Ultrasonography of the equine foot is limited to the sagittal midline and the presence of the artefacts may lead to difficulties in interpretation (Busoni & Denoix 2001). Although scintigraphy can provide highly reliable sensitive information about normal bone activity, anatomical localisation is limited and there is a relatively high incidence of false negative results (Dyson et al. 2003). Computed tomography can provide highly sensitive information that could be used to give an accurate assessment of the 3D distribution of osseous and soft tissue abnormalities, but general anaesthesia is required (Tietje et al. 2001). MRI in the equine practice has been widely used to diagnose pathology of the carpal and metacarpal regions and the foot (Nagy & Dyson 2012; King et al. 2013).

1.7.2. The Fetlock

The normal anatomy of the metacarpo-phalangeal and metatarsophalangeal joint has been fully described by the use of low-field magnetic resonance imaging (Martinelli & Baker 1996). Unfortunately, there are currently no published descriptions of normal anatomy based on the higher resolution images that it is possible to acquire with high field (or ultra high field) MRI systems (Dyson & Murray 2007a). On the other hand, there are several studies that describe the lesions of the equine fetlock joint, particularly in the subchondral bone, in clinical cases. The equine metacarpo-phalangeal joint is a more accessible region compared with other regions in the distal limb to different diagnostic techniques such as radiography, ultrasonography, nuclear scintigraphy, arthroscopy, and endoscopy. Therefore, the use of the MRI is less common than in the foot (Dyson & Murray 2007b).

1.8. Cadaver Studies

A previous MRI study of equine distal limbs used cadaver material to describe the normal appearance of the anatomic structures of the metacarpophalangeal joint in images obtained using high-field and low-field systems (Smith, et al. 2011).. They found that different layers of articular cartilage were clearly visible on the distal aspect of the third metacarpal bone, proximal aspect of the proximal phalanx and the dorsal surface of the proximal sesamoid bones on 1.5 T high-field images. Whereas in 0.27T low field MRI, separation between the articular cartilage surfaces was not clearly distinguished or defined in the weight bearing area of the joint, but could be distinguished in other areas of the joint such as the dorsal surface of the proximal sesamoid bone (Smith et al. 2011). Another study by the same group also using equine cadaver limbs, found that there was an increased likelihood of false positive results in using both high (T2*W-GRE) and low (T2W-FSE) MRI pulse sequences in detection of cartilage lesions, and a moderate-high likelihood of false positives for detection of subchondral bone lesions when compared with histopathology, whereas there was better interpretation agreement for subchondral bone changes (Smith et al. 2012).

There is good information available on normal MR anatomy of the proximal metacarpal and metatarsal regions, based on a study in which 30 cadaver metacarpal regions of mature horses with no history of carpal or proximal metacarpal pain were scanned (Nagy & Dyson 2009). It has been suggested that proton MR is an inaccurate technique for measuring early degenerative changes such as osteoarthritis as this technique does not provide insight into the molecular composition of cartilage (Fragonas et al. 1998; Braun & Gold 2012). Yet, gadolinium-containing contrast media has been used to assess equine articular cartilage (Carstens et al. 2012).

1.9. Articular Cartilage Morphology

Articular cartilage is a dense connective tissue that covers the ends of bones and assists load-bearing movement at the joint by providing a low wear, low friction and shock absorbing surface (Mow et al. 1984; Mow et al. 1993). Articular cartilage contains relatively few active cells which are immersed in a matrix composed of three types of molecule: collagen (as fibres), water and proteoglycans (PG) (Kuettner 1992). In order to meet the functional demands placed upon it, articular cartilage displays a number of unique mechanical properties and morphological features (Camarero-Espinosa S. et al., 2016). Hyaline cartilage, which covers the surface of the diarthrodial joints, is essential to normal articular cartilage physiological function and is capable of distributing and transforming the high compressive forces which occur during weight bearing and locomotion, across the joint without sustaining any substantial wear.

1.10. Articular Cartilage Zones

The structure of the articular cartilage varies according to depth and it may therefore be divided into four zones or layers. Collagen content structure and proteoglycan concentration vary throughout the layers. The zones are superficial (tangential), transitional, deep and calcified. Articular cartilage varies in thickness over the joint surface in the horse, with the variations likely to be correlated with biomechanical demands, e.g. in the metacarpophalangeal joint, the cartilage on the dorsal and palmar surface is thin and covering a large joint articulation surface (Brama et al. 2001; Moger et al. 2007).

1.10.1. Superficial (Tangential) Zone

The superficial (tangential) zone makes up to 20% of the articular cartilage thickness. It plays an important role in absorbing stresses and preventing the deeper layers from sharing stress (Fox et al. 2009). It contains primarily collagen (type II and IV) fibrils and is approximately 50µM thick (Moger et al. 2007). The collagen fibrils are packed tightly and aligned parallel (tangential) to the articular surface of the cartilage. This cartilage zone contains a relatively high number of chondrocytes. The main purpose of this layer is protecting and maintaining of the cartilage deeper layers.

This superficial layer is in direct contact with the synovial fluid, which assists movement of the contact joint. Moreover, it is very important to the most of the tensile features of the articular cartilage (Cohen et al. 1998).

1.10.2. Middle (Transitional) Zone

This layer is located immediately deep to the superficial zone and provides an anatomic and functional bridge between the superficial and deeper layers. It occupies around 60% of the total cartilage volume. It is mainly composed of proteoglycans and thick collagen fibrils. The collagen fibrils are aligned in an oblique manner besides low-density spherical chondrocytes. This layer is the first line of resistance to compressive forces (Cohen et al. 1998; Fox et al. 2009).

1.10.3. Calcified Zone

This layer is in a direct contact with the subchondral bone and there is a tidemark demarcating this layer from the deep layer. The cell density is very low and the chondrocytes are hypertrophic. It plays an essential role in keeping the cartilage secured to the bone, through attaching collagen fibrils from the deep layer to the underlying subchondral bone surface (Fox et al. 2009; Kuettner 1992).

1.11. Articular Cartilage Physiology

Articular cartilage is mainly composed of proteoglycans (PGs), water and collagen, the latter playing an important role in the mechanical function of the cartilage. The extracellular matrix (ECM) is made up of type II collagen occupying 15-20% and proteoglycans (PGs) occupying 5-10% (Heinegard 1989). It contains 65-85% water and a small population of chondrocytes only occupying about 5% of the tissue by weight (Roughley & Lee 1994). The matrix is structured as a collagen framework with glycoproteins, including proteoglycans, interspersed between the collagen fibres. Proteoglycans are made up of a protein core and negatively charged glycosaminoglycan side chains (GAGS), which give cartilage a negative fixed charge density (FCD). There are three main side chains in the articular cartilage: chondroitin 4-sulphate (CS4), chondroitin 6-sulphate (CS6) and keratin sulphate (KS). Chondroitin sulphate occupies 55-90% of total glycosaminoglycan (GAGS) (Carney & Muir 1988).

The FCD attracts free-floating positive counter-ions, such as sodium ions (Na^+). These ions attract water molecules in the articular cartilage via osmotic pressure. Additionally, these ions produce strong electro-static repulsive forces between proteoglycan molecules, consequently cartilage stiffness occurs due to aggregation of PG molecules (Regatte & Schweitzer 2008; Madelin et al. 2011; Matzat et al. 2013).

1.12. Physiologic MRI of Articular Cartilage

Normal articular cartilage composed of approximately 70% water by weight and 30% of other components such as type II collagen and proteoglycans. Approximately 30% of the water component of the articular cartilage is associated with the intrafibrillar space inside collagen fibre; the remaining amount is located in the intercellular space (Maroudas et al. 1991). There is some variation in water content between zones: 80% in the superficial zone of the cartilage and 65% in the deeper layer, which provides and helps to transport and distribute nutrients to the cartilage cells (chondrocytes). The increased water content in the cartilage will influence T2 time and signal intensity of the cartilage as the T2 time is sensitive to the body fluids (Liess et al. 2002). Collagen represents approximately 50% of articular cartilage on a dry weight basis (Mayne 1989; Eyre 1991). Proteoglycans of the articular cartilage contain negative charge density, thus mobile positively charged ions, such as sodium ($^{23}\text{Na}^+$), and contrast media such as gadolinium will distribute in articular cartilage in relation to the proteoglycan content. Due to the structural order of the collagen fibres, the water molecules associated with the collagen fibres exhibit both cartilage magnetization transfer and magic-angle effect. So, physiological MRI of articular cartilage yields the benefit of these characteristics that articular cartilage exhibit in order to investigate the integrity of the collagen fibres and proteoglycans matrices (Gold et al. 2006).

1.13. Protocols For Articular Cartilage Measurements

There are many protocols that have been used to evaluate and measure the articular cartilage morphology and pathology such as proton density (Gold et al. 2006), fat suppressed T1 weighted 3D spoiled gradient recalled acquisition in the steady state (SPGR) and fast low angle shot sequence (FLASH), which are regarded as gold standard MRI protocols for quantitative articular cartilage MRI assessment and have

been used in both 1.5T and 3.0T MRI systems (F. Eckstein et al. 2006; Gold et al. 2006; Peterfy et al. 2006).

It has been found that MRI is capable of providing extremely accurate information on articular cartilage volume (Sittek et al. 1996), and is able to provide information about articular cartilage thickness if high-resolution fat-suppressed T1-weighted 3D gradient echo sequences are used and transverse, longitudinal and oblique plane images obtained (Eckstein et al. 1996). The double-echo steady state MRI protocol (DESS) with water excitation has attracted interest recently due to the lower slice thickness that can be achieved with a fast acquisition time.

Research has led to the development of methods to build 3D virtual computer models of the articular cartilage from data acquired from normal MRI that offer the potential to assess cartilage morphology with better accuracy than 2D MRI (Stammberger et al. 1999; Koo et al. 2011).

1.14. Normal Appearance of The Articular Cartilage

MRI has been found to be one of the promising techniques for assessing articular cartilage. Despite the large number of research studies performed however, there remains controversy over the normal MRI appearance of articular cartilage and what causes this appearance (Mlynarik et al. 1996), and only a few studies have described the normal appearance of articular cartilage. It is crucial for the clinician to be able understand the normal anatomical appearance of the articular cartilage to differentiate between normal and abnormal. Several cartilage MRI studies have found that normal articular cartilage has a laminar-like homogeneous appearance (Chalkias et al. 1994) with the number of these laminae differing according to the source of the articular cartilage tissue (bovine, human etc.). Another study found that this trilaminar appearance of the articular cartilage corresponded to the histological layers of the articular zones, except the calcified layer, which was found to be indistinguishable from subchondral bone. The difference in the MRI descriptions of articular cartilage may be due to differences in MRI techniques used, such as field strength, coil and pulse sequence.

A trilaminar appearance of the articular cartilage has been described featuring superficial and deep hypointense layers in all MRI sequences along with an intermediate zone appreciated as moderately hyperintense on a spin echo SE T1-weighted (longitudinal relaxation time) MRI and hyperintense on T2-weighted (transverse relaxation time) on gradient recall echo (GRE) MRI (Chalkias et al. 1994).

1.15. Technical Factors Affecting MRI of Articular Cartilage Measurements

There are other factors which affect the articular cartilage MRI quality such as the strength of the magnet, radio frequency coils used in scanning, pulse sequence and selected voxel dominions (Behr et al. 2009).

Voxel size of the articular cartilage can be acquired by multiple slice thickness, thus the smaller voxel size the better spatial resolution. However, if the voxel size decreases the number of the hydrogen protons decreases as well, which leads to a lower signal to noise ratio. Thus, high- resolution MRI requires a sufficient (SNR) ratio in order to support the small voxel size of the images.

There are a number of ways in which (SNR) ratio could be increased in order to increase the quality of the MRI, for example, shortening the echo time, increasing the total number of excitations averaged (NEX), greater T1 magnetization or using very specialised small coils (Kneeland & Hyde 1989; Mosher et al. 2000).

1.16. Sodium Content in The Biological Tissues

Sodium is one of the most dominant and vital components of living bodies. Normally, intercellular sodium concentration is between 10 to 15mM; while extracellular concentration is approximately 145mM (Constantinides et al. 2001). Sodium concentration in the tissue is very sensitive to any changes in the integrity of cell membranes and metabolic state of the tissue. In theory sodium ^{23}Na is a quadrupolar nucleus which exhibits complex behaviour as a consequence of the spin quantum number $3/2$ and which is considered to be the second strongest nuclear magnetic resonance nuclei after protons (^1H).

Na emits a relatively low signal compared with proton signal. Moreover, sodium MRI has an average of signal to noise ratio (SNR) 3000 – 20,000 times lower than proton signal to noise ratio depending on the organ imaged (Berendsen & Edzes 1973; Pabst et al. 2002; Jerecic et al. 2004; Murphy & Eisner 2009).

Recently it has been possible to achieve reasonable ^{23}Na MRI scan times (around ~14 min) for high resolution images with low slice thickness by using high field MRI systems with enhanced hardware capability and double-tuned radio frequency coils, (Madelin & Regatte 2013). However, the impact of sodium ^{23}Na MRI has been reduced by technical challenges that arise from the inherent biological and MRI properties of the ^{23}Na nucleus, as well as hardware and software requirements (Staroswiecki et al. 2010).

1.17. Osteoarthritis

1.17.1. Pathophysiology

Osteoarthritis is considered to be the most common disease of human joints, affecting more than 10% of the adult population (Borthakur et al. 1999). A considerable number of studies have reported that more than 50% of the human population over 65 years suffers from osteoarthritis in the United States (Sarzi-Puttini et al. 2005). Osteoarthritis (OA) is one of the most degenerative and progressive diseases of the articular cartilage and is accompanied by severe joint pain, which results in joint immobilization (Eckstein et al. 2006). It has been defined by the American College of Rheumatology as a "heterogeneous group of conditions that lead to joint symptoms and signs which are associated with the defective integrity of articular cartilage, in addition to related changes in the underlying bone at the joint margins" (Sarzi-Puttini et al. 2005). Loss of articular cartilage is the primary gross pathological defect in OA. In early stages of the disease, proteoglycan loss occurs from cartilage but the collagen component is largely unaffected. The reduction in proteoglycan content is reflected in the colour change of cartilage to yellow-gray or brownish gray. Another microscopic change that has been recognised by light microscopy is the loss of metachromasia in the matrix surface. Whether this occurs due to rupture of the superficial collagen network or as a result of depletion of the proteoglycan due to the release of enzymes from chondrocytes remains speculative (Okimura et al. 1997).

Matrix changes to articular cartilage are usually followed by erosion of the articular cartilage surface, which may extend to deep fissuring. The proliferation of chondrocytes and increased production of the matrix in the area adjacent to the fissure is unable to heal the cartilage (Okimura et al. 1997). Macroscopic loss of cartilage may progress to subchondral bone exposure (Borthakur et al. 2000); however the early stage of OA is mostly associated with proteoglycan loss accompanied with little change in collagen.

1.17.2. Diagnostic Imaging

Osteoarthritis in horses is usually diagnosed by the use of radiography. However, osteoarthritis is an insidious disease that may feature pathological lesions, including substantial damage to the articular cartilage, before radiographic changes become visible. One focus of current research is therapeutic intervention in the early stages of cartilage degeneration, which relies on early detection of disease. The use of molecular markers, which are synovial fluid or serum based, has been explored but is hampered by the lack of methods for quantitative assessment of the severity of osteoarthritis for the entire articular joint surface (Brommer et al. 2003). Recently, a number of qualitative and semi-quantitative techniques have been used to measure or grade the extent of cartilage degeneration in OA. These techniques include the use of Indian ink to assess cartilage changes over the entire joint surface; the intensity of Indian ink uptake correlates with proteoglycan content reduction in horse cartilage (Cantley et al. 1999).

Quantitative MRI techniques have been used for clinical evaluation of the health status of cartilage and soft tissue. Recently, advanced quantitative MRI techniques have been described and used for assessing and detecting early degenerative changes of the equine articular cartilage (Carstens et al. 2013). Mainly those quantitative MRI techniques are important in assessing articular cartilage health, functional status and pathological changes that occur in the articular cartilage. Moreover, these quantitative MRI techniques are sensitive to the glycosaminoglycan content of the articular cartilage and the collagen network integrity such as T2 mapping, delayed gadolinium enhanced MRI of cartilage (Bashir et al. 1996; Saveraid & Judy 2012; Matzat et al. 2013) and sodium MRI of the articular cartilage (Shapiro et al. 2002b; Newbould et al. 2013).

1.17.3. Classification

Osteoarthritis in the horse was classified by McIlwraith in 1996 (Kidd et al. 2001):

- I. Primary: (Type A) which is commonly seen in the carpus and fetlock, distal tarsal and distal interphalangeal joints.
- II. Secondary: (Type B) that is usually associated with other known injuries or damage to the joint for example, intra-articular fractures or septic arthritis.
- III. Osteoarthritis, which occurs incidentally or due to non-progressive damage to the articular cartilage.

1.17.4. Osteoarthritis in The Horse

Osteoarthritis is considered to be a joint disease of a multifactorial etiology. It is recognised by degradation of the cartilage matrix and is accompanied clinically by joint stiffness, swelling and pain (Shapiro et al. 2002b). Osteoarthritis has been classified into three main types (Kidd et al. 2001). Osteoarthritis affects horses leading to lameness which is considered to be the most common cause of days lost from training (Bailey et al. 1999) and a cause of significant economic loss to horse owners (Kidd et al. 2001). The lower limb joints are the most frequently affected by osteoarthritis; typically secondary to traumatic injury (Rydell et al. 1970). Forelimbs are significantly more susceptible to musculoskeletal injuries than the hindlimbs, and many of these injuries lead to osteoarthritis (Menarim et al. 2012).

There are several abnormalities that could occur in the equine MCPJ/MTPJ such as synovitis or osteoarthritis, with the latter being a common cause of lameness among racehorses (Brokken et al. 2007). The gross pathology has been described as variable degrees of articular cartilage destruction (Pool & Meagher 1990), subchondral bone sclerosis, marginal osteophyte formation and, occasionally, eburnation of subchondral bone. Joint effusion and synovitis are often clinically associated with the chronic disease (McIlwraith 1982).

There is no curative treatment for osteoarthritis but early stage detection followed by efficient treatment could inhibit its detrimental effects.

1.18. Hypotheses

The first hypothesis of this study was that the ultra-high field 7T MRI magnet would produce images of excellent anatomical detail, that would allow identification of the major anatomical structures of the equine fetlock region, and that the MR images would be superior to those acquired using a high field 1.5T magnet. Secondly, the measurements of articular cartilage thickness in the MCPJ/MTPJ of the horse made from MRI would compare favourably with measurements made directly from histological sections but that 7T MRI enables more accurate and precise measurement than 1.5T MRI. The third hypothesis was that novel MRI methods could quantify body tissue biochemical properties associated with the early onset of articular cartilage degeneration in equine articular cartilage. In addition, this study hypothesised that dGEMRIC and T2 will correlate with the early arthritic change markers of proteoglycan concentration and water content. It was further hypothesised that sodium MRI would be able to quantify cartilage properties associated with the early stages of osteoarthritis in equines. In particular, it was hypothesised that sodium MRI signal intensity values would correlate with the cartilage sodium ion and sGAG content. The fourth hypothesis was that quantitative 7T sodium MRI techniques could detect changes in sodium and proteoglycan content in equine articular cartilage using a model of osteoarthritis. Specifically, this study hypothesized that trypsin degradation would result in a concentration dependent decrease in sodium signal intensity of the acquired 7T MR images. The final hypothesis of this study was that the 7T sodium MR image signal intensity would correlate with proteoglycan and sodium concentration.

Chapter 2 High- And Ultra-high Field Magnetic Resonance Anatomy Of The MCIII/MTIII Region Of The Horse

2.1. Introduction

Several epidemiological studies have shown that the MCPJ/MTPJ is the most common site of lameness in Thoroughbred racehorses, with bone related injuries of the metacarpo/metatarsophalangeal region representing the most usual cause of catastrophic fracture of the distal limb in the Thoroughbred racehorse (Verheyen & Wood 2004; Ely et al. 2009; Gonzalez et al. 2010). For instance, P1 and biaxial proximal sesamoid bone fractures are the most frequent fracture types in National Hunt racing (Parkin et al. 2004). Moreover, soft tissue such as collateral ligaments injury occur secondary to trauma which could occur either in the body of the collateral ligament or at the ligament bone junction (Rodgerson & Spirito 2001). Furthermore, injury to the straight, oblique and short distal sesamoidean ligaments can occur in combination with distal sesamoid bone fractures or other problem (Moyer & Raker 1980).

MRI has been used in veterinary practice since 1987 particularly in small animal hospitals, whereas there have been a number of procedural difficulties associated with taking images from live horses, for example, a MRI compatible table which is suitable for horses and appropriate coils (Pancieria et al. 1987).

In 1987 Park and colleagues published a description of 0.15T MRI of equine limbs; despite the low resolution of their images they concluded that MRI had great potential for imaging the equine musculoskeletal system (Park et al. 1987). After that, in 1996, the low-field 0.15T MRI appearance of the equine MCPJ/MTPJ was described accurately before the clinical use of the MRI systems in equine practice (Martinelli et al. 1996).

Recently, anatomical studies of the equine MCPJ/MTPJ have been conducted to describe the normal appearance of the equine MCPJ/MTPJ using a 1.5T MRI magnet (Dyson & Murray 2007a).

Subsequently, MRI has been used extensively in equine practice to investigate foot pain due to the high prevalence of foot disease and the difficulty of imaging the soft tissues of the equine foot by other means compared with the more proximal limb (Whitton et al. 1998). There has been an increasing interest in the use of 3T and ultra-high-field 7T systems for in vivo studies because of the high resolution images that they can produce. These systems are only available in a small number of research centres, and have mostly been used for neuroimaging. A study describing the normal anatomical appearance of the equine metacarpal region from high resolution MR images acquired by a 7T system is needed. A 7T system can provide gold standard reference images with superior resolution morphologic detail (Regatte & Schweitzer 2007).

In order to improve our understanding of the normal anatomical appearance this study aimed to describe the normal anatomy of the MCPJ/MTPJ using 7T MRI and thus aid recognition and evaluation of fetlock pathology.

2.2. Aims And Objectives

The aim of this study was to describe the appearance of the normal equine MCPJ/MTPJ region on 1.5T and 7T MR images.

The following specific objectives were set in order to accomplish this aim:

- I. Describe the MRI appearance of the major structures of the equine MCPJ/MTPJ region using T1-weighted 7T MR images to produce anatomical reference images
- II. Compare 1.5T images with 7T images to illustrate the ability of ultra-high field MRI to produce MR images of greater anatomical detail than high-field images
- III. Describe the appearance of the major soft tissues of the MCPJ/MTPJ region, especially the superficial digital flexor tendon, deep digital flexor tendon, distal sesamoidean ligaments and collateral ligaments of the MCPJ/MTPJ

The hypothesis was that the ultra-high field 7T MRI magnet produces images of excellent anatomical detail, which allows identification of the major anatomical structures of the equine fetlock region, and that the MR images are superior to those acquired using a high field 1.5T magnet.

2.3. Materials And Methods

2.3.1. Limbs Collection

Eight limbs were collected from horses aged 7-12 years that had been euthanized for reasons unrelated to this study with no history of distal MCPJ/MTPJ region pain. The limbs were harvested by sectioning proximal and distal to the fetlock joint, thoroughly cleaned and labeled. The shoes were removed. Then, the limbs were frozen directly at -20°C upon collection until the study commenced. All limbs were defrosted for 24 hours at room temperature prior to the MRI study.

2.3.2. MRI Imaging

The limbs were imaged with a system based on a 1.5T magnet (Magnetom 1.5T, Siemens Healthcare GmbH Henkestrasse, Erlangen, Germany) and a 7T magnet (BioSpec, Bruker Corporation 70/30 system Bruker, Germany). T1-weighted images were acquired, followed by T2-weighted images using both systems. Sagittal, dorsal and transverse planes were acquired from using both systems (Table 1.1).

Table 2-1: Image Acquisition Parameters.

Magnet strength	Sequence	TR/TE (ms)	Flip angle	Matrix	Resolution	Slice thickness	Scan time
7T	T1	3.5/100	30	262x280	250x250	3.5mm	1hour 47min
	T2	6424/56	30	280x280	250x250	3.5mm	1 hour 14 min
1.5T	T1	11/600	130	384x384	250x250	2.2mm	11 mins 3 sec
	T2	113/6620	150	320x288	250x250	2.2mm	10 min 31 sec

2.3.3. Data Analysis

MRI data sets were downloaded from the MRI systems using the associated workstations and software (Bruker ParaVision 5.0 software; Siemens Syngo MR B13 software) in DICOM file format and then transferred to a MacBook Pro computer with a screen resolution of 2880 X 1800 resolution using a flash drive. OsiriX imaging software (Pixmeo SARL, 266 Rue de Bernex, CH-1233 Bernex, Switzerland) was used to view and manipulate the MR studies. Several sagittal, transverse, dorsal and oblique views were obtained for this study. As previously described, the ability of an observer to identify anatomical structures was classified as either 'seen' when clearly visible (Dyson et al. 2003), or indistinct where they could not be accurately identified (Smith et al. 2011).

2.4. Results

2.4.1. The Appearance of The Articular Cartilage, Synovial Fluid and Bone In T1-Weighted 7T and 1.5T MR Images of The MCPJ/MTPJ Region

The articular cartilage of the MCPJ/MTPJ was visible as a thin layer of homogeneous high signal intensity on T1-weighted 7T and 1.5T MR images. On 7T images the cartilage surfaces were separated by synovial fluid of intermediate to low signal intensity, whereas on the comparable 1.5T images the synovial fluid had high to intermediate signal intensity (Fig 2.1). As a consequence of the differences in contrast between articular cartilage and synovial fluid on images produced by the ultra-high 7T and high 1.5T field strength MR systems, the articular cartilage surface of distal MCIII/MTIII, proximal P1 and the proximal sesamoid bones was clearly defined on 7T images but indistinct on 1.5T MR images. This was a consistent findings in all five limbs imaged.

The subchondral bone plate on 7T & 1.5T MR images had low signal intensity. It was clearly defined by cartilage (intermediate to low signal intensity) towards the articular surface in dorsal and palmar regions of distal MCPJ/MTPJ. The interface between the subchondral bone plate and the trabecular bone on both MR images was usually smooth. The trabecular bone had high to intermediate signal intensity on 7T MR images with lower signal intensity spots creating a pattern suggesting the architecture

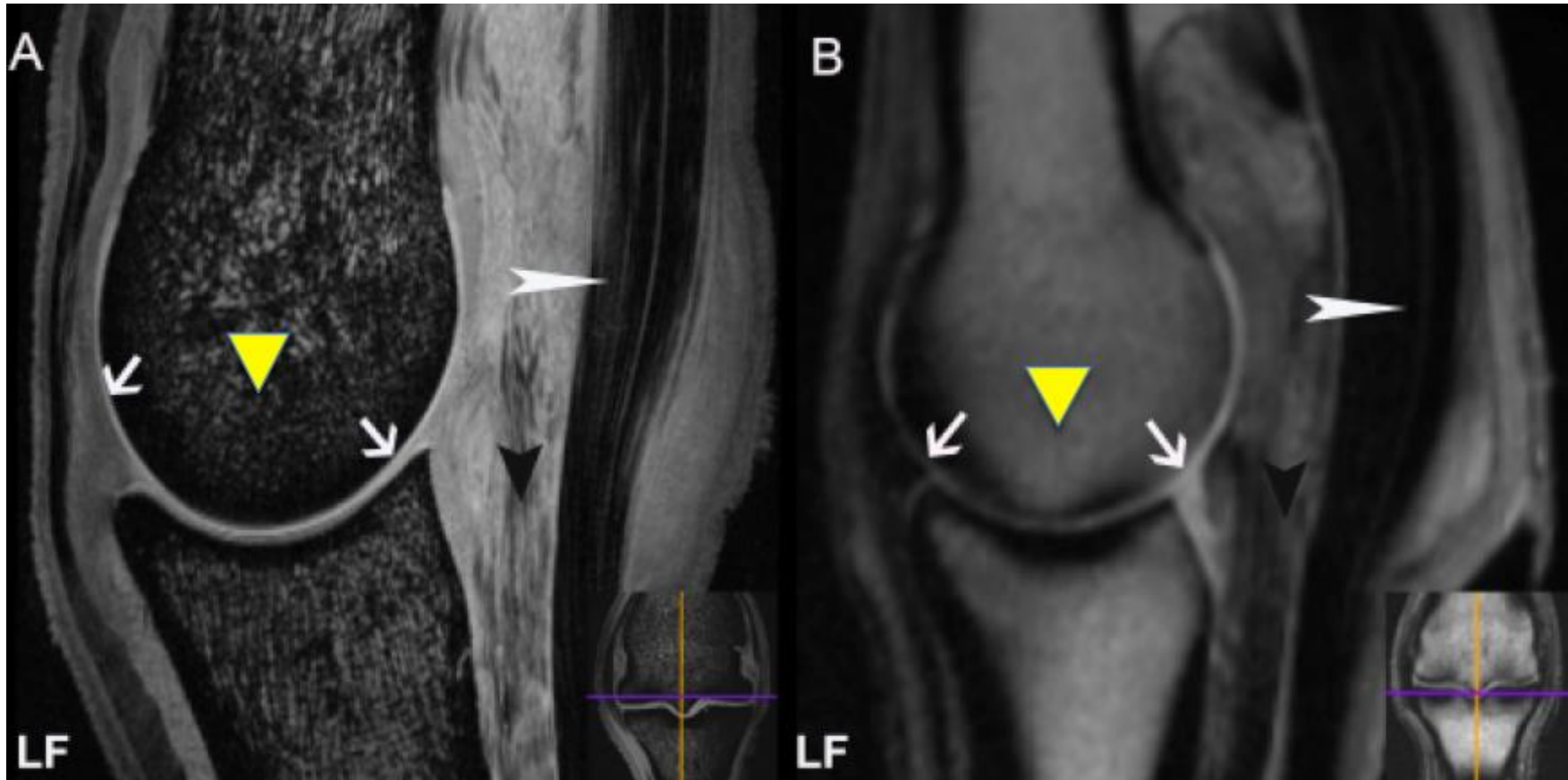
of trabecular bone. However, on 1.5T MR images, the trabecular bone had a more homogeneous intermediate to low signal intensity signal.

On sagittal, parasagittal, and dorsal images through the midpoint of the MCIII/MTIII articulation and transverse images at the level of metacarpo-sesamoidean articulation acquired at either field strength the cortical bone of the distal MCIII/MTIII and P1 had homogeneous low signal intensity. The dorsal and palmar thirds of the condyles at the level of mid sagittal ridge of distal MCPJ/MTPJ had low signal intensity compared with middle third of the metacarpal condyle on (C&D) sagittal images (Fig 2.1).

On the parasagittal MR images, well-defined foci of intermediate to high signal intensity were present within the trabecular bone which represented vascular channels (Fig 2.2). Additionally, on these images there was an increase in the thickness of subchondral bone at the mid point of the distal condyle of distal MCIII/MTIII and the mid point of the lateral and medial aspects of proximal P1 related to adaptation to the pattern of exercise induced loading. The trabecular bone was relatively high signal intensity when compared with cortical bone (Fig 2.2).

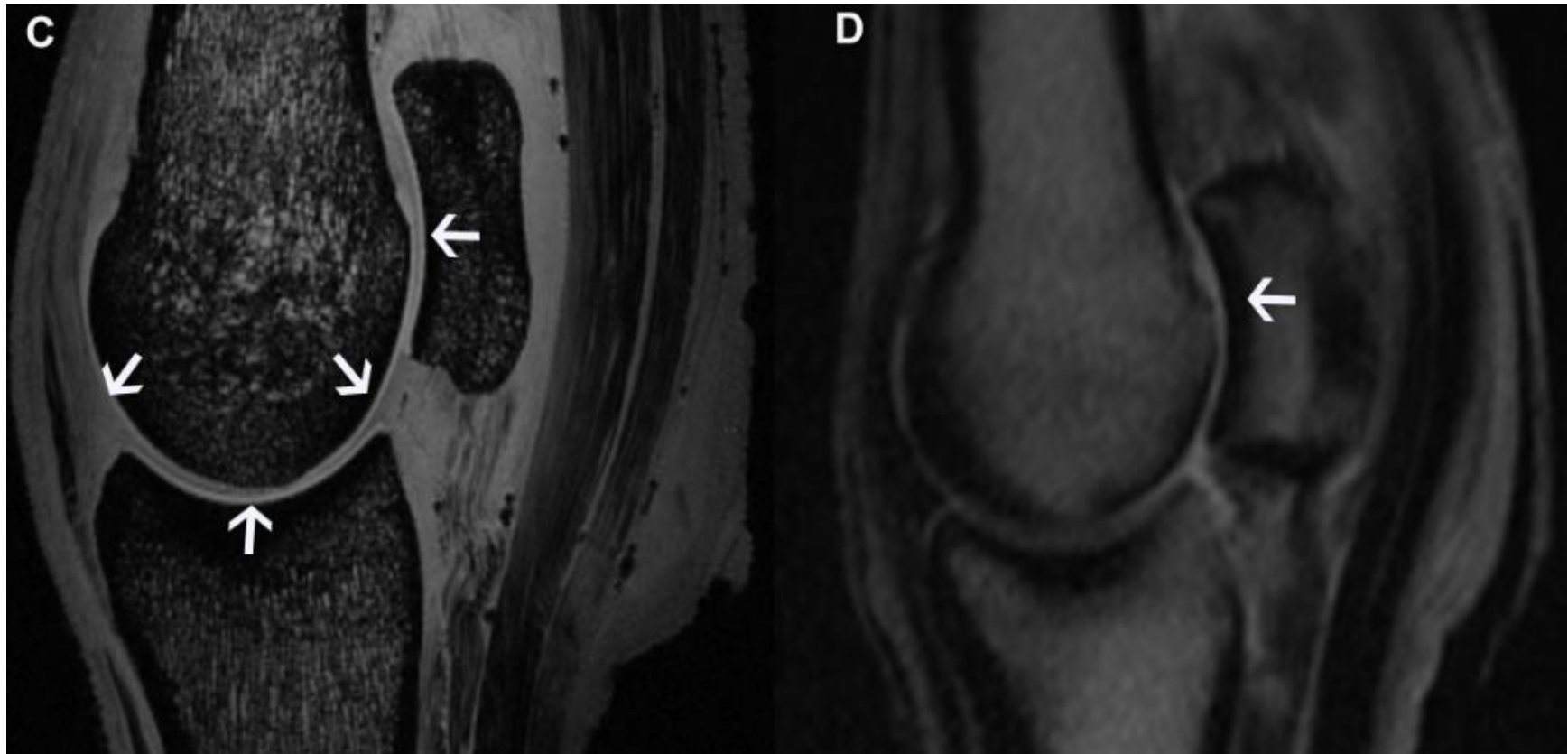
The periosteal and endosteal surface of the MCIII/MTIII and P1 at the level of the attachment of the lateral and medial collateral ligaments of the P1 and MCPJ/MTPJ were smooth, and both lateral and medial sides of superficial and deep collateral ligaments were more clearly defined on T1 7T MR images compared with 1.5T T1 MR images at the similar anatomical position. However on 1.5T sagittal MRI plane at the level of metacarpo-sesamoidean articulation the collateral ligaments were indistinct (Fig 2.5).

The proximal sesamoid bones had low to intermediate signal intensity on sagittal, parasagittal and transverse 7T MR images but a lower intensity on the equivalent 1.5T images. The articular cartilage of the proximal sesamoid bones was clearly visible as homogeneous high to intermediate signal intensity in sagittal and parasagittal 7T images, this was due to the hyper-intense signal of the synovial fluid and the intermediate to low signal intensity of the subchondral bone (Fig 2.2) (C&D). Whereas on 1.5T MR images it was difficult to differentiate between the cartilage of the proximal sesamoid bone and each MCIII/MTIII bones.



See figure 2-1

Figure 2-1: Sagittal plane 7T (A, C) & 1.5T (B, D) T1-weighted MR images of the metacarpophalangeal region. A & B are from the mid-sagittal plane (through the sagittal ridge of distal MCIII) and C & D from an abaxial parasagittal plane including a proximal sesamoid bone. Articular cartilage has an intermediate signal intensity in images acquired at either field strength (thin white arrows) but a thin zone of reduced intensity delineates the articular surface of distal MCIII from that of P1 in the 7T images only (white arrow). This zone represents synovial fluid. The articular cartilage of the proximal sesamoid bone is clearly visible in 7T images (C, white arrow), whereas in 1.5T images it is poorly visualized (D). The subchondral bone of the dorsal distal aspect of the condyles of MCIII is thicker than at the mid and palmar aspects (C & D) The trabecular bone of distal MCIII and proximal P1 produces a punctate pattern of mixed signal intensity due to low intensity trabecular bone interspersed by high intensity bone marrow; the trabecular bone structure is only resolved in 7T images (A & B, yellow arrow heads). Linear intermediate signal intensity is visible within dorsal DDFT in the 7T image through the sagittal ridge of MCIII (A, white arrowhead) but this cannot be identified in the other images. The feature is due to structural change in the DDFT tendon in this location as a consequence of compressive forces. The straight sesamoidean ligament has low to intermediate signal intensity in images acquired at either field strength, however, the striated pattern created by the fascicular structure is only clearly visible in 7T images (A, black arrowhead).



See figure 2-2

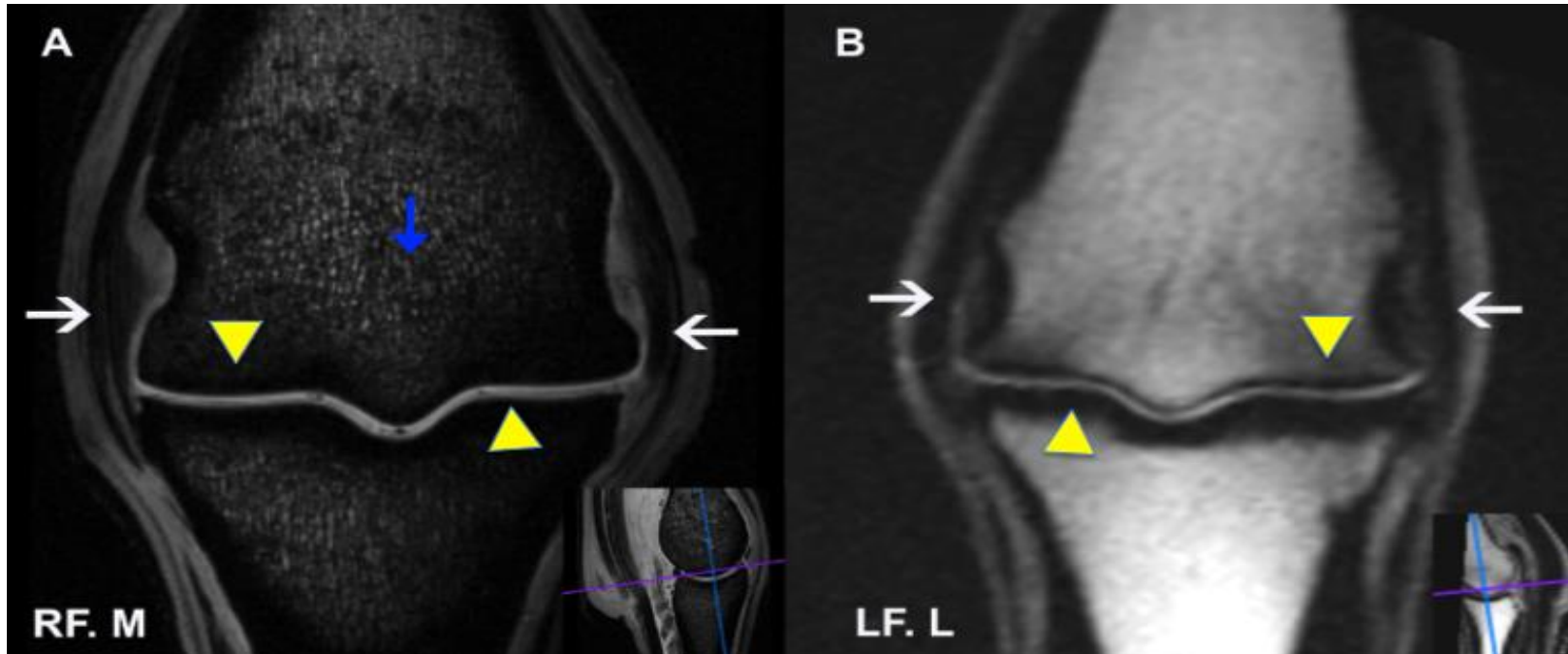
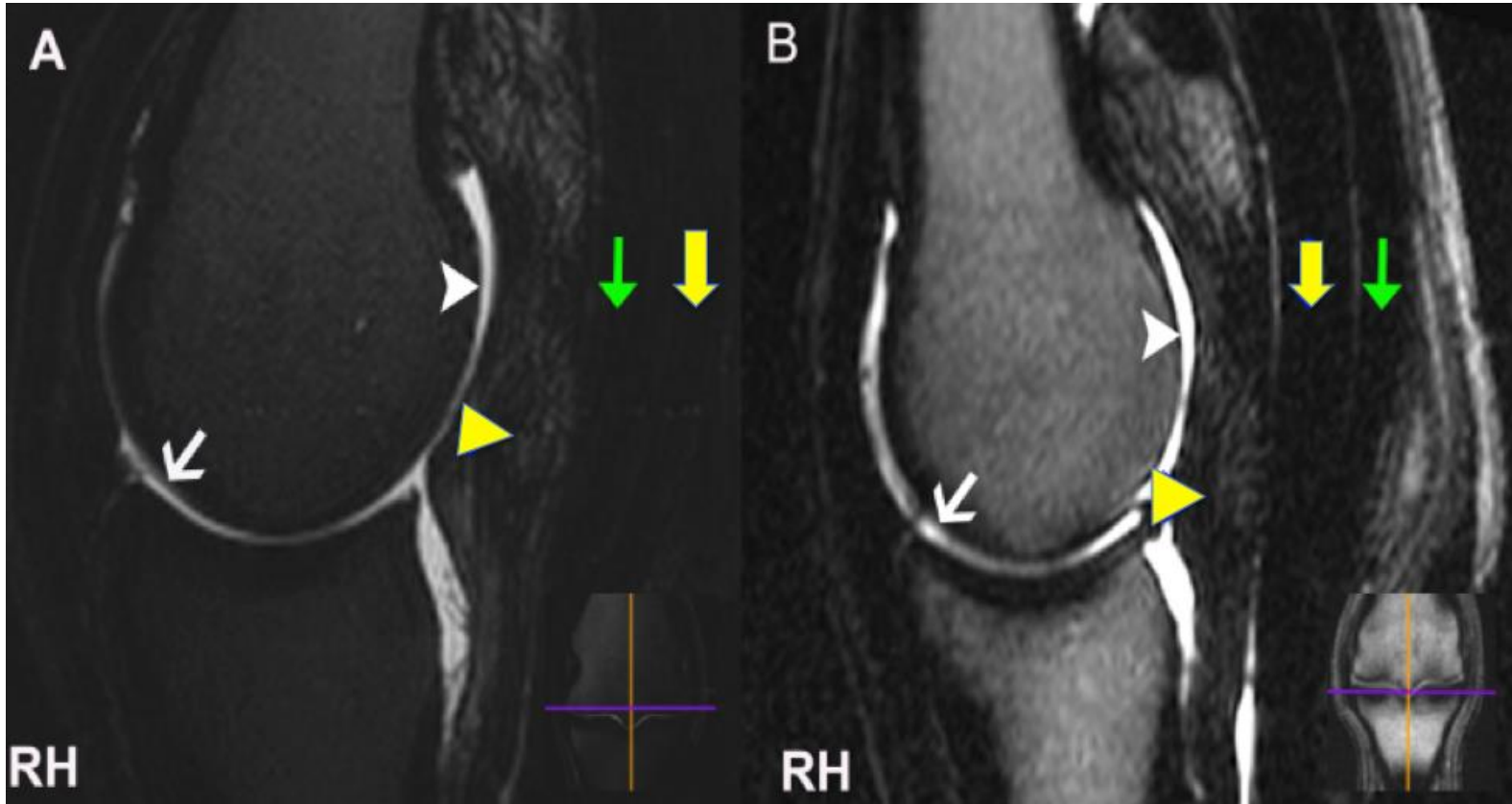


Figure 2-2: Dorsal plane 7T (A) and 1.5T (B) T1-weighted MR images of the metacarpophalangeal region. Images obtained from a dorsal plane through the midpoint of the metacarpophalangeal articulation and were matched as closely as possible but differences remain due to limb positioning and slice thickness. There is an increase in the thickness of the subchondral bone of the distal condyles of MCIII and proximal P1 midway between sagittal ridge/ sagittal groove and the abaxial margin (A & B, yellow arrowhead) in comparison to the remaining condyle. This feature reflects bone adaptation to exercise. The trabecular bone of distal MCIII and proximal P1 produces a punctate pattern of mixed signal intensity due to low intensity trabecular bone interspersed by high intensity bone marrow; the trabecular bone structure is only resolved in the 7T images (A). The periosteal and endosteal surfaces at the site of attachment of lateral and medial collateral ligaments of the metacarpophalangeal articulation to distal MCIII are smooth; the collateral ligaments are only clearly defined in 7T images compared to 1.5T images (A & B, white arrow).

2.4.2. The appearance of the articular cartilage, synovial fluid and bone in T2-weighted 7T and 1.5T MR images of the metacarpo/metatarsophalangeal region

The trabecular bone on T2-weighted 7T & 1.5T MR images was heterogeneous low signal intensity, which is characteristic of mineralized tissue. On 7T images, the trabeculae were best appreciated in the mid-sagittal plane at the level of the sagittal ridge of distal MCIII, parasagittal plane through a proximal sesamoid bone and transverse plane through the metacarpo-sesamoidean articulation. The cortical bone had homogeneous low signal intensity signals in 7T MR images compared with intermediate to high signal intensity signal on 1.5T MR images. The articular cartilage and synovial fluid of the MCIII/MTIII joint had high signal intensity and in the case of the synovial fluid, this outlined the normal limits of the MCIII/MTIII joint capsule (A, B, C & D) (Fig 2.3). There was decrease in signal intensity in the palmar and abaxial aspects of the proximal sesamoid bones reflecting increased mineralization in these two regions of cortical bone compared with the trabecular bone present centrally (Fig 2.3, C & D).

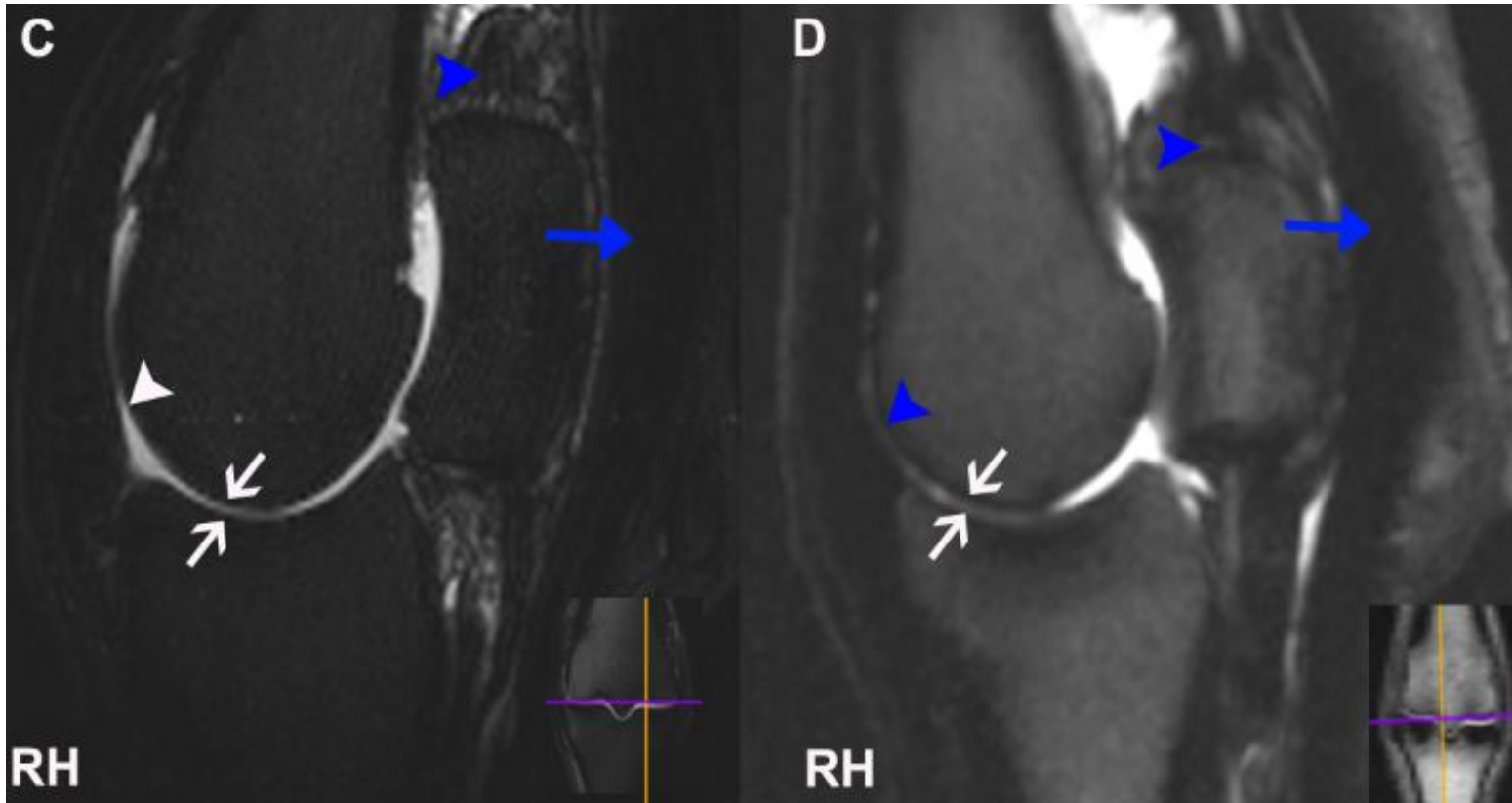
On both 7T and 1.5T images the articular cartilage of MCIII/MTIII, P1, both proximal sesamoid bones and synovial fluid had high signal intensity. The articular cartilage of proximal P1 and distal MCIII/MTIII could be distinguished in 7T images, whereas in the 1.5T images no interface could be identified between these layers at the distal aspect of the sesamoid bones because the intensity of cartilage and synovial fluid was too similar at this field strength to produce any contrast (Fig 2.3). However, the cartilage of the dorsal aspect of MCIII/MTIII and the dorsal aspect of the proximal sesamoid bones was visible (Fig 2.3, C&D).



See figure 2-3.

Figure 2-3 Sagittal plane 7T (A, C) & 1.5T (B, D) T2-weighted MR images of the metatarsophalangeal joint. A & B were obtained in the mid-sagittal plane (through the sagittal ridge of distal MTIII); C & D in a parasagittal plane through a proximal sesamoid bone. The increased signal intensity of the synovial fluid compared to the surrounding tissues outlines the limits of the joint cavity, which extends further proximally in the parasagittal plane than the mid-sagittal plane. In the 7T images articular cartilage of distal MTIII and P1 is not readily differentiated from synovial fluid due their similar (intermediate) intensity (white arrows facing each other in C & D). The boundary between cartilage and subchondral bone is indistinct in some regions in the 7T images due to the similar signal intensity of the tissues but is not visible in the 1.5T images because of their lower resolution.

The straight distal sesamoidean ligament (yellow arrowhead), deep digital flexor tendon (yellow arrow) and superficial digital flexor tendon (green arrow) are of low signal intensity; this is relatively homogeneous for the flexor tendons but heterogeneous for the straight distal sesamoidean ligament as a result of striations of intermediate signal intensity produced by the fascicular structure.



See figure 2-3.

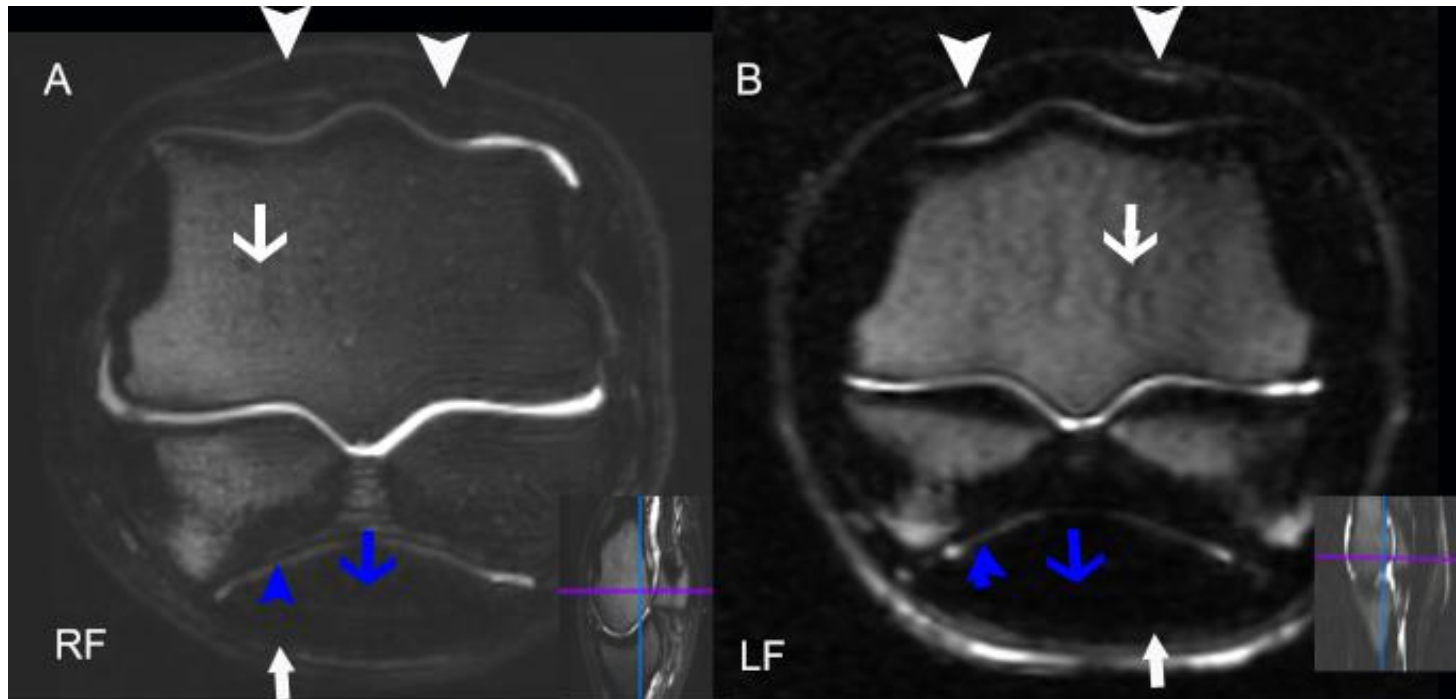


Figure 2-4: Transverse plane 7T (A) & 1.5T (B) T2-weighted MR images of the metacarpo/metatarsophalangeal joint obtained through the metacarpo-sesamoidean articulation. The trabecular bone is of heterogeneous signal intensity as the result of a pattern of high intensity foci and low intensity streaks on an intermediate intensity background (white arrow in A & B). The palmar annular ligament of the fetlock (thick white arrow) and superficial and deep digital flexor tendons (blue arrow) are of low signal intensity and cannot be readily distinguished as separate structures in either image, although the high signal intensity of synovial fluid within the digital flexor tendon sheath delineates the dorsal border of the deep digital flexor tendon. Similarly the dorsal and lateral digital extensor tendons are of low signal intensity and not readily visualized as discrete structures (white arrowhead).

2.4.3. The appearance of the soft tissues in T1- and T2-weighted 7T and 1.5T MR images of the metacarpo/metatarsophalangeal region

The margins of the MCPJ/MTPJ capsule were clearly defined by the contrasting intensity of the adjacent tissues in both T1- and T2-weighted sequences: the intermediate intensity of the fibrous part of the joint capsule was outlined by lower intensity synovial membrane on its luminal aspect in T1-weighted images and by high intensity synovial fluid in T2-weighted images. Synovial plica (folds) of synovial membrane were visualized at the dorsal proximal aspect of the MCPJ/MTPJ as short linear or curvilinear structures of intermediate to high signal intensity in both T1- & T2-weighted sequences, visible against a high intensity background (synovial fluid) in T2 images (Fig 2.6).

The major blood vessels and nerves (palmar and palmar digital vein, artery and nerve) were only clearly visualized in transverse plane images, appearing as small fattened ovoid structures. The blood vessels had intermediate intensity in T1-weighted but high intensity in T2-weighted images. The anatomical detail of the 7T T2-weighted images enabled visualization of a very thin low intensity zone at the outer margin of the blood vessels, which presumably represented the connective tissue of the outer vessel wall (tunica externa). The nerves had low intensity in both image sequences and were difficult to distinguish from the surrounding tissues in all but the 7T T1-weighted images (Fig 2.5).

The collateral ligament of the lateral and medial aspects of the MCPJ/MTPJ had homogeneous low signal intensity. The ligament was most clearly visualized in the transverse plane at the level of the distal portion of the metacarpo-sesamoidean articulation and dorsal plane through the midpoint of the MCPJ/MTPJ articulation, particularly on T1-weighted 7T images. Axially, contrast with synovial fluid enabled the sharp margin of the ligament to be distinguished whereas abaxially the intermediate intensity of the fascia and other subcutaneous connective tissue adjacent to the ligament made the margin less clear (Figs 2.2, 2.5). The superficial longitudinally orientated part of the ligament was thicker than the deep obliquely orientated part. At the insertions of the collateral ligaments, the endosteal and periosteal surfaces of distal MCIII/MTIII and proximal P1 were smooth (Fig 2.2).

The superficial and deep digital flexor tendons had homogeneous low signal intensity on T1-weighted 7T & 1.5T MR images acquired in the mid-sagittal plane at the level of the distal MCPJ/MTPJ and parasagittal plane through a proximal sesamoid bone. The DDFT had smooth well-defined margins with uniform striations of intermediate to low signal intensity in sagittal plane images, running from proximal to distal at the palmar aspect of the MCPJ/MTPJ within the dorsal third of the DDFT where the tendon conformed to the angulation of the MCPJ/MTPJ. These striations, which represented the fascicular structure of the tendon, were more clearly visible on 7T than 1.5T MR images (Fig 2.6). The boundary between the SDFT and DDFT was clearly visible on transverse plane T1-weighted 7T MR images through the metacarpo-sesamoidean articulation, which enabled the crescent-shaped outline of the SDFT and the oval-shaped outline of the DDFT in this region to be seen (Fig 2.6).

The boundary between the tendons was less distinct on transverse plane T2-weighted 7T images and transverse plane 1.5T image of either sequence type, which made assessment of the shape of individual tendons difficult.

The paratenon of the flexor tendons most usually visualized in transverse images, it was more distinct in T1 7T compared with T1 1.5T MRI. The palmar paratenon of the DDFT was considerably thicker compared with dorsal paratenon of the DDFT and the palmar border of the SDFT.

On transverse plane at the level of the distal portion of the metacarpo-sesamoidean articulation the manica flexoria was visible as thin linear structure of homogeneous high to intermediate signal intensity on T1-weighted 7T MR images. On T2-weighted 7T MR images and 1.5T MR images however it was indistinct. The dorsal common and lateral digital extensor tendon were thin structures of homogeneous low signal which were not readily identifiable as discrete structures on the transverse plane T1-weighted MR images obtained at either field strength (Fig 2.3). On T2-weighted 1.5T MR images the palmar/plantar margins of the extensor tendons was highlighted by the high signal intensity signal of the synovial fluid present in the dorsal pouch of the MCPJ/MTPJ (Fig 2.4). The palmar (plantar) annular ligament (of the fetlock) was visible as a thin but distinct low signal intensity structure in both MRI fields (Fig 2.5).

The suspensory ligament branches were mostly well-defined low signal intensity structures. On the sagittal 7T and 1.5T MR images, at the palmar aspect of the suspensory ligament branches at the level of MCPJ/MTPJ. They had a diffuse region of intermediate to high signal intensity, which extended distally to the level of the proximal sesamoid bones, which likely to be due to a combination of the ligament fibre divergence as each branch attaches onto the proximal aspect of the sesamoid bone as well as due to volume averaging. The extensor branches of the suspensory ligament had low signal intensity, and were visible as thin structures in both 1.5T and 7T MR images (Fig 2.5 C&D). Moreover, the lateral and medial branches on the parasagittal plane through a proximal sesamoid bone at the level of their distal insertion they had heterogeneous high signal intensity signals (Fig C&D 2.3).

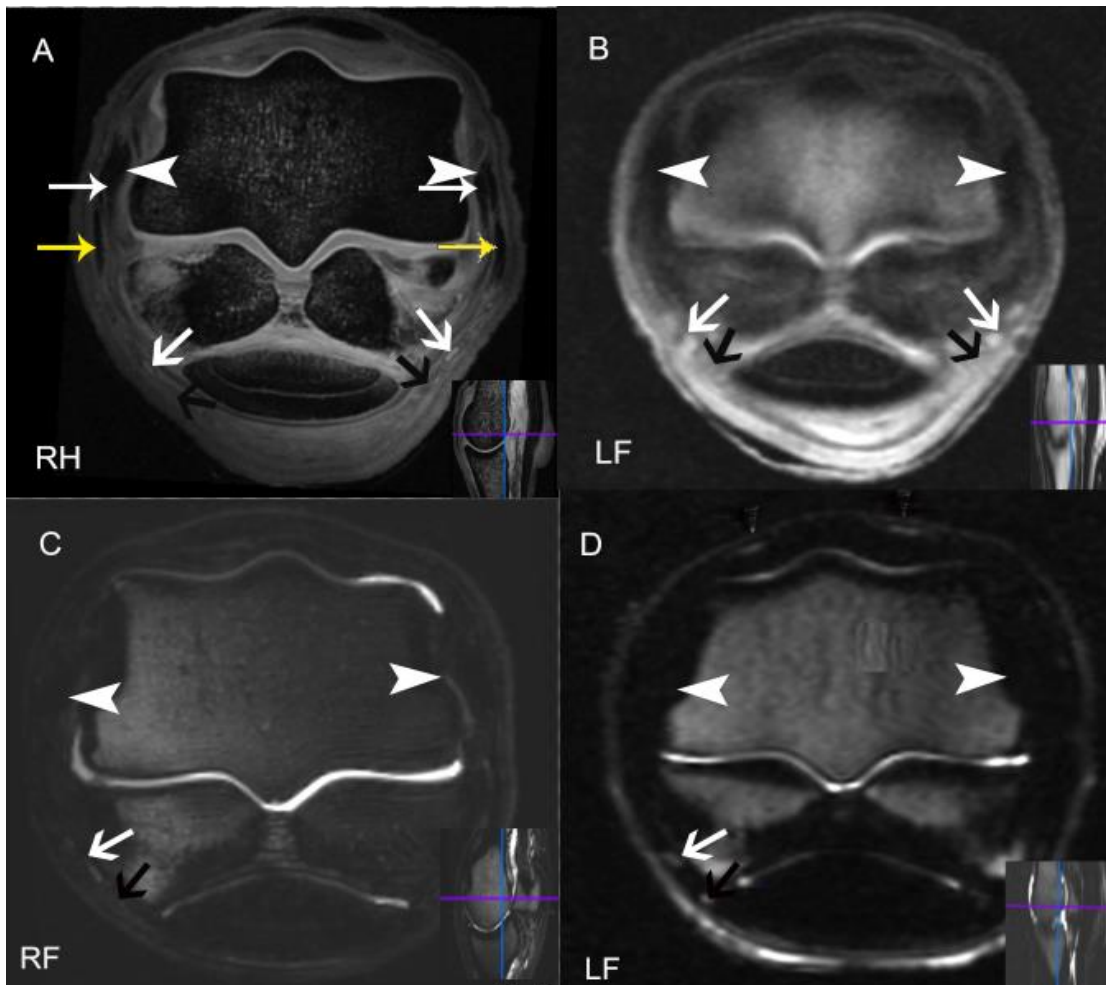
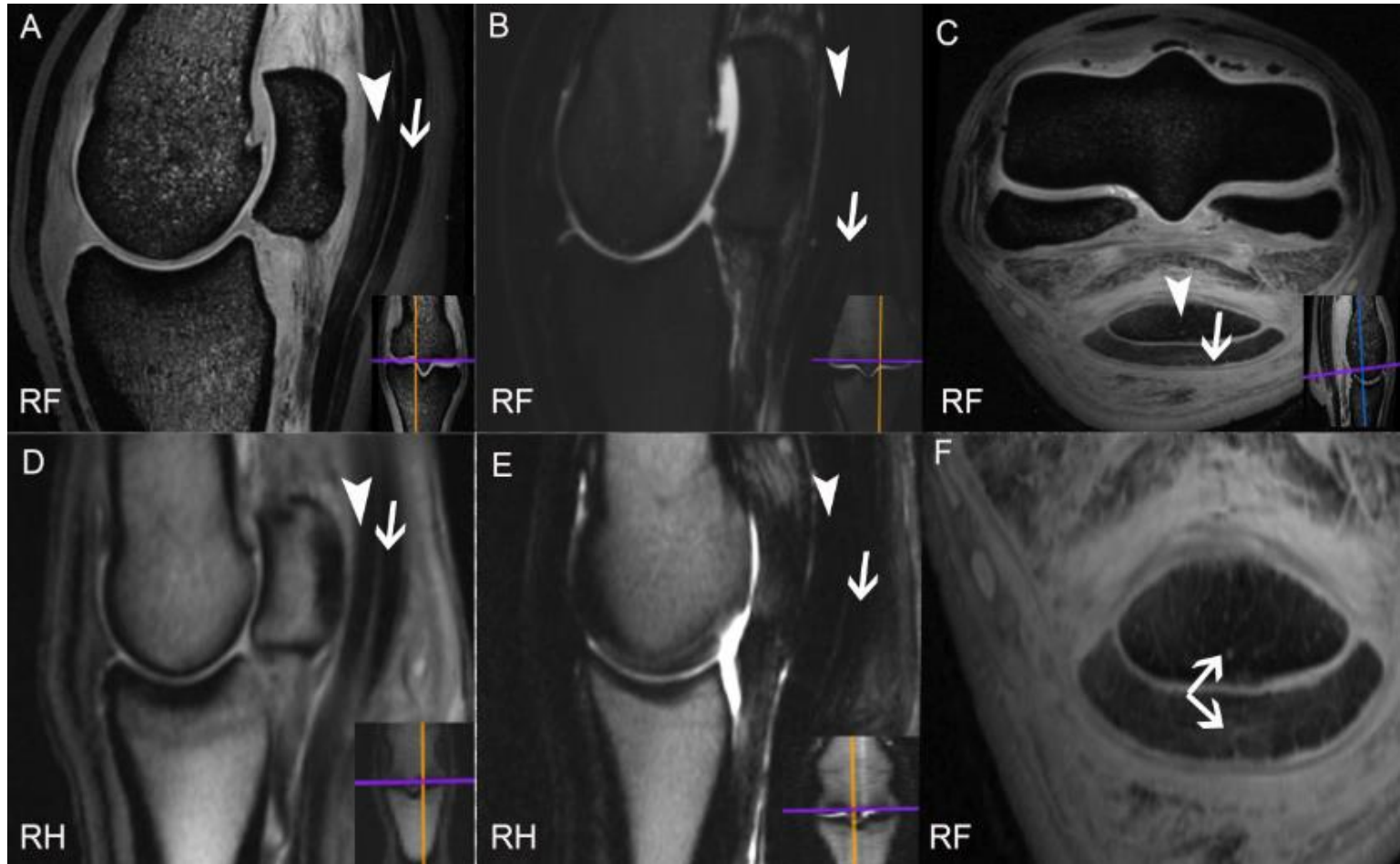


Figure 2-5: Transverse plane 7T (A & B) & 1.5T (C & D) MR images of the metacarpophalangeal joint obtained through the distal portion of the metacarposesamoidean articulation. A & C are T1-weighted, B & D T2-weighted images. The superficial collateral ligaments (thin yellow arrows) and deep (thin white arrows) of the metacarpophalangeal joint are of low signal intensity in both MRI sequences (white arrowheads). In the T1-weighted images (A & C) there is sufficient contrast with the surrounding tissues to be able to distinguish the ligaments but it is only in the 7T T1-weighted image (A) that the margins of the ligament can be clearly visualized. The digital vessels (white arrows) and nerves (black arrows) are visualized as intermediate-high signal intensity structures surrounded by a narrow low signal intensity zone, which are most clearly visualized in the 7T T1-weighted image (A).



See figure 2-6.

Figure 2-6: Sagittal plane 7T (A & B) & 1.5T (D & E) MR images of the metacarpophalangeal joint; transverse plane 7T MR image (C) obtained through the distal portion of the metacarpo-sesamoidean articulation. Of the sagittal plane images, A, B & E are parasagittal, including a proximal sesamoid bone, and D is mid-sagittal. A, C & D are T1-weighted, B & E T2-weighted images. The superficial digital flexor tendon (white arrow) and deep digital flexor tendons (white arrowhead) are of low signal intensity and are visible in all images. The boundary between the tendons is indistinct in the T2-weighted images and the striated pattern reflecting the fascicular structure of the tendons can only be seen clearly in the 7T T1-weighted sagittal plane image (A). The pattern is faintly visible in the 1.5T T1-weighted sagittal plane image (D) and not in the T2-weighted images. In the 7T T1-weighted transverse plane image (C&F), the fascicular structure is visualized as a fine speckled pattern (thin white arrows).

2.4.4. Appearance of the distal sesamoidean ligaments in T1-weighted 7T and 1.5T MR images

2.4.4.1. Distal Sesamoidean Ligaments

The cruciate, straight and oblique distal sesamoidean ligaments were better visualised on 7T MR images compared to 1.5T images. The cruciate and short sesamoidean ligaments were more readily distinguished in 7T MR images. In general on sagittal 7T MRI the distal sesamoidean ligaments had homogeneous intermediate to high signal intensity and a coarse striated pattern reflecting their fascicular structure. Whereas on 1.5T MRI the sesamoidean ligaments had homogeneous low signal intensity signals compared with comparable 7T MR images.

2.4.4.2. Cruciate Sesamoidean Ligaments

On transverse 7T MR images the cruciate ligaments had intermediate to high signal intensity in a striated pattern, which was consistent with their fascicular structure. In dorsal plane the distal portions of the cruciate sesamoidean ligaments were visualized but their orientation took them dorsal when they run distally (Fig 2.7 A, B & C).

2.4.4.3. Oblique Sesamoidean Ligaments

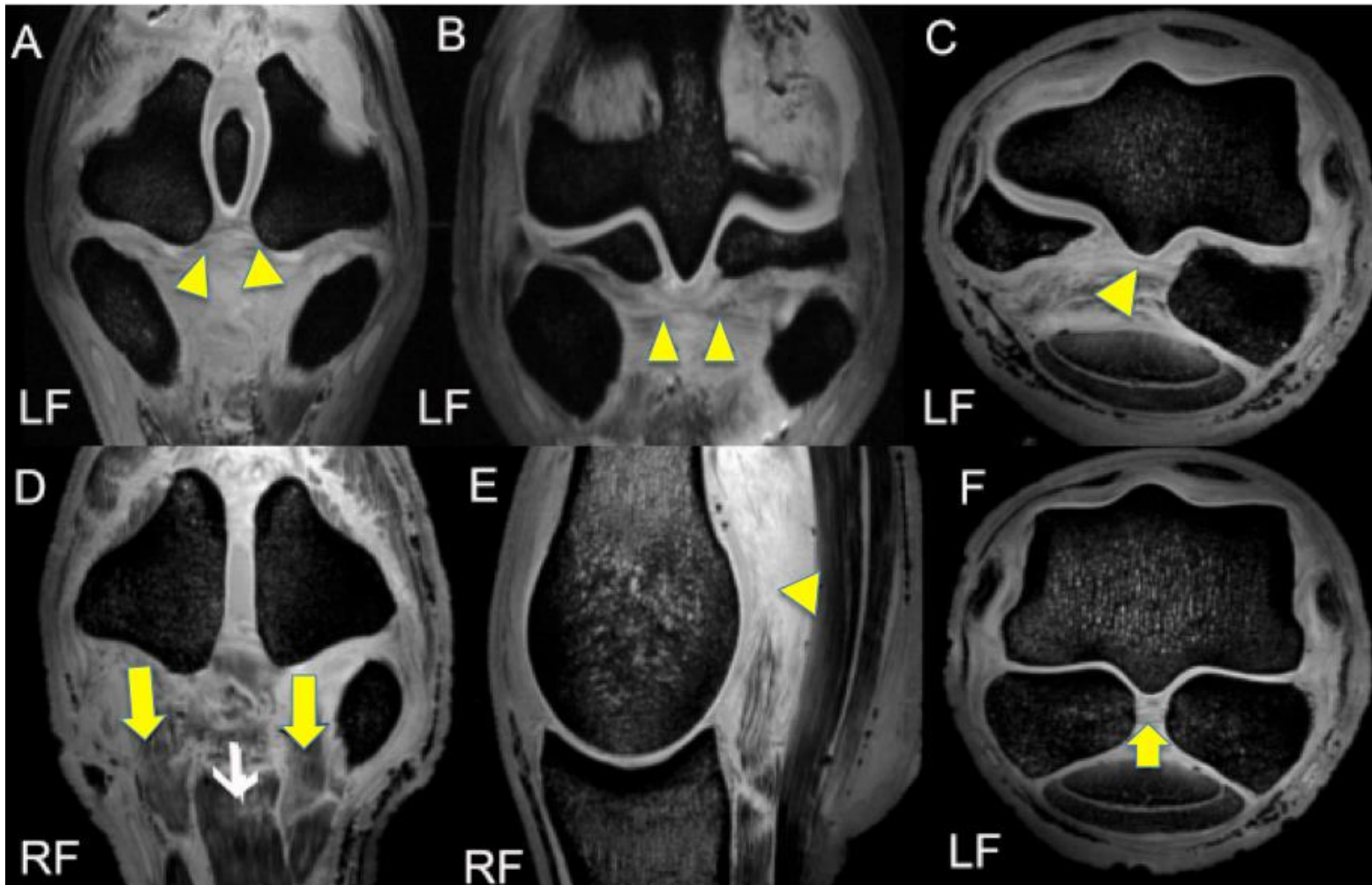
The oblique sesamoidean ligaments originated proximally from the dorsal abaxial portion of the distal margin of the proximal sesamoid bones. In transverse, sagittal and dorsal MRI planes they had high to intermediate signal intensity, with a heterogeneous pattern because of the striations resulting from their fascicular structure, which was most distinct towards their attachment with proximal sesamoid bone. Dorsal plane images clearly showed the cross-shape configuration of the ligament. The individual ligaments were triangular in appearance with sharp margins towards the abaxial aspects of the limb. The oblique ligaments were seen in transverse plane images with high to intermediate signal intensity signals due to the fat closely associated with the ligaments' margins. On sagittal views the oblique sesamoidean ligaments had a number of fine lines within the ligaments of high signal intensity (Fig 2.7), (D). However, the oblique ligaments were indistinct on in 1.5T images.

2.4.4.4. Straight Sesamoidean Ligaments

The straight sesamoidean ligament was clearly seen on dorsal views through the dorsal portion of proximal sesamoid bone, sagittal views which had homogeneous high to intermediate signal intensity compared with the oblique sesamoidean ligaments that had heterogeneous intermediate to low signal intensity. Both sets of ligaments were clearly seen on dorsal plane images, which showed the anatomical relationship of axial straight ligament and the adjacent abaxial oblique sesamoidean ligaments and the differing fiber direction of the ligaments. On the transverse plane images the straight sesamoidean ligament was oval in outline (Fig 2.5, 2.7).

2.4.4.5. Intersesamoidean ligament

The main body of the intersesamoidean ligament had a heterogeneous intermediate signal intensity, featuring small focal areas of intermediate to high signal intensity signal on a lower signal intensity background, and with sharp margins on transverse plane T1-weighted 7T and 1.5T MR images. Whereas, at their proximal sesamoid bone insertions the intensity was lower (low to intermediate signal intensity signal) (Fig 2.7), (E&F).



See figure 2-7.

Figure 2-7: 7T T1-weighted MR images of the metacarpophalangeal region obtained in the dorsal (A, B & D), sagittal (E), transverse oblique (C) and transverse (F) planes. A & D are through the dorsal portion of the proximal sesamoid bones, B through the palmar portion of the metacarpophalangeal articulation, E is mid-sagittal, C & F transverse through the distal portion of the metacarposesamoidean articulation, although slight distolateral to proximomedial obliquity has been used in C to highlight the intersesamoidean ligament. The cruciate, oblique and straight distal sesamoidean and the intersesamoidean ligaments are highlighted in the images. The ligaments are of intermediate to high signal intensity and have a coarse striated pattern reflecting their fascicular structure. The proximal portions of the cruciate distal sesamoidean ligaments are visualized in A (yellow arrowhead) but their orientation takes them dorsal to the image slice distally (so that they are overlaid by the oblique distal sesamoidean ligaments); in B the more dorsal image plane allows the entire ligament to be visualized (yellow arrowheads), clearly showing the cross-shaped configuration of the ligament. The oblique and straight distal sesamoidean ligaments are visualized in D (yellow arrows and white arrow respectively), which show the anatomical arrangement of axial straight ligament and adjacent, abaxial, oblique ligaments and the differing fibre directions of the ligaments. The signal intensity of the straight distal sesamoidean ligament is greater than the oblique (high compared to intermediate). The intersesamoidean ligament is highlighted in E (yellow arrowhead) and F (yellow arrow) but is more distinct in F where the image plane is parallel to the fibre direction.

Table 2-2: Comparison of anatomical structures in 7T&1.5T MR images. Structures were classified as ‘seen’ or ‘indistinct’ as previously described (Dyson et al. 2003; Smith et al. 2011).

Bone structure	7T MRI	1.5T MRI
Bone	Seen	Seen
SDDT	Seen	Seen
DDFT	Seen	Seen
Distinguish articular cartilage surface	Seen	Indistinct
Cartilage	Seen	Seen
Fascicular structure of the DDFT	Seen	Indistinct
Cruciate sesamoidean ligaments	Seen	Indistinct
Straight sesamoidean ligaments	Seen	Indistinct
Collateral ligaments boundary	Seen	Indistinct
Manica flexoria	Seen	Indistinct

2.5. Discussion

There is no publication which describes the MR appearance of the complex anatomical structures of the equine metacarpo/metatarsophalangeal joint based on images obtained with an ultra-high MR system and therefore no direct comparison with the work of others is possible. However, there is an animal study, which reported an alternative method to histopathology in the evaluation of early onset of osteoarthritic changes in canine articular cartilage (Pepin et al. 2009). Furthermore, another study showed the benefit of the cartilage imaging of the human knee joint using 7T MR images (Krug et al. 2007) and another human study has shown the possible superiority of 7T MR images of the knee joint compared to 3T MR images (Welsch et al. 2012).

The normal anatomy of the equine MCPJ/MTPJ region has been described from both 7T and 1.5T MR images. The results indicated that most of the structures seen on the 7T MR images could be also seen on 1.5T MR images but with lower resolution and more indistinct margins. On T1-weighted MR images acquired from the 7T MRI system however, the anatomical structures were clearly seen in all planes, which was not always the case with 1.5T images, and in superior anatomical detail. The margins of the smaller structures were very sharp on 7T MR images, whereas they were indistinct or difficult to appreciate on 1.5T MR images. These findings were consistent with the hypothesis that the 7T MRI magnet provides excellent anatomical details and allows identification of the major anatomical structures of the equine MCPJ/MTPJ, and that 7T MR images are superior to 1.5T images.

On 7T MR images the majority of bony and soft tissues were of lower intensity than on comparative 1.5T images due to the relatively low abundance of protons on T1-weighted sequences as well as a very short T2-weighted time compared lower field strength units (Regatte & Schweitzer 2007; Krug et al. 2011).

The separate cartilage layers at the surface of the articular cartilage can be clearly seen on 7T MR images and this could be due to the low slice thickness, which increased the resolution of the images in comparison to the higher slice thickness 1.5T MR images.

The greater image resolution and higher signal to noise ratio of 7T MR images can enable better interpretation and detection of morphological changes (Krug et al. 2007; Regatte & Schweitzer 2007). That is to say 7T MRI has more anatomical information that could be used in the equine clinical practice as a reference guide for veterinary clinicians as they interpret MRI acquired from their clinical magnet system.

The cruciate distal sesamoidean ligaments have not been described in previous studies. A study concluded that cruciate sesamoidean ligament were indistinct in 30% of limbs in low-field MR images (Smith et al. 2011). However, this study described the appearance of the ligament with the potential to see the cross like appearance in the dorsal plane T1-weighted 7T MR images. This study found that it is possible to appreciate the ligaments in 1.5T, but 7T MRI can distinguish them clearly. Therefore,

the anatomical information learned from 7T MRI could assist the observer in gaining more information from the 1.5T images.

The bundles or fascicles of the superficial and deep digital flexor tendons were clearly appreciated in 7T MR images, but were indistinct in 1.5T MR images. The margins of both superficial and deep digital flexor tendons were clearly seen in 7T MRI images within the manica flexoria, but were indistinct on 1.5T MR images. The insertion of the suspensory ligaments branches into the proximal sesamoidean bone was clearly appreciated in 7T MR images. Moreover, manica flexoria was clearly seen in 7T MR images with distinct smooth borders, which could be due to the smaller slice thickness and greater resolution giving better visualization of such a small structure compared with 1.5T images (Werpy 2007).

It has been suggested that understanding the normal anatomic appearance of a specific anatomic region of the body is crucial to accurate diagnostic interpretation of MR images. Inhomogeneity in the 7T MRI appearance of a number of soft tissue structures was identified in this study.

For instance, in 7T MRI there was linear intermediate signal intensity in the dorsal third of the deep digital flexor tendon in the MCPJ/MTPJ region in all the limbs due to local compressive changes in the DDFT tendon. This feature is constant when the tendon is not under tension and thus was seen in specimens used in this study. This appearance can be seen in sagittal and transverse views at the level of mid sagittal ridge on 7T due to the structural changes in the tendon resulting from compression against the proximal scutum of the intersesamoidean ligament (Smith et al. 2011).

The relaxation times as well as imaging parameters of 7T MR images are believed to be the major determinants of contrast between cartilage and other surrounding tissues such as lipids, muscles, and menisci (Regatte & Schweitzer 2007). Several research centres are currently using ultra-high magnets ranging from 7T to 12T; these magnets can provide high resolution MRI images that characterize the articular cartilage layers and provide detailed imaging of the tissue samples (Werpy 2007).

Motion artefacts were not seen in this study due to scanning cadaver equine limbs. Inevitably, cadaver MR images are superior to those acquired from living horses imaged without anaesthesia.

2.6. Conclusion

To conclude, the normal MRI appearance of the major structures of the equine MCPJ/MTPJ region have been described using T1-weighted 7T MR images and anatomical reference images were produced. Most of the anatomical structures of the equine MCPJ/MTPJ were clearly seen in ultra-high MRI with clear margins. Moreover, this study compared T1 and T2-weighted 7T MRI images of the equine MCPJ/MTPJ region with 1.5T MRI images, and found that 7T MRI was able to produce MR images of greater anatomical detail than lower-field images. Moreover, the margins of the smaller structures were very sharp on 7T MR images, whereas they were indistinct or difficult to appreciate on 1.5T MR images, due to the influence of the field strength of the magnet, relaxation times, as well as the imaging parameters of the 7T MR images. Finally, the results obtained with 7T MRI allow the production of high quality “gold standard” images of the equine fetlock that are sufficiently detailed for use as reference images to aid interpretation of images produced by lower field strength, clinical MRI systems. 7T MRI, although not available for clinical cases, could therefore help indirectly to provide more accurate diagnoses and a better outcome for horses.

Chapter 3 Accuracy and Precision of Articular Cartilage Thickness Measurement Using Ultra-High 7T and 1.5T High-Field Magnetic Resonance Imaging (MRI)

3.1. Introduction

Osteoarthritis is one of the most common joint disorders that occurs in equines and may lead to disability and economic loss (McIlwraith 1982). It is considered to be one of the most chronic diseases, causing degeneration of the cartilage resulting in pain and lameness of the affected horse (Kidd et al. 2001). The MCPJ/MTPJ joint of horse is most frequently affected by degenerative changes, such as osteoarthritis lesions (McIlwraith 1982). Cartilage loss (thinning) is a characteristic feature of OA (Jaremko et al. 2007). Therefore, assessment of the articular cartilage thickness is very crucial for diagnosing and assessing the progression of the osteoarthritis (Wang et al. 1990).

Magnetic resonance imaging (MRI) has been used to investigate cartilage thickness in the human and equine. For instance, it has been used to assess the third carpal bone articular cartilage of the equine providing useful information on the cartilage due to its ability to produce high resolution images (Murray et al. 2005). However, MRI assessment of the equine MCPJ/MTPJ cartilage is likely to be more difficult because the thickness of the cartilage is approximately 2 mm, which is relatively thin, and the lateral and medial condyle surfaces are lightly curved (Recht et al. 2005; Olive et al. 2010).

1.5T MRI magnets have been in use for diagnostic purposes in equine practices for a number of years (Bolen et al. 2010; Carstens et al. 2013). Recently, higher field strength magnets (3T) have been introduced to a number of equine practices such as in the University of Zurich and Ohio State University equine centres (Gutiérrez-Crespo et al, 2014; <https://vet.osu.edu/vmc/about-us/news/now-available-site-3-tesla-magnet-mri-large-and-small-animals>).

I proposed to determine the accuracy and precision of cartilage thickness measurements obtained using 1.5T MRI and ultra-high field MRI (7T) by comparing these measurements with histology.

3.2. Aims And Objectives

The hypotheses for this work were that measurements of articular cartilage thickness in the MCPJ/MTPJ of the horse made from MRI compare favourably with measurements made directly from histological sections but that 7T MRI enables more accurate and precise measurement than 1.5T MRI, although measurements made from images at the two field strengths are well correlated.

This study's principal aim was to validate the use of T1 sequence MRI for determining articular cartilage thickness in the MCPJ/MTPJ of the horse, using histological measurements as the gold standard. A further aim was to compare measurements made from high field (1.5T) MR and ultra high (7T) field MR images.

The following objectives were developed in order to achieve these aims:

- I. To measure articular cartilage thickness on the metacarpal/metatarsal condyles, proximal phalanx (P1) and proximal sesamoid bones (PSB) from T1-weighted 1.5T & 7T MR images and directly from histological sections in horses
- II. To evaluate the accuracy of MRI by comparing MRI and histological measurements
- III. To evaluate the precision of MRI by determining the variation between repeated measurements
- IV. To compare measurements made from 1.5T & 7T MR images

3.3. Materials And Methods

3.3.1. Sample Collection

Three cadaver equine limbs were collected from horses aged 7-12 years euthanised for reasons other than this study. The limbs were collected immediately after euthanasia labelled and stored at -20°C until use. A previous study demonstrated that cadaver material can go through two freeze-thaw cycles without affecting image quality (Bolen et al. 2011). Prior to imaging they were thawed at room temperature over a 24h period. After MR imaging the limbs were dissected and osteochondral samples harvested from the metacarpal/metatarsal condyles, proximal P1 and PSBs.

3.3.2. MRI Study

The metacarpophalangeal/metatarsophalangeal regions of the limbs were imaged using 1.5T (Magnetom 1.5T, Siemens Healthcare GmbH Henkestrasse, Erlangen, Germany), and 7.0T MRI systems (Bruker BioSpec70/30 system, Bruker Corporation, Ettlingen, Germany). T1-weighted images were acquired as described in the table below (Table 3.1).

Table 3-1: MR image acquisition parameters.

	T1 1.5T	T1 7T
Image size	320x288	280x270
View size	1337x695	1337x704
Slice thickness (mm)	3	3.56
Slice number	30	280
Echo time (ms)	12	3.5
Planes	Sagittal, transverse & dorsal	Sagittal, transverse & dorsal
Tr time (ms)	550	100
Flip angle (deg)	150	30
Scan time	22 m	1 h, 47 m

3.3.2.1. T1-weighted Image Analysis – Measurement of Cartilage Thickness from MR Images

After image acquisition, DICOM image files were transferred to a MacBook Pro computer with the screen resolution of 2880X1800 and 220 pixels per inch using an ordinary flash drive. Images were viewed and measurements made using a commercially available medical imaging application (OsiriX v.6.5.1 32-bit; Pixmeo SARL, Bernex, Switzerland). In order to consistently identify measurement sites the following protocol was followed:

In sagittal plane images the MCIII/MTIII condyle and proximal P1 were divided into dorsal and palmar halves. Cartilage thickness was measured from the interface between low signal intensity subchondral bone and high signal intensity cartilage, and high signal intensity cartilage and medium signal intensity joint space using the measurement tool (Fig 3.1). Measurements were performed at three sites on both the dorsal and palmar halves of the condyle measurements were repeated in triplicate during a single session.

Each proximal sesamoid bone was divided into proximal and distal halves (Fig 3.1). Cartilage thickness was measured from the interface between low signal intensity subchondral bone and high signal intensity cartilage, and high signal intensity cartilage and medium signal intensity joint space using the measurement tool (Fig 3.1). Measurements were performed at three sites on both the proximal and distal halves and each measurement was repeated in triplicate during a single session.

For each measured site the mean and standard deviation of the triplicate measurements was calculated.

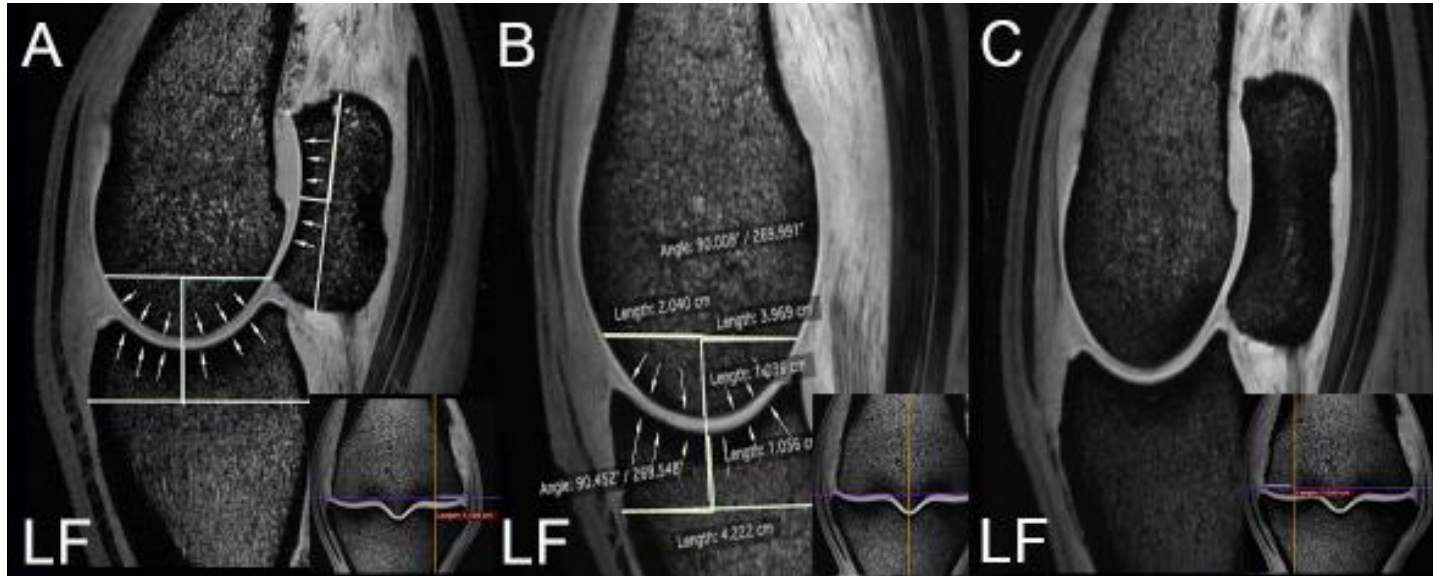


Figure 3-1: Sagittal plane T1-weighted images of left fore metacarpophalangeal joint acquired using the 7T MR system, illustrating the sites at which cartilage thickness was measured. (A) Through the lateral proximal sesamoid bone, (B) through the mid-sagittal ridge and (C) through the medial proximal sesamoid bone. Sagittal plane images were used for all measurements. The MCIII/MTIII condyle and proximal P1 was divided into dorsal and palmar halves. Cartilage thickness was measured from the interface between low signal intensity subchondral bone and high signal intensity cartilage, and high signal intensity cartilage and medium signal intensity joint space using the measurement tool. Measurements were performed at three sites on both the dorsal and palmar halves and each measurement was repeated in triplicate. Each proximal sesamoid bone was divided into proximal and distal halves. Cartilage thickness was measured from the interface between low signal intensity subchondral bone and high signal intensity cartilage, and high signal intensity cartilage and medium signal intensity joint space using the measurement tool. Measurements were performed at three sites on both the proximal and distal halves and each measurement was repeated in triplicate. For each measured site the mean and standard deviation of the triplicate measurements was calculated.

3.3.3. Cartilage Sample Collection And Processing

After MR imaging, the MCPJs/MTPJs were disarticulated and distal MCIII/MTIII, P1 and PSBs dissected free of the major soft tissues. A sagittally orientated 5mm slice of cartilage and subchondral bone was harvested using a handsaw from lateral, mid and medial metacarpal/metatarsal condyle and proximal P1. Similar samples were harvested from the PSBs but this was achieved by dividing the bones transversely into proximal and distal halves. The samples were immediately placed in labelled containers containing 10% buffered formalin and fixed for 24 hours before further processing.

3.3.4. Histology

Subchondral bone was decalcified in formic acid for 2-3 weeks prior to processing in paraffin. 2.5µm thick sections were cut from the embedded samples and stained with Harris haematoxylin and eosin.

3.3.5. Measurement of articular cartilage thickness from histological sections

Sections from the 42 cartilage samples were examined microscopically using an Olympus microscope BX51TF and representative views photographed with a 12.5 megapixel microscope-mounted Olympus DP71 camera (Olympus Corporation, Shinjuku Monolith, 3-1 Nishi-Shinjuku 2-chome, Shinjuku-ku, Tokyo, Japan). The images were downloaded as JPEG files to the same computer system as used for the MRI measurements (MacBook Pro computer with the screen resolution of 2880X1800 resolution and 220 pixels per inch). Measurements were made using the image viewing software Adobe Photoshop CS6 version 13.0.4 (Adobe Systems Incorporated, 345 Park Avenue, San Jose, CA 95110-2704). Briefly, a line was drawn parallel to the cartilage-bone interface to eliminate the effect of irregularity of this boundary on cartilage thickness measurement and three measurements made from the line to the cartilage surface as shown in Figure 3.2. All the measurements were calibrated using the reference scale bar included in each image and the mean of the three measurements used for subsequent statistical analysis.

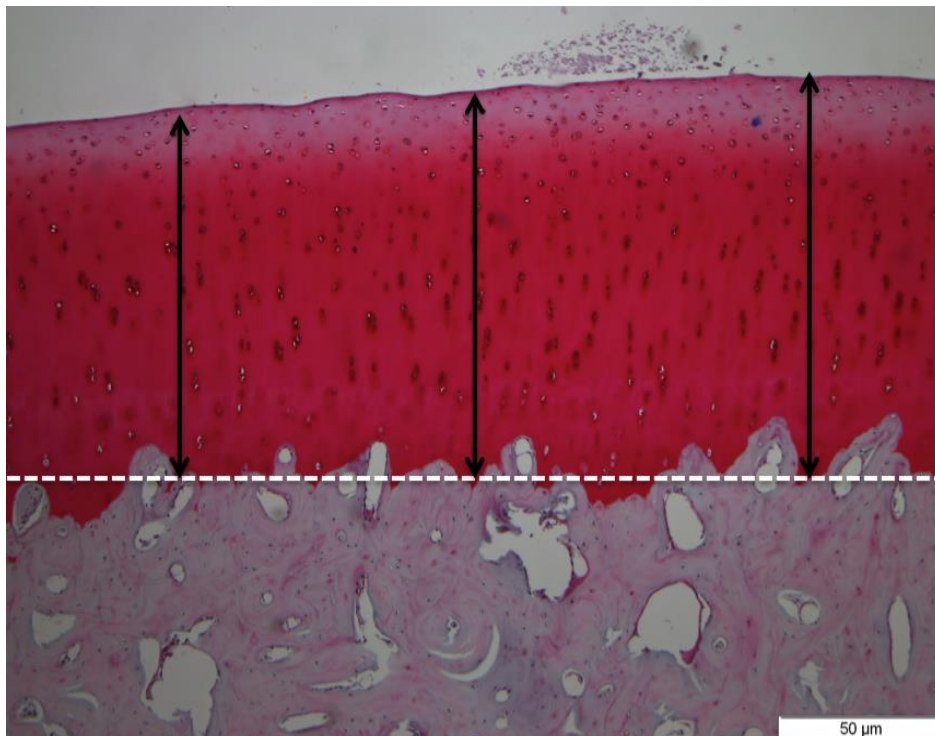


Figure 3-2: Photomicrograph of haematoxylin & eosin section from sample prepared from proximal P1 magnified 100 times. The dashed white line at the cartilage-bone interface was used to eliminate the effect irregularity of this boundary on cartilage thickness measurements. The three black double-headed arrows represent the three measurements of cartilage thickness made for each sample.

3.3.6. Statistical Analysis

Data were analysed using IBM SPSS advanced statistics 20.0 (IBM Corporation Armonk U.S.A) at 95% confidence level. The accuracy and precision calculations were completed using Microsoft Excel 2010 software (Microsoft corporation Redmond U.S.A). All of the MRI and histological measurement data were confirmed to have a normal statistical distribution using the Shapiro-Wilks test prior to further statistical analysis. Students T-test was used to evaluate the effect of cartilage location, e.g. MCIII/MPIII cartilage, P1 cartilage etc and one-way ANOVA test for the difference between all cartilage sites. The correlation between MRI (1.5T and 7T) and histological measurements was determined using Pearson rank correlation (r value) as shown in the scatter plot figures.

Accuracy was defined as the mean difference between the MRI and histology measurements (bias). Accuracy was expressed as a percentage according to the formula:

$$\text{Percentage accuracy} = (\text{Mean Histology} - \text{Mean MRI}) / \text{Mean Histology} * 100.$$

Precision was defined as the variance of the mean difference between the MRI and histology measurement (accuracy) expressed as a percentage.

3.4. Results

3.4.1. MRI And Histological Measurements

3.4.1.1. T1-weighted 7T MRI Measurements

The overall mean \pm standard deviation of the articular cartilage thickness in the MCPJ/MTPJ of the six limbs imaged was 0.783 mm \pm 0.0621 mm. There were however differences in thickness depending on location, specifically in relation to whether the surface was metacarpal/metatarsal condyle, proximal P1 or PSB, and to the site on the surface.

The mean \pm standard deviation thickness of articular cartilage covering the metacarpal/metatarsal condyles based on the measurements made was 0.785 mm \pm 0.055 mm; the equivalent result for proximal P1 was 0.790 mm \pm 0.060 mm, for the lateral PSB was 0.769 mm \pm 0.061 mm and for the medial PSB was 0.768 mm \pm 0.0871 mm (Fig 3.3). There was no significant difference in articular cartilage thickness between sites.

The results of cartilage thickness measurements for each anatomical site are shown graphically in Figure 3.4. There were no significant differences between sites on an anatomical surface but there was a trend for palmar/plantar cartilage to be thicker than dorsal for the metacarpal/metatarsal condyles and proximal P1. For the lateral and medial PSBs, the trend was for proximal cartilage to be thicker than distal.

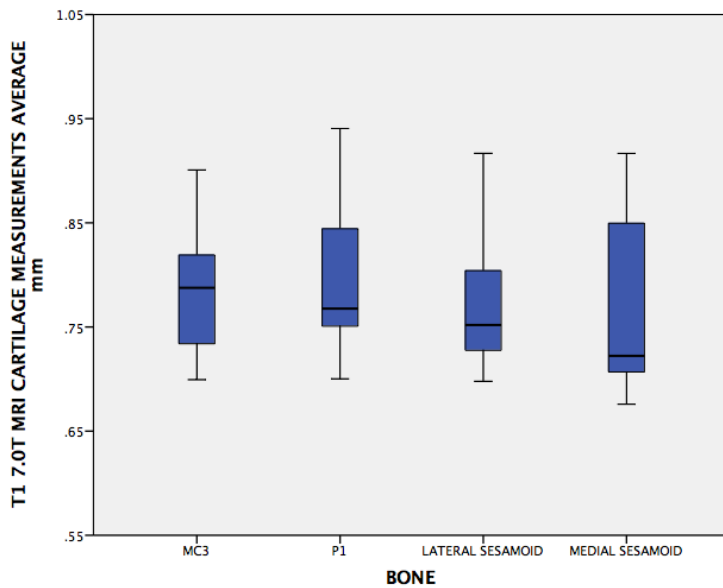


Figure 3-3: Box plot of articular cartilage thickness measurements made from T1-weighted 7T MR images: anatomical location. MC3 = metacarpal/metatarsal condyles; P1 = proximal phalanx; lateral/medial sesamoid = lateral/medial proximal sesamoid bone.

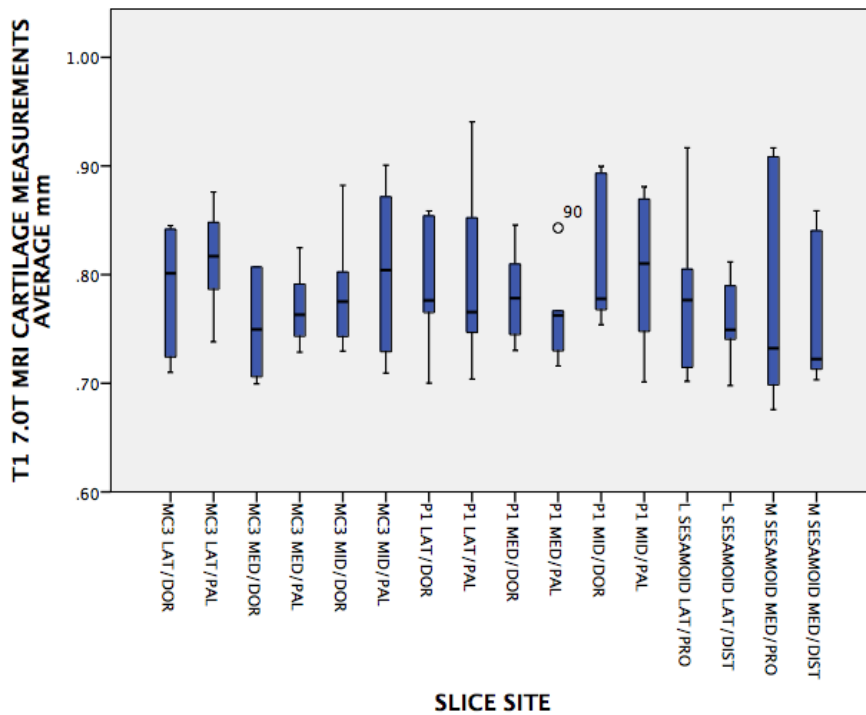


Figure 3-4: Box plot of articular cartilage thickness measurements made from T1-weighted 7T MR images: anatomical location and site. MC3 = metacarpal/metatarsal condyle; P1 = proximal phalanx; sesamoid = proximal sesamoid bone.

3.4.1.2. T1-weighted 1.5T MRI Measurements

The mean \pm standard deviation articular cartilage thickness in the MCPJ/MTPJ of the six limbs imaged was 0.78mm \pm 0.05mm. There were differences in cartilage thickness depending on location, specifically in relation to whether the surface was metacarpal/metatarsal condyle, proximal P1 or PSB, and to the site on the surface.

The mean \pm standard deviation thickness of articular cartilage covering the metacarpal/metatarsal condyles based on the measurements made was 0.799mm \pm 0.05mm; the equivalent result for proximal P1 was 0.786 \pm 0.05mm; for the lateral PSB was 0.792 mm \pm 0.06 and for the medial PSB cartilage thickness was 0.772mm \pm 0.08mm (Fig 3.5). There were no statistically significant differences observed in relation to anatomical surface. The cartilage covering the PSBs was thinner than metacarpal/metatarsal condyles and P1. There were no statistical differences between sites on an anatomical surface. There was a trend for palmar/plantar cartilage sites to be thicker than dorsal for metacarpal/metatarsal condyles and P1. For the lateral and medial PSBs, the trend was for proximal cartilage to be thicker than distal cartilage (Fig 3.6).

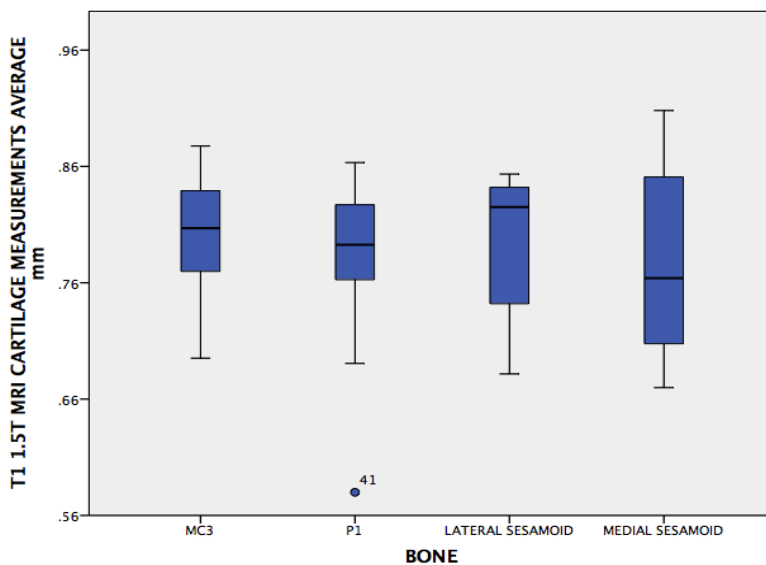


Figure 3-5: Box plot of articular cartilage thickness measurements made from T1-weighted 1.5T MR images: anatomical location. MC3 = metacarpal/metatarsal condyles; P1 = proximal phalanx; lateral/medial sesamoid = lateral/medial proximal sesamoid bone.

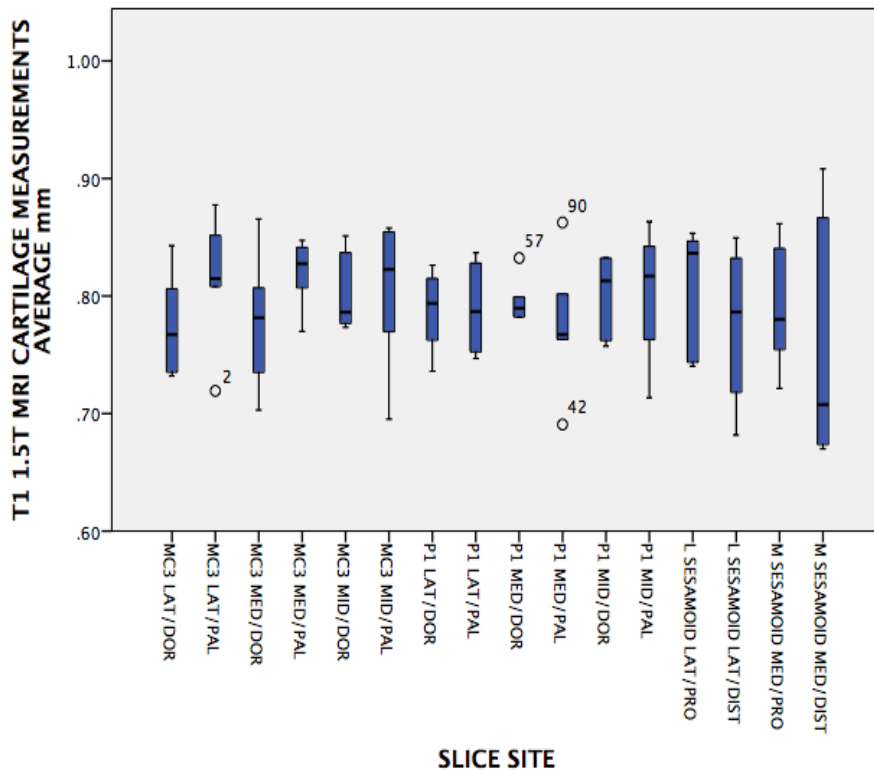


Figure 3-6: Box plot of articular cartilage thickness measurements made from T1-weighted 7T MR images: anatomical location and site. MC3 = metacarpal/metatarsal condyle; P1 = proximal phalanx; sesamoid = proximal sesamoid bone.

3.4.1.3. Histological Measurements

The mean \pm standard deviation articular cartilage thickness in the MCPJ/MTPJ of the six limbs was 0.96 mm \pm 0.11mm. There were no significant differences in cartilage thickness depending on location, specifically in relation to whether the surface was metacarpal/metatarsal condyle, proximal P1 or PSB, and to the site on the surface.

The mean \pm standard deviation thickness of articular cartilage covering the metacarpal/metatarsal condyles based on the measurements made was 0.922 mm \pm 0.10mm; the equivalent result for proximal P1 was 0.99mm \pm 0.10mm, for the lateral PSB was 0.985mm \pm 0.14 mm and for the medial PSB was 0.929 mm \pm 0.11mm (Fig 3.7). There were no significant differences in relation to anatomical surface.

The results for cartilage thickness at the different sampling sites for each anatomical site are shown graphically in Figure 3.8. There were no significant differences in cartilage thickness according to anatomical locations.

There was a trend for the proximal cartilage to be thicker than distal for the lateral and medial PSBs. Whereas, there was no trend found for the metacarpal/metatarsal condyles and P1.

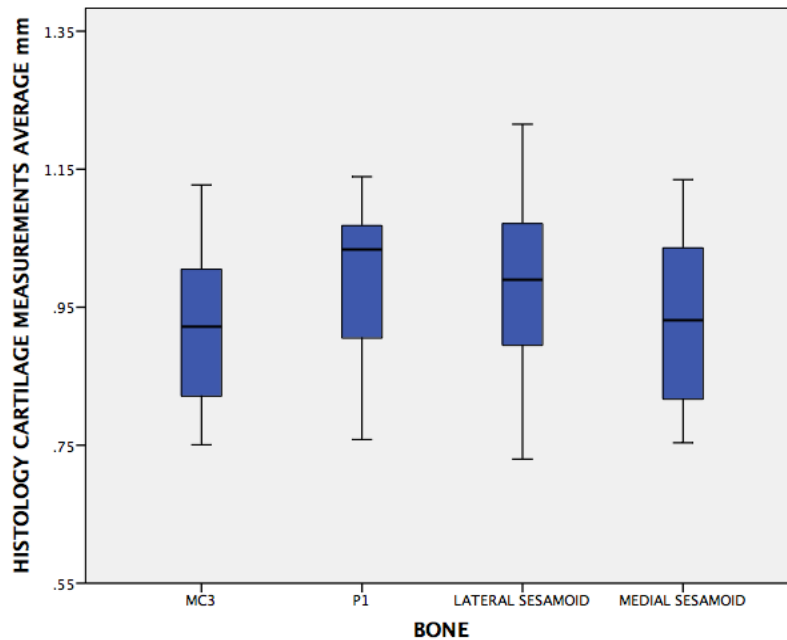


Figure 3-7: Box plot of articular cartilage thickness measurements made from histological measurements: anatomical location. MC3 = metacarpal/metatarsal condyles; P1 = proximal phalanx; lateral/medial sesamoid = lateral/medial proximal sesamoid bone.

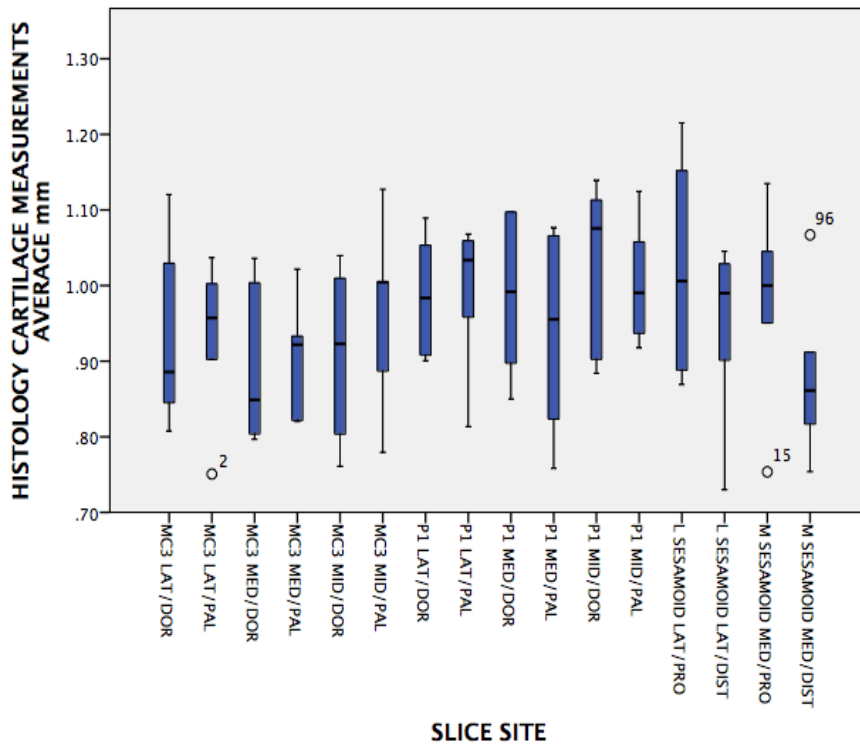


Figure 3-8: Box plot of articular cartilage thickness measurements made from histological measurements: anatomical location and site. MC3 = metacarpal/metatarsal condyle; P1 = proximal phalanx; sesamoid = proximal sesamoid bone.

3.4.2. Correlation Between T1-weighted (7T/1.5T) MRI and Histological Measurements

Using mean values from all anatomical surfaces and sites for analysis, there were moderate positive correlations between 7T MRI and histological measurement of cartilage thickness, 1.5T MRI and histological measurement of cartilage thickness measurements, and between 7T and 1.5T MRI measurement of cartilage thickness (Table 3.2).

Table 3-2: Correlation coefficient (r value) of T1 7T MRI, 1.5T MRI and histology cartilage thickness measurements.

Cartilage thickness measurements		7T MRI measurement	1.5T MRI measurement
Histological measurement	Pearson Correlation (r -value)	0.472	0.414
	P Value	0.000	0.000

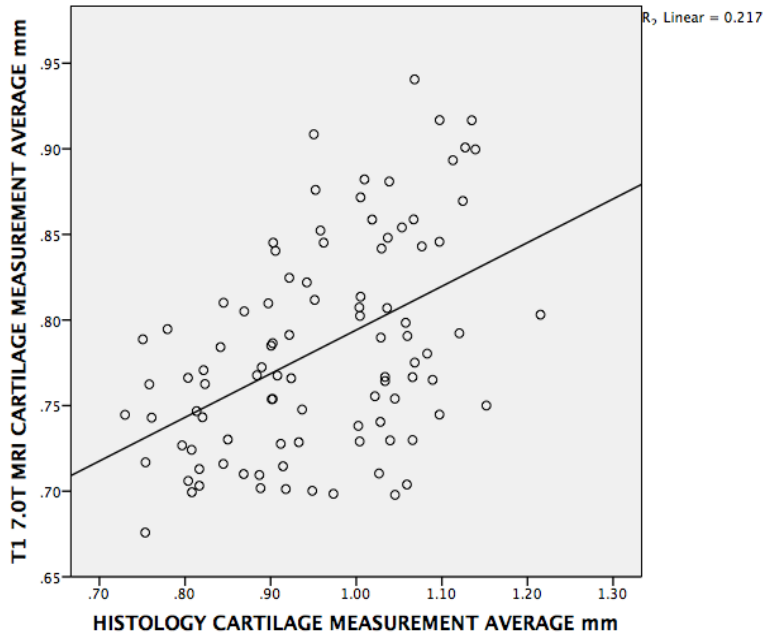


Figure 3-9: Scatter plot of 7T MRI articular cartilage thickness measurement means against histological articular cartilage thickness measurement means. There was moderate positive correlation of T1-weighted 7T MRI cartilage thickness measurements and histology cartilage thickness measurements for MCIII/MTIII, P1 and lateral & medial PSBs ($P < 0.05$) correlation coefficient ($r = 0.472$).

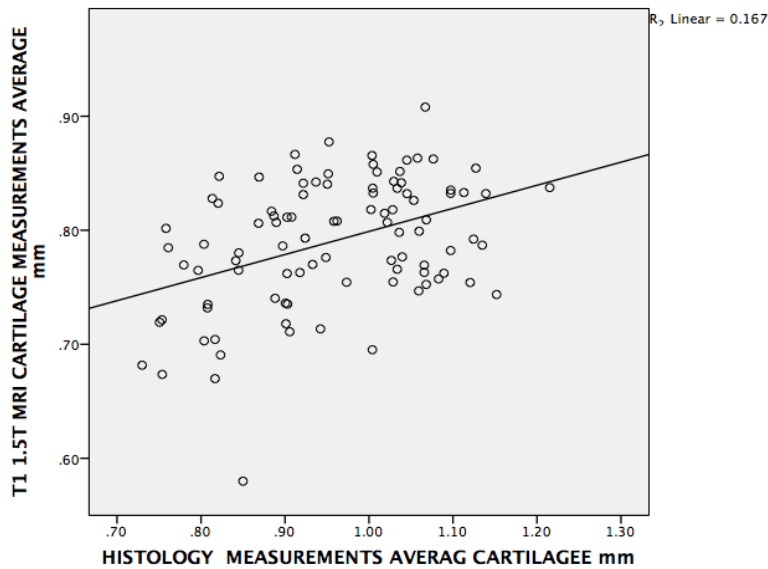


Figure 3-10: Scatter plot of 1.5T MRI cartilage thickness measurements against histological cartilage thickness measurements. There was moderate positive correlation of T1-weighted 1.5T MRI cartilage thickness measurements and histology cartilage thickness measurements of MCIII/MTIII, P1 and lateral & medial PSBs ($P < 0.05$) correlation coefficient ($r = 0.414$).

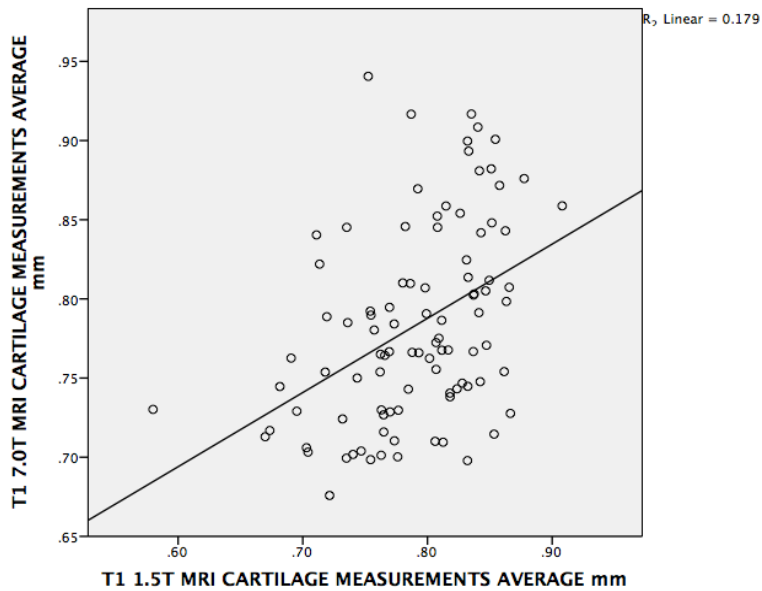


Figure 3-11: Scatter plot of T1-weighted 7T MRI cartilage measurements against T1 1.5T MRI cartilage measurements. There was moderate positive correlation between 7T MRI cartilage measurements and T1-weighted 1.5 T MRI cartilage measurements of the MCIII/MTIII, P1 and lateral & medial PSBs ($P < 0.05$) correlation coefficient ($r = 0.426$).

Table 3-3: Mean of articular cartilage thickness (mm) measured using T1 7T MRI, 1.5T MRI and histology.

Anatomical surface	7T MRI (mm)	Histology (mm)	1.5 MRI (mm)
Metacarpal/metatarsal condyles	0.785	0.92	0.799
Proximal P1	0.790	0.99	0.786
Lateral proximal sesamoid bone	0.769	0.985	0.792
Medial proximal sesamoid bone	0.768	0.929	0.772

3.5. Accuracy and Precision of 7T and 1.5T T1-weighted Measurements of the Articular Cartilage Thickness Compared with Histological Measurements

The accuracy of 7T MRI measurement articular cartilage thickness based on data from all anatomical surfaces and sites was 83.46% (0.835) and the accuracy of 1.5T MRI measurement was 83.13% (0.831); the precision of 7T MRI measurements was 8.67% (0.086) and of the 1.5T MRI measurements 9.46% (0.094) when expressed as variance of all the measurements per MRI system. When all the samples were divided into different cartilage surfaces, measurement accuracy for MCIII/MTIII was 86.11% (0.861) and 86.5% (0.865) for 7T and 1.5T MRI respectively. The accuracy of 7T MRI measurements of P1 was 80.90% (0.809) compared with 80.05% (0.800) for the 1.5T MRI measurement. The measurement accuracy for the medial PSB was 83.43% (0.834) for 7T MRI and 83.61% (0.836) for 1.5T MRI, and 7T MRI measurement accuracy for the lateral PSB 83.23% (0.832) compared with 81.49% (0.814) achieved using 1.5T MRI (Table 3.4).

Table 3-4: Accuracy and precision (STDEV) of the 7T and 1.5T MRI cartilage thickness measurements to the histological measurements.

	7T MRI		1.5 MRI	
	Accuracy %	Precision %	Accuracy %	Precision %
Overall	83.46 (0.834)	8.67 (0.086)	83.13 (0.831)	9.46 (0.094)
Metacarpal/ metatarsal condyles	86.11 (0.861)	8.19 (0.0819)	86.50 (0.865)	10.51 (0.1051)
Proximal P1	80.90 (0.809)	7.57 (0.075)	80.05 (0.8)	9.05 (0.0905)
Medial proximal sesamoid bone	83.43 (0.834)	9.34 (0.093)	83.61 (0.836)	7.98 (0.0798)
Lateral proximal sesamoid bone	83.23 (0.832)	9.59 (0.0959)	81.49 (0.814)	10.33 (0.1033)

3.6. Discussion

This study was conducted in order to identify the accuracy and precision of 1.5T MRI for measuring cartilage thickness by comparing measurements from 1.5T MR images with those made from ultra-high field MRI (7T) images and histological sections. Moreover, comparisons were made in order to assess the accuracy and precision of measurements of 7T MRI measurement of the equine cartilage which could be a useful tool in the future for assessing equine articular cartilage. This study found that 7T MRI is fairly accurate and precise however, it consistently underestimated articular cartilage thickness (histological measurement). This could be due to several factors that may have influenced our measurements, such as partial volume averaging producing systemic errors in thin cartilage plates (Koo et al. 2005), the low intensity appearance of calcified cartilage in MR images leading to this layer being misidentified as subchondral bone (Sittek et al. 1996), or observer error.

3.6.1. Measurement Variation

There were some differences between these two MRI modalities and histopathology which may involve the alteration of histological cartilage tissue during processing and the difference in spatial resolution of MR images (Bischofberger et al. 2006). Furthermore, some differences may have arisen from the variation of MRI plane sections, MRI slice thickness as well as the lack of resolution at the lower boundary of the equine articular cartilage (most superficial tide-mark zone) for both MRI cartilage thickness measurements. For instance, the calcified cartilage layer might be underestimated, as the MRI signal intensity of this layer was lower than the other superficial cartilage layers. Moreover, it has been found that the articular cartilage thickness is theoretically affected by hydration factor, which could decrease cartilage thickness (Blumenkrantz & Majumdar 2007).

3.6.2. Difference in Thickness Mean

No significant differences were found in the mean cartilage thickness between 1.5T and 7T MRI measurements and their values were similar to the histological measurements, particularly 7T MRI cartilage thickness measurements. This could have been due to the higher resolution of the 7T versus 1.5T images. Also it has been found that 7T MRI and histopathological measurements follow the same thickness patterns such that the proximal P1 articular cartilage was thicker than MCIII/MTIII, lateral proximal sesamoid bone and medial sesamoid bone articular cartilage (Table 3.3). Moreover, the articular cartilage thickness measurements of the lateral and middle MCIII/MTIII were higher on the palmar aspect than the dorsal aspect for all measurement techniques. However, this was not the case for the medial aspect of the MCIII/MTIII.

The lateral dorsal aspect of P1 articular cartilage mean thickness was greater than the palmar aspect for all measurement techniques. The middle and medial dorsal aspects of P1 cartilage was higher in both histological and 7.0T MRI measurement, while on 1.5T MRI was lower. The articular cartilage thickness of both proximal sesamoid bones was higher at the proximal aspect than distally for all variables (Table 3.3). A previous study found that the mean thickness 0.99 ± 0.17 mm of

cartilage thickness measured using 1.5T MRI, whereas the mean cartilage thickness measures using histology was 0.79 ± 0.16 mm with a significant difference between both measurement methods (Olive et al. 2010). Our results were similar to those reported by Olive and colleagues in 2010 but lower than those found by Carstens and colleagues in their study (Carstens et al. 2013). However, they used delayed gadolinium enhanced dGEMRIC MRI techniques in measuring the articular cartilage of equine MCIII/MTIII joint.

3.6.3. Correlation Between MRI vs. Histology

It was hypothesised that histological cartilage thickness measurements were highly correlated to articular cartilage measurement from both high 1.5T and ultra-high 7T MRI cartilage thickness measurements. Our MRI results showed that there was no significant difference between both MRI measurements and the histological measurements. Moreover, it has been found that both MRI measurements were significantly correlated to each other as well as the histological measurements when they individually compared to the histological measurements. A previous study has shown that 1.5T MR images provide reasonable accuracy in measuring articular cartilage thickness. Nevertheless, this study found a significant moderate correlation of articular cartilage thickness measurements between histological and 1.5T high-field MR images measurements $r= 0.44$; $P=0.0001$ (Olive et al. 2010). Additionally, a significant correlation has been found between T1 three-dimensional gradient echo (3D GRE) sequence of 7T MRI and histological measurements of articular cartilage (Pepin et al. 2009).

3.6.4. Accuracy And Precision Of The Articular Cartilage Thickness

The accuracy and precision of the cartilage thickness measurements made from 7T MR images was higher than those made from 1.5T images. This study found that the accuracy of the 7T and 1.5T MRI measurement were close to each other for all the examined cartilages except of the lateral sesamoid, there was around 2% difference in the accuracy. It has been found that when 1.5T MRI is compared with 7T MRI ultra-high field magnet the 7T MRI system produces images with far superior contrast as well as higher resolution. Thus, articular cartilage can be appreciated with greater

clarity, although it is possible to appreciate different cartilage surfaces on the distal metacarpal cartilage, P1 and both proximal sesamoid bones in 1.5T MR images. The 1.5T MR images do not allow detailed appreciation of the individual articular cartilage surfaces and as a consequence articular cartilage thickness was measured across adjacent articular surfaces (between MCIII/MTIII and P1 or MCIII/MTIII and both sesamoid bones). However, when measuring the articular cartilage thickness using 7T MRI, there was not a well-defined margin of the subchondral bone and the area between it and the calcified layer of the articular cartilage, which could also have affected our measurement results. Our histological mean was around 0.9 mm, so some of our readings may have been overestimated using MRI measurement tool. Moreover, previous research showed that tissues are subjected to shrinkage during standard histology preparation due to dehydration (Bischofberger et al. 2006).

A study of equine cartilage using 1.5T MRI of the third carpal bone compared cartilage thickness using MRI and histology. The study found that there was no significant difference between MRI and histology measurements and there was strong correlation between these two methods with significant positive bias between observers as the MRI technique provides a good representation of the articular cartilage thickness. It was suggested that MRI could be used for clinical evaluation of osteochondral structure and alteration (Murray et al. 2005), which supports our results.

There are several factors that could affect the accuracy of this technique such as variation in the pixel intensity ratio between subchondral bone and the cartilage. Despite these limitations, the MRI measurement technique described could be used to evaluate cartilage pathology in horses.

3.7. Limitations Of The Study

This study used a 7T MRI magnet, however ultra high field systems have not been introduced into equine clinical practice yet. No intra-observer or inter-observer validation of the MRI or histology measurement techniques used in this study was performed. This validation process should be performed before these methods are adopted in practice.

3.8. Future Study

Future work should include the use of clinically applicable low field MRI magnets, increased sample size and the number of observers in order to compare between their measurements. Also, validation of MRI techniques with other novel techniques such as laser scanner technique using 3D desktop laser scanner (Koo et al. 2005), which could allow more accurate cartilage thickness measurements is warranted.

3.9. Conclusion

To conclude, this study measured the equine cartilage thickness using T1-weighted images acquired from 1.5T and 7T MRI systems as well as by histology. Then these three modalities were compared to evaluate how accurate and precise both MRI measurements are in comparison with the gold standard histological measurement of the cartilage thickness. This study hypothesised that measurements of articular cartilage thickness in the MCPJ/MTPJ of the horse acquired from MRI magnets are accurate, however that 7T MRI enabled more accurate and precise measurement than 1.5T MRI although measurements made from images at the two field strengths were well correlated. From the results, this study found that there was a significant correlation between both MRI of cartilage thickness measurements and histological measurements of equine cartilage thickness. Moreover, 7T MRI measurements were closer, than 1.5T measurements to the histology measurement as they follow the same pattern of cartilage thickness.

It has also been found that MRI is able to provide useful information about the thickness of equine articular cartilage, similar to histological evaluation. This is very crucial because the use of the MRI in equine practice in evaluating articular cartilage will allow the potential detection of any pathological changes *in vivo*. This study compared these different methods in a relatively simplistic way; others have used more sophisticated methods to compare these different articular cartilage measurements. The results from this study indicated that 7T MRI can provide better information and more accurate and precise measurements than high field MRI magnets due to its better spatial resolution. Future work to increase the number of observers, which could improve the results and could give extra validation of this MRI

technique in measuring equine articular cartilage is warranted. It is acknowledged that 7T MRI systems are not currently being used in equine clinical practice, however higher field strength systems are being introduced into equine clinics so the conclusions of this study may have clinical, as well as research, application in the future.

Chapter 4 A Comparison of Quantitative MR Imaging Techniques of the Normal Equine Fetlock Joint to Assess Articular Cartilage: Transverse Relaxation Time (T2-time), T1 signal intensity and dGEMRIC Study

4.1. Introduction

Osteoarthritis (OA) is a degenerative chronic disease that occurs in equines that is characterized initially by loss of the affected articular cartilage surface, which consequently leads to inflammation, pain and occurrence of pathological lesions such as a growth of new vasculature and development of osteophytes, culminating in the narrowing of the joint space. From a biochemical point of view, OA is characterized by the following changes in the articular cartilage surface: decrease in proteoglycan (PG) concentration, changes in the size of the collagen fibrils, change in the aggregation of the PG, an increase in water content in the cartilage, as well as increased production and degradation of the matrix macromolecules of the cartilage. It has been suggested that the partial breakdown in the proteoglycan matrix and decrease in the total content of collagen could be a sign of the early changes in articular cartilage due to OA. It has been reported that the total number of collagen fibres remains unaffected at the onset of the earliest stage, even if there is a general change of the aggregation and size of the fibres (Borthakur et al. 2006; Taylor et al. 2009).

4.2. T2 relaxation Time Mapping

Quantitative MR imaging techniques have shown promising results using what are referred to as 'biomarkers' such as transverse (T2) relaxation time mapping, T1 rho and dGEMRIC studies. Validation of these techniques has demonstrated sensitivity in the assessment or detection of biochemical alteration within tissue of interest such as articular cartilage (Matzat et al. 2013). T2 relaxation time techniques look at the spin-echo time of the nuclei, which reflects the speed by which the nuclei loses its phase coherence after radio frequency (RF) excitation, ending by decay of the T2 magnetisation (Choi & Gold 2011; Matzat et al. 2013). T2 mapping has been used as

a non-invasive technique that can characterise the structure and organization of hyaline articular cartilage (Goodwin 2001). Moreover, several studies have suggested that T2 MRI studies are beneficial for diagnosis of early OA due to the fact that T2-time is very sensitive to the water content of the cartilage. OA decreases the total number of proteoglycans (PG) and increases the osmotic pressure and swelling which is followed by destruction of the collagen matrix (Surowiec et al. 2014). Several studies examining quantitative T2 MRI mapping of bovine articular cartilage confirmed the ability and the sensitivity of T2 mapping in identifying the changes in the articular cartilage and collagen content (Nieminen et al. 2000; Nissi et al. 2004). A human study found it sensitive to these changes (Taylor et al. 2009). Moreover, another research group found that that *in vivo* T2 transverse relaxation time is increased in patients that have severe osteoarthritis when compared with healthy people (Mosher et al. 2000; Li et al. 2007). T2 time significantly correlated with the loss of proteoglycans (PG) in a previous study suggesting that the negatively charged GAGs influence the interaction of water molecules that causes an elevation of T2 time after proteolytic degeneration of the articular cartilage (Wayne et al. 2003). Nieminen et al concluded that T2 mapping could be used to evaluate the structure of collagen network fibres and is sensitive to PG content (Nieminen et al. 2001).

T2 relaxation mapping has a number of limitations, which reduce its usage in routine clinical practice (Surowiec et al. 2014), despite optimistic results in many clinical studies (Nishii et al. 2008). T2 mapping requires a long scan time, which could be very expensive (Keenan et al. 2011). Poor spatial resolution of the thin distal third metacarpal-tarsal equine cartilage is an issue that could potentially be improved in the future using a dedicated surface coil and field view (Carstens et al. 2013).

4.3. Delayed Gadolinium Enhanced Contrast MRI of Articular Cartilage (dGEMRIC)

Gadolinium (GdDTPA²⁻) enhanced T1 imaging (dGEMRIC) to assess the structure of articular cartilage *in vivo* has previously been described (Nieminen et al. 2001). The term delayed in the delayed gadolinium study refers to the time needed to allow large amounts of Gd-DTPA²⁻ to invade the full articular cartilage thickness. This takes

around 30 min and the tissue is ready to MRI (Crema et al. 2011; Wucherer et al. 2012; Surowiec et al. 2014). It has been widely used in human and animal research and routine practice such as neurology studies, but few studies have used this technique in equine medicine (Saveraid & Judy 2012; Carstens et al. 2013).

This technique is based on the observation that the ions in the interstitial fluid of the articular cartilage are distributed in relation to the negatively charged glycosaminoglycans molecules, and this is strongly related to the total proteoglycan (PG) content of the articular cartilage. After injecting Gd-DTPA²⁻ intravenously into the body or intra-articularly, the anionic molecules enter the cartilage and concentrate in areas of relatively low glycosaminoglycan concentration. This reduces the T1 relaxation time of the cartilage and the concentration can be estimated by measuring the T1 time of the articular cartilage, thus allowing an indirect quantitative assessment of glycosaminoglycans content. Thus, T1 values are high in the areas of cartilage that have low concentrations of glycosaminoglycans, and low in high concentration areas (Williams et al. 2005; Krishnan et al. 2007; Crema et al. 2011).

Quantitative dGEMRIC studies have shown promising quantitative results in the assessment of articular cartilage health status. However, acquiring precise quantitative MRI techniques and clinically valuable MRI data of the scanned tissue has proven challenging, and the reproducibility of the quantitative MRI mapping techniques and its results are crucial. The data acquired using this technique can be very time consuming, which restricts its usage on a routine basis. Furthermore, it has been limited by variations in contrast diffusion and challenges determining the actual plasma content of the dGEMRIC contrast media (Watanabe et al. 2009). However, despite all of these limitations which influence dGEMRIC technique, it is considered to be a more promising method for assessing GAG content of the articular cartilage, especially with OA pathology, than standard MRI protocols (Bashir et al. 1999; Gold et al. 2009). However, no study has yet compared these techniques to biochemical properties such as GAG content. Therefore, this study aims to investigate and compare between these techniques.

4.4. Aims and Objectives

It was hypothesised that novel MRI methods can quantify body tissue biochemical properties associated with the early onset of articular cartilage degeneration in equine articular cartilage. In addition, it was hypothesised that dGEMRIC and T2 will correlate with the early arthritic change markers of proteoglycan concentration and water content.

The specific objectives of this study were as follows:

- I. To establish T1 signal intensity of the normal horse articular cartilage pre and post gadolinium contrast (dGEMRIC).
- II. To describe transverse relaxation time (T2) of normal equine articular cartilage.
- III. Measure the proteoglycan content and hydration in normal equine articular cartilage and describe any topographical variation within normal equine cartilage.
- IV. Describe the relationship between MRI measurements and biochemical parameters.

4.5. Materials and Methods

4.5.1. Samples Collection and Preparation

Seven limbs of adult horses aged 5-11 years and various breeds, euthanised for other reasons unrelated to this study were collected with owner consent. All limbs were labeled and frozen at -20°C until preparation and imaging. Limbs were defrosted at room temperature for 24h prior to cartilage collection. Then, the forelimbs were disarticulated at the level of the third distal metacarpal MCIII bone, surrounding soft tissue was removed and the cartilage surface kept moist by covering with wet surgical gauze soaked in isotonic normal saline (Baxter). After that the medial and lateral distal condyles were sectioned by handsaw (width= 5mm, height 3-4 cm) (Fig 4.1). During cutting the samples were washed with normal saline several times to avoid dehydration. Cartilage samples were labeled then kept in tissue container filled with isotonic normal saline until MRI.

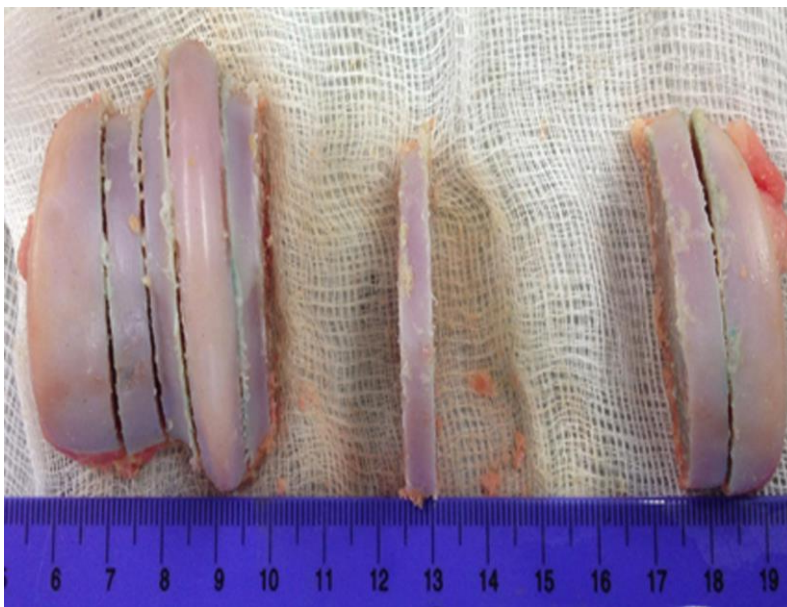


Figure 4-1: This image represents cartilage samples preparation. 4 semi-circular cartilage and bone sections were taken (5mm width, 3cm height) of equine MC3 bone, and were labeled 1-4 from lateral to the medial aspect of the bone. Subsequently, kept in a container filled with isotonic solution (normal saline) for MRI and biochemical study.

4.5.2. MRI imaging (T1, T2 Relaxation Time Images and GdDTPA²⁻ Enhanced Measurements)

Markers were prepared using copper sulphate (1.5g/l) solution (Sigma) in clear glass vials. These were used during measurement of the two sets of MRI images to provide more accuracy during slice positioning.

All cartilage samples were scanned by ultra-high field (7T) magnet (BioSpec, Bruker Corporation 70/30 system Bruker, Germany) by using a dual tuned quadrature ²³Na/1H coil custom built by a commercial coil manufacturer (PulseTeq Limited, Chobham, Surrey, UK) (Fig 4.2). Samples were placed in a container filled with inert Fomblin (Solvay Solexis) to avoid air bubble interference during scanning.

Firstly, T1-weighted images were obtained using a gradient echo (FLASH) sequence with TR/TE= 120/3.5ms, flip angle= 30⁰, FOV=6cm and 3.5cm, matrix= 240x140, resolution= 250x250 microns, slice thickness= 3mm, bandwidth= 81.3kHz and scan time of 17mins 55 seconds. Secondly, the T2 relaxation time was determined using 16 echo sequences with TR/TE= 6/8ms, average= 10ms, flip angle= 180⁰, FOV=6cm and 3.5cm, matrix= 240x140, resolution= 250x250 microns, slice thickness= 3mm, bandwidth= 101kHz and scan time of 2hrs 20mins (Fig 4.4).

After the baseline MRI scans and the data was obtained for both T1-weighted and T2-weighted times, the Fomblin was removed. A 0.51mM solution of Gd-DTPA (Magnevist®, gadopentetate dimeglumine, Bayer) was prepared in by diluting a 1mM solution in 0.9% sodium chloride. Cartilage samples were incubated for 2 hours in 0.5mM Gd-DTPA (Mlynárik et al. 1999). T1-relaxation time gadolinium-enhanced MRI (Gd-DTPA) was performed using the same parameters (Fig 4.3).

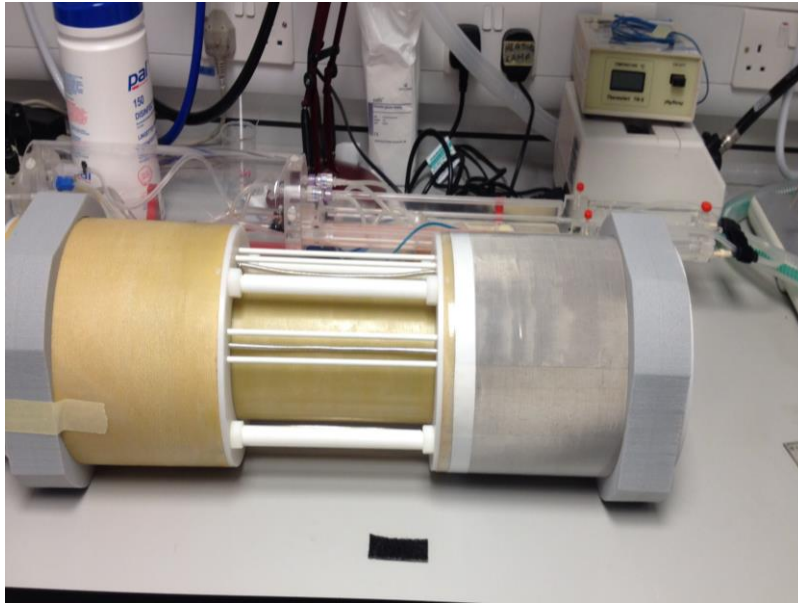


Figure 4-2: A dual tuned quadrature $^{23}\text{Na}/^1\text{H}$ coil designed by PulseTeq Limited Chobham, Surrey, UK, for this project.



Figure 4-3: A plastic container containing metacarpal condyle fixed at the bottom with fixing MRI-friendly material to avoid signal alteration of the plastic container as well as fixing the samples in order to get the same slice parameters in each MRI scans.

4.6. MRI Data Analysis

4.6.1. T1- Weighted Image Analysis (Signal Intensity)

All MR images obtained pre- and post-contrast were analysed using commercially available software (Bruker ParaVision version 5.0). Digital subtraction was performed, although there was a shift in signal between pre-and post-copper sulphate contrast phantom due to magnetic shift. So, in order to resolve this problem, four regions of interest, two from dorsal (A&B) and the others from palmar aspect (C&D), were measured manually using track tool on the central dorsal and central palmar cartilage regions and the circular phantom in both pre (Spre) and post contrast (Spost). T1 (Fig 4.4) was subsequently worked out using the following equation:

$$\text{True T1 signal pre} = \frac{S_{post}}{S_{pre}} \times \text{Observed T1 signal Pre}$$

Each of four ROI were drawn manually three times and each ROI was repeated in triplicate. Mean and standard deviation of T1 signal intensity or pre and post contrast were calculated in each T1 trial.

4.6.2. T2-Relaxation Time Analysis

MR images were reconstructed and processed to measure T2 relaxation times using commercially available software (Bruker ParaVision version 5.0). ROI were drawn again manually, 4 regions of interest, two from dorsal (A&B) and the others from palmar aspect (C&D), were performed manually using track tool on the central dorsal and central palmar cartilage regions again as T1 time technique (Fig 4.4). These ROI regions were measured three times, mean as well as standard deviation of T2 time were carried out for pre and post contrast study measurements.

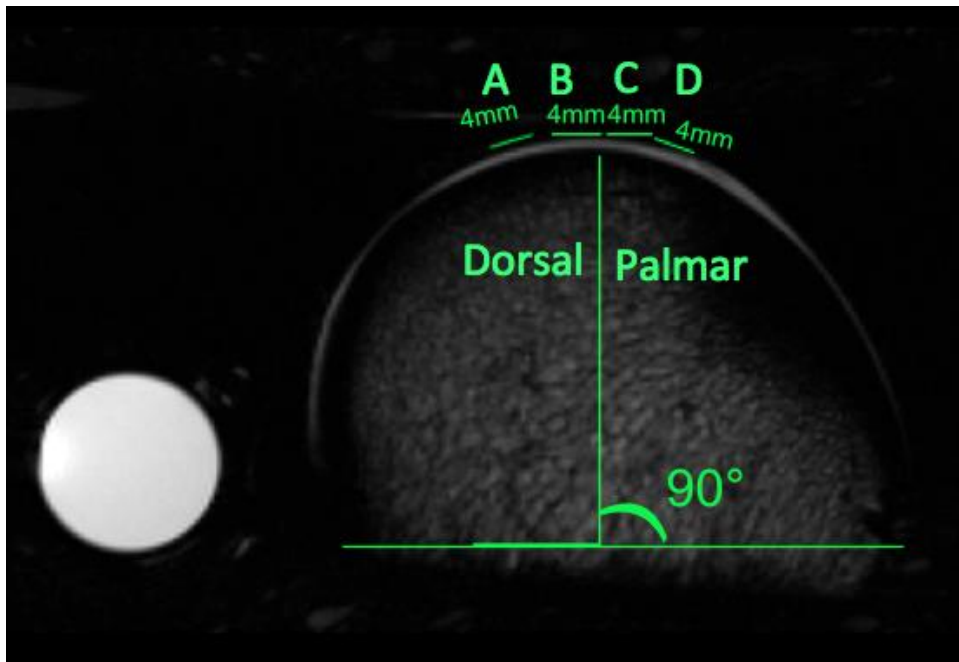


Figure 4-4: T2-weighted (relaxation time) image MRI analysis. By using a geometry tool, a straight line was drawn between the dorsal and palmar end points of the semi-circular cartilage sample, in which a 90° angle was created from the centre of the straight line. From this centre 4 lines were drawn two from dorsal (A&B) and the others from palmar aspect (C&D) of the cartilage sample ROIs. Then, the track tool was used to manually track the cartilage ends, making sure that this tracking tool included the cartilage area only. The value obtained represented the average T1 signal intensity within the ROIs. The geometry afterward was overlaid onto the corresponding post or pre contrast imaging sample to make sure that the two pre and post contrast imaging sets ROIs were similar to each other in their slice position.

4.7. Biochemical Study (Cartilage Collection)

After the MRI study, cartilage samples were kept in isotonic normal saline (Baxter) and then the cartilage samples were harvested as cylindrical disks at specific regions using 4mm biopsy punch (Steifel, a GSK Company, Research Triangle Park, USA). The cylindrical punches were obtained by trephining down the long axis through the cartilage and bone to make sure that the cartilage layers were included (Fig 4.5). All samples were then labeled as the same area of interest that was analyzed in the MRI study.

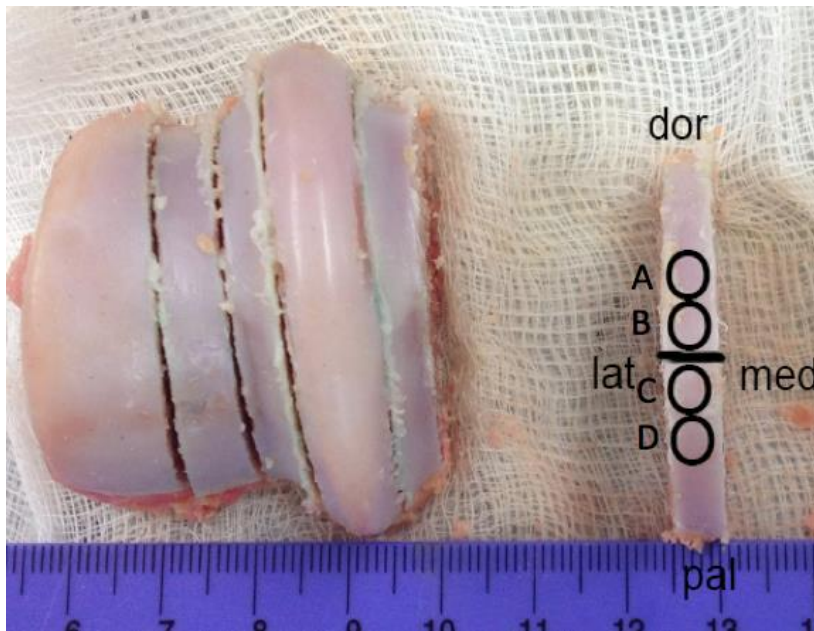


Figure 4-5: This diagram represents cartilage collection for biochemical assay study. Four cylindrical disks were harvested using 4mm biopsy punches and labelled A and B from the dorsal site and C and D from the palmar site. Samples were removed at specific regions and totally separated from the subchondral bone using a surgical scalpel making sure that full thickness of cartilage was carefully removed. These were then used to determine water and proteoglycan content.

4.7.1. Water Content (Dry Weight)

All cartilage samples were placed in labelled 96 well microplates filled with isotonic solution (normal saline) to equilibrate and avoid dryness of cartilage. Wet weight was measured. Then, samples were kept in a 50°C oven for 24 hours (Keenan et al. 2011). Subsequently, dry weight was taken to measure the water percentage. Water percentage of the samples was calculated using the formula $[(ww-dw)/ww]*100\%$. Afterward, every cartilage punch was placed in labelled Eppendorf tube until glycosaminoglycan measurement.

$$\text{Water percentage} = \frac{\text{wet weight} - \text{dry weight}}{\text{wet weight}} \times 100$$

4.7.2. Proteoglycan Assay

Dried articular cartilage samples (1-5mg) were weighed, placed in 1.5ml Eppendorf tubes (Sigma) and 1ml of papain extraction reagent, prepared according to manufacturer's manual was added (Sulphated Glycosaminoglycan Assay, Biocolor, County Antrim, UK). Then, they were kept overnight in an oven at 60°C. During this time the cartilage digestion occurred. Afterward, 1,9- dimethyl methylene blue reagent (Blyscan) was added and the assay commenced according to manufacturer's manual instructions (Blyscan). Then, the microplate tube was moved to the spectrophotometer to measure the absorbance, the absorbance reading was carried out at 650nm with a spectrophotometer reader filter, with the absorbance being calibrated with known concentration of bovine tracheal chondroitin 4-sulphate (Blyscan) making sure that the standard curve had an r^2 value of ≥ 0.95 (Fig 4.6).

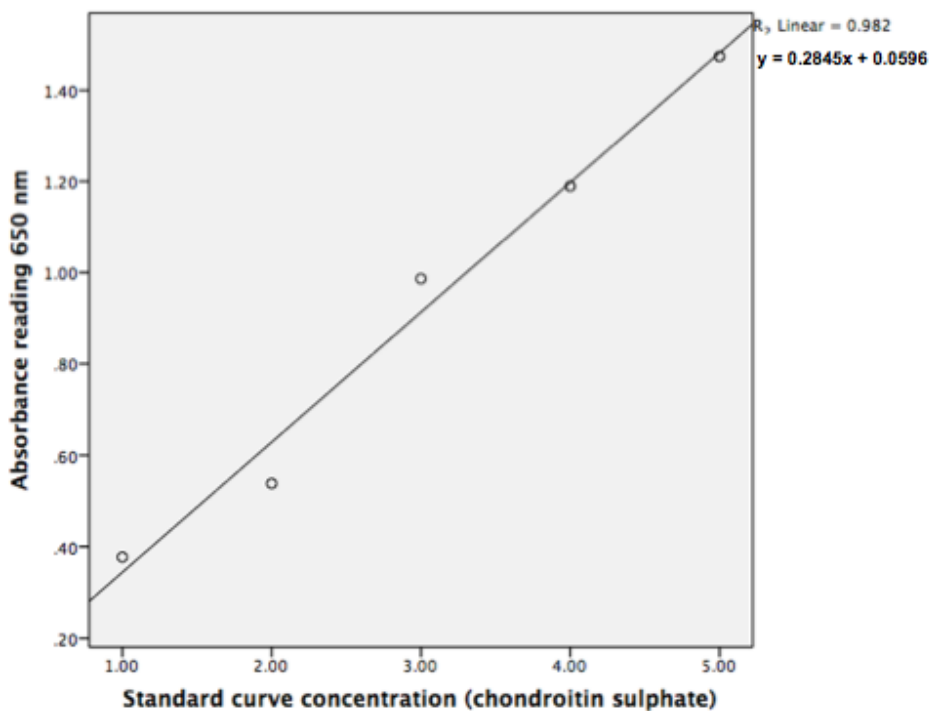


Figure 4-6: This figure shows the scatter plot of the standard curve, used to measure the concentration of cartilage glycosaminoglycans, acquired from 5 standards with different concentrations measured by 650nm filter using a spectrophotometer.

4.7.3. Statistical Analysis

All data variables were analysed using IBM® SPSS® statistics 20 software with the confidence level of 95%. All variables were confirmed to have a normal distribution using Shapiro-Wilks test prior to further statistical analysis. The variability of intraobserver ROI placement of T2 relaxation time and T1 signal intensity values was determined by calculating the Correlation coefficient (r value) between three trials of T2 relaxation time and T1 signal intensity value readings. The effect of punch location factor (e.g. dorsal vs. palmar sites, lateral vs. medial sites) on biochemical content such as GAG glycosaminoglycans and hydration as well as MRI parameter readings (i.e. T1-signal intensity, T2 relaxation time and gadolinium enhancement) was determined using ANOVA test for independent variables. The correlation between biochemical characteristics and different MRI parameters was calculated using Pearson rank correlation test.

4.8. Results

4.8.1. Biochemical Evaluation

4.8.1.1. sGAG Content

The mean GAG content for all of the articular cartilage samples was (39.45 µg/mg/dw ±10.65 µg/mg/dw) (Table 4.1). There was significantly greater sGAG content in dorsal 44.34±10.64 µg/mg/dw than palmar (34.56 µg/mg/dw ±8.19 µg/mg/dw) samples ($P<0.05$) (Table 4.2). The mean sGAG content of lateral site was (39.05 µg/mg/dw ± 10.25 µg/mg/dw), medial (39.85 µg/mg/dw ±11.11 µg/mg/dw) with no significant difference found between these two sites of the equine cartilage ($P=0.69$). However, there was significant difference between different punch locations found. Punch A had higher sGAG content 44.94±9.66 µg/mg/dw than punch C (32.75 µg/mg/dw ±6.02µg/mg/dw) and punch D (36.37 µg/mg/dw ±9.68µg/mg/dw) ($P<0.05$).

There was a significant difference of sGAG content found between punches B, C and D as punch B (43.74 µg/mg/dw ±11.68 µg/mg/dw) was higher than C (32.75 µg/mg/dw± 6.02µg/mg/dw) and punch D 36.37 (µg/mg/dw ±9.68 µg/mg/dw) ($P<0.05$) (Table 4.2, 4.3) and Figures (4.7-4.9).

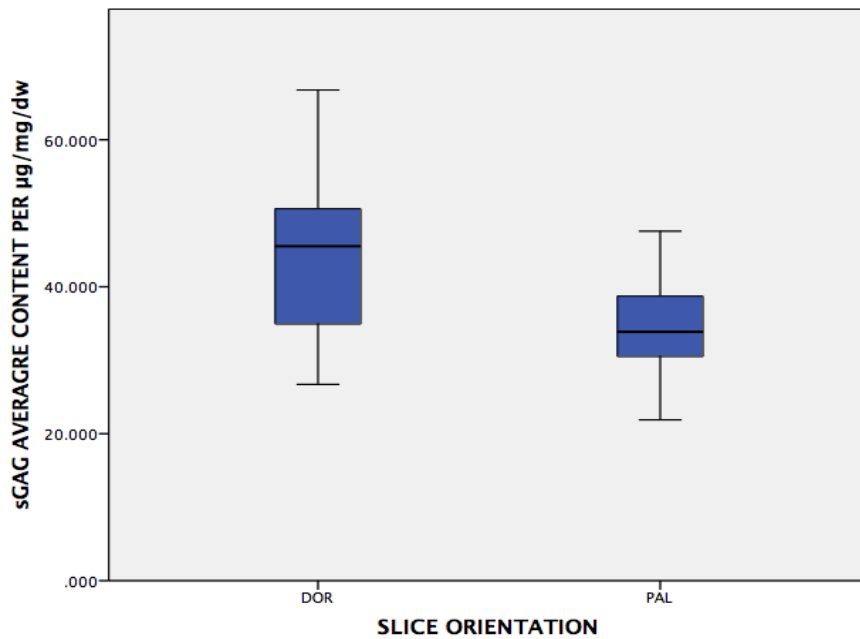


Figure 4-7: Box plot shows the mean sGAG content ($\mu\text{g}/\text{mg}/\text{dw}$) over dorsal and palmar sites of the equine metacarpal-tarsal articular cartilage. The dorsal cartilage punches had higher GAG content ($44.34 \pm 10.64 \mu\text{g}/\text{mg}/\text{dw}$) than palmar punches ($34.56 \mu\text{g}/\text{mg}/\text{dw} \pm 8.19 \mu\text{g}/\text{mg}/\text{dw}$) ($P < 0.05$).

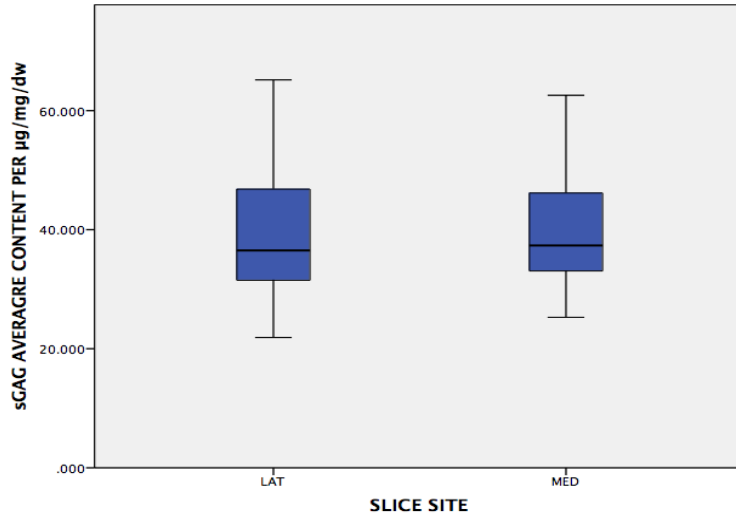


Figure 4-8: Box plot shows the mean of sGAG content ($\mu\text{g}/\text{mg}/\text{dw}$) of lateral and medial aspects of the equine metacarpal-tarsal articular cartilage. No significant difference was observed between lateral sites ($39.05 \mu\text{g}/\text{mg}/\text{dw} \pm 10.25 \mu\text{g}/\text{mg}/\text{dw}$), medial site ($39.85 \mu\text{g}/\text{mg}/\text{dw} \pm 11.11 \mu\text{g}/\text{mg}/\text{dw}$) ($P = 0.69$).

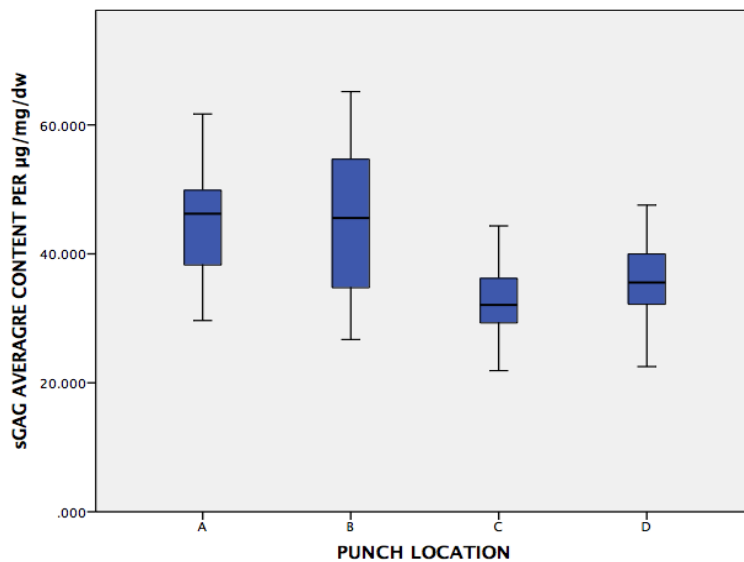


Figure 4-9: Box plot shows the mean of sGAG content ($\mu\text{g}/\text{mg}/\text{dw}$) of different punch locations of the equine metacarpal-tarsal articular cartilage. A is most dorsal, B dorsal & C palmer and D most palmar sites of the articular surface of the metacarpal-tarsal articular cartilage. A punch had higher sGAGS content $44.94 \pm 9.66 \mu\text{g}/\text{mg}/\text{dw}$ than B punch ($43.74 \mu\text{g}/\text{mg}/\text{dw} \pm 11.68 \mu\text{g}/\text{mg}/\text{dw}$), C punch ($32.75 \mu\text{g}/\text{mg}/\text{dw} \pm 6.02 \mu\text{g}/\text{mg}/\text{dw}$) and punch D ($36.37 \mu\text{g}/\text{mg}/\text{dw} \pm 9.68 \mu\text{g}/\text{mg}/\text{dw}$) ($P < 0.05$).

Table 4-1: Mean and standard deviation of all variables (sGAG (mg), T1 signal intensity, T2 relaxation time (ms) and T1 dGEMRIC).

	Mean	Standard deviation
sGAG content $\mu\text{g}/\text{mg}/\text{dw}$	39.45	10.65
T2 time (ms)	30.76	4.38
T1 Pre signal intensity	1.74	0.498
T1 post signal intensity	1.88	0.491
Water content %	72.60	4.3

Table 4-2: Paired Student's T-test of topographical difference in cartilage GAG content $\mu\text{g}/\text{mg}/\text{dw}$.

PUNCH LOCATION	GAG content $\mu\text{g}/\text{mg}/\text{dw}$	Std Dev	P value
Dorsal	44.34	10.64	$P < 0.05$
Palmar	34.56	8.19	
Lateral	39.05	10.25	$P = 0.69$
Medial	39.85	11.11	

Table 4-3: ANOVA Post hoc t-test of sGAG content ($\mu\text{g}/\text{mg}/\text{dw}$) in different punch locations: Multiple comparisons dependent variable: sGAG content per mg Tukey HSD.

PUNCH LOCATION	PUNCH LOCATION	P Value.
A	B	0.96
	C	0.000 *
	D	0.006 *
B	A	0.96
	C	0.000 *
	D	0.023 *
C	A	0.000 *
	B	0.000 *
	D	0.483

* The mean difference is significant at the 0.05 level.

Table 4-4: Mean and standard deviation of sGAG content ($\mu\text{g}/\text{mg}/\text{dw}$), water (%), average T2 relaxation time, T1 intensity pre contrast and T1 post contrast vs. different punch location (A, B, C & D).

	Punch Location	N	Mean	Std. Deviation
sGAG CONTENT PER MG	A	28	44.94	9.66
	B	28	43.74	11.68
	C	28	32.75	6.02
	D	28	36.37	9.68
	Total	112	39.45	10.65
T1 POST	A	28	1.810	0.486
	B	28	1.896	0.489
	C	28	1.926	0.503
	D	28	1.895	0.504
	Total	112	1.882	0.491
T1 PRE	A	28	1.665	0.469
	B	28	1.801	0.554
	C	28	1.793	0.508
	D	28	1.707	0.472
	Total	112	1.742	0.498
T2 PRE	A	28	30.314	4.922
	B	28	31.646	4.851
	C	28	31.875	3.538
	D	28	29.215	3.724
	Total	112	30.762	4.382
WATER PERCENTAGE	A	28	73.29	3.980
	B	28	72.89	3.095
	C	28	72.93	3.877
	D	28	71.29	5.766
	Total	112	72.60	4.305

4.8.1.2. Percentage Water

The mean water content for all samples was 72.60% \pm 4.3% (Table 4.5). The mean water % for the dorsal site was 73.09% \pm 5.53%, palmar site 72.11% \pm 4.93%. There were no significant differences found between dorsal and palmar sites (Fig 4.10) ($P=0.229$). The mean water % for the lateral site (72.46% \pm 4.71%) and medial sites 72.73% \pm 3.88% (Fig 4.11) (Table 4.6) were not significantly different ($P=0.744$). When all data set were split to evaluate the difference between different punch locations (A, B, C & D), the mean water content of A punch was 73.29% \pm 3.98%, B 72.89% \pm 3.09%, C 72.93% \pm 3.87% and D was 71.29% \pm 5.76% (Table 4.7), there was no significant difference found between them (Fig 4.12), (Table 4.8).

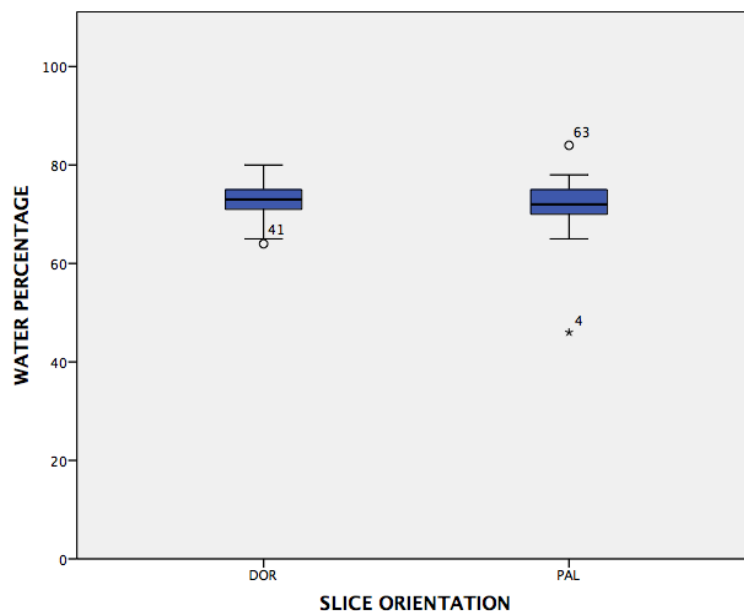


Figure 4-10: Box plot showing the water content (%) in dorsal and palmar aspects of the cartilage. The mean water % for the dorsal site was 73.09% \pm 5.53%, palmar site 72.11% \pm 4.93%. There was no significant difference found between dorsal and palmar sites ($P=0.229$).

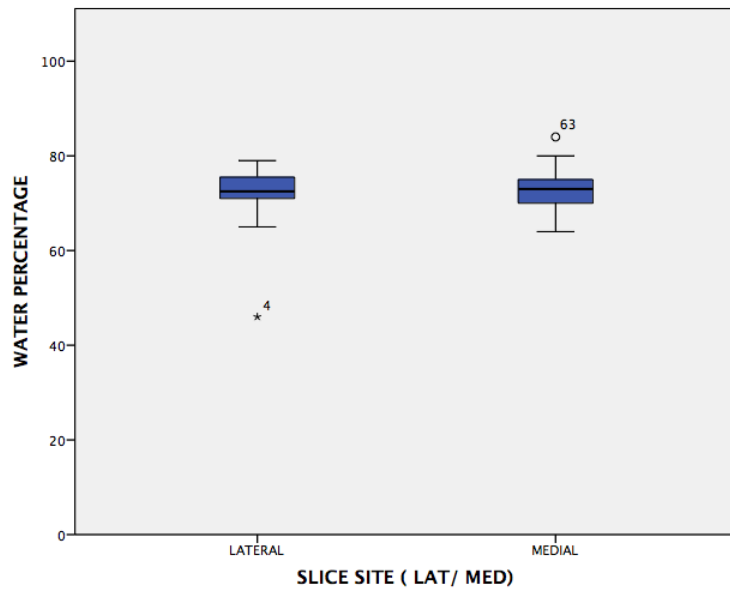


Figure 4-11: Box plot showing the water content (%) of lateral and medial aspects of the equine metacarpal-tarsal articular cartilage. Lateral site $72.46\% \pm 4.71\%$ and medial sites $72.73\% \pm 3.88\%$ with no significant difference was found between these sites ($P=0.744$).

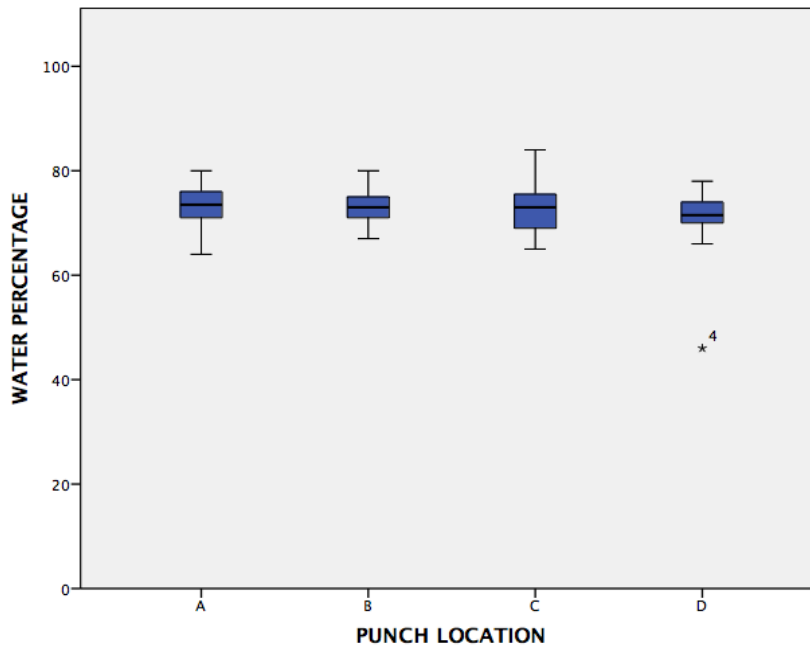


Figure 4-12: Box plot showing the water content (%) of different punch location as (A, B, C & D) of the equine metacarpal-tarsal articular cartilage. There was no significant difference found between them.

Table 4-5: Paired Student's T-test of topographical difference in cartilage water content %.

	Mean % Water	Std Dev	P value
Dorsal	73.09	5.53	<i>P</i> =0.229
Palmar	72.11	4.93	
Lateral	72.46	4.71	<i>P</i> =0.744
Medial	72.73	3.88	

Table 4-6: Mean and standard deviation of water % vs. punch location (A, B, C, and D).

PUNCH LOCATION	Mean % Water	Std. Deviation
A	73.29	3.98
B	72.89	3.09
C	72.93	3.87
D	71.29	5.76

Table 4-7: ANOVA Post hoc t-test of water content % in different punch locations: Multiple comparisons dependent variable: water content % per mg/dw Tukey HSD.

PUNCH LOCATION	PUNCH LOCATION	Sig.
A	B	0.986
	C	0.989
	D	0.307
B	A	0.986
	C	1
	D	0.502
C	A	0.989
	B	1
	D	0.482

4.9. MRI Image Evaluation

4.9.1. T2 relaxation Time Analysis of Equine Cartilage

The mean T2 relaxation time of the equine cartilage for all data was 30.76 ms \pm 4.38 ms (Table 4.5). When palmar and dorsal sites were analysed, dorsal site was 30.98 ms \pm 4.8 ms and palmar site was 30.54 ms \pm 3.84 ms (Table 4.8), (Fig 4.13). Whereas lateral site, was 30.23 ms \pm 4.22 ms and medial site was 31.29 ms \pm 4.51 ms (Fig 4.14). The mean T2 relaxation time in punch A was 30.31 ms \pm 4.92 ms, B 31.64 ms \pm 4.85 ms, C 31.87 ms \pm 3.53 ms and in D punch was 29.21 ms \pm 3.72 ms (Table 4.9), (Fig 4.15). There was no significant difference was found between punch locations (Table 4.10).

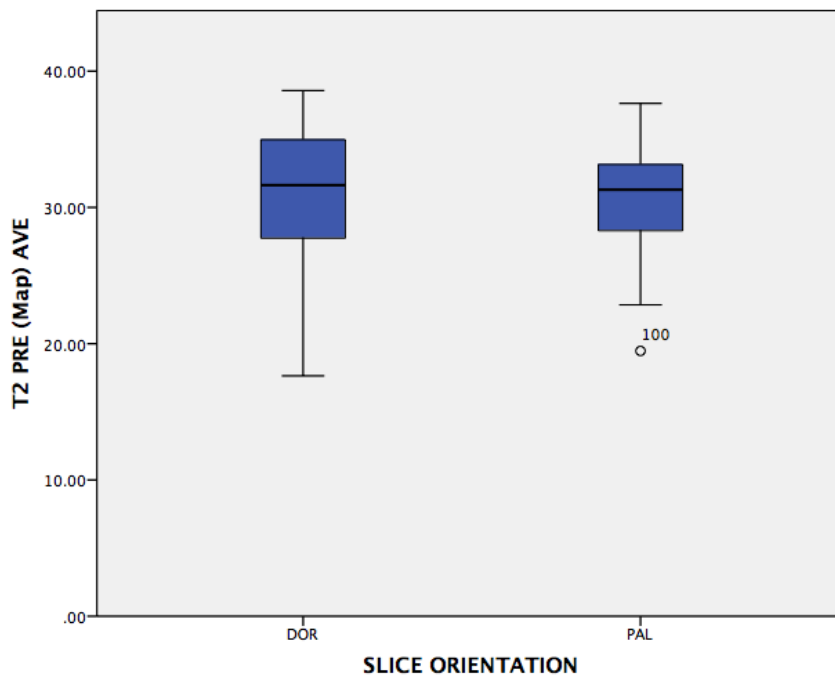


Figure 4-13: Box plot showing the T2 relaxation time (ms) for dorsal and palmar aspects of the equine cartilage. There was no significant difference between dorsal (30.98 ms \pm 4.8 ms) and palmar sites (30.54 ms \pm 3.84 ms), ($P= 0.602$).

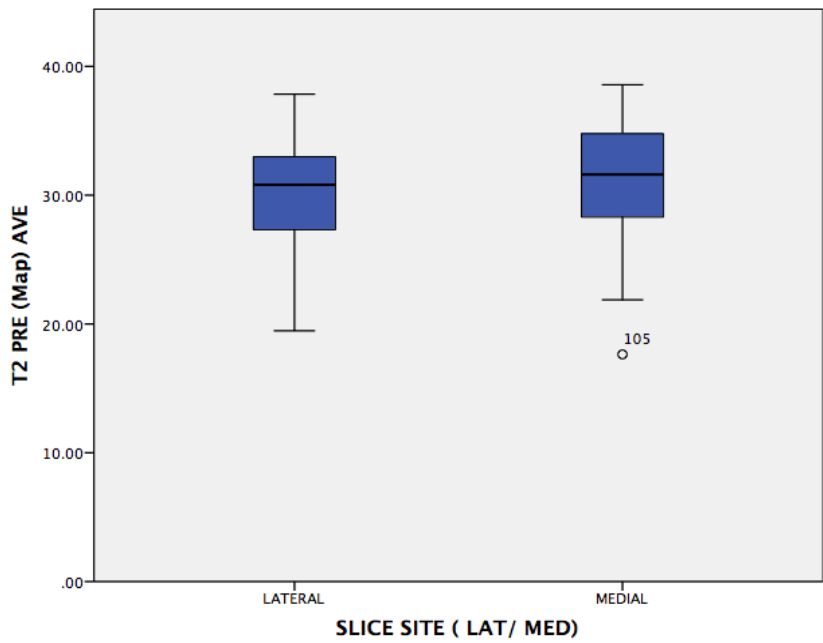


Figure 4-14: Box plot showing the T2 relaxation time (ms) in lateral and medial aspects of the equine cartilage. There was no significant difference between medial (30.23 ms \pm 4.22 ms) and lateral sites (31.29 ms \pm 4.51 ms) ($P=0.20$).

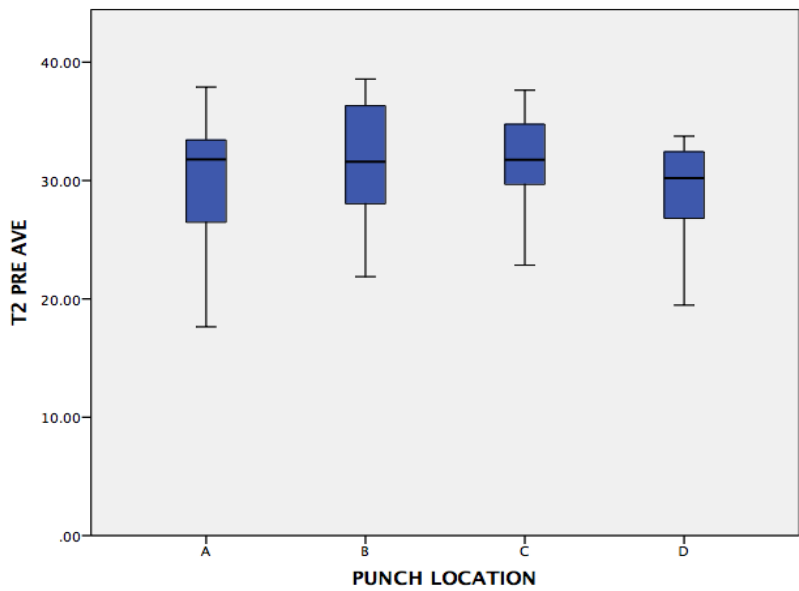


Figure 4-15: Box plot showing the T2 relaxation time (ms) of different punch location as (A, B, C & D) of the equine metacarpal-tarsal articular cartilage. There was no significant difference found between them.

Table 4-8: Paired Student's T-test of topographical difference in cartilage T2 relaxation time (ms).

	T2-wighted time ms	Std Dev	P value
Dorsal	30.98	4.8	<i>P</i> =0.602
Palmar	30.54	3.84	
Lateral	30.23	4.22	<i>P</i> =0.20
Medial	31.29	4.51	

Table 4-9: Mean and standard deviation of T2 relaxation time (ms) vs. punch location (A, B, C, and D).

PUNCH LOCATION	Mean T2 relaxation time (ms)	Std. Deviation
A	30.31	4.92
B	31.64	4.85
C	31.87	3.53
D	29.21	3.72

Table 4-10: ANOVA Post hoc t-test of T2 relaxation time (ms) in different punch locations: Multiple comparisons dependent variable: T2 relaxation time (ms) Tukey HSD.

PUNCH LOCATION	PUNCH LOCATION	Sig.
A	B	0.655
	C	0.529
	D	0.775
B	A	0.655
	C	0.997
	D	0.156
C	A	0.529
	B	0.997
	D	0.102
D	A	0.775
	B	0.156
	C	0.102
A	B	0.655
	C	0.529
	D	0.775

4.9.2. T1-weighted Pre and Post dGEMRIC Analysis (Signal Intensity)

The mean T1 signal intensity of all data points pre-contrast and post-dGEMRIC incubation was $1.74 \times 10^6 \pm 0.49 \times 10^6$, and $1.88 \times 10^6 \pm 0.49 \times 10^6$ respectively. The mean T1- signal pre- and post-dGEMRIC of the dorsal site was $1.73 \times 10^6 \pm 0.51 \times 10^6$ and $1.85 \times 10^6 \pm 0.48 \times 10^6$ respectively. The mean T1- signal pre- and post-dGEMRIC of the palmar site, was $1.75 \times 10^6 \pm 0.48 \times 10^6$ and $1.91 \times 10^6 \pm 0.49 \times 10^6$ respectively (Fig 4.16).

T1-signal pre- and post-dGEMRIC of the lateral site was $1.71 \times 10^6 \pm 0.33 \times 10^6$ and $1.85 \times 10^6 \pm 0.47 \times 10^6$ respectively; the medial site was $1.77 \times 10^6 \pm 0.62 \times 10^6$ and $1.9 \times 10^6 \pm 0.51 \times 10^6$ respectively (Fig 4.17) and (Table 4.11). When the data set was analysed according to punch location, T1 signal intensity pre- and post-contrast for punch A was $1.66 \times 10^6 \pm 0.46$ and $1.81 \times 10^6 \pm 0.48$, B was $1.80 \times 10^6 \pm 0.55$ and $1.89 \times 10^6 \pm 0.48$, C was $1.79 \times 10^6 \pm 0.50$ and $1.92 \times 10^6 \pm 0.50$, and D was $1.70 \times 10^6 \pm 0.47$, and $1.89 \times 10^6 \pm 0.50$ (Fig 4.18), (Table 4.12). When an ANOVA test was performed to investigate the difference between these groups no significant difference was found (Table 4.11).

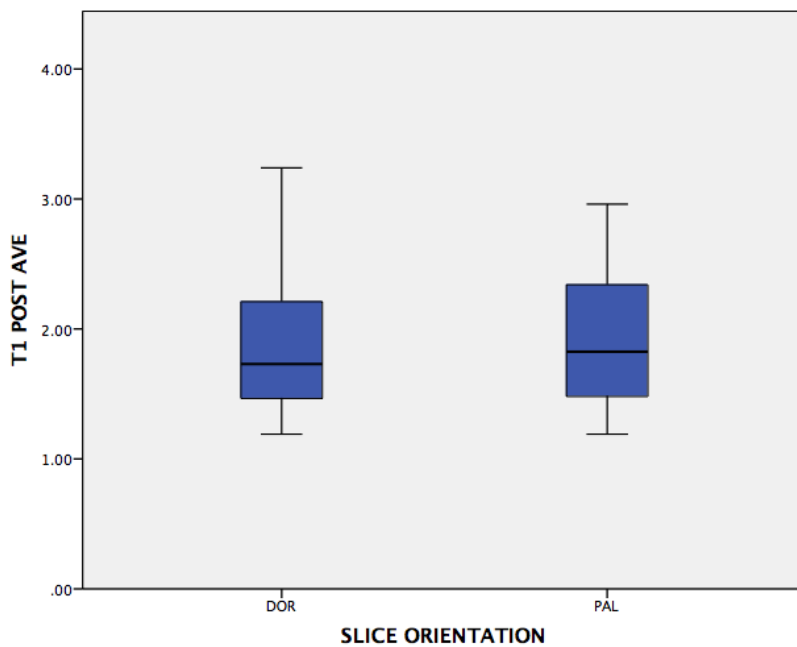


Figure 4-16: Box plot showing the T1-signal intensity post dGEMRIC incubation of dorsal and palmar aspects of the equine cartilage. There was no significant difference between palmar ($1.91 \times 10^6 \pm 0.49 \times 10^6$) and dorsal aspects ($1.85 \times 10^6 \pm 0.48 \times 10^6$).

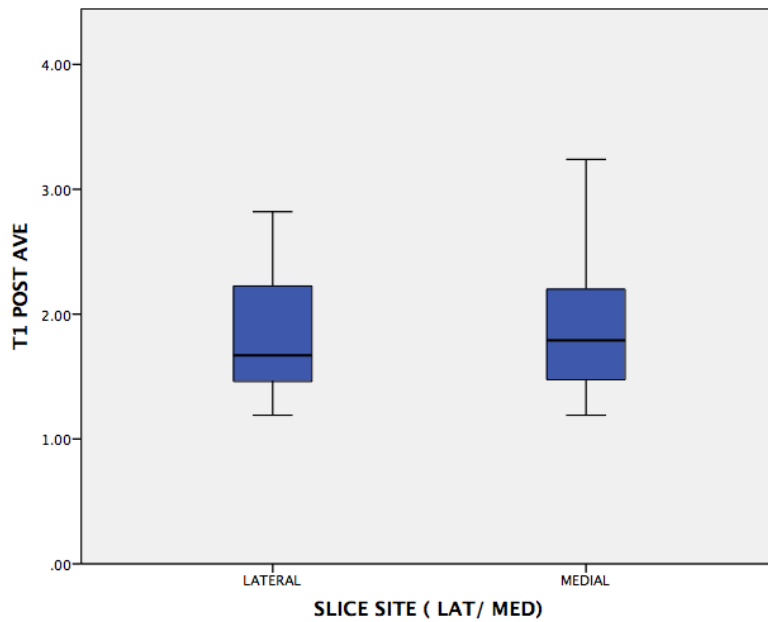


Figure 4-17: Box plot showing the T1-signal intensity post dGEMRIC incubation of lateral and medial aspects of the equine cartilage. There was no significant difference between medial ($1.9 \times 10^6 \pm 0.51 \times 10^6$) and lateral sites ($1.85 \times 10^6 \pm 0.47 \times 10^6$).

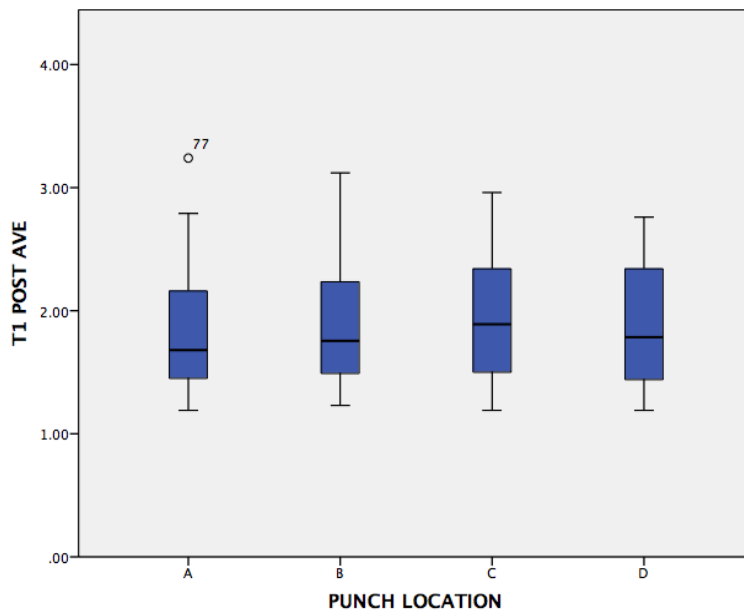


Figure 4-18: Box plot showing the T1 signal intensity of different punch location as (A, B, C &D) of the equine metacarpal-tarsal articular cartilage. No significant difference was found between them.

Table 4-11: Paired student's T-test of topographical difference in cartilage T1 signal intensity pre and post dGEMRIC.

	T1 PRE AVE x10⁶	Std Dev	P value	T1 POST AVE x10⁶	Std Dev	P value
Dorsal	1.73	0.51	<i>P</i> =0.86	1.85	0.48	<i>P</i> =0.58
Palmar	1.75	0.48		1.91	0.49	
Lateral	1.71	0.33	<i>P</i> =0.5	1.85	0.47	<i>P</i> =0.62
Medial	1.77	0.62		1.9	0.51	

Table 4-12: Mean and standard deviation of T1 signal intensity (pre & post) vs. punch location (A, B, C, and D).

PUNCH LOCATION	Mean & Standard deviation	T1 PRE AVE	T1 POST AVE
A	Mean	1.66	1.81
	Standard deviation	0.46	0.48
B	Mean	1.80	1.89
	Standard deviation	0.55	0.48
C	Mean	1.79	1.92
	Standard deviation	0.508	0.50
D	Mean	1.70	1.89
	Standard deviation	0.47	0.50

4.10. Correlation between MRI parameters and the biochemical properties of equine cartilage

4.10.1. Correlation of T1 signal intensity post (dGEMRIC) with GAG Content

T1 signal intensity post gadolinium enhancement had a moderate negative significant correlation with GAG content of all cartilage samples ($P < 0.05$) ($r = -0.354$) (Fig 4.18).

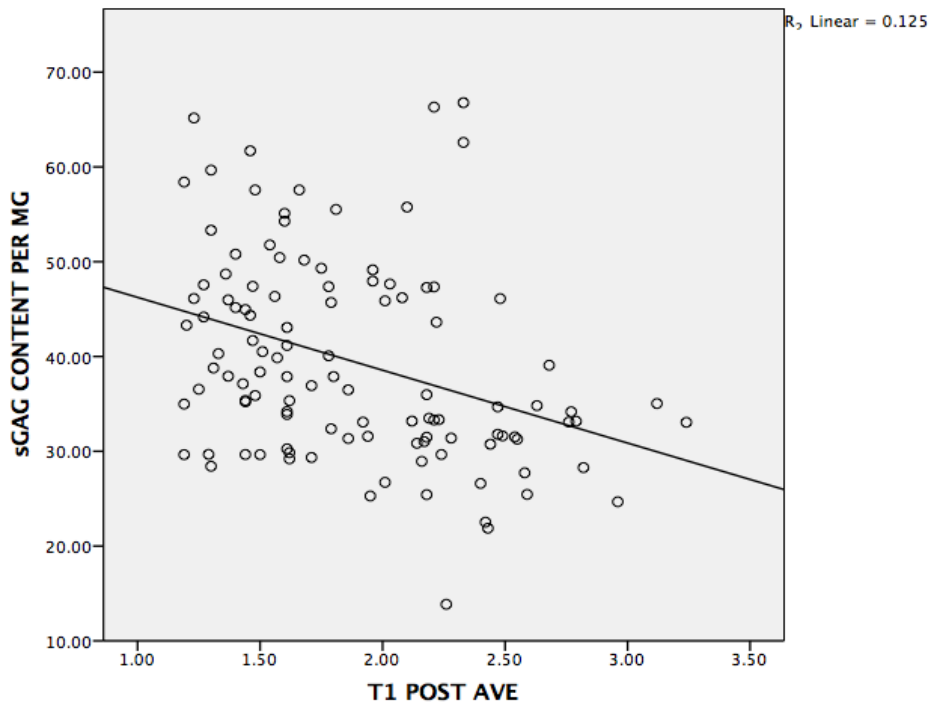


Figure 4-19: Scatter plot of glycosaminoglycan content per mg dry weight vs. T1 signal intensity post gadolinium GdDTPA²⁻. T1 signal intensity post Gadolinium was found to negatively correlate with GAG ($P < 0.05$, $r = -0.354$).

4.10.2. Correlation between water % and T2 relaxation time (ms)

There was no significant correlation observed between the water content of the equine articular cartilage and T2 relaxation time (ms) ($P=0.92$) (Fig 4.14) and (Table 4.14).

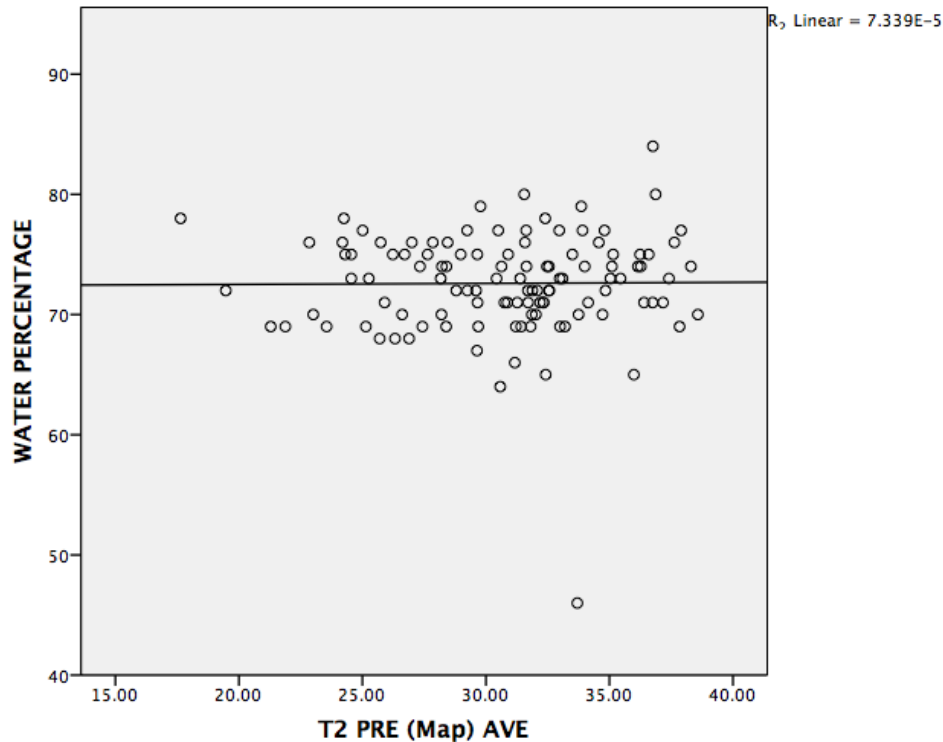


Figure 4-20: Scatter plot of the percentage water content of the equine cartilage vs. T2 relaxation time (ms).. There was no significant correlation found between the water content and T2 relaxation time of the equine cartilage ($P=0.92$).

4.11. Discussion

Recently, quantitative MRI techniques have shown promising results with several biomarkers such as dGEMRIC or T2 relaxation time mapping of the cartilage, demonstrating ability and sensitivity in detection of biochemical alteration of the articular cartilage as well as detection of early stage OA. So, in order to be applied in the clinical practice it is essential that future research studies include optimization and establishment of normal and abnormal reference ranges in order to develop sensible clinical protocols, which can be applied to the detection and assessment of early stage OA.

The results of this study suggest that dGEMRIC is worth further investigation because it has the potential to be a useful OA research tool in the future. Several studies have reported the use of dGEMRIC using clinical MRI in the human field (Welsch et al. 2008) but reports of contrast MRI in horses are very limited (Saveraid & Judy 2012). No previous validation of this technique using 7T MRI in the horse has been performed despite the potential of 7T MRI for equine research.

4.11.1. Analysing the effect of contrast agent on MRI parameters

Delayed gadolinium-enhanced MRI of the cartilage (dGEMRIC) is reportedly very sensitive to the content of glycosaminoglycan (GAG) in the articular cartilage, while T2 transverse relaxation time is sensitive to water content, the structure of collagen network and collagen content in the cartilage (Nieminen et al. 2001; Menezes et al. 2004). Since GAG and collagen molecules are the two solid components of the articular cartilage, an assessment of these components with these techniques is very useful in order to determine the quality and function of the cartilage. Several studies have described dGEMRIC techniques (Tiderius et al. 2004; Williams et al. 2005; Watanabe et al. 2009). Recently, high resolution and T1 weighted images of equine articular cartilage were acquired with and without delayed gadolinium-enhancement (Carstens et al. 2013). Several studies have found that the T1-time decreased in areas of low GAG content, as the gadolinium material accumulated in these areas (Bashir et al. 1996).

The concentration of GAG can be estimated by measuring the T1 time (signal intensity) of the articular cartilage and comparing it with the T1-time before the application of gadolinium contrast, thus allowing an indirect quantitative assessment of glycosaminoglycan content. Thus, T1 values are high in the areas of cartilage that have low concentrations of glycosaminoglycans, and low in high concentration areas (Williams et al. 2005; Krishnan et al. 2007; Crema et al. 2011). This was confirmed by this study where a negative correlation was found between T1 signal intensity and GAG concentration i.e. increasing signal intensity was correlated with decreasing GAG content.

In this study, signal intensity of T1-weighted MRI was significantly greater post gadolinium-enhancement. These findings are in agreement with low T1 signal intensity post gadolinium-enhancement in repaired human cartilage tissue (Trattnig et al. 2007), but in disagreement with after studies that have been done in both the human and equine studies (Taylor et al. 2009; Carstens et al. 2013). This disagreement could be due to different MRI protocols and scanning time (Trattnig et al. 2007). Disagreement might also be due to the unknown history of cartilage samples that were used in this study. Gross postmortem examination was performed to exclude joints with gross signs of joint disease, and therefore dGEMRIC could not infiltrate the cartilage layers and reduce the T1 time. The T1-signal intensity acquisition method used in this research does induce a variability and investigator bias in both pre and post MRI time reading. This could be due to the manual positioning of the ROI and of the samples in the scanner as the scanner does not have an automatic sample table with laser indicator. This potentially affected our measured values, as there was variation in the T1 per reading showing variability in manual RIO positioning. Moreover, these variations could be due to the demarcation between subchondral bone and cartilage, which was subjectively less clear in dGEMRIC than pre dGEMRIC. Moreover, inaccurate positioning of the ROI could be due to partial volume averaging of the MRI (Keenan et al. 2011; Wucherer et al. 2012).

4.11.2. Topographical variation in the cartilage biochemistry

Several quantitative MRI studies have shown significant variation exists in the biochemical composition of the cartilage surface of the equine metacarpal-tarsal joint. This variation between locations, such as lateral or medial sites, is due to different load-bearing demands. This variation could alter the MRI parameters, resulting in site-specific differences in quantitative MRI results (Brama et al. 2000; Lee et al. 2014).

The results of this study revealed that there was a significant variation in sGAG between different site locations, as the dorsal condyle had higher sGAG content than the palmar condyle. This result is in agreement with the findings of Brama and colleagues (Brama et al. 2000). There was also no significant difference appreciated between lateral and medial aspects in this study, which again is in agreement with the

findings of Brama and colleagues. However, the mean cartilage GAG content found by Brama et al was between 45.5 µg/mg/dw and 50.4 µg/mg/dw (Brama et al. 2000), whereas our value was only 39.45± 10.65µg/mg/dw.

The difference in GAG content could be due to several reasons. First, specimen history was unavailable in this study and only gross postmortem examination was undertaken to check for early signs of OA. Therefore there is the potential that the cartilage specimens had lowered GAG content as a direct result of early onset OA (Mosher et al. 2000). Second, the PG assay cartilage samples were taken after considerably long MRI scanning time and the presence of the contrast medium may have resulted in some degree of PG degradation mainly since the gadolinium is known to alter surrounding macromolecules (Wheaton et al. 2004b). Finally, the PG assay is known to be subject to several fundamental errors making comparison between studies difficult, mainly due to the issue with GAG complex precipitation (Goldberg & Kolibas 1990). The PG assay is also mainly responding to the chondroitin sulphated and keratin sulfate, and the assay is only sensitive to 70% of the keratin sulfate. Thus, individual samples may vary in the relative amounts of chondroitin sulphated and keratin sulfate and this could affect the GAG content (Stevens et al. 1982).

4.11.3. Correlation between MR imaging parameters and biochemical features of the equine cartilage

Correlation analysis of T1-signal intensity and GAG showed significant negative correlation, which is in agreement with what was found by Nieminen et al. (Nieminen et al. 2002). Furthermore, injection of gadolinium resulted in overall shortening of T1-relaxation time, so GAG concentration can be measured by a change in signal intensity on T1 MRI (Bashir et al. 1999). That is to say the presence of gadolinium shortens T1-signal intensity relaxation time, so, cartilage with low GAG concentration had a relatively low T1 gadolinium-enhanced (dGEMRIC) value.

The GAG concentration is proportional to the dGEMRIC value, and the areas that have low T1 values can be interpreted as low GAG regions (Xia et al. 2008). When T2-weighted time and water data points were analysed, there was no significant

relationship found between them. This result was not expected, as T2 time should increase linearly as increase in the water content of all cartilage samples (Chou et al. 2009). Such a positive result was not have been observed, but could be due to the small range of water content values analysed in this study.

4.12. Conclusion

Quantitative MRI techniques such as dGEMRIC or T2 relaxation time are thought to be key to increasing our understanding of the pathogenesis of OA. It is hoped that in the future this will lead to more accurate diagnosis and provide appropriate treatment leading to a better outcome for horse with OA. This study demonstrates that MRI can be used quantitatively in the research setting; potentially future work may take this technique in to the clinical setting. This unique study looked into this complex relationship between the early onset OA marker and its quantitative MRI parameters in the horse using ultra-high 7T MRI. However, ultra-high field magnets are not used in equine practice due to its limited availability and high cost. However, 3T MRI is now available in at least two equine hospitals worldwide and will likely increase. Delayed gadolinium-enhanced (dGEMRIC) technique appears to provide a feasible quantitative tool for assessing articular cartilage properties, which could be used in clinical trials.

However, these quantitative parameters cannot fully characterise the biochemical properties of the cartilage. Delayed gadolinium-enhanced (dGEMRIC) techniques are time-consuming and T2 mapping is very complex, however there may be other quantitative MRI techniques to examine the biochemical properties of the equine cartilage. Recently, people have been using sodium MRI to study cartilage and it has shown promise to image the biochemistry of the cartilage potentially leading to early diagnosis of OA. Therefore, the next two chapters are going to validate sodium MRI techniques and biochemical assays such as flame photometry and PG assay using 7T MRI of equine cartilage.

Chapter 5 *In Vitro* Quantitative Sodium MRI of Equine MC3/MT3 Articular Cartilage

5.1. Introduction

Articular cartilage degeneration is a major component of the pathology of osteoarthritis (OA), which leads to joint pain. Poor performance as a result of OA is one of the most important musculoskeletal diseases affecting horses and causes economical loss through loss of days and racing (Rossdale et al. 1985). Recently, researchers have used sodium MRI to look at the health status of articular cartilage in humans and to assess articular cartilage degeneration (Madelin et al. 2014). Sodium concentration is associated with the proteoglycan (PG) content in the articular cartilage (Paul et al. 2000). Therefore, Na MRI is potentially a non-invasive technique to quantify PG loss in the cartilage (Lesperance et al. 1992; Jelicks et al. 1993), which is suggested to be the early signature of osteoarthritis (Mankin et al. 1981; Van De Loo et al. 1994).

So far, no study has examined the potential of T1-weighted sodium MRI to quantify the Na content of equine articular cartilage, which could be useful to identify early stage OA in equines. Therefore, the goal of this study was to measure the sodium content of equine articular cartilage and compare these findings with biochemical parameters including sulphated glycosaminoglycans (sGAG) and sodium ions (Na⁺).

5.2. Sodium MRI

OA is usually diagnosed in clinical practice by conventional radiography as the presence or absence of osteophytes, narrowing of articular space and abnormality of the adjacent anatomical structures (Rogers et al. 1990). The early degenerative changes of articular cartilage associated with OA are usually accompanied by proteoglycan depletion in the articular cartilage matrix (Reddy et al. 1998). During the early stage of OA, the articular cartilage loses proteoglycans molecules, which have negative charge density and play an essential role in controlling tissue integrity through providing fixed charge density of the articular cartilage. The sulphate and carboxylate groups of the PG attract free-floating positive Na^+ from the extracellular matrix (ECM), where the Na concentration is 10 times higher than the intracellular concentration. Since PGs are hydrophilic water molecules are accumulated due to osmotic pressure in the cartilage. Then, due to the strong electrostatic repulsive force between glycosaminoglycans molecules, PG molecules are separated and causes compressive stiffness of the cartilage (Lesperance et al. 1992; Insko et al. 1999; Zbýň et al. 2014).

Several MRI studies have investigated articular cartilage structure abnormalities using both *in vivo* and *ex vivo* techniques (Brossmann et al. 1997). Numerous studies found that Na MRI is correlated with the proteoglycan content, and is sensitive to small changes in proteoglycan concentration (Shapiro et al. 2002a; Wheaton et al. 2004a). Na MRI can be used as a method of detecting and looking at the early stages of proteoglycans depletion and a non-invasive technique to look at the cartilage health status within the body (Borthakur et al. 2000; Shapiro et al. 2000a). Furthermore, quantitative Na MRI study has shown that Na concentration is helpful in detecting small loss of PG in degenerative bovine cartilage (Insko et al. 1999). However, to date no studies have examined the ability of Na MRI to quantify biochemical parameters in equine cartilage.

Sodium (^{23}Na) ions in the living body play an essential role in cellular homeostasis and cell viability. Na MR image studies have shown that the relaxation times of Na nuclei are altered in degraded cartilage, which is linked to PG loss. Positively charged

Na ions are attracted to negatively charged GAGs to maintain overall electroneutrality and therefore distribute according to the GAG content (Shapiro et al. 2000a). Therefore, Na MRI images are less intense for degraded cartilage. Several *in vitro* studies have shown that sodium MRI can measure cartilage GAG content indirectly.

Several efforts have been made to develop this technique and make it a useful tool to use *in vivo*. Presently, sodium MRI has been used to evaluate articular cartilage health status as well as a predictive method for osteoarthritis. For instance, a recent study described the ability of sodium MRI to detect the early onset of osteoarthritis in human ballet dancers (Chang et al. 2014). However, MRI is challenging, as sodium emits a low detectable MR signal in the articular cartilage due to comparatively low Na content in the body biological tissues. So high magnetic field strength and additional hardware and software are required to improve the image quality and make it reliable tool for clinical imaging (Zbýň et al. 2014).

5.3. Aims and Objectives

This study aimed to investigate the ability of sodium MRI to non-invasively assess the biochemical characteristics of the equine articular cartilage. It was hypothesised that sodium MRI would be able to quantifying tissue (cartilage) properties that are associated with the early stages of osteoarthritis in equines. In particular, it was hypothesised that sodium MRI signal intensity values would correlate with the cartilage sodium ion and sGAG content.

The specific objectives of this study were as follows::

- I. To determine sodium MRI signal intensity in normal equine articular cartilage as well as investigate whether topographical variation exists.
- II. To measure proteoglycan content of normal equine articular cartilage and describe any topographical variations within normal equine cartilage.
- III. Measure sodium content in normal equine articular cartilage using gold standard flame photometer technique.

Investigate whether any correlations exist between sodium MRI parameters and biochemical properties.

5.4. Materials and Methods

5.4.1. Samples Collection and Preparation

Nine forelimbs were collected from eight Welsh ponies aged 16-18 months that were euthanised for reasons unrelated to this study. The metacarpal/tarsal condyles were harvested and kept in a freezer (-20°C) until the study. Samples were defrosted 24h prior to MRI study.

5.4.2. Agarose Phantom Preparation

To determine the agarose concentration with a T2 relaxation time equal to cartilage a series of agarose phantoms (1, 2, 4, 6 and 7.5%) were produced by adding the required amount of ultrapure agarose to 100 ml of deionised water (Shapiro et al. 2000b; Nagel et al. 2013). This part of the study aimed to establish the agar concentration that has a similar T2 signal as cartilage, as knowing the T1 and T2 properties of the cartilage and the agar gel phantoms allowed appropriate calibration of the Na phantoms (Shapiro et al. 2000a). Then, T2 mapping of the phantoms and a slice of equine articular cartilage was performed using 7T ultra-high field magnet using a dual tuned quadrature $^{23}\text{Na}/^1\text{H}$ coil (Table 5.1) and (Fig 5.1). MR images were reconstructed and processed to measure T2 relaxation times using MRI software (Fig 5.1). The T2 relaxation time of the phantoms and articular cartilage was determined. A standard curve of agar percentage and T2 relaxation time was produced (Fig 5.4) and the agar percentage with the same T2-relaxation time (42 ms) as the equine articular cartilage was calculated. Afterward, sodium phantoms were prepared with different sodium concentration to establish a sodium standard curve (Madelin et al. 2010; Chang et al. 2012), that has the same T2- times as the articular cartilage.

Table 5-1: MRI Technical Information.

	T2 map MRI
Slice thickness (mm)	3
Repetition time (RE)	100
Echo time (TR/TE)	6/8
MRI acquisition type and Flip angle	2D, 30°
Matrix	240x140
Resolution (microns)	250x250
Flip angle	30

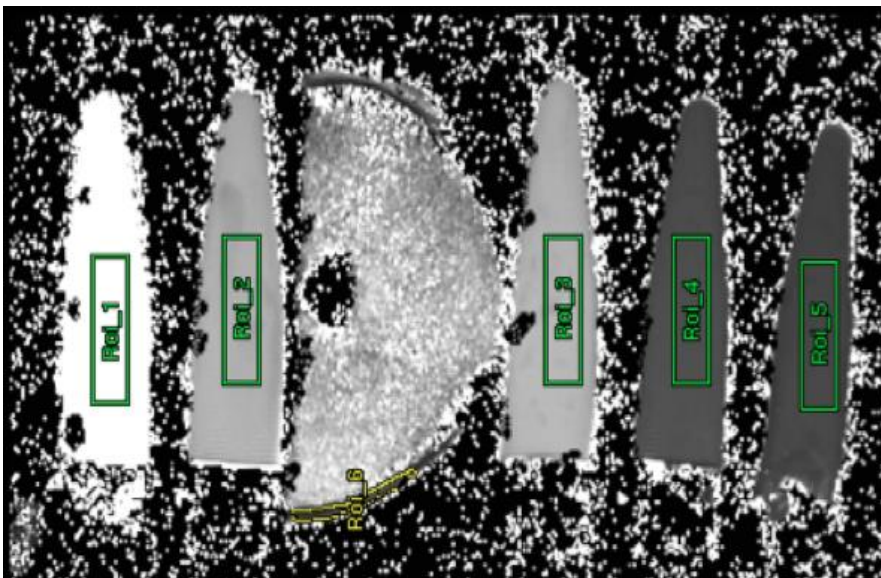


Figure 5-1: T2-time mapping image analysis. Using the geometry tool, a triangular track tool was used to draw a triangular ROI (ms) in each agarose phantom. Then 4mm line was plotted. The track tool was used to manually draw the ROI around the cartilage, making sure that only the cartilage area was included. The value obtained from this image represent the T2-weight time map.

5.4.3. Sodium Phantom Preparation

A series of sodium phantoms were prepared as 50, 100, 150, 200, 220 and 300 mM in 6.2 % ultrapure agar in 1.5 ml Eppendorf Microcentrifuge tubes (Shapiro et al. 2000a).

5.4.4. Sodium MR Imaging Technique

All cartilage samples were scanned with a 7T ultra-high field magnet using a dual tuned quadrature $^{23}\text{Na}/^1\text{H}$ coil (PulseTeq Limited, Chobham, Surrey, UK). Firstly, high field T1-weighted H^+ images were obtained using a gradient echo (FLASH) sequence with TR/TE= 120/3.5ms, scan time of 17mins 55 seconds. Secondly, T1-weighted Na^+ MR scans were performed of the entire metacarpal condyle (Table 5.2).

Table 5-2: Table describing the sodium MRI protocol information.

	Sodium MRI protocol	T1-weighted protocol
Slice thickness	4mm	4mm
Repetition Time	123ms	120/3.5ms
Echo time	3.6756ms	120/3.5ms
Scanning type	23Na_FLASH2D_Tr75_1_1_4mm	FLASH2D_3D_Tr30ms
Flip angel	12.97°C	30°
Resolution	250x250 microns	250x250 microns
Scan time	6 hour 65 min	17mins 55 seconds
Matrix	1325x762	240x140

5.4.5. T1-weighted Hydrogen Images

Standard T1-wighted H^+ localizer images were acquired, which were then used to plan the sodium scans using a dual tuned quadrature $^{23}\text{Na}/^1\text{H}$ coil.

5.4.6. Sodium Image Analysis

All images were acquired with the Na phantom at the same time. After Na MRI scanning all images were analyzed, reconstructed and processed to measure Na mapping using MRI software (Bruker ParaVision version 5.0). Several rectangular RIO were drawn in the Na phantoms. 4mm RIO were drawn manually, in dorsal, middle and palmar areas of the articular cartilage (Fig 5.2).

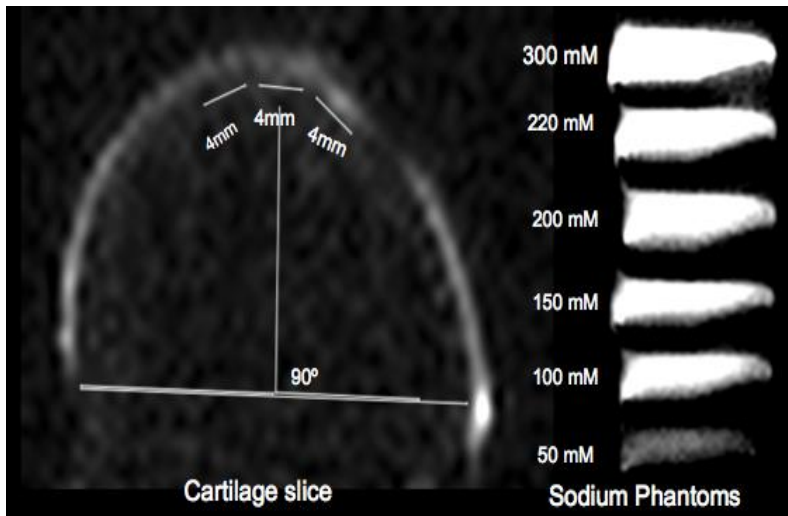


Figure 5-2: Sodium MR image analysis. Using the geometry tool, a straight line was drawn between the two end points of the semi-circular blocks. Then, a perpendicular line was plotted from the centre of the straight line. From this centre line two other 4mm lines were drawn to represent the central palmar and the central dorsal ROIs. To ensure that only the cartilage area was included, the track tool was used to manually draw around the cartilage (A). Afterwards, a triangular track tool was used to draw triangular area ROIs, to measure sodium signal in each phantom. The value obtained represents the average sodium signal intensity with in the ROI (A&B).

5.4.7. Collection of Articular Cartilage Samples for GAG and Flame Photometer Assays

Articular cartilage samples (n=68) were harvested from the regions of interest following imaging using a 4mm biopsy punch. Half of these samples were used for sGAG measurement and the other half were used to measure Na concentration using flame photometry. After harvesting of the articular cartilage, each sample was weighed using a laboratory balance and placed in a 1.5ml Eppendorf tube. All tubes were placed in a dry oven at 60°C overnight and then weighed again to measure the dry weight and calculate GAG amount using PG assay and sodium content using flame photometer method.

5.4.8. Proteoglycan Assay

Dried cartilage samples (1-4mg) were weighed after overnight incubation in the oven at 60°C, and placed in 1.5ml polypropylene tubes (Sigma). Sulphated glycosaminoglycans were quantified using a commercially available assay as previously described (page 90). Dried cartilage samples were digested in 1ml of papain extraction reagent (Blyscan, Sulphated Glycosaminoglycan Assay, Biocolor, County Antrim, UK).

5.4.9. Sodium Concentration Measurement Using Flame Photometer Method

Each sample was placed in a 10ml plastic test tube containing 5ml of 6mM nitric acid and vortexed to ensure that the cartilage sample was fully covered with nitric acid. Samples were incubated in a hot water bath (80°C) for 120 min and vortexed every 30 min until dissolved completely. All cartilage samples and sodium standard samples were analyzed using a flame photometer (410 Flame Photometer, Sherwood Scientific Ltd, Cambridge, UK). A standard calibration curve was calculated using sodium solutions of known sodium concentration (20, 40, 60, 80 and 100µg/ml). After calibration of the flame photometer, all cartilage samples were analyzed and the amount of sodium for each sample was determined using the standard curve (Fig 5.3). Sodium content was expressed as sodium per mg of dry weight.

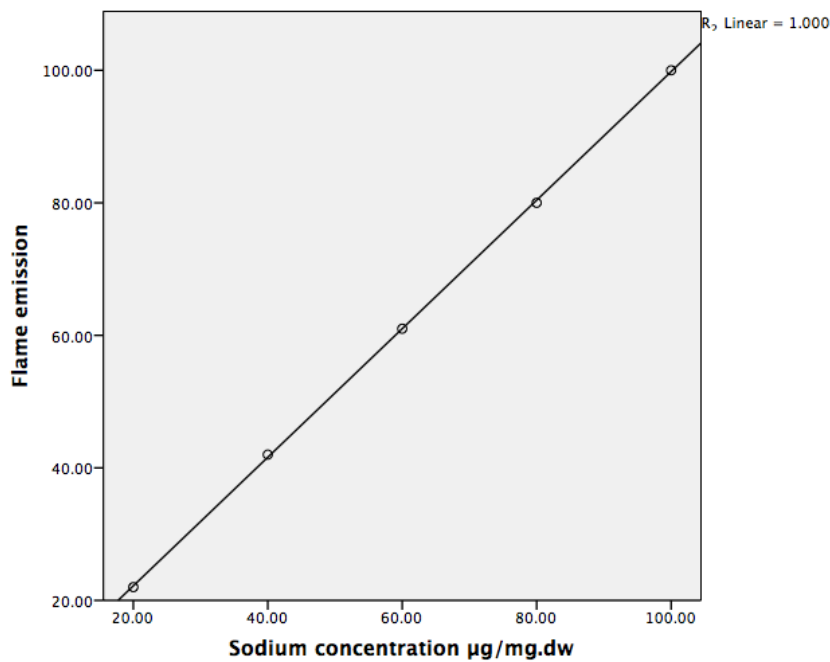


Figure 5-3: Standard curve, used to measuring the concentration of cartilage sodium, acquired from 5 standards with different concentrations measured by flame photometer ($r=1$).

5.5. Statistical Analysis

All variables were analysed using a commercially available statistical software program (SPSS Advanced Statistics 20.0, BM Corporation Armonk U.S.A). All data was confirmed to have a normal distribution using Shapiro-Wilks statistical tests before further statistical tests were performed. The effect of topography (i.e. dorsal, middle, palmar site) in biochemical characteristics such as GAG content, sodium content and MRI parameter of sodium MR images was determined using one-way ANOVA at 95% confidence significant level. The correlation between sodium MRI value and biochemical characteristics was determined using Pearson rank correlation test.

5.6. Results

5.6.1. Agarose T2 Time Mapping

Using the standard curve equation an agarose percentage of 6.2% was calculated to have a T2-relaxation time equal to that of articular cartilage (42 ms) (Fig. 5.4).

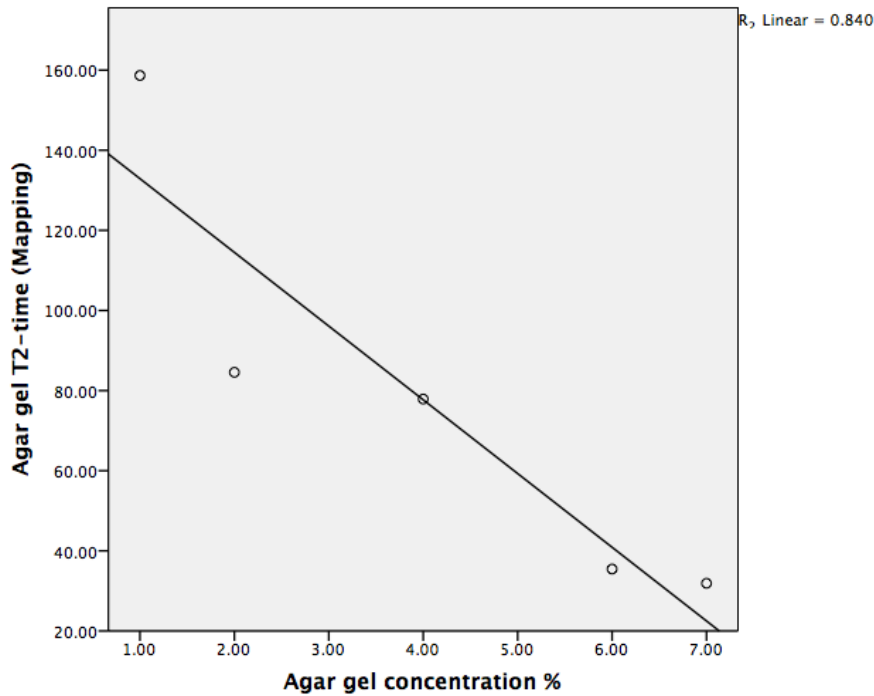


Figure 5-4: Standard curve scatter plot of the agarose T2-time (ms) and agar concentration (%) ($r=-0.917$). The agarose concentration for Na study phantom was calculated using this standard curve equation.

5.6.2. Sodium MRI Standard Curve

The standard curve of sodium signal intensity from the sodium concentration phantoms was used to determine the amount of sodium in the cartilage (Fig 5.5).

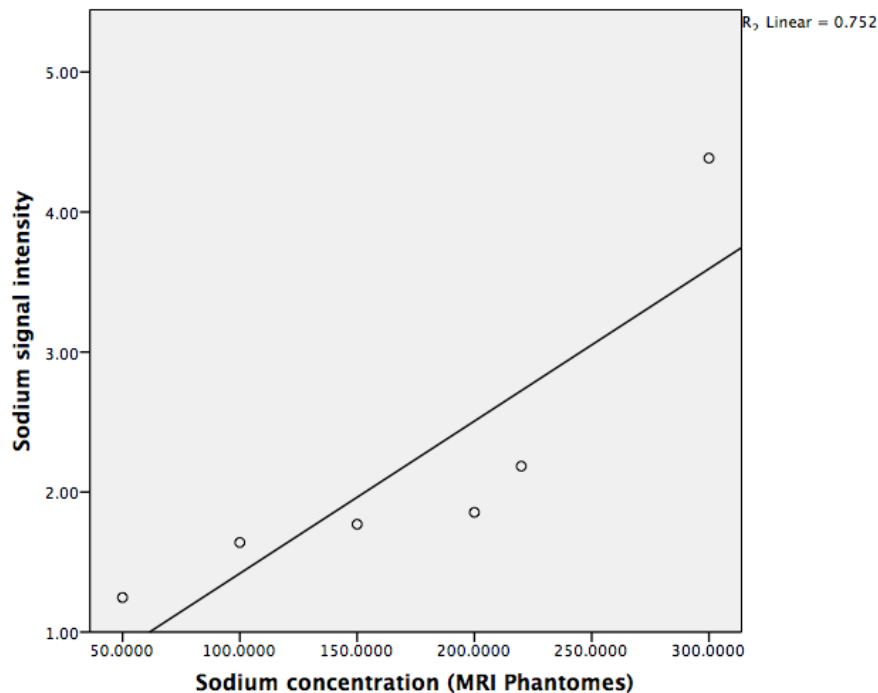


Figure 5-5: Standard curve used to determine the amount of cartilage sodium, acquired from 6 standards with different concentration measured using 7T sodium MR images ($r=0.867$).

5.6.3. Sodium MRI Analysis vs. GAG

5.6.3.1. Sodium MRI Analysis

The mean sodium content for all samples was 224.93 mM/l \pm 84.25 mM. When these samples were analysed by punch location, the mean sodium content of dorsal samples was 234 mM \pm 88.32, middle 236.56 mM \pm 95.94 mM and palmar 201mM \pm 62.70 mM. The middle samples had the highest sodium content then dorsal and palmar respectively (Fig 5.6). There was no significant difference found between the various punch locations ($P= 0.363$) (Fig 5.6).

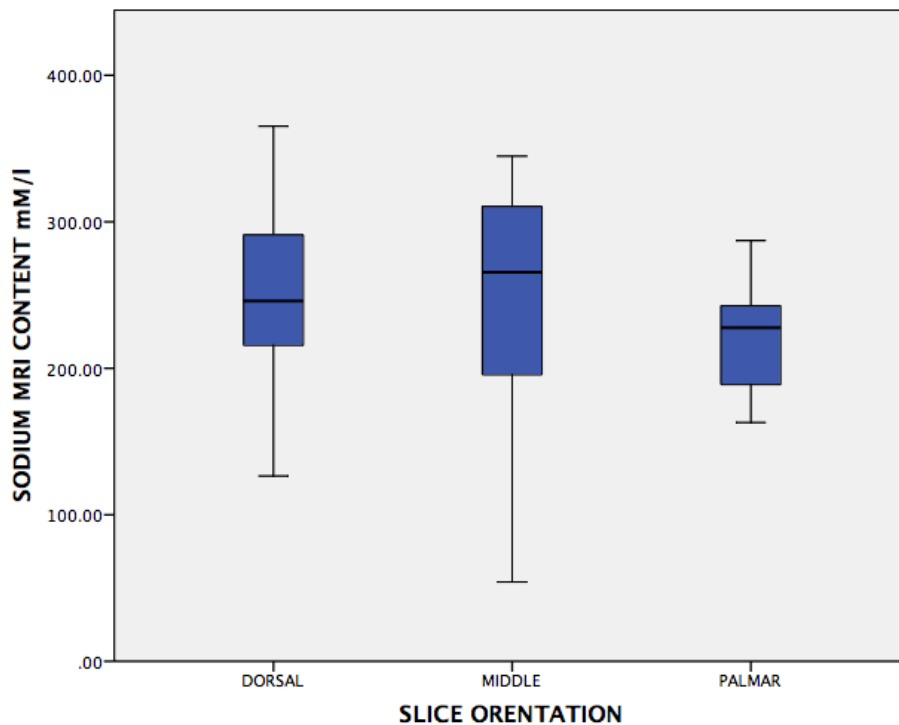


Figure 5-6 Box plot describing the sodium content determined by MRI at three articular surface sites. There was no significant difference observed between sites.

5.6.3.2. Proteoglycan Assay

The mean GAG content for all samples was $33.41 \pm 6.71 \mu\text{g}/\text{mg}/\text{dw}$. The middle cartilage samples had the highest GAG content ($36.65 \pm 4.92 \mu\text{g}/\text{mg}/\text{dw}$). The dorsal and palmar sites contained $31.85 \pm 7.25 \mu\text{g}/\text{mg}/\text{dw}$ and $31.22 \pm 6.74 \mu\text{g}/\text{mg}/\text{dw}$ respectively. There was significant difference between dorsal and palmar sites ($P=0.021$). GAG content was significantly greater in the middle punch site than the palmar site ($P=0.036$). There was no significant difference found between dorsal and middle sites ($P=0.056$) (Fig 5.7).

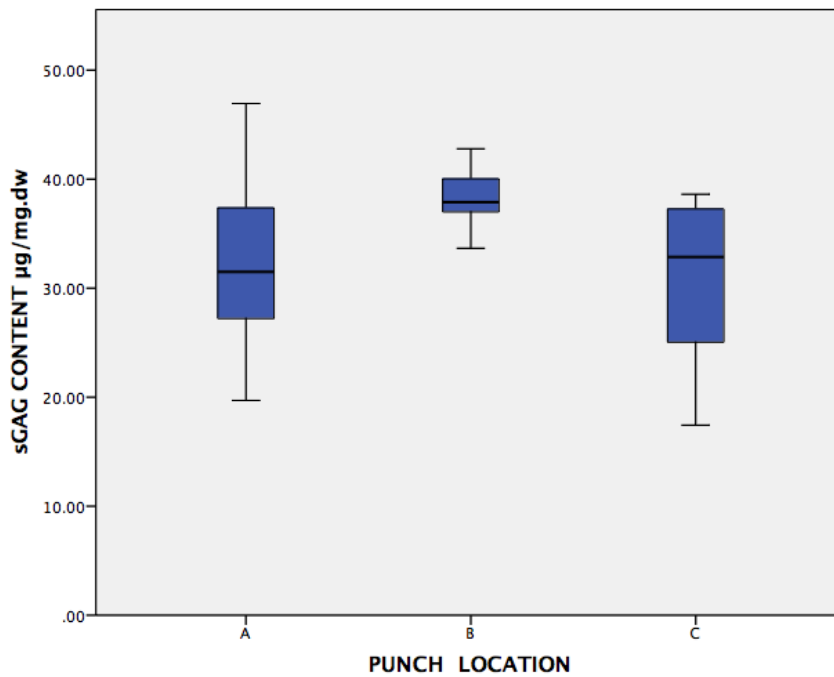


Figure 5-7: Box plot describing the GAG content at different punch locations. A= dorsal, B= middle and C= palmar. The middle site of the articular surface had a significantly greater GAG content than palmar sites ($P=0.036$).

5.6.4. Sodium MRI vs. Sodium (Flame Photometer)

5.6.4.1. Sodium MRI

Overall the mean sodium MRI content for the second part of this study was 319.16 mM \pm 137.88 mM. The middle cartilage samples had greater amount of sodium content 343.34 mM \pm 170.04 mM than dorsal 342.81 mM \pm 96.68 mM and palmar site 275.87 mM \pm 129.18 mM. There was no significant difference between sites ($P=0.203$) (Fig 5.8).

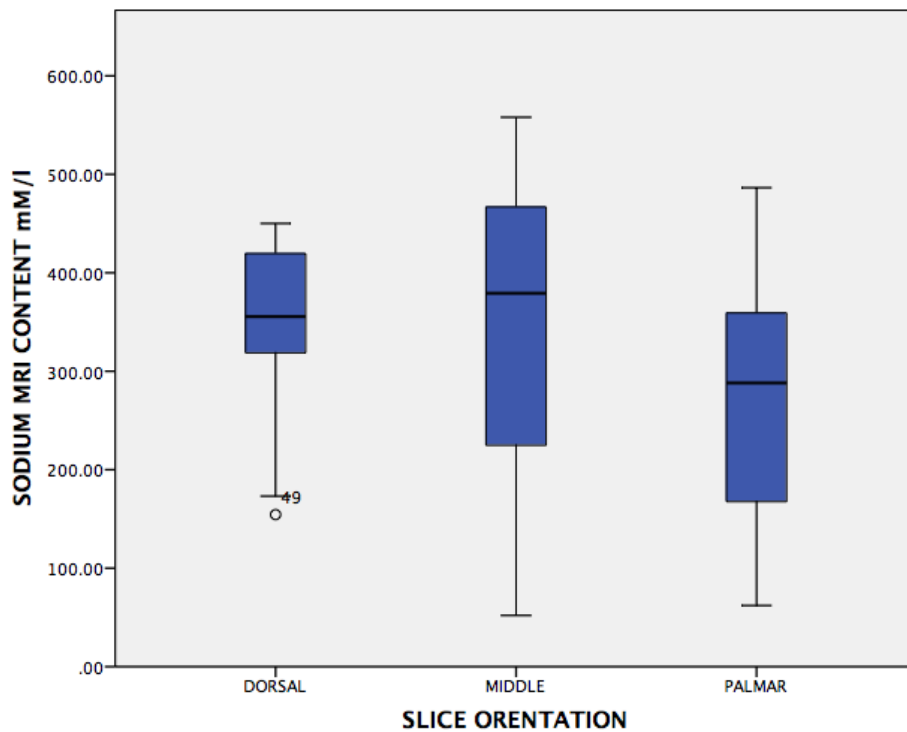


Figure 5-8: Box plot describing the distribution of sodium content MRI in the articular cartilage samples. The middle site had the greatest sodium content 343.34 mM \pm 170.04 mM. There was no significant difference between sites ($P= 0.203$).

5.6.4.2. Sodium content (Flame Photometer)

When all sodium content (flame photometer) data was analysed the overall sodium content was 136.92 $\mu\text{g}/\text{mg}/\text{dw}$ \pm 41.51 $\mu\text{g}/\text{mg}/\text{dw}$. When ANOVA test was performed, there was significant difference effect of site on sodium content of all cartilage samples ($P=0.05$). The middle cartilage samples had significantly greater sodium content (161.11 \pm 45.91 $\mu\text{g}/\text{mg}/\text{dw}$) than the dorsal (123.60 \pm 36.67 $\mu\text{g}/\text{mg}/\text{dw}$) and palmar sites (125.19 \pm 31.48 $\mu\text{g}/\text{mg}/\text{dw}$). When all cartilage samples were analysed by cartilage site, a statistically significant difference was found between middle and palmar sites ($P=0.013$), as well as between middle and dorsal ($P= 0.015$) (Fig 5.9).

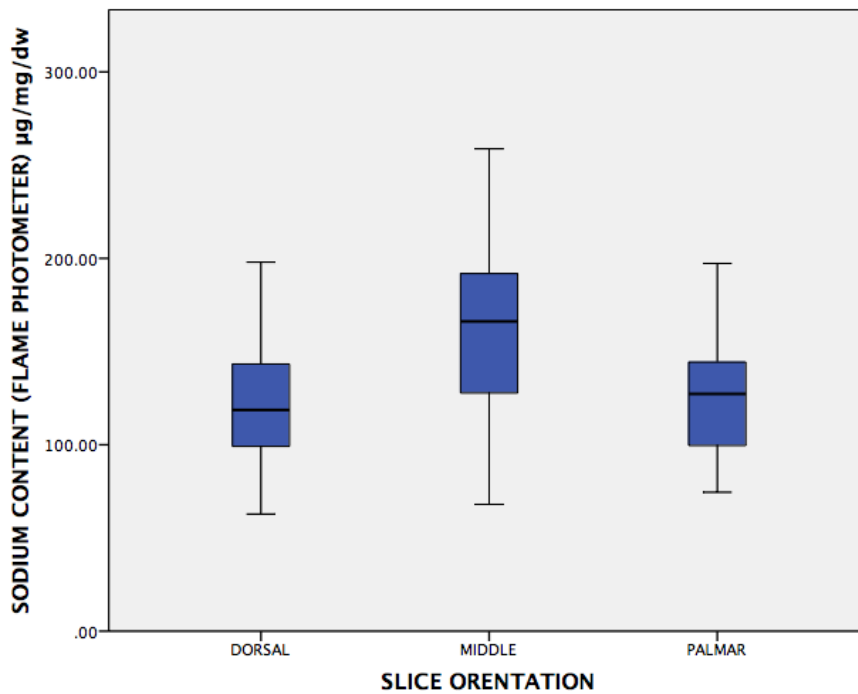


Figure 5-9: Box plot describing the distribution of sodium content determined using flame photometry for the dorsal, middle and palmar sample sites. Significantly greater sodium content was observed in the middle site compared with other sites ($P=0.006$), whereas no significant difference ($P=>0.05$) was observed between dorsal and palmar sites.

5.6.5. Correlation

5.6.5.1. Correlation Between Sodium MRI and GAG Content

Overall, a moderate positive significant correlation was observed between sodium MRI results and GAG content ($P=<0.004$, $r= 0.38$) Figure (5.10), Table (5.3). When the dorsal site was analysed separately sodium MRI content was not significantly correlated with GAG content ($P=>0.05$), $r= 0.115$) (Figure 5.11), (Table 5.4). Sodium MRI content of the middle site had a statistically significant positive correlation with GAG content ($P=0.002$), $r= 0.640$) (Figure 5.11), (Table (5.4). There was no significant correlation between sodium MRI content palmar site with GAG content ($P=0.77$), $r= 0.079$) (Figure (5.11), (Table 5.4).

Table 5-3 Pearson rank correlation test between sodium MRI content vs. GAG content all the data set.

		Correlations	
		sGAG CONTENT $\mu\text{g}/\text{mg}\cdot\text{dw}$	
SODIUM MRI CONTENT mM/l	Pearson Correlation	0.381 **	
	Sig. (2-tailed)	0.004	
	N	55	

** Correlation is significant at the 0.01 level (2-tailed).

Table 5-4: Pearson rank correlation test between sodium MRI content vs. GAG content for all cartilage punches.

		GAG CONTENT $\mu\text{g}/\text{mg}/\text{dw}$		
		Dorsal	Middle	Palmar
SODIUM MRI CONTENT mM	Pearson Correlation	0.140	0.640 **	0.079
	Sig.(2 tailed)	0.58	0.002	0.77
	Number	20	20	20

** Correlation is significant at the 0.01 level (2-tailed).

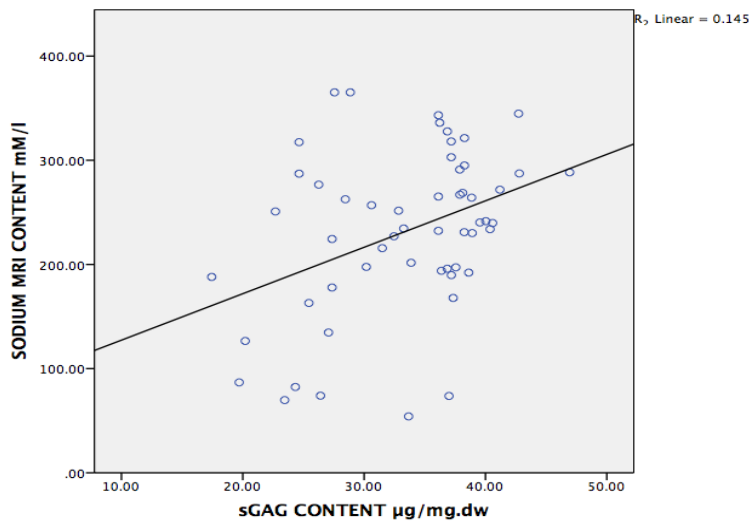


Figure 5-10: A scatter plot of sodium MRI content (mM/l) and glycosaminoglycan content ($\mu\text{g}/\text{mg}$ dry weight). Pearson correlation plot for all data points. A moderate positive correlation was observed between sodium MRI content and glycosaminoglycan content ($P < 0.004$, $r = 0.38$).

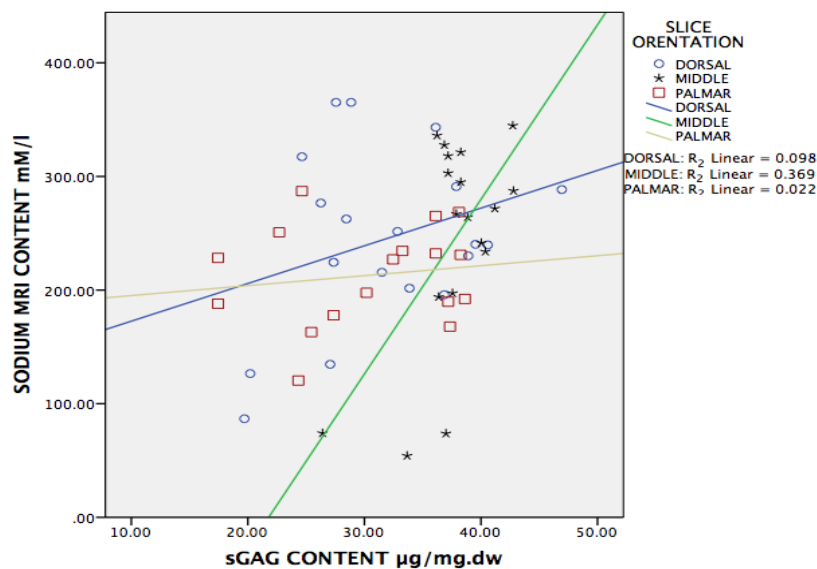


Figure 5-11: Scatter plot of sodium MRI content (mM/l) and glycosaminoglycan content ($\mu\text{g}/\text{mg}$ dry weight). Pearson correlation plot for all data points. When only dorsal site data points are analysed, there was no significant correlation between sodium MRI content and glycosaminoglycan content (purple circles). When only middle data points are analysed, there was a statistically significant positive correlation between sodium MRI content and GAG content (black stars). When only the palmar data points were analysed there was a strong positive correlation observed between sodium MRI content and glycosaminoglycan content (red squares).

5.6.5.2. Correlation Between Sodium MRI vs. Sodium (Flame Photometer) Content

When all the sodium MRI data results were analysed against sodium content (flame photometer), sodium MRI content was found to moderately and positively correlate with sodium content (flame photometer) ($P=0.001$), $r= 0.451$) (Figure 5.12), (Table 5.5). When dorsal site data points were analysed separately sodium MRI content was found to not correlate with sodium (flame photometer) content (Figure 5.13), (Table 5.6). Sodium MRI content had a strong positive correlation with sodium (flame photometer) content when only middle data points were analysed ($P=0.001$), $r= 0.71$) (Figure 5.13), (Table 5.6). However, when palmar site data points were analysed individually, sodium MRI content was found to weakly correlate with sodium (flame photometer) content (Figure 5.13), (Table 5.6).

Table 5-5: Pearson rank correlation test between sodium MRI content vs. sodium content (flame photometer).

	Correlations	
SODIUM MRI CONTENT mM/l	SODIUM CONTENT (FLAME PHOTOMETER) $\mu\text{g}/\text{mg}/\text{dw}$	
	Pearson Correlation	0.451 **
	Sig. (2-tailed)	0.001
	N	63

** Correlation is significant at the 0.01 level (2-tailed).

Table 5-6 Pearson rank correlation test between sodium MRI content vs. sodium content (flame photometer) for different punch locations.

		SODIUM CONTENT (FLAME PHOTOMETER) $\mu\text{g}/\text{mg}/\text{dw}$		
		Dorsal	Middle	Palmar
SODIUM MRI CONTENT mM	Pearson Correlation	0.297	0.71**	0.107
	Sig.(2 tailed)	0.282	0.001	0.643
	Number	21	21	21

** Correlation is significant at the 0.01 level (2-tailed).

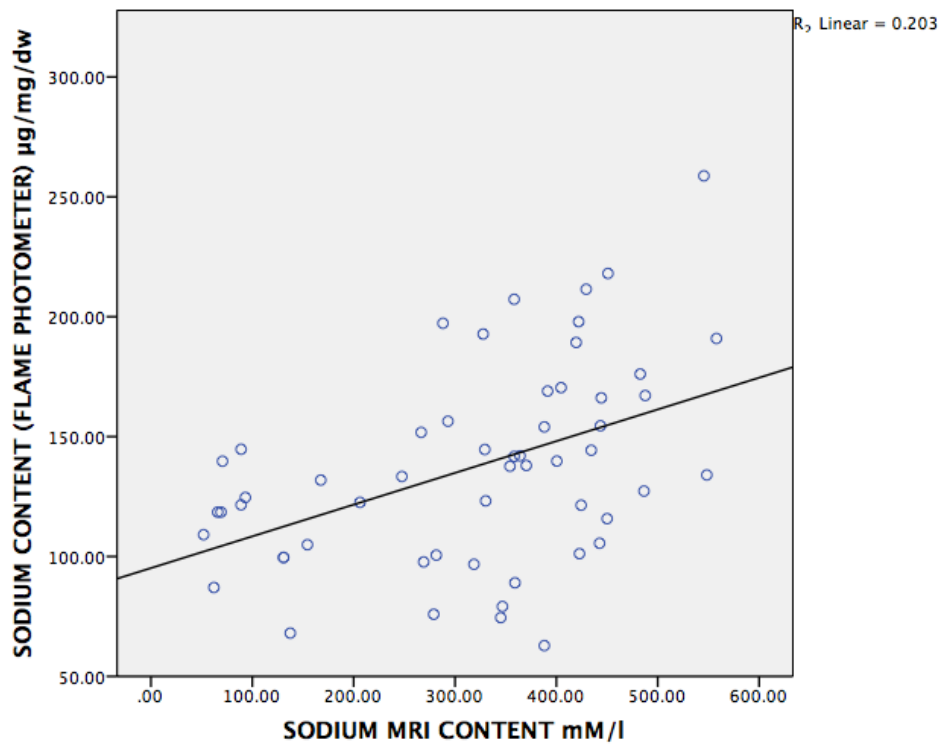


Figure 5-12: Scatter plot of all data points for sodium MRI content mM/l vs. sodium content (flame photometer) per mg dry weight. When all the data points were analysed, sodium MRI content has a statistically moderate positive correlation with sodium content (flame photometer) ($P=0.001$, $r=0.451$).

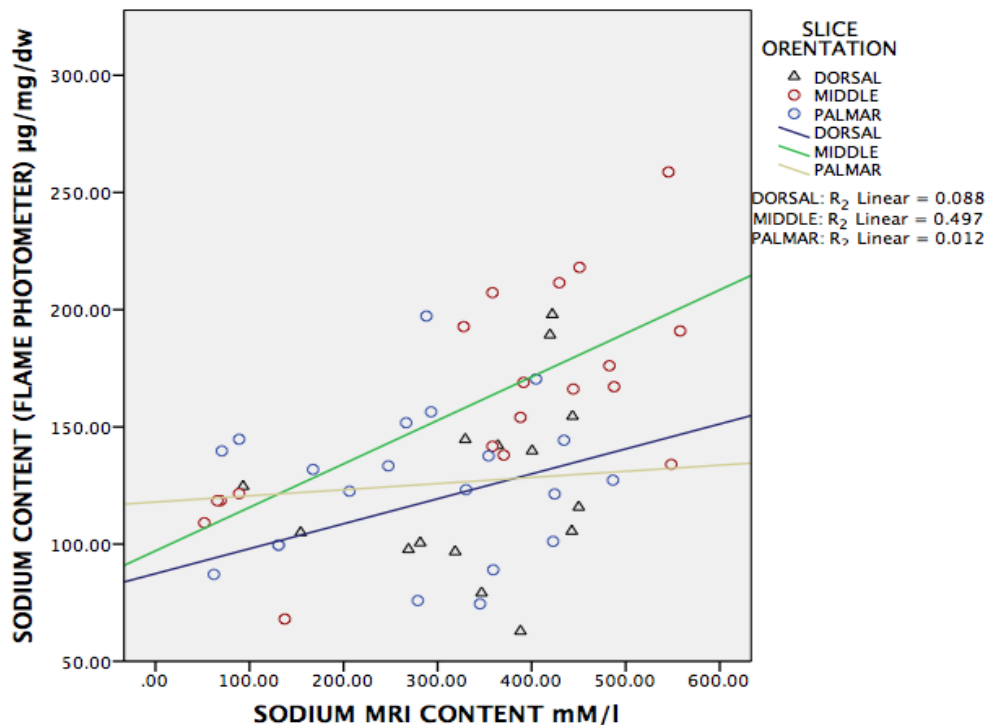


Figure 5-13: Scatter plot of sodium MRI contents mM/l vs. sodium content (flame photometer) per mg dry weight. When only dorsal site data points are analysed, there was weak correlation between sodium MRI content vs. sodium content (flame photometer) (purple circles). When only middle data points are analysed, there was a statistically significant positive correlation of sodium MRI content vs. sodium content (flame photometer) ($P=0.001$, $r=0.71$) (green circles). When only the palmar data points were analysed there was weak positive correlation was observed between: Sodium MRI content vs. sodium content (flame photometer) (red circles).

5.7. Discussion

There has been increasing in the interest in using non-invasive MRI techniques to quantitatively assess cartilage health status and pathological changes. This work aimed to measure sodium content in equine articular cartilage using an *in vivo* study. However, this technique was challenging due to relatively low signal to noise ratio of sodium ions, relatively long scanning time which resulted in low resolution sodium MR images compared to T1-weighted or T-2 weighted hydrogen MR images (Madelin et al. 2010).

However, the strength of the MR magnet as well as imaging software capability are able to minimise the effect of such low resolution and image artifact (Zbýň et al. 2014).

5.7.1. Sodium MRI Map and Topographical Variation in Cartilage

Quantifying sodium content in biological tissues has been the subject of investigation for several years. Shapiro et al, had addressed this issue with a very simplistic and straightforward technique, which can be used to measure sodium content in all biological tissue type using high field sodium MRI technique (Shapiro et al. 2000b). Sodium content in normal cartilage is proportional to the glycosaminoglycans due to the fixed charge density in the cartilage, thus any loss of PG content during the early onset stage of OA would influence and reduce the amount of sodium (Lesperance et al. 1992).

Many human and animal sodium MRI studies have measured sodium content in the cartilage. For instance, a human study showed that sodium content changed due to age. This study found that people aged between 30-40 had 150-250 mM sodium content in their cartilage and as those with 60-70 had 80-200 mM sodium content (Madelin et al. 2010), these results were dependant on site location (Maroudas 1968; Shapiro et al. 2002a). The sodium content of normal healthy human cartilage usually has a range of 240-300 mM (Borthakur et al. 2006; Wang et al. 2009). Another study found that repaired cartilage had lower sodium content 174 ± 53 mM than normal reference cartilage 267 ± 42 mM (Zbýň et al. 2014). Sodium MRI of bovine patellar cartilage found the sodium content was 335.62 ± 12.71 mM (Shapiro et al. 2000b). Another bovine articular cartilage study found that the average of sodium content in normal bovine cartilage was 316 mM in the central part, while the peripheral edges had around 150mM (Shapiro et al. 2002a). However, the sodium results found using MRI technique were within ~93% compared to those gained by spectroscopy of the cartilage plugs, with partial volume averaging at the periphery likely causing the 7% discrepancy (Shapiro et al. 2002a). The use of a gradient coil would allow lower slice thickness and resolve this issue (Shapiro et al. 2000b).

This study found that the sodium content average of all cartilage samples was 265.79 mM, with some variation in sodium content among different cartilage sites. The central middle (most load-bearing surface) cartilage samples had the highest relative sodium content, followed by dorsal and palmar sites. These results are in agreement with that found by Shapiro and colleagues (Shapiro et al. 2000b; Shapiro et al. 2002a), who noted a similar pattern of sodium distribution in bovine patellar articular cartilage. This variation in sodium content trends in the cartilage tissue can most likely be associated with variation of glycosaminoglycans as well as collagen content in normal loaded joint compared with unloaded joint (Maroudas 1979; Karvonen et al. 1994; Fragonas et al. 1998).

5.7.2. Topographical Variation in Cartilage Glycosaminoglycans

Several studies have shown that there is significant variation in the biochemical composition of normal articular cartilage, these variations were found between weight-bearing sites of equine joints (Brama et al. 2000). Consequently, this variation in load bearing and biochemistry between different sites can affect the characteristics of the MR images.

From the results, a significant variation in GAG content and sodium were found between the various sites measured. The mean sodium content measured by flame photometry was $143.587 \mu\text{g}/\text{mg}/\text{dw} \pm 55.22 \mu\text{g}/\text{mg}/\text{dw}$; the middle cartilage samples had significantly greater sodium content compared with dorsal and palmar sites. Similarly, there was significantly higher amount of GAG in the middle site than dorsal and palmar sites. This result is in agreement with a previous study by Brama and colleagues, who found the central sites of the fetlock had significantly higher amount of GAG content, due to this part of the joint is receiving constant regular loading compared with far dorsal sites (Brama et al. 2000). Another study found that there was a significant effect of weight-bearing on biochemical parameters including GAGs, as well as an effect of exercise on biochemical parameters when trained young horses and pasture rested young horses were compared (Van Weeren et al. 2008).

The mean GAG content found in this study was 32.296 µg/mg/dw ±7.464 µg/mg/dw which was lower than what was reported by Brama and colleagues (45-50µg/mg/dw) (Brama et al. 2000).

Several reasons would at once present themselves as to why this difference in mean GAG content occurred. Complete specimen history was unavailable in this study. Gross post-mortem examination was undertaken to check for gross signs of OA, but there is still the possibility that these ponies had low amounts of GAG as a result of early OA. Moreover, It has been reported that GAG content would differ according to exercise regime. One study found that there was significant difference in GAG content in young horses that had been subjected to different exercise regime (Van Weeren et al. 2008). The ponies used in this study were previously used for vaccine trials and had therefore been restricted to small paddock turnout without training or exercise. Additionally, the glycosaminoglycan assay cartilage samples were obtained after a long sodium MRI analysis. Lastly, the PG assay is know suffer from to a number of fundamental errors, mainly involving precipitation of the GAG (Shapiro et al. 2002a) , making comparing between studies difficult.

5.7.3. Relationship Between Quantification of Sodium by MRI and Flame Photometer

It was hypothesised in this study that sodium MRI values would correlate with sodium values of the same samples. Yushmanov and colleagues found that sodium MRI values of the rat brain were acceptably correlated with those measured using a flame photometer, and there was a decrease in sodium content in the ischemic brain tissue of the rat (Yushmanov et al. 2009; Yushmanov et al. 2013). A study of myocardial tissue found that the sodium MRI value was about two fold higher than the sodium content measured using flame photometry (Constantinides et al. 2001). These results are in agreement with this current study, which found moderate significant positive correlation between sodium MRI values and flame photometer results.

This study observed that sodium MRI content of the middle punches of equine cartilage had the greatest positive correlation with sodium (flame photometer) content when only middle data points were analysed ($P=0.001$, $r=0.71$ Figure 5.13). As

observed in many studies, the variation in the cartilage tissue sodium is likely to be associated with variation in the biochemical components of the cartilage such as glycosaminoglycans and collagen content (Maroudas 1979; Karvonen et al. 1994; Fragonas et al. 1998).

5.8. Conclusion

There are a number of limitations to this study. A low number of the cartilage samples from a limited number of ponies were used. Furthermore, ROIs to measure sodium concentration using MRI software (Bruker ParaVision version 5.0) were drawn manually, which introduces the possibility of operator error and missing some parts of the curved metacarpal condyle. However, as an initial demonstration of the feasibility of measuring sodium in equine cartilage by MRI this study was able to demonstrate statistical significance and relationships between all of the three different techniques used to assess the sodium content of equine cartilage. As hypothesised previously, quantitative MRI could be beneficial in non-invasively quantifying tissue (cartilage) properties that are associated with early stage onset osteoarthritis in equines. In conclusion, this non-invasive quantitative MRI technique is able to assess the total sodium content of equine cartilage, which could be interesting in the future to know if the findings, using these techniques, correlate with the clinical symptoms as well as histology findings. It is hoped that this technique could be used in the future in equine clinical practices for the evaluation of the cartilage biochemical composition in degenerative equine cartilage, in which an objective technique of proteoglycan quantification is needed.

Chapter 6 Sodium MRI Evaluation of Equine Cartilage (Enzymatic Degradation)

6.1. Introduction

The limited intrinsic ability to repair of articular cartilage means articular cartilage health is crucial for the health of joints (Zbýň et al. 2014). Mechanical injuries are one of the most common causes of articular cartilage damage, which lead to degenerative changes and osteoarthritis. These early degenerative changes are mainly accompanied by a loss of proteoglycans (PG) and there might be only little change in the collagen molecules in cartilage. Currently most of the diagnostic techniques detect structural changes in cartilage, yet, the early onset of articular osteoarthritis happens earlier, before structural abnormalities of the articular cartilage are detectable (Venn & Maroudas 1977; Bashir et al. 1996). Development of chondroprotective drugs which aim to support the regeneration of chondrocytes and consequently cartilage, means that a valid diagnostic technique is required to help clinicians evaluate the early articular cartilage changes, and deal with the degeneration in its early stages (Recht & Resnick 1994). Several non-invasive sodium MRI studies have shown this technique is able to quantify the cartilage glycosaminoglycan (GAG) content, as it plays an essential role in cartilage homeostasis. These studies suggest that this technique could be extremely useful for both assessment of articular cartilage health status and to predict osteoarthritis (Zbýň et al. 2014). Sodium (^{23}Na) ions in the living body play an essential role in cellular homeostasis and cell viability. Sodium concentration in healthy tissues is 10 times higher in the extracellular fluid than intracellular fluid (Nagel et al. 2009). Sodium MR imaging studies have shown that the relaxation times of Na nuclei are altered in degraded cartilage, which is linked to PG loss. Positive sodium ions are attracted to negative GAGs to maintain overall electroneutrality and therefore distribute according to the GAG content. This results in Na MRI images being less intense for degraded cartilage.

One of the most common effects of cartilage pathology, such as osteoarthritis is the loss of proteoglycans from the matrix of the cartilage. Thus, by using a model of osteoarthritic change, in which the articular cartilage has been enzymatically degraded (digested) with different trypsin enzyme concentrations, then the sodium MRI characteristics of the articular cartilage can be evaluated as a function of changes in the proteoglycans content.

This study aims to quantify sodium concentration of equine articular cartilage which are subjected to three different concentration of digestion solution in a model of osteoarthritis using 7T MRI images. These findings will then be compared with GAGs and sodium quantified by flame photometer assay.

6.2. Aims and Objectives

After estimating sodium content of the normal equine articular cartilage in the previous chapter, it was hypothesized that quantitative 7T sodium MRI technique can detect changes in sodium and proteoglycan content in equine articular cartilage using a model of osteoarthritis. Specifically, this study hypothesized that trypsin degradation would result in a concentration dependent decrease in sodium signal intensity of the acquired 7T MR images. Furthermore, it was also hypothesised that the 7T sodium MR image signal intensity would correlate with proteoglycan and sodium concentration.

The specific objectives of this study were as follows:

- I. Establish a model of osteoarthritis using trypsin enzymatic digestion.
- II. Quantify the sodium content of normal equine cartilage and enzymatically-digested cartilage using sodium MRI.
- III. Determine cartilage proteoglycan and sodium content using proteoglycan assay and flame photometry technique respectively.
- IV. Determine the relationship between sodium MRI, proteoglycan concentration and sodium concentration.

6.3. Materials And Methods

6.3.1. Sample Collection And Preparation

Nine fetlock joints were collected from horses age 6-10 years, euthanized for reasons unrelated to this study. They were cleaned, dissected and MCIII articular surface exposed and then placed in labelled phosphate buffered saline containers. Each MCIII bone was cut into three osteochondral slices (Fig 6.1). Then, a groove was created in the middle of each of the three remaining slices to divide each in to dorsal and palmer aspects. Afterwards, each slice was numbered 1-3 from the lateral to medial aspect (Fig 6.1).



Figure 6-1: Representation of the sample preparation. Semi-circular slices (width 5mm, height around 3cm) were prepared for this study from the distal aspect of the third metacarpal bone. All slices were labelled 1-3. Then they were cleaned labelled and maintained in isotonic saline for MRI and subsequent biochemistry analysis.

6.3.2. Sample Enzymatic Degradation (Trypsin Enzyme)

Proteolytic degradation of the equine articular cartilage was performed using trypsin as previously described study using a bovine patellar model (Borthakur et al. 2000). A stock trypsin solution was made using trypsin enzyme tables (Sigma-Aldrich, Poole, Dorset, UK) dissolved in 137mM phosphate buffered saline solution. Three different concentrations of solution (10, 50 and 100 $\mu\text{g}/\text{ml}$) were prepared for articular cartilage digestion. The dorsal aspect of three of the slices was immersed in trypsin solution (10, 50 and 100 $\mu\text{g}/\text{ml}$). Nine replicate slices were obtained for each concentration. The palmer aspect was covered with surgical gauze soaked with equilibrated phosphate buffered solution. The remaining slice was kept as a control and was not subjected to trypsin treatment. The samples were left to equilibrate for 30 min (Fig 6.2). Then they were rinsed with PBS and kept in PBS until imaged. In this way, each articular cartilage served as a self-control specimen for the imaging (Borthakur et al. 2000).

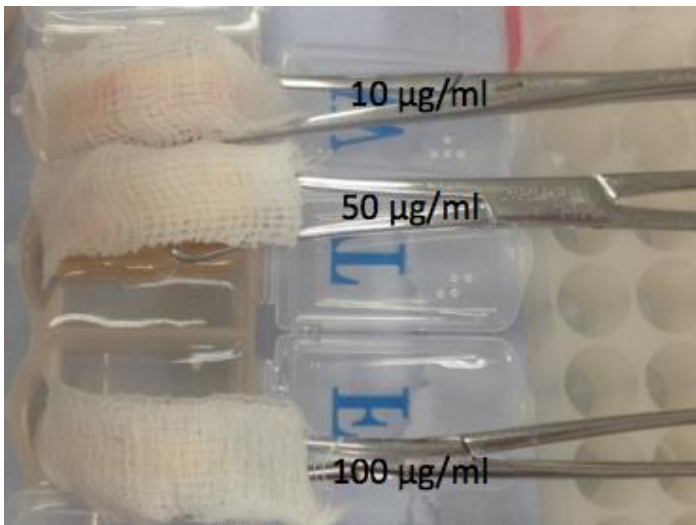


Figure 6-2: Demonstration of the articular cartilage digestion process. The top slice degraded with 10 $\mu\text{g}/\text{ml}$ trypsin, middle one degraded with 50 $\mu\text{g}/\text{ml}$ and last slice degraded with 100 $\mu\text{g}/\text{ml}$ trypsin solution. Only the dorsal aspect aspects were immersed in the enzymatic solution (trypsin) for 30 min, while the palmer aspect in each slice covered by surgical gauze soaked with normal saline to avoid dryness of the articular cartilage surface, as they were used as a control.

6.3.3. Sodium MRI and MRI Data Acquisition

Sodium MRI was performed using an ultra-high field 7T magnet (BioSpec, Bruker Corporation 70/30 system Bruker, Germany). A dual tuned quadrature $^{23}\text{Na}/^1\text{H}$ coil designed by (PulseTeq Limited, Chobham, Surrey, UK) was used to acquire the Na MRI (Table 6.1).

Table 6-1: This table shows the technical information for the Na MRI protocol.

Acquisition type	2D acquisition
Slice thickness	4 mm
Repetition time	123ms
Echo time	3.6756ms
Scanning type	^{23}Na _FLASH2D_Tr75_1_1_4mm
Coil type	Dual tuned quadrature $^{23}\text{Na}/^1\text{H}$ coil
Number of averages	4048
Flip angle	12.97°
Matrix	250X250
Scan time	3 hours 20 min

6.3.4. Sodium MRI T1-Signal Intensity

Following image acquisition, T1 weighted sodium MR images were analysed using the MRI workstation (Bruker ParaVision 5.0 software). Sodium signal intensity was measured separately in each punch location corresponding to the GAG and flame photometer punches. A 4mm region of interest (ROI) was drawn manually using the track tool to measure sodium signal intensity. Each measurement was repeated three times separately and the average calculated. A standard curve was created from sodium phantoms in order to determine the sodium content in each site using the average signal intensity (Fig 6.3) (Shapiro et al. 2000a). Images were visualised in OsiriX and the Image Fusion tool was used to merge T1-weighted and sodium MRI images for the purposes of illustration (Fig 6.3)

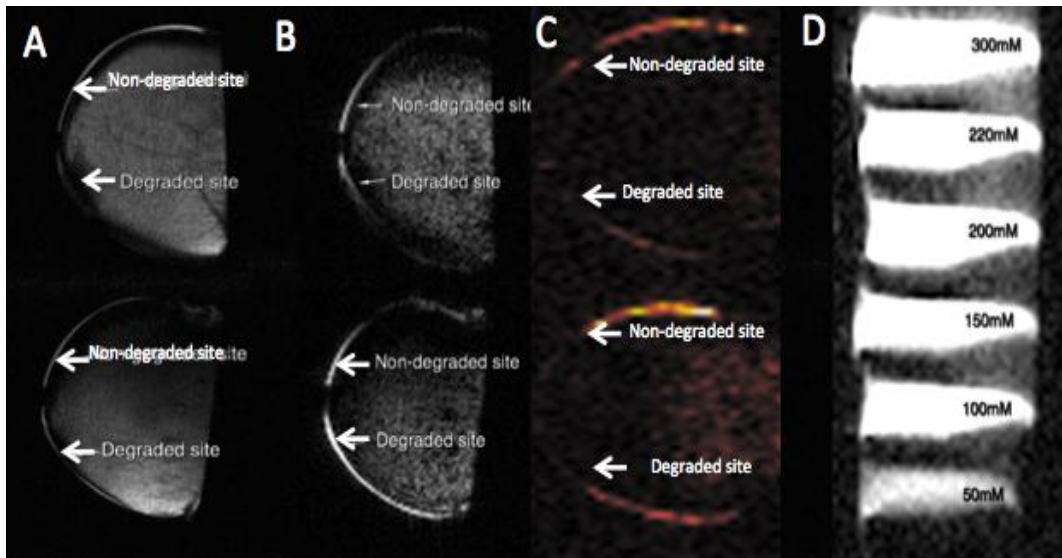


Figure 6-3: A sagittal sodium MR image of equine MCIII and its articular cartilage. (A) T1-weighted MRI; (B) Sodium MRI; (C) sodium image merged with T1-weighted image and (D) sodium MRI of the phantoms containing different concentration of sodium. Sodium MRI analysis using geometry tool, a straight line was drawn between the two end points of the semi-circular slices a 90° angle plotted from the center of the central line. Two 4mm lines were plotted from the central point to represent two dorsal RIOs (digested part) and other two palmar (control) RIOs. The track tool was used to manually draw around the articular cartilage, making sure that only the cartilage area was included. The values obtained show the average sodium signal intensity within the RIO.

6.3.5. Articular Cartilage Slice Collection for GAG and Flame Photometer Analysis

After MRI scanning, a 4mm sterile biopsy punch (Steifl, a GSK Company, Research Triangle Park, USA) was used to collect cartilage samples (Fig 6.4). Cartilage punches were removed from each specimen and maintained in isotonic saline (Baxter). Then all punches were labelled and weighed to estimate the cartilage wet weight and placed into labelled 1.5ml polypropylene tube (Sigma). Afterward they were placed in a 60°C oven for 24hrs, then dry weight was calculated. All samples were divided in to two halves, one half for glycosaminoglycan assay and the other half for sodium flame photometry.

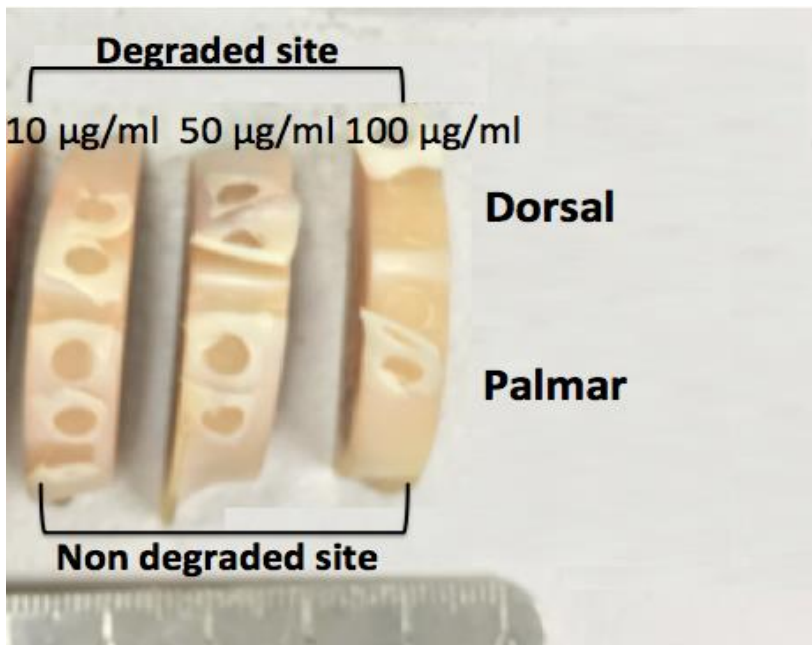


Figure 6-4: Diagrammatic presentation of the biochemical assays preparation. Four 4mm biopsy punches were harvested and separated from the MCIII subchondral bone using scalpel; making sure the full thickness of the cartilage was included. Half of these punches were used for GAG assay and the other half went for flame photometer technique. Peeling of the cartilage was due to sample collection and occurred after MRI.

6.3.6. GAG Assay (Glycosaminoglycans)

Cartilage samples (1-6mg) for GAG determination were placed into 1.5ml polypropylene tubes (Sigma), and 1ml of papain extraction reagent was added according to manufacture's instructions (Blycan, Sulphated Glycosaminoglycan Assay, Biocolor, County Antrim, UK) to digest the cartilage. After the assay finished, the 96 well assay plate was placed in a spectrophotometer (Borthakur et al. 1999). The absorbance readings of the samples were measured at 650nm. Known concentrations of bovine tracheal chondroitin sulphate 4-sulphate (Blycan) was used to make sure that the standard curve had a significant r^2 value of ≥ 0.95 as described in chapter 4 (page 90).

6.3.7. Flame Photometer

Samples for flame photometry were placed in Corning 15ml labelled centrifuge tubes (Sigma), as described in Chapter 5 (page 123).

6.4. Statistical Analysis

All MR images were analysed using Bruker ParaVision version 5.0 (Bruker, Germany) (Figure 8.4). Then, all data were statistically analysed using IBM SPSS advanced statistics 20.0 (IBM Corporation Armonk U.S.A). All study variables were confirmed to have a normal statistical distribution using Shapiro-Wilks statistical test before further statistical analysis. After Na MRI quantification and biochemical analysis, the effect of trypsin (degradation) on articular cartilage biochemical analysis (GAG and flame photometer techniques) and sodium MRI results were determined using a paired student's T-test and ANOVA test at 95% confidence level. The correlation between biochemical characteristics and sodium MRI results was determined using Pearson rank correlation.

6.5. Results

6.5.1. Sodium Content (MRI) vs. GAG Content

6.5.1.1. Overall Sodium Content (MRI) Degraded Samples and Control Samples

Overall the mean sodium content determined by MRI of degraded samples was 49.22 ± 5.05 mM/l and 82.97 ± 7.25 mM/l for the controls. There was significant difference in sodium content (MRI) between degraded and control samples ($P < 0.01$) (Fig 6.5).

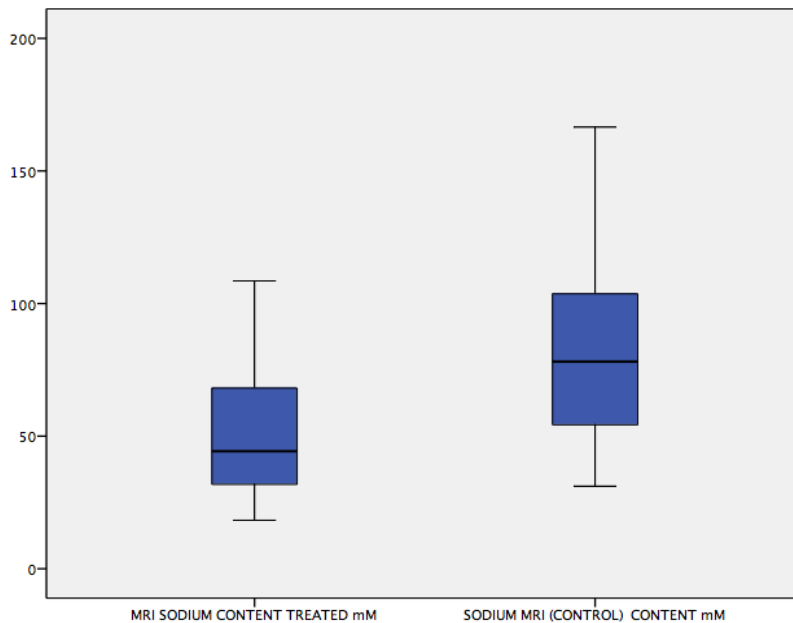


Figure 6-5: Difference in mean sodium (MRI) concentration in articular cartilage samples degraded trypsin solution and its control group. There was significant difference in sodium content determined by MRI between degraded and control samples ($P < 0.01$).

6.5.1.2. Sodium Content (MRI) of Cartilage Samples Degraded by Different Trypsin Concentration

The mean sodium content determined by MRI of samples degraded with 10 µg/ml trypsin was 52.77 ±26.9. mM/l and 71.60 ±23.9 mM/l for control samples. There was a statistically significant difference between samples degraded with 10 µg/ml trypsin and the controls ($P= 0.049$) (Fig 6.6). The mean sodium content determined by MRI of samples degraded with 50 µg/ml trypsin was 46.16 ±9.55 mM/l and for control samples was 78.53 ±10.67 mM/l. There was significant difference between degraded cartilage samples with 50 µg/ml trypsin with its control samples ($P= 0.031$) (Fig 6.7). The mean sodium content determined by MRI of samples degraded with 100 µg/ml trypsin was 48.70 ±8.41 mM/l and 98.75 ±16.63 mM/l was for control samples. There was statistically significant difference between samples degraded with 100µg/ml trypsin and the control samples ($P<0.01$) (Fig 6.8) (Table 6.2).

Table 6-2: Table describing the results of MRI quantification of the amount of cartilage sodium (mM/l)

	Sodium MRI mean (mM/l)	Standard deviation (mM/l)
Sodium MRI content for cartilage treated with 10 µg/ml	52.77	26.9
Controls	71.60	23.9
Sodium MRI content for cartilage treated with 50 µg/ml	46.16	9.55
Control	78.53	10.67
Sodium MRI content for cartilage treated with 100 µg/ml	48.70	8.41
Control	98.75	16.63

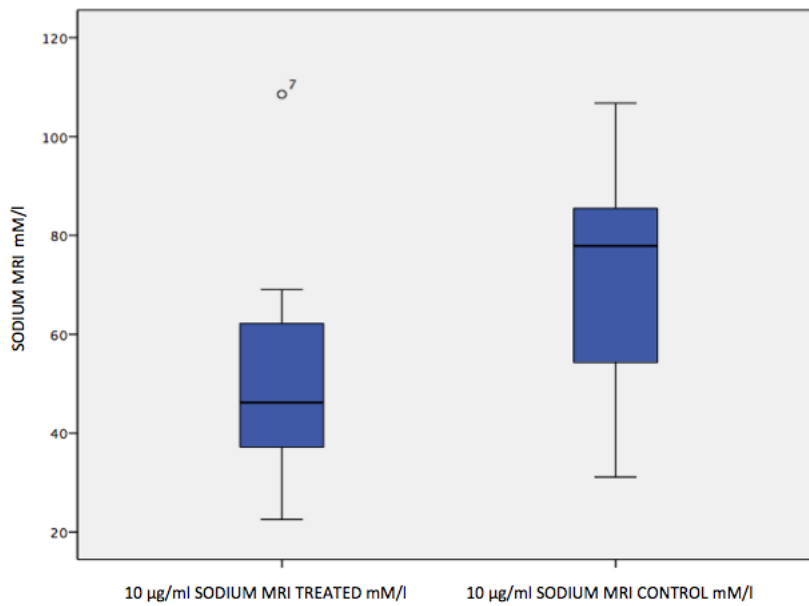


Figure 6-6: Difference in mean sodium (MRI) concentration in articular cartilage samples degraded trypsin solution (10 µg/ml) and its control group. There was significant difference in sodium content (MRI) between degraded and control samples ($P=0.049$).

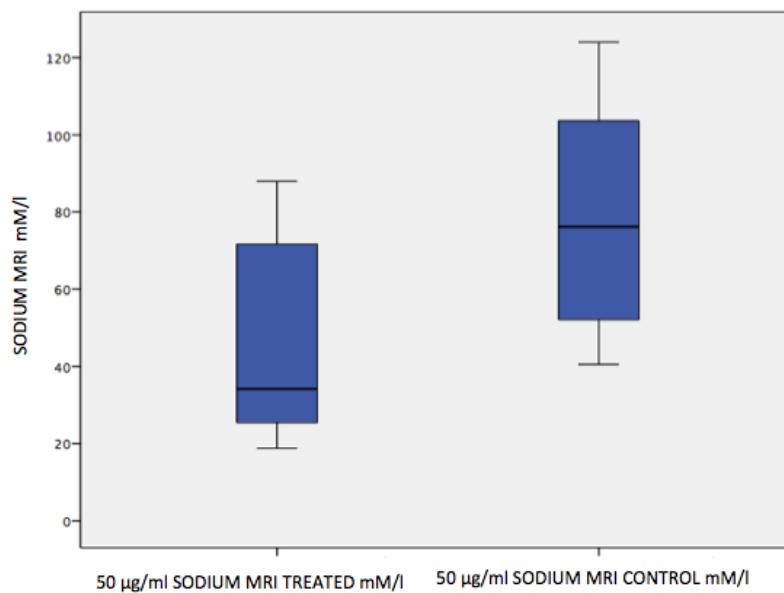


Figure 6-7: Difference in mean sodium (MRI) concentration in articular cartilage samples degraded trypsin solution (50 µg/ml) and the control group. There was a significant difference in sodium content (MRI) between degraded and control samples ($P=0.031$).

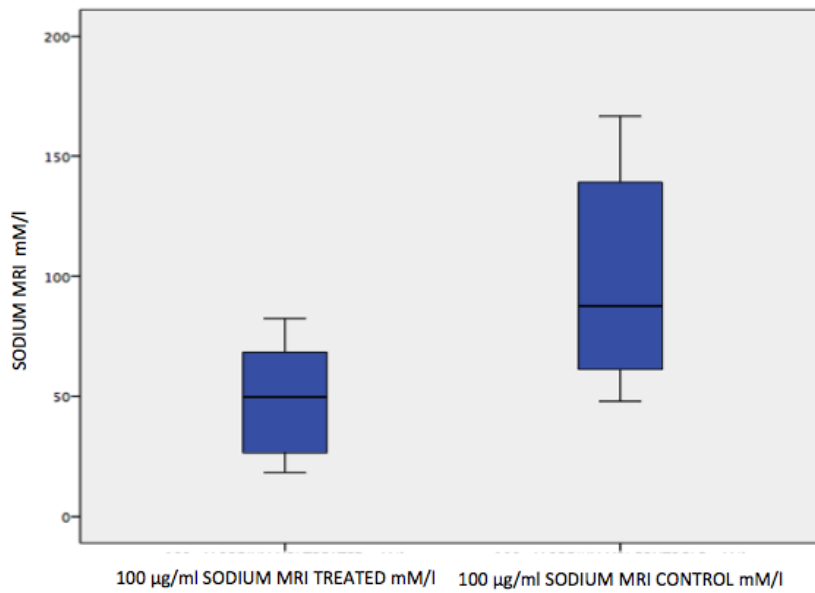


Figure 6-8: Difference in mean sodium (MRI) concentration in articular cartilage samples degraded trypsin solution (100 µg/ml) and the control group. There was a significant difference in sodium content (MRI) between degraded and control samples ($P<0.01$).

6.5.1.3. Overall GAG Content

The mean GAG content of all degraded samples was 16.55 ± 1.0 µg/mg/dw, while the mean GAG for control samples was 24.57 ± 1.09 µg/mg/dw. There was a statistically significant difference in GAG content between degraded and control samples ($P<0.01$) (Fig 6.9).

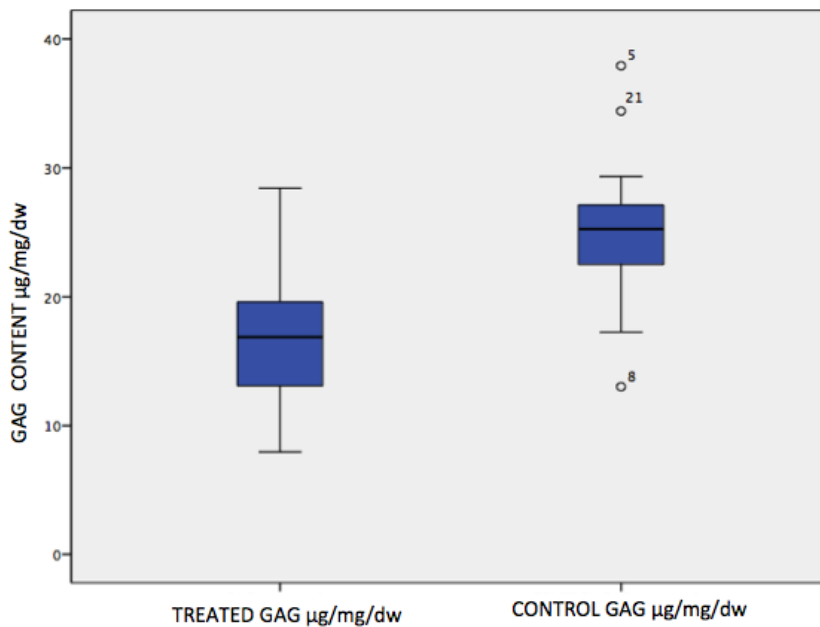


Figure 6-9 Difference in overall mean GAG content of the articular cartilage samples degraded in trypsin solution and the control group. There was a significant difference in overall GAG content between degraded and control samples ($P<0.01$).

6.5.1.4. GAG Content of Samples Degraded with Different Trypsin Concentration

The mean GAG content for samples degraded with 10µg/ml trypsin was significantly lower (19.77 ± 1.79 µg/mg/dw) than control samples (24.66 ± 2.65 µg/mg/dw) ($P<0.01$) (Fig 6.10). The mean GAG content for samples degraded with 50 µg/ml trypsin was significantly lower (15.41 ± 1.54 µg/mg/dw) than control samples (23.73 µg/mg/dw ± 1.09 µg/mg/dw) ($P<0.01$) (Fig 6.11). The mean GAG content for samples degraded with 100µg/ml trypsin was significantly lower (14.44 ± 1.41 µg/mg/dw) than control samples (25.29 ± 1.84 µg/mg/dw) (Fig 6.12) ($P=0.001$).

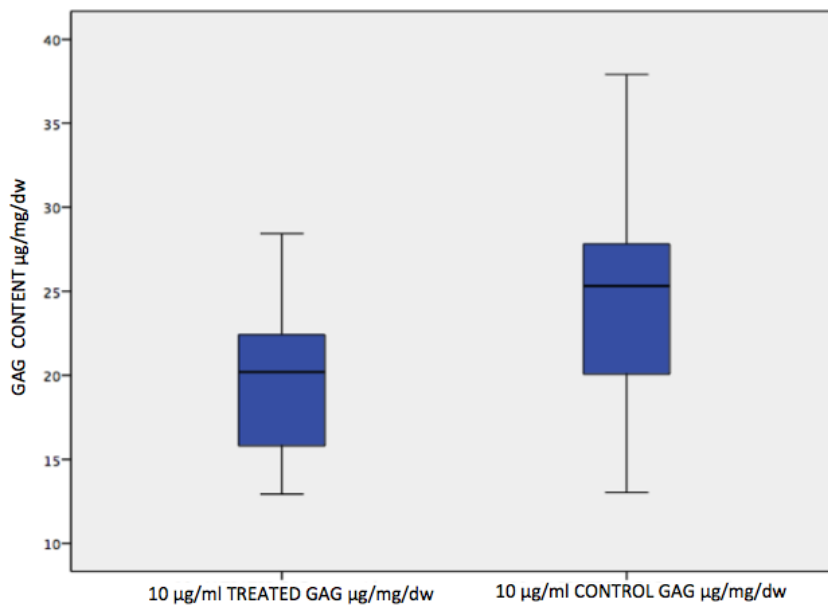


Figure 6-10: Difference in mean GAG content of the articular cartilage samples degraded with (10 µg/ml) trypsin solution and the control group. There was a significant difference in GAG content between degraded and control samples ($P < 0.01$).

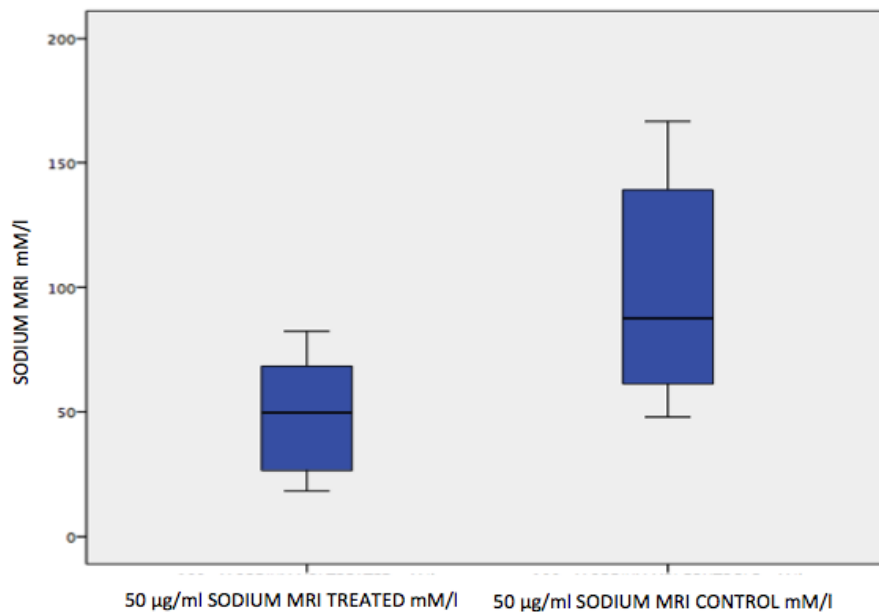


Figure 6-11: Difference in GAG content mean of the articular cartilage samples degraded with 50 µg/ml trypsin solution and its control group. There was a significant difference in GAG content between degraded and control samples ($P < 0.01$).

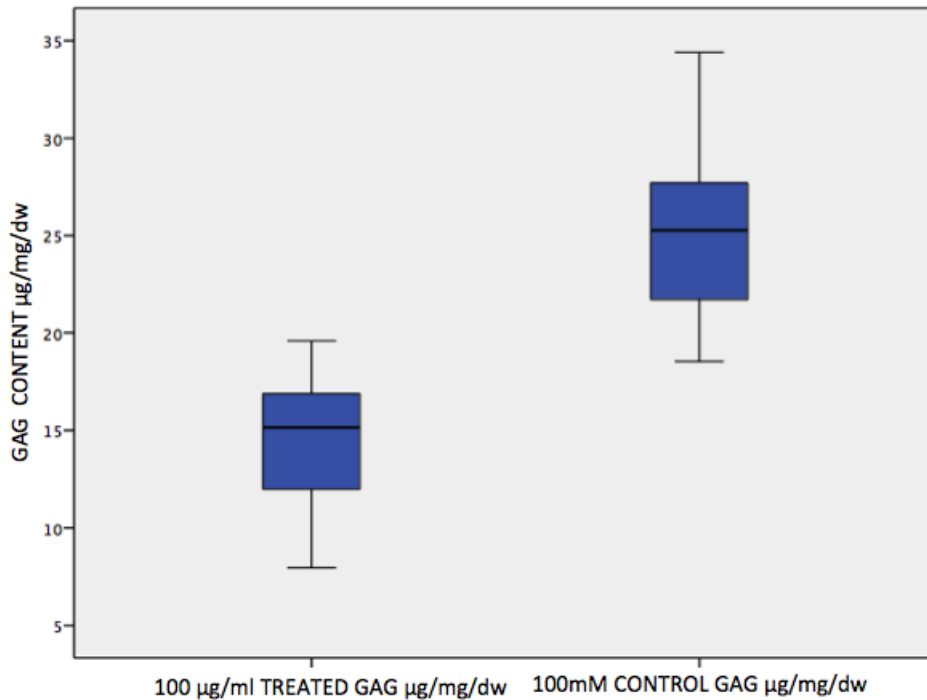


Figure 6-12: Difference in GAG content mean of the articular cartilage samples degraded with 100 µg/ml trypsin solution and its control group. There was a significant difference in GAG content between degraded and control samples ($P=0.001$).

6.5.2. Sodium Content (MRI) vs. Sodium Content (Flame Photometer)

6.5.2.1. Overall Sodium Content Measured by Flame Photometer

The mean sodium content measured by flame photometer for degraded samples was 51.45 ± 1.69 µg/mg/dw, and the mean sodium content for control group was 68.29 ± 4.37 µg/mg/dw. There was a statistically significant difference in sodium content measured by flame photometer between the degraded and control groups ($P<0.01$) (Fig 6.13).

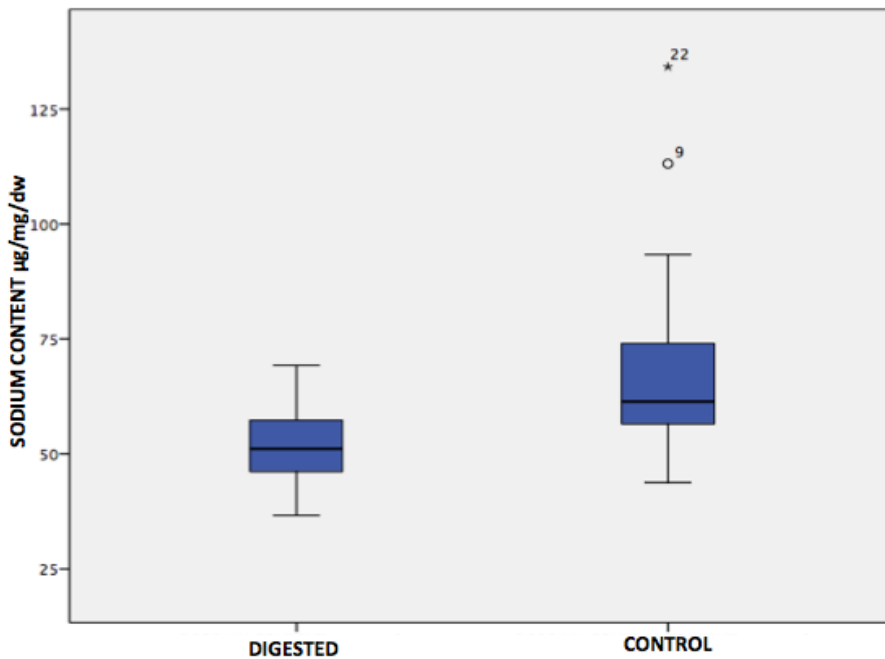


Figure 6-13: Box plot describing the sodium content of all articular cartilage samples degraded with trypsin solution and control. There sodium content was significantly lower in degraded than control samples ($P=0.001$).

6.5.2.2. Sodium Content (flame photometer) of Samples Degraded with Different Trypsin Concentration

The mean sodium content (flame photometer) of cartilage samples degraded with 10 µg/ml trypsin was 111.34 ± 7.93 µg/mg/dw; control 116.76 ± 12.32 µg/mg/dw. There was no significant difference in sodium content (flame photometer) between degraded and control samples of the same group ($P=0.702$) (Fig 6.14).

The mean sodium content (flame photometer) of cartilage samples degraded with 50 µg/ml trypsin was 101.79 ± 9.03 µg/mg/dw; control mean 121.60 ± 6.9 µg/mg/dw. There was statistically significant difference in sodium content (flame photometer) between samples degraded with 50 µg/ml trypsin and control samples ($P=0.034$) (Fig 6.15). The mean sodium content (flame photometer) of cartilage samples degraded with 100 µg/ml trypsin was 101.86 ± 6.79 µg/mg/dw; mean of control 132.57 ± 5.85 µg/mg/dw. There was a significant difference in mean sodium content (flame photometer) between cartilage samples degraded with 100 µg/ml trypsin and control samples of the same group found ($P<0.01$) (Fig 6.16).

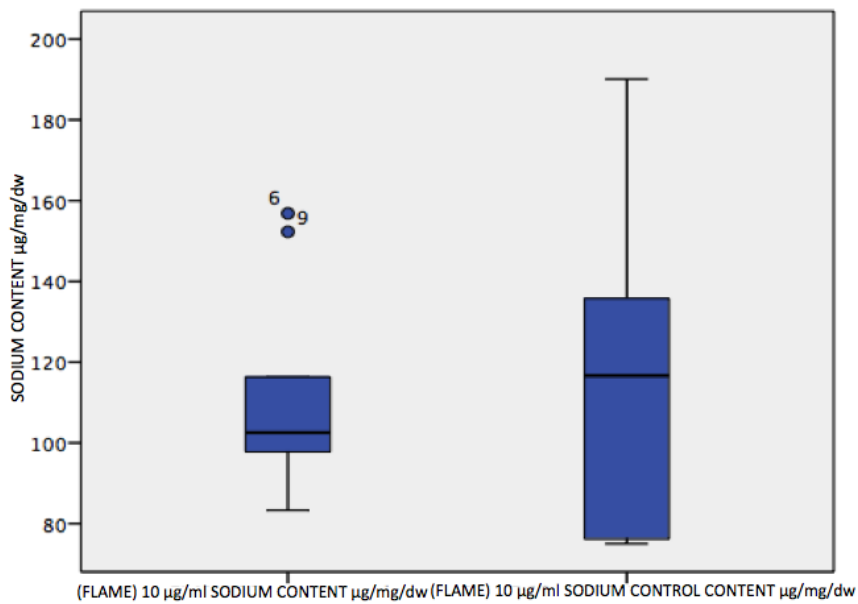


Figure 6-14: Box plot describing the difference in sodium content (flame photometer) of the articular cartilage samples degraded with 10 µg/ml trypsin solution and its control group. There was no significant difference in sodium content (flame photometer) between degraded and control samples ($P=0.702$).

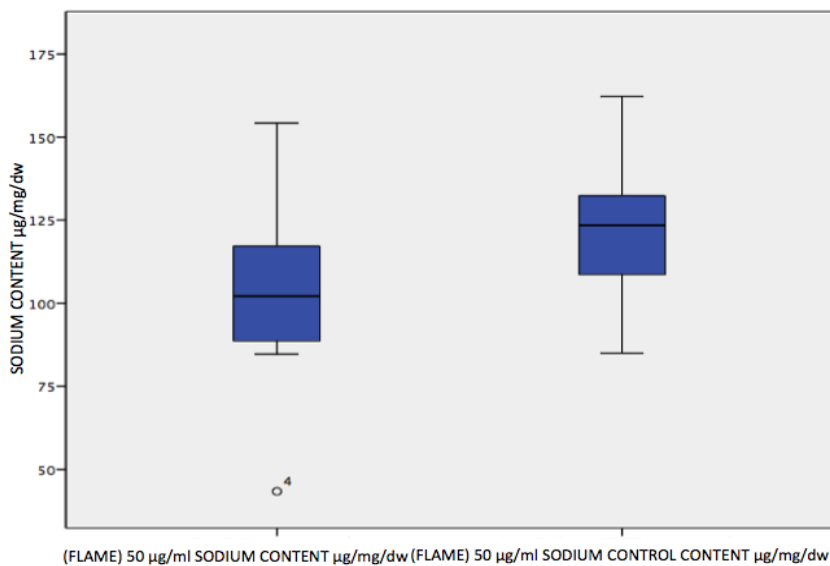


Figure 6-15: Box plot describing the difference in sodium content (flame photometer) content mean of the articular cartilage samples degraded with 50 µg/ml trypsin solution and its control group. There was significant difference in sodium content (flame photometer) between degraded and control samples ($P=0.034$).

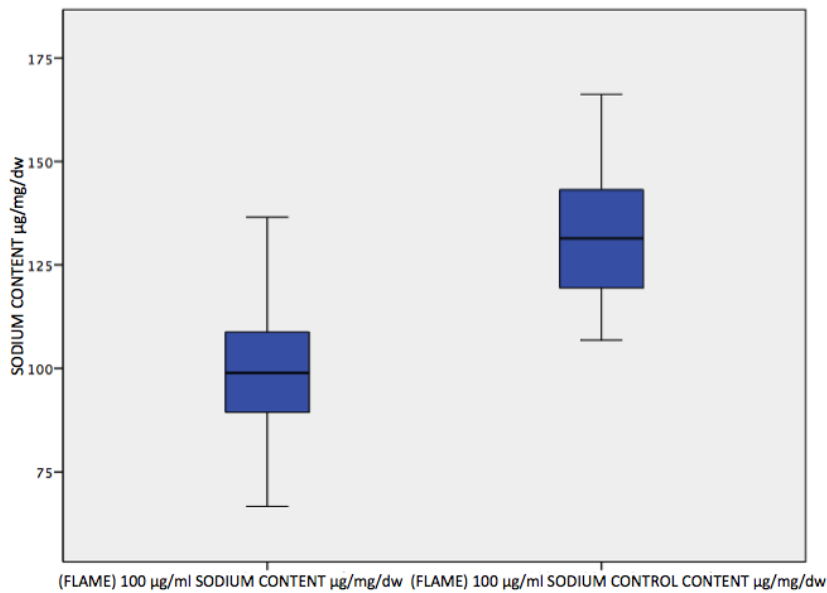


Figure 6-16: Box plot describing the difference in mean sodium content (flame photometer) of the articular cartilage samples degraded with 100 µg/ml trypsin solution and the control group. There was significant difference in sodium content (flame photometer) between degraded and control samples ($P<0.01$).

6.5.3. Correlation

6.5.4. Correlation Between Sodium MRI vs. Sodium Flame Photometer Results

Sodium content (MRI) was found to significantly and positively correlate with sodium content (flame photometer) in trypsin treated samples ($P<0.01$, $r=0.670$) (Fig 6.17). A significant strong positive correlation was found between sodium content (flame photometer) and sodium content (flame photometer) in control samples ($P=<0.01$, $r=0.702$) (Fig 6.18).

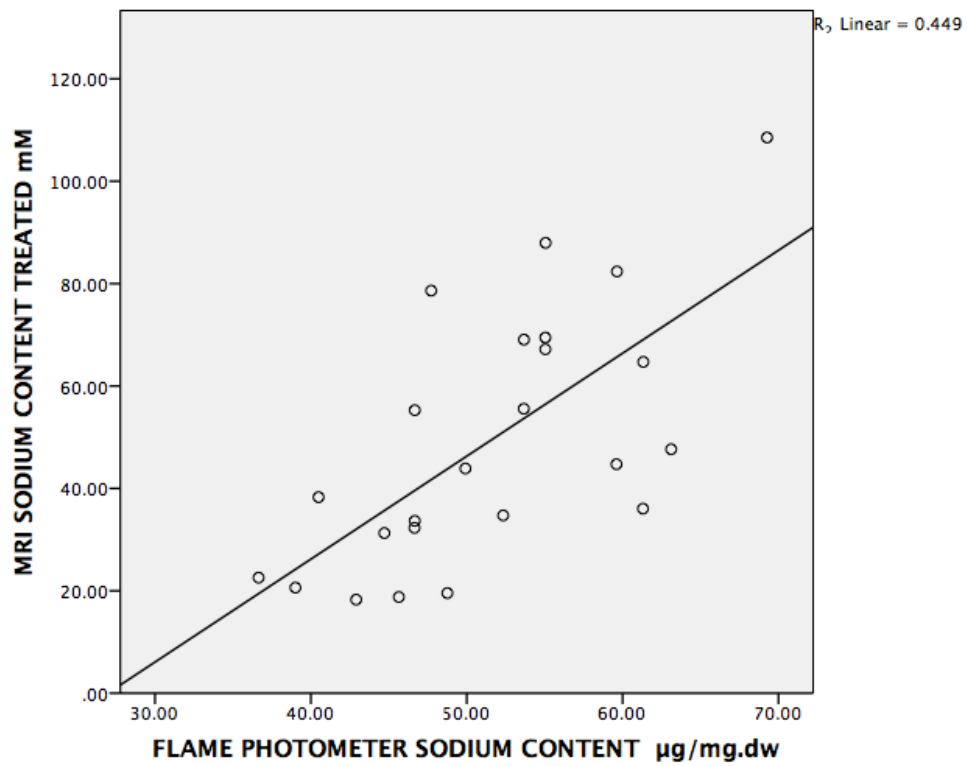


Figure 6-17: Sodium content treated (MRI) mM/L vs. sodium content treated (flame photometer) per mg dw. When sodium MRI results and sodium results measured by flame photometer of the same correspondent punches were analysed there was strong positive relation ship between them ($P=<0.01$, $r=0.670$).

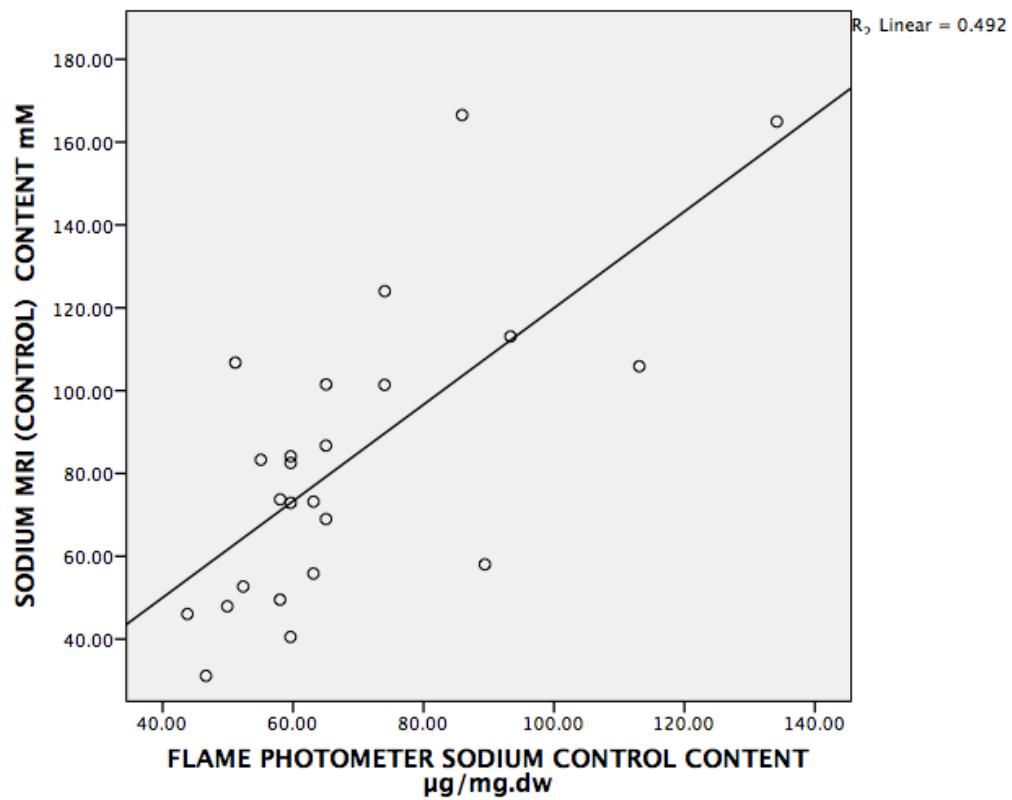


Figure 6-18: Sodium content (MRI) control mM per litre vs. sodium content control (flame photometer control) per mg dry weight. When sodium MRI results (control) and sodium results measured by flame photometer (control) of the same correspond punches were analysed there was strong positive relationship between them ($P < 0.01$, $r = 0.702$).

6.5.5. Correlation between sodium MRI vs. GAG content

There was a significant moderate positive correlation between sodium content (MRI) and GAG content ($P<0.01$; $r=0.367$) (Fig 6.19).

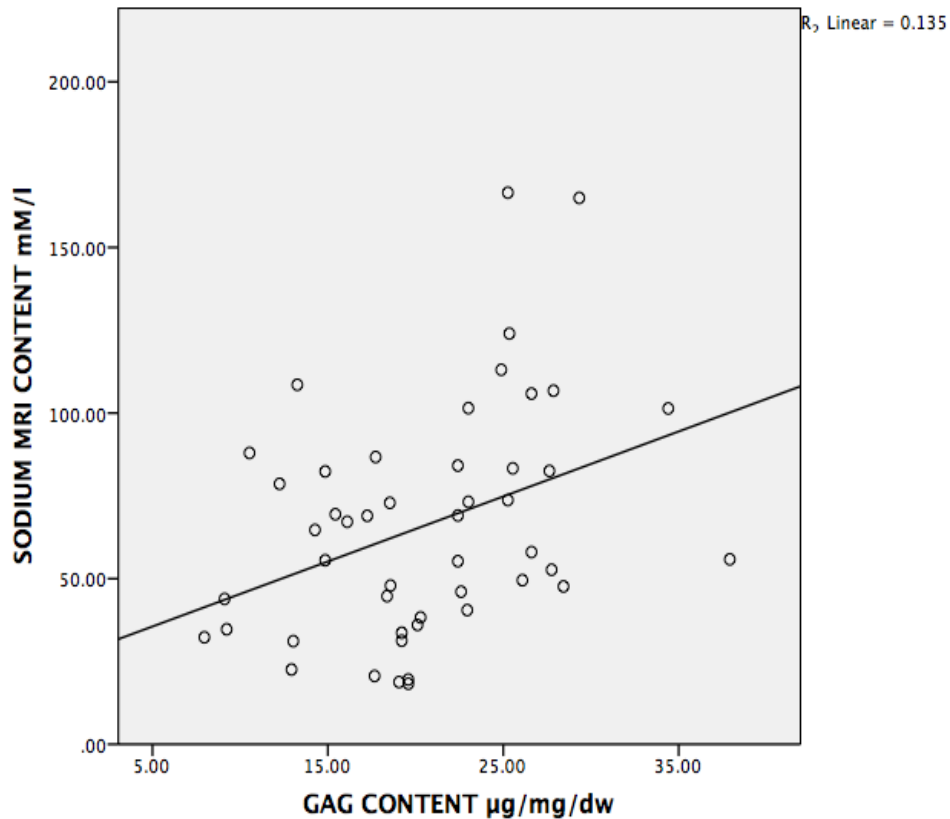


Figure 6-19: Sodium MRI contents mM/l vs. GAG content per mg/dw (all samples). There was significant correlation between data sets ($P<0.01$; $r=0.367$).

6.6. Discussion

Several MRI studies have used sodium MRI for evaluation of cartilage tissue after cartilage repair surgery to evaluate the difference in sodium content before and after surgery (Trattning et al. 2010; Chang et al. 2012; Zbýň et al. 2012). Another sodium MRI study found significantly lower sodium content in repair tissue than normal control cartilage (Marlovits et al. 2006). Furthermore, a study found that GAG had a similar pattern to sodium, and that GAG content in control cartilage samples was higher than repaired cartilage tissue and concluded that sodium MRI could be used as a non-invasive method to evaluate the performance of new cartilage tissue repair

techniques in human femoral condyles (Zbýň et al. 2012). In this study, the aim was to use cartilage digestion with different trypsin concentrations as a model of equine osteoarthritis. MR images were compared with cartilage GAG content and sodium. To date, no studies have compared MRI values with flame photometer quantification of cartilage sodium. So, as part of this study I aimed to further validate sodium MRI.

6.6.1. Sodium MRI Data Analysis

In this study cartilage was subjected to enzymatic degradation using trypsin to evaluate the effect of proteoglycan degradation on sodium imaging studies. There was a substantial decrease of between 20~50% in the sodium signal at the proteoglycan (PG) degraded site. The reduced sodium signal at the degraded site correlated with a lower PG content and sodium signals. That is to say the sodium MRI technique can clearly detect the changes associated with the loss of PG content in the cartilage. These results are in agreement with a sodium MRI study of degraded bovine cartilage (Reddy et al. 1998).

6.6.2. Exploring the Effect of Trypsin Enzymatic Degradation on the Equine Cartilage sodium (MRI) content

Previously described techniques (Reddy et al. 1998; Borthakur et al. 2000) have demonstrated the effect of enzymatic degradation on cartilage proteoglycan (PG). It has been found that sodium MRI can measure change in PG content (Borthakur et al. 2000). However, in the study by Reddy et al degradation was performed in bovine patellar cartilage for a relatively long time (12 h). The results presented in this study demonstrate that enzymatic degradation reduces PG content within equine cartilage in a concentration dependent manner, and this is associated with a decrease in sodium signal intensity. This study found that sodium MRI content was different according to trypsin concentration, as it had maximum effect in the cartilage slices degraded with 100 µg/ml solution.

This study demonstrated that there was around a 45% reduction in the sodium signal intensity of cartilage after enzymatic degradation. This result was in agreement with previous studies (Jelicks et al. 1993; Reddy et al. 1998; Insko et al. 1999; Borthakur et al. 2000)

6.6.3. Exploring the Effect of Trypsin Enzymatic Degradation on the Equine Cartilage PG Content

Degradation in trypsin solution for 30min resulted in the loss of about 8 $\mu\text{g}/\text{mg}/\text{dw}$ of GAG from equine MCIII cartilage when compared with control cartilage. When considering each degraded group with its control group, there was a significant difference between degraded cartilage samples and controls. That is to say that there was substantial reduction (~57%) in the PG content on degraded samples when compared with the control group. This effect was most apparent in the 50 $\mu\text{g}/\text{ml}$ and 100 $\mu\text{g}/\text{ml}$ trypsin concentration groups. These findings are in agreement with a bovine patella study that showed that there was a reduction in the PG content of between 50 and 70% compared with the original content before PG depletion (Insko et al. 1999). The PG loss in the cartilage was appreciated as loss of sodium MRI signal. These findings were in agreement with bovine patella study, which found that there was loss in sodium signal in the degraded cartilage site (Reddy et al. 1998).

6.6.4. Exploring the Effect of Trypsin Enzymatic Degradation on the Equine Cartilage sodium content

So far no sodium MRI studies have compared MRI results with sodium content by flame photometry. However, this study did compare and correlate sodium MRI results with sodium content measured using flame photometry of equine cartilage samples. This study demonstrated that sodium signal intensity does correspond with actual sodium content and there is a correlation between MRI sodium signal and sodium flame photometry results.

The effect of enzymatic degradation on the equine cartilage sodium content was similar to that which had been observed between sodium signal intensity loss and depletion of the PG content in the cartilage matrix. The enzymatic degradation had a substantial effect in the cartilage samples treated with higher enzymatic concentrations; there was around 20% loss in the sodium content after enzymatic degradation with 100 $\mu\text{g}/\text{ml}$. Moreover there was around 17% loss in the sodium content in the cartilage degraded with 50 $\mu\text{g}/\text{ml}$ trypsin, a significant difference was found between both degraded and non-degraded cartilage samples. A weaker effect

was observed in the samples degraded with the lower enzymatic concentration of 10µg/ml, with no significant difference observed between degraded and non-degraded cartilage samples. However, there was a significant decrease in glycosaminoglycans following degradation in 10µg/ml trypsin.

6.6.5. Exploring the Correlations Between Sodium MRI, GAG Content and Flame Photometry

Sodium MRI research of bovine patella found a strong correlation between GAG content and sodium signal intensity (Borthakur et al. 2000). However, in their study they did not compare directly between PG content and its corresponding sodium MRI signal intensity or sodium content. This study found a statistically significant positive moderate relationship between overall sodium MRI signal intensity and overall GAG content.

When each enzymatic degradation group was analysed separately, there were only weak relationships observed between sodium MRI and biochemical parameters. However, this could be due to the reduced sample size and reduced spread of data that did not reflect the whole trend of the relationship. Furthermore, the mechanisms associated with early onset of the OA are not completely understood, and there is still argument in whether GAG content is increased (Matyas et al. 1999; Lorenzo et al. 2004) or changed (Lorenz et al. 2005).

No previous studies have compared sodium MRI with sodium content by flame photometry in cartilage. So this study aimed to evaluate and compare cartilage sodium content using sodium MRI and validate these results with flame photometer sodium content. Therefore, when sodium MRI data was compared with sodium content (flame photometer) data, there was a statistical significant positive strong relationship when sodium MRI results plotted vs. sodium content (flame photometer). This finding is logically true because sodium content of the equine cartilage was measured in a direct way.

6.7. Limitations of the study

This study used 7T MRI for acquiring sodium MR images, and 7T MRI is not been used so far in equine studies. Moreover, this study used an *in vitro* ultra-high field sodium MRI method to detect small changes in the sodium content of the cartilage. This study used a simple model GAG loss to simulate osteoarthritis. Future studies using cartilage samples from naturally occurring osteoarthritis would therefore be valuable.

6.8. Conclusion

Several studies presently have proven that sodium MRI can assess the cartilage GAG content, which plays an essential role in cartilage homeostasis in healthy as well as osteoarthritic cartilage. Sodium MRI has the benefits of being both a non-invasive and a quantitative technique. Sodium MRI therefore has the potential to be a non-invasive technique to evaluate early stages of cartilage degeneration, which is related to osteoarthritis. Sodium MRI has the potential to be clinically useful to evaluate the early stage onset of OA. Moreover, sodium MRI is specific as well as sensitive in detecting small changes in PG content of the equine articular cartilage. This study compared sodium signal intensity with the biochemical components of the cartilage using a PG assay and flame photometry in an enzymatic model of osteoarthritis. Significant relationships between sodium MRI, GAG content and sodium flame photometer were described.

Sodium MRI has not been used in equine practice, however researchers in human medicine have reported the use of this technique as an *in vivo* method for looking at the cartilage tissue integrity. Therefore, this technique could be used in future studies as a research tool by providing more information on the biochemistry of equine cartilage across the surface of the joint, rather than limited samples. Ultimately, 7T MRI could allow non-invasive study of osteoarthritis in the horse and limit the need for terminal studies.

Chapter 7 Overall Discussion and Conclusion

7.1. Overall Discussion

This study aimed to use novel MRI techniques to describe and quantify the anatomy and biochemistry of the equine fetlock joint. The first anatomical study described and evaluated the hard and select soft tissue structures such as the sesamoidean ligaments SDFT and DDFT of the equine fetlock using 7T and 1.5T MRI (Chapter 2); a second study evaluated the accuracy and precision of cartilage thickness measurement by MRI compared with histopathological measurement (Chapter 3). The following studies focused on quantitative evaluation of articular cartilage biochemistry. In Chapter 4, previously described techniques including delayed gadolinium-enhanced (dGEMRIC) MRI, and T2-time measurement, were examined in equine articular cartilage. In the final two chapters, a novel dual tuned quadrature $^{23}\text{Na}/^1\text{H}$ coil was used to investigate the topographical variation and biochemical properties (water, sodium and GAG) of normal equine cartilage and in a model of osteoarthritis.

The novelty of the first chapter is the description of the ultra-high field MRI anatomy of the equine fetlock, in comparison to the current clinically used 1.5T MRI system. The anatomical atlas of the equine fetlock could help clinical veterinarians and students not only when examining MRI images, but when performing other procedures such as ultrasonography, by giving them more understanding of the normal anatomical appearance.

Chapter 4 examined the relationship between quantitative MRI parameters including delayed gadolinium-enhanced MRI (dGEMRIC) and T2 relaxation time measurement, demonstrating the ability to quantify biochemical parameters of the articular cartilage, which could be a useful tool in the detection of the early stage of osteoarthritis (OA).

In the final two Chapters, a dual tuned quadrature $^{23}\text{Na}/^1\text{H}$ coil was used to compare the topographical variation examine the biochemical properties (sodium and glycosaminoglycans) of both normal equine fetlock cartilage and degraded equine

cartilage in a model of osteoarthritis. As the sodium MRI technique is used in human practice to evaluate OA, it seems reasonable that the technique could be used in future equine research to look at the joint quantitatively and non-invasively (Chapters 5 and 6).

From the results presented of the second chapter, 7T MR images could be used in equine practice as a reference for clinical images, especially in soft tissues such as SDFT and DDFT, which were appreciated in high-resolution. This study described the normal appearance in the anatomy atlas of soft tissues especially SDFT, DDFT and DSL of the equine fetlock using 7T MRI, in comparison to 1.5T MR. The normal anatomy of the equine fetlock region has been described from both 7T and 1.5T MR images. The results indicated that most of the structures seen clearly on the 7T MR images could also be seen on 1.5T MR images, with indistinct margins as well as less morphological information. On T1-weighted MR images acquired from the 7T MRI system, however, the anatomical structures were clearly seen in all planes, which was not always the case with 1.5T images, and in superior anatomical detail. The margins of the smaller structures were very sharp on 7T MR images, although they were indistinct or difficult to appreciate on 1.5T MR images. For example, the cruciate sesamoidean ligaments can be appreciated in dorsal planes T1-weighted 7T MRI, but not clearly seen in 1.5T MR images. Moreover, the observer can see the articular cartilage layers using T1-weighted 7T MRI, whereas in T1-weighted 1.5T MRI they were indistinct.

In the third part of the study, a difference was found in the measurement of the equine cartilage between 7T MRI and 1.5T MRI, in comparison to histology cartilage thickness measurements. This could be due to the higher resolution of the articular cartilage in 7T MR images versus 1.5T MRI images. A significant correlation between 7T MRI cartilage thickness measurement and histologic cartilage thickness measurement was found. The correlation with histologic cartilage thickness was greater for 7T than 1.5T MRI ($r=0.47$ and 0.41 respectively). However, the accuracy of the 7T and 1.5T MRI were similar, with both methods consistently underestimating the thickness of the cartilage layer. Overall, the articular cartilage thickness measured by 7T and 1.5T were 83.46% and 83.13% of the histologic cartilage measurement.

The reasons for this consistent underestimation may reflect the effects of volume averaging in the images, or the MRI appearance of the calcified cartilage layer.

This study evaluated the delayed gadolinium-enhanced MRI of cartilage (dGEMRIC) biomarker technique and T2-time measurement, demonstrating a capability to quantify biochemical parameters of equine articular cartilage, which could be a useful tool in the detection of the early stage of OA. This study found that T1-weighted time was shorter after incubation of the cartilage samples in delayed gadolinium-enhanced (dGEMRIC) solution in agreement with of Trattnig and colleagues (Trattnig et al. 2007). However, our results disagreed with other human and equine studies (Taylor et al. 2009; Carstens et al. 2013); this disagreement could be due to the different MRI protocols and scanning time (Trattnig et al. 2007), as well as signal changes that occurred in post-gadolinium enhanced material. The pre- and post-gadolinium enhancement T1-signal intensity acquisition method used in this part of the study introduced a source of variability and investigator bias in both pre- and post-MRI time readings. This might be due to the positioning of the ROI manually. This affected some of our results as pre- dGEMRIC MRI material was subtracted from post-gadolinium enhanced dGEMRIC material MR images to see the T1-weighted time difference between pre and post dGEMRIC study. Moreover, this variation could be due to the demarcation between subchondral bone and cartilage, which was subjectively less clear in dGEMRIC and differences in the partial volume averaging of the MRI (Keenan et al. 2011; Wucherer et al. 2012).

When the GAG content of cartilage samples was measured, it was found that there were variations at different locations; the dorsal condyle had a higher sulphated GAG content than the palmer condyle, in agreement with the results of Brama and his colleagues. Our results were around 7 $\mu\text{g}/\text{mg}/\text{dw}$ higher than was found in the Brama and colleagues study (Brama et al. 2000); this difference could be for several reasons, such as unknown history and age of the cadaver cartilage examined.

Furthermore, cartilage was taken from scanned limbs after considerably long scanning time in the presence of the dGEMRIC material and time may influence to some degree the proteoglycan degradation, since the gadolinium is known to affect

the surrounding macromolecules (Wheaton et al. 2004b). Another factor which might have affected our results was that the proteoglycan assay suffers from a number of different fundamental errors, mainly involving precipitation of the DMMB-GAG complex as well as different linearity patterns present in the GAG standard calibration curves; the GAG complex precipitation made it difficult to compare several studies (Goldberg & Kolibas 1990). Future studies using a more accurate proteomic approach to quantifying specific GAGs are warranted.

A negative correlation was observed between T1-signal intensity and GAG which is in agreement with what was found by Nieminen et al. (Nieminen et al. 2002). This is because injection of gadolinium resulted in overall shortening T1-relaxation time, so GAG concentration can be measured by a change in signal intensity on T1- signal intensity MRI (Bashir et al. 1999). When the relationship between MRI parameters such as T2 time and dGEMRIC was examined, they were significantly negatively correlated with GAG content at all the data points; this result is discussed in the literature as the gadolinium penetrates the cartilage matrix according to the fixed charge density, as GAG and gadolinium in the cartilage matrix are inversely proportional.

After this investigation, other techniques that might be useful or have any relation to the biochemical components within the cartilage, related to the cartilage GAG content were examined. Sodium ions in the body are considered to be the second strongest magnetic field after hydrogen atoms. The relationship between sodium ions and the GAG content of cartilage has previously been described in human and bovine cartilage. This led to evaluating the sodium content in the equine cartilage using the 7T MRI ultra-high field magnet, due to the importance of sodium content in the tissue as well its relationship with the glycosaminoglycan content of the cartilage. Two studies were conducted to look at this relationship. In the first, described in Chapter 5, the sodium content of normal equine cartilage from the metacarpal condyle was measured and in the second, described in Chapter 6, the amount of sodium in cartilage in a model of osteoarthritis that involved subjecting the cartilage to degradation using different concentrations of degradation enzyme was measured. These techniques have been previously reported in the human literature to validate

the measurement of sodium content, using a sodium MRI technique. The results of this novel sodium quantification MRI technique were compared with GAG content as well as sodium content using a flame photometry assay. It was found that 7T MRI is a useful method for detecting sodium content in the equine cartilage, despite the fact that the sodium MRI method is expensive and time-consuming. However, advances in coil technology such as increasing the number of channels can dramatically decrease scan time. For example, using a 20-channel dual-tuned quadrature $^{23}\text{Na}/^1\text{H}$ coil would reduce the time and the cost of this technique; it has been used recently in human medicine to evaluate cartilage *in vivo*.

7.2. Overall Conclusion

Overall conclusions of this thesis focus on whether 7T MRI of the equine fetlock would allow better visualisation of the fetlock structures and assessment, and whether the 7T MRI magnet would allow a quantitative and non-invasive technique to assess physiological and biochemical properties of the equine cartilage associated with the early onset of articular cartilage degenerative conditions such as osteoarthritis. The findings of the experiments described in the second chapter confirm that 7T MRI can provide high-resolution MRI, superior to that of 1.5T MR images. It was found that although the ligaments can be seen in 1.5T, 7T MRI allows closer examination and gives more information. Moreover, 7T MRI allows better investigation of articular cartilage measurements, with a greater correlation with histology measurements. Despite the fact that the dGEMRIC technique is complicated and time-consuming, a moderate correlation between 7T MRI value and glycosaminoglycan content in equine cartilage was found. Finally, sodium MRI can be used to investigate the cartilage status, given the other technical difficulties in using this technique.

7.3. Limitations of The Study

Unfortunately, in the 2nd, 3rd and 6th chapters, the clinical case history of the equine specimens was not available. It is suggested in the future to include cartilage scoring systems, such as Harris haematoxylin and eosin and toluidine blue staining. This will allow investigation of any gross cartilage changes.

An additional technique would be histological assessment following MRI studies using alcian blue or Safranin-O to indicate whether or not the cartilage samples were damaged or had any proteoglycan loss. The number of equine limbs used in the different parts of this study was relatively low, presenting another limitation that could affect the validity of our results, given the long wait for the busy MRI system. Lack of inter-observer comparison of MRI ROI values was another limitation, previous studies having shown good positive inter-observer correlation results (Wucherer et al. 2012). Another limitation is that a 7T MRI magnet was in the study rather than a clinical magnet; to date the highest field strength used in equine clinical MRI is 3T. Currently, the lack of the 7T MRI in equine practices limits its applicability of the findings of this research.

7.4. Future Work

The results of this study have laid the basis of several future studies.

The equine cartilage thickness measurements in Chapter 3 could include the use of a specific sequence in taking the measurements, a larger sample size, and involving more than one observer would allow better validation of the MRI measurements. Use of cartilage plugs would provide greater accuracy in measuring the exact site of cross-bonds for the histological measurements. Extra validation of this technique using a laser scanner technique (3D desktop laser scanner), could allow better outcome of the cartilage thickness measurements of equine.

In the dGEMRIC technique, scanning cartilage specimens subjected to different degrees of mechanical cartilage damage as well as appropriate normal cartilage as control would ensure conclusive results between biochemical indicators such as glycosaminoglycan and MRI parameters.

Looking into the relationship between T2 relaxation time and the collagen content instead of the proteoglycan content could show the true cause of T2-time variation in OA studies.

Modification of the dual tuned quadrature $^{23}\text{Na}/^1\text{H}$ coil should also be considered, as this coil has 12 channels as compared with the 20-channel resonator used in recent human studies (Wetterling et al. 2012).

This modification will reduce time and effort in conducting the researchers, enabling more samples to be scanned in less time and at less cost than in this study.

Appendix A

Fomblin (Solvay Solexis, Thorofare, New Jersey, USA)

Blyscan, Sulphated Glycosaminoglycan Assay (Biocolor, County Antrim, UK)

Trypsin enzyme (Sigma, Poole, Dorset, UK)

7T Bruker scanner (BioSpec, Bruker Corporation 70/30 system Bruker, Germany)

Dual tuned quadrature $^{23}\text{Na}/^1\text{H}$ coil (PulseTeq Limited, Chobham, Surrey, UK).

Fomblin (Solvay Solexis, Thorofare, New Jersey, USA)

List of references

- Aime, S. & Caravan, P., 2009. Biodistribution of gadolinium-based contrast agents, including gadolinium deposition. *Journal of Magnetic Resonance Imaging*, 30(6), pp.1259–1267.
- Akella, S.V et al., 2001. Proteoglycan-induced changes in T1rho-relaxation of articular cartilage at 4T. *Magnetic Resonance in Medicine*, 46(3), pp.419–423.
- Arnett, F. et al., 1988. The American Rheumatism Association 1987 revised criteria for the classification of rheumatoid arthritis. *Arthritis & Rheumatism*, 31(3), pp.315–324.
- Asher, K. et al., 2010. Radiofrequency coils for musculoskeletal MRI. *Topics in Magnetic Resonance Imaging*, 136(3), pp.315–323.
- Axel, L. & Hayes, C., 1985. Surface coil magnetic resonance imaging. *Archives of Physiology and Biochemistry*, 93(5), pp.11–18.
- Bailey, C. et al., 1999. Impact of injuries and disease on a cohort of two- and three-year-old thoroughbreds in training. *Veterinary Record*, 145, pp.103–110.
- Banerjee, S. et al., 2008. Rapid in vivo musculoskeletal MR with parallel imaging at 7T. *Magnetic Resonance in Medicine*, 59(3), pp.655–660.
- Bashir, A., Gray, M. & Burstei, D., 1996. Gd-DTPA 2- as a measure of cartilage degradation. *Magnetic Resonance Imaging of the Skeletal Musculature*, 36(28), pp.665–673.
- Bashir, A. et al., 1997. Glycosaminoglycan in articular cartilage: In vivo assessment with delayed Gd (DTPA)(2-)-enhanced MR imaging. *Radiology*, 205(2), pp.551–558.
- Bashir, A. et al., 1999. Nondestructive imaging of human cartilage glycosaminoglycan concentration by MRI. *Magnetic Resonance in Medicine*, 41(1), pp.857–865.
- Behr, B. et al., 2009. MR imaging of the human hand and wrist at 7T. *Skeletal Radiology*, 38(9), pp.911–7.
- Berendsen, H.J. & Edzes, H.T., 1973. The observation and general interpretation of sodium magnetic resonance in biological material. *Annals of the New York Academy of Sciences*, 204(1), pp.459–85.
- Bischofberger, A. et al., 2006. Magnetic resonance imaging, ultrasonography and histology of the suspensory ligament origin: a comparative study of normal anatomy of warmblood horses. *Equine Veterinary Journal*, 38(6), pp.508–516.
- Blumenkrantz, G. & Majumdar, S., 2007. Quantitative magnetic resonance imaging of articular cartilage in osteoarthritis. *European Cells & Materials*, 13, pp.76–86.
- Bogner, W. et al., 2009. Assessment of 31P relaxation times in the human calf muscle: A comparison between 3T and 7T in vivo. *Magnetic Resonance in Medicine*, 62(3), pp.574–582.
- Bolas, N., 2011. Basic MRI principles. In: Murray RC, ed. *Equine MRI*. Chichester, West Sussex: Wiley-Blackwell, 1, pp.3–37.
- Bolen, G. et al., 2010. Qualitative Comparison of 0.27T, 1.5T, and 3T Magnetic resonance images of the normal equine foot. *Journal of Equine Veterinary Science*, 30(1), pp.9–20.
- Bolen, G.E. et al., 2011. Impact of successive freezing-thawing cycles on 3-T magnetic resonance images of the digits of isolated equine limbs. *American Journal of Veterinary Research*, 72(6), pp.780–790.
- Borthakur, A. et al., 1999. In vivo triple quantum filtered twisted projection sodium

- MRI of human articular cartilage. *Journal of Magnetic Resonance*, 141(2), pp.286–290.
- Borthakur, A. et al., 2000. Sensitivity of MRI to proteoglycan depletion in cartilage: Comparison of sodium and proton MRI. *Osteoarthritis & Cartilage*, 8(4), pp.288–293.
- Borthakur, A. et al., 2006. Sodium and T1p MRI for molecular and diagnostic imaging of articular cartilage. *NMR in Biomedicine*, 19, pp.781–821.
- Brama, P. et al., 2000. Topographical mapping of biochemical properties of articular cartilage in the equine fetlock joint. *Equine Veterinary Journal*, 32(1), pp.19–26.
- Brama, P. et al., 2001. Contact areas and pressure distribution on the proximal articular surface of the proximal phalanx under sagittal plane loading. *Equine Veterinary Journal*, 33(1), pp.26–32.
- Braun, H. & Gold, G., 2012. Diagnosis of osteoarthritis: Imaging. *Bone*, 51(2), pp.278–288.
- Brokken, M.T. et al., 2007. Magnetic resonance imaging features of proximal metacarpal and metatarsal injuries in the horse. *Veterinary Radiology & Ultrasound*, 48(6), pp.507–517.
- Brommer, H., Van Weeren, R. & Brama, P., 2003. New approach for quantitative assessment of articular cartilage degeneration in horses with osteoarthritis. *American Journal of Veterinary Research*, 64(1), pp.83–87.
- Brossmann, J. et al., 1997. Short echo time projection reconstruction MR imaging of cartilage: comparison with fat-suppressed spoiled GRASS and magnetization transfer contrast MR imaging. *Radiology*, 203, pp.501–507.
- Burstein, D. & Gray, M.L., 2006. Is MRI fulfilling its promise for molecular imaging of cartilage in arthritis? *Osteoarthritis and Cartilage*, 14(11), pp.1087–1090.
- Busoni, V. & Denoix, J., 2001. Ultrasonography of the podotrochlear apparatus in the horse using a transcuneal approach: Technique and reference images. *Veterinary Radiology & Ultrasound*, 42(6), pp.534–540.
- Butler, J. et al., 2008. Foot, Pastern and Fetlock. In Butler, JA. Colles, C. Dyson, SJ. Kold, SE. & Poulos, PW., eds. *Clinical Radiology of the Horse*. Oxford: Blackwell Science Ltd, 3, pp. 27–130.
- Camarero-Espinosa S. et al., 2016. Articular cartilage: from formation to tissue engineering. *Biomaterials Science*. 26(4), pp734-67.
- Cannon, P. et al., 1986. Sodium nuclear magnetic resonance imaging of myocardial tissue of dogs after coronary artery occlusion and reperfusion. *Journal of the American College of Cardiology*, 7(3), pp.573–579.
- Cantley, C.E. et al., 1999. Naturally occurring osteoarthritis in the metacarpophalangeal joints of wild horses. *Equine Veterinary Journal*, 31(1), pp.73–81.
- Carney, S.L. & Muir, H., 1988. The structure and function of cartilage proteoglycans. *Physiological Reviews*, 68(3), pp.858–910.
- Carstens, A. et al., 2012. Validation of delayed gadolinium-enhanced magnetic resonance imaging of cartilage and T2 mapping for quantifying distal metacarpus/metatarsus cartilage thickness in thoroughbred racehorses. *Veterinary Radiology & Ultrasound*, 54(2), pp.139–148.

- Carstens, A. et al., 2013. Feasibility for mapping cartilage T1 relaxation times in the distal metacarpus3/metatarsus3 of thoroughbred racehorses using delayed gadolinium-enhanced magnetic resonance imaging of cartilage (dGEMRIC): normal cadaver study. *Veterinary Radiology & Ultrasound*, 54(4), pp.365–72.
- Chalkias, S. et al., 1994. Hyaline articular cartilage: relaxation times, pulse-sequence parameters and MR appearance at 1.5 T. *European Radiology*, 4(4), pp.353–359.
- Chang, G. et al., 2012. Improved assessment of cartilage repair tissue using fluid-suppressed ²³Na inversion recovery MRI at 7 Tesla: Preliminary results. *European Society of Radiology*, 22, pp.1341–1349.
- Chang, G. et al., 2014. Early knee changes in dancers identified by ultra-high-field 7T MRI. *Scandinavian Journal of Medicine and Science in Sports*, 24(4), pp.678–682.
- Choi, J.A. & Gold, G.E., 2011. MR imaging of articular cartilage physiology. *Magnetic Resonance Imaging Clinics of North America*, 19(2), pp.249–282.
- Chou, M.-C. et al., 2009. Correlation between the MR T2 value at 4.7 T and relative water content in articular cartilage in experimental osteoarthritis induced by ACL transection. *Osteoarthritis and Cartilage*, 17(4), pp.441–7.
- Cohen, N., Foster, R. & Mow, V., 1998. Composition and dynamics of articular cartilage: Structure, function, and maintaining healthy state. *Journal of Orthopaedic & Sports Physical Therapy*, 28, pp.203–215.
- Constantinides, C. et al., 2001. Noninvasive quantification of total sodium concentrations in acute reperfused myocardial infarction using ²³Na MRI. *Magnetic Resonance in Medicine*, 46(6), pp.1144–1151.
- Crema, M.D. et al., 2011. Articular cartilage in the knee: Current MR imaging techniques and applications in clinical practice and research. *Radiographics*, 31(1), pp.37–61.
- Damadian, R. et al., 1976. Field focusing nuclear magnetic resonance (FONAR): visualization of a tumor in a live animal. *Science*, 194(4272), pp.1430–1432.
- Dyson, S. et al., 2003. Lameness in 46 horses associated with deep digital flexor tendonitis in the digit: diagnosis confirmed with magnetic resonance imaging. *Equine Veterinary Journal*, 35(7), pp.134–138.
- Dyson, S.J., Murray, R. & Schramme, M.C., 2005. Lameness associated with foot pain: Results of magnetic resonance imaging in 199 horses (January 2001–December 2003) and response to treatment. *Equine Veterinary Journal*, 37(2), pp.113–121.
- Dyson, S. & Murray, R., 2007a. Magnetic resonance imaging of the equine fetlock. *Clinical Techniques in Equine Practice*, 6(1), pp.62–77.
- Dyson, S. & Murray, R., 2007b. Magnetic resonance imaging of the equine foot. *Clinical Techniques in Equine Practice*, 6(1), pp.46–61.
- Eckstein, F. et al., 1996. Determination of knee joint cartilage thickness using three-dimensional magnetic resonance chondro-crassometry (3D MR-CCM). *Magnetic Resonance in Medicine*, 36(2), pp.256–265.
- Eckstein, F. et al., 2006. Magnetic resonance imaging (MRI) of articular cartilage in knee osteoarthritis (OA): morphological assessment. *Osteoarthritis and Cartilage*, 14(Suppl. 1), pp.46–75.

- Eckstein, F., Burstein, D. & Link, T.M., 2006. Quantitative MRI of cartilage and bone : degenerative changes in osteoarthritis. *NMR in Biomedicine*, 19, pp.822–854.
- Ely, E.R. et al., 2009. Descriptive epidemiology of fracture, tendon and suspensory ligament injuries in national hunt racehorses in training. *Equine Veterinary Journal*, 41(4), pp.372–378.
- Eyre, D.R., 1991. The collagens of articular cartilage. *Seminars in Arthritis and Rheumatism*, 21(Suppl 2), pp.2–11.
- Fishbein, K.W., McGowan, J.C. & Spencer, R.G., 2005. Hardware for magnetic resonance imaging. In: Filippi, M., de Stefano, N., Dousset, V., & McGowan, J.C., eds. *MR Imaging in White Matter Diseases of the Brain and Spinal Cord*. Berlin Heidelberg: Springer-Verlag, 1, pp.13–28.
- Fox, A.J., Bedi, A. & Rodeo, S.A, 2009. The basic science of articular cartilage: structure, composition, and function. *Sports Health*, 1(6), pp.461–468.
- Fragonas, E. et al., 1998. Correlation between biochemical composition and magnetic resonance appearance of articular cartilage. *Osteoarthritis and Cartilage*, 6, pp.24–32.
- Gambarota, G. et al., 2008. Characterisation of tumour vasculature in mouse brain by USPIO contrast-enhanced MRI. *British Journal of Cancer*, 98(11), pp.1784–9.
- Gibby, W., 2000. MRI Hardware, Signal-to-noise ratio, and safety. In: Zimmerman, RA., Gibby, WA., & Carmody, RF. eds. *Neuroimaging: Clinical and Physical Principles*. New York: Springer, 1, pp.125–157.
- Gold, G.E. et al., 2006. MRI of articular cartilage in OA: novel pulse sequences and compositional/functional markers. *Osteoarthritis and Cartilage*, 14, pp.76–86.
- Gold, G.E. et al., 2009. Recent advances in MRI of articular cartilage. *American Journal of Roentgenology*, 193(3), pp.628–638.
- Goldberg, R.L. & Kolibas, L.M., 1990. An improved method for determining proteoglycans synthesized by chondrocytes in culture. *Connective Tissue Research*, 24(3–4), pp.265–75.
- Gonzalez, L.M. et al., 2010. MRI features of metacarpo(tarso)phalangeal region lameness in 40 horses. *Veterinary Radiology & Ultrasound*, 51(4), pp.404–414.
- Goodwin, D.W., 2001. Visualization of the macroscopic structure of hyaline cartilage with MR imaging. *Seminars in Musculoskeletal Radiology*, 5(4), pp.305–12.
- Gutiérrez-Crespo, B., Kircher, P.R. & Carrera, I., 2014. 3 Tesla magnetic resonance imaging of the occipitoatlantoaxial region in the normal horse. *Veterinary Radiology and Ultrasound*, 55(3), pp.278–285.
- Gutierrez-Nibeyro, S.D. et al., 2009. Magnetic resonance imaging findings of desmopathy of the collateral ligaments of the equine distal interphalangeal joint. *Veterinary Radiology and Ultrasound*, 50(1), pp.21–31.
- Heinegard, D. & Ake, O., 1989. Structure and biology of cartilage and bone matrix noncollagenous macromolecules. *American Societies for Experimental Biology*, 3(9), pp.2042–2051.
- Insko, E.K. et al., 1999. Sodium NMR evaluation of articular cartilage degradation. *Magnetic Resonance in Medicine*, 41(1), pp.30–34.
- Jaremko, J.L. et al., 2007. Accuracy and reliability of MRI vs. laboratory measurements in an ex vivo porcine model of arthritic cartilage loss. *Journal of Magnetic Resonance Imaging*, 26(4), pp.992–1000.
- Jelicks, L. et al., 1993. Hydrogen-1, sodium-23, and carbon-13 MR spectroscopy of cartilage degradation in vitro. *Magnetic Resonance Imaging*, 3(4), pp.565–568.

- Jerecic, R. et al., 2004. ECG-gated ^{23}Na -MRI of the human heart using a 3D-radial projection technique with ultra-short echo times. *Magnetic Resonance Materials in Physics, Biology and Medicine*, 16, pp.297–302.
- Karvonen, R.L. et al., 1994. Factors affecting articular cartilage thickness in osteoarthritis and aging. *Journal of Rheumatology*, 21(7), pp.1310–1318.
- Keenan, K.E. et al., 2011. Prediction of glycosaminoglycan content in human cartilage by age, T1 ρ and T2 MRI. *Osteoarthritis and Cartilage*, 19(2), pp.171–9.
- Kidd, J.A., Fuller, C. & Barr, A., 2001. Osteoarthritis in the horse. *Equine Veterinary Education*, 13(3), pp.160–168.
- King, J.N. et al., 2013. MRI findings in 232 horses with lameness localized to the metacarpo(tarso)phalangeal region and without a radiographic diagnosis. *Veterinary Radiology & Ultrasound*, 54(1), pp.36–47.
- Kneeland, J.B. & Hyde, J.S., 1989. High-resolution MR imaging with local coils. *Radiology*, 171(1), pp.1–7.
- Koo, S., Gold, G.E. & Andriacchi, T.P., 2005. Considerations in measuring cartilage thickness using MRI: factors influencing reproducibility and accuracy. *Osteoarthritis and Cartilage*, 13(9), pp.782–789.
- Koo, S., Rylander, J.H. & Andriacchi, T.P., 2011. Knee joint kinematics during walking influences the spatial cartilage thickness distribution in the knee. *Journal of Biomechanics*, 44(7), pp.1405–1409.
- Krishnan, N. et al., 2007. Delayed gadolinium-enhanced magnetic resonance imaging of the meniscus: an index of meniscal tissue degeneration? *Arthritis and Rheumatism*, 56(5), pp.1507–11.
- Krug, R. et al., 2007. In vivo bone and cartilage MRI using fully-balanced steady-state free-precession at 7 Tesla. *Magnetic Resonance in Medicine*, 58(6), pp.1294–1298.
- Krug, R. et al., 2011. High-resolution imaging techniques for the assessment of osteoporosis. *Radiologic Clinics of North America*, 48(3), pp.601–621.
- Kuettner, K.E., 1992. Biochemistry of articular cartilage in health and disease. *Clinical Biochemistry*, 25(3), pp.155–163.
- Kulkarni, M. V, Patton, J.A. & Price, R.R., 1986. Technical considerations for the use of surface coils in MRI. *American Journal of Roentgenology*, 147(2), pp.373–8.
- Lee, J.H. et al., 2014. Topographical variations of the strain-dependent zonal properties of tibial articular cartilage by microscopic MRI. *Connective Tissue Research*, 55(3), pp.205–16.
- Lesperance, L.M., Gray, M.L. & Burstein, D., 1992. Determination of fixed charge density in cartilage using nuclear magnetic resonance. *Journal of Orthopaedic Research*, 10(1), pp.1–13.
- Li, X. et al., 2007. In vivo T(1 ρ) and T(2) mapping of articular cartilage in osteoarthritis of the knee using 3 T MRI. *Osteoarthritis and Cartilage*, 15(7), pp.789–797.
- Liess, C. et al., 2002. Detection of changes in cartilage water content using MRI T2-mapping in vivo. *Osteoarthritis and Cartilage*, 10(12), pp.907–913.
- Van De Loo, A. et al., 1994. Proteoglycan loss and subsequent replenishment in articular cartilage after a mild arthritic insult by IL-1 in mice: Impaired proteoglycan turnover in the recovery phase. *Inflammation Research*, 41(3–4), pp.200–208.

- Lorenz, H. et al., 2005. Early and stable upregulation of collagen type II, collagen type I and YKL40 expression levels in cartilage during early experimental osteoarthritis occurs independent of joint location and histological grading. *Arthritis Research & Therapy*, 7(1), pp.R156–R165.
- Lorenzo, P., Bayliss, M.T. & Heinegård, D., 2004. Altered patterns and synthesis of extracellular matrix macromolecules in early osteoarthritis. *Matrix Biology*, 23(6), pp.381–391.
- Madelin, G. et al., 2010. Sodium inversion recovery MRI of the knee joint in vivo at 7T. *Journal of Magnetic Resonance*, 207(1), pp.42–52.
- Madelin, G. et al., 2014. Sodium MRI: Methods and applications. *Progress in Nuclear Magnetic Resonance Spectroscopy*, 79, pp.14–47.
- Madelin, G., Jerschow, A. & Regatte, R.R., 2011. Sodium MRI with fluid suppression: Will it improve early detection of osteoarthritis? *Imaging in Medicine*, 3(1), pp.1–4.
- Madelin, G., Jerschow, A. & Regatte, R.R., 2012. Sodium relaxation times in the knee joint in vivo at 7T. *NMR in Biomedicine*, 25(4), pp.530–537.
- Madelin, G. & Regatte, R.R., 2013. Biomedical applications of sodium MRI in vivo. *Journal of Magnetic Resonance Imaging*, 38(3), pp.511–29.
- Mankin, H.J., Johnson, M.E. & Lippiello, L., 1981. Biochemical and metabolic abnormalities in articular cartilage from osteoarthritic human hips. III. Distribution and metabolism of amino sugar-containing macromolecules. *The Journal of Bone and Joint Surgery. American Volume*, 63(1), pp.131–139.
- Marlovits, S. et al., 2006. Magnetic resonance observation of cartilage repair tissue (MOCART) for the evaluation of autologous chondrocyte transplantation: Determination of interobserver variability and correlation to clinical outcome after 2 years. *European Journal of Radiology*, 57(1), pp.16–23.
- Maroudas, A., 1968. Physicochemical properties of cartilage in the light of ion exchange theory. *Biophysical Journal*, 8(5), pp.575–595.
- Maroudas, A., 1970. Distribution and diffusion of solutes in articular cartilage. *Biophysical Journal*, 10(5), pp.365–379.
- Maroudas, A., 1979. Physicochemical properties of articular cartilage. In Freeman, M.A.R. ed. *Adult articular cartilage*, Pitman Medical, Kent, England, 2, pp.215–290.
- Maroudas, A. et al., 1991. The effect of osmotic and mechanical pressures on water partitioning in articular cartilage. *Biochimica et Biophysica Acta*, 1073(2), pp.285–294.
- Martinelli, M. & Baker, G., 1996. Magnetic resonance imaging of degenerative joint disease in a horse: a comparison to other diagnostic techniques. *Equine Veterinary Journal*, 28(5), pp.410–415.
- Martinelli, M.J. et al., 1996. Correlation between anatomic features and low-field magnetic resonance imaging of the equine metacarpophalangeal joint. *American Journal of Veterinary Research*, 57(10), pp.1421–1426.
- Matyas, J.R. et al., 1999. The early molecular natural history of experimental osteoarthritis: I. Progressive discoordinate expression of aggrecan and type II procollagen messenger RNA in the articular cartilage of adult animals. *Arthritis and Rheumatism*, 42(5), pp.993–1002.
- Matzat, S.J. et al., 2013. Quantitative MRI techniques of cartilage composition. *Quantitative Imaging in Medicine and Surgery*, 3(3), pp.162–174.

- Mayne, R., 1989. Cartilage collagens. What is their function, and are they involved in articular disease? *Arthritis and Rheumatism*, 32(3), pp.241–246.
- McIlmraith, C.W., 1982. Current concepts in equine degenerative joint disease. *Journal of the American Veterinary Medical Association*, 180(3), pp.239–250.
- Menarim, B.C. et al., 2012. Radiographic abnormalities in barrel racing horses with lameness referable to the metacarpophalangeal joint. *Journal of Equine Veterinary Science*, 32(4), pp.216–221.
- Menezes, N. et al., 2004. T2 and T1rho MRI in articular cartilage systems. *Magnetic Resonance in Medicine*, 51(3), pp.503–509.
- Mlynarik, V. et al., 1996. Investigation of laminar appearance of articular cartilage by means of magnetic resonance microscopy. *Magnetic Resonance Imaging*, 14(4), pp.435–442.
- Mlynárik, V. et al., 1999. The role of relaxation times in monitoring proteoglycan depletion in articular cartilage. *Journal of Magnetic Resonance Imaging*, 10(4), pp.497–502.
- Moger, C.J. et al., 2007. Regional variations of collagen orientation in normal and diseased articular cartilage and subchondral bone determined using small angle x-ray scattering (SAXS). *Osteoarthritis and Cartilage*, 15(6), pp.682–687.
- Mosher, T.J., Dardzinski, B.J. & Smith, M.B., 2000. Human articular cartilage: influence of aging and early symptomatic degeneration on the spatial variation of T2-- preliminary findings at 3 T. *Radiology*, 214(1), pp.259–266.
- Mosher, T.J. & Dardzinski, B.J., 2004. Cartilage MRI T2 relaxation time mapping: overview and applications. *Seminars in Musculoskeletal Radiology*, 8(4), pp.355–368.
- Mow, V.C., Holmes, M.H. & Lai, W.M., 1984. Fluid transport and mechanical properties of articular cartilage: a review. *Journal of Biomechanics*, 17(5), pp.377–394.
- Mow, V.C., Ateshian, G.A. & Spilker, R.L., 1993. Biomechanics of diarthrodial joints: a review of twenty years of progress. *Journal of Biomechanical Engineering*, 115, pp.460–467.
- Moyer, W. & Raker, C.W., 1980. Diseases of the suspensory apparatus. *The Veterinary Clinics of North America: Large animal practice*, 2(1), pp.61–80.
- Murphy, E. & Eisner, D.A., 2009. Regulation of intracellular and mitochondrial sodium in health and disease. *Circulation Research*, 104(3), pp.292–303.
- Murray, R.C. et al., 2005. Validation of magnetic resonance imaging for measurement of equine articular cartilage and subchondral bone thickness. *American Journal of Veterinary Research*, 66(11), pp.1999–2005.
- Murray, R. et al., 2006. Magnetic resonance imaging characteristics of the foot in horses with palmar foot pain and control horses. *Veterinary Radiology & Ultrasound*, 47(1), pp.1–16.
- Nagel, A.M. et al., 2009. Sodium MRI using a density-adapted 3D radial acquisition technique. *Magnetic Resonance in Medicine*, 62(6), pp.1565–1573.
- Nagel, A.M. et al., 2013. Skeletal muscle MR imaging beyond protons: With a focus on sodium MRI in musculoskeletal applications. In Webber, M.A., ed. *Magnetic Resonance Imaging of the Skeletal Musculature*. Berlin: Springer-Verlag, pp. 115–133.

- Nagy, A. & Dyson, S., 2009. Magnetic resonance anatomy of the proximal metacarpal region of the horse described from images acquired from low- and high-field magnets. *Veterinary Radiology & Ultrasound*, 50(6), pp.595–605.
- Nagy, A & Dyson, S., 2012. Magnetic resonance imaging findings in the carpus and proximal metacarpal region of 50 lame horses. *Equine Veterinary Journal*, 44(2), pp.163–8.
- Newbould, R. et al., 2012. Reproducibility of sodium MRI measures of articular cartilage of the knee in osteoarthritis. *Osteoarthritis and Cartilage*, 20(1), pp.29–35.
- Newbould, R.D. et al., 2013. T1-Weighted sodium MRI of the articular cartilage in osteoarthritis: A cross sectional and longitudinal Study. *PLoS ONE*, 8(8), pp.1–9.
- Nieminen, M.T. et al., 2000. Quantitative MR microscopy of enzymatically degraded articular cartilage. *Magnetic Resonance in Medicine*, 43(5), pp.676–681.
- Nieminen, M.T. et al., 2001. T2 Relaxation reveals spatial collagen architecture in articular cartilage: A comparative quantitative MRI and polarized light microscopic Study. *Magnetic Resonance in Medicine*, 49(3), pp.487–493.
- Nieminen, M.T. et al., 2002. Spatial assessment of articular cartilage proteoglycans with Gd-DTPA-enhanced T1 imaging. *Magnetic Resonance in Medicine*, 48, pp.640–648.
- Nishii, T. et al., 2008. Evaluation of cartilage matrix disorders by T2 relaxation time in patients with hip dysplasia. *Osteoarthritis and Cartilage*, 16(2), pp.227–233.
- Nissi, M.J. et al., 2004. Proteoglycan and collagen sensitive MRI evaluation of normal and degenerated articular cartilage. *Journal of Orthopaedic Research*, 22(3), pp.557–564.
- Okimura, A., Yasunori, O. & Seicho, M., 1997. Enhancement of the cartilage matrix protein synthesis in arthritic cartilage. *Arthritis & Rheumatism*, 40(6), pp.1029–1036.
- Olive, J. et al., 2010. Fat-suppressed spoiled gradient-recalled imaging of equine metacarpophalangeal articular cartilage. *Veterinary Radiology & Ultrasound*, 51(2), pp.107–115.
- Pabst, T. et al., 2002. Sodium T2* relaxation times in human heart muscle. *Journal of Magnetic Resonance Imaging*, 15(2), pp.215–218.
- Pancier, D.L. et al., 1987. Magnetic resonance imaging in two dogs with central nervous system disease. *Journal of Small Animal Practice*, 28(7), pp.587–596.
- Park, R.D., Nelson, T.R. & Hoopes, P.J., 1987. Magnetic resonance imaging of the normal equine digit and metacarpophalangeal joint. *Veterinary Radiology*, 28(4), pp.105–116.
- Parkin, T.D.H. et al., 2004. Risk of fatal distal limb fractures among thoroughbreds involved in the five types of racing in the United Kingdom. *The Veterinary Record*, 154(16), pp.493–497.
- Paul, P.K. et al., 2000. Magnetic resonance imaging reflects cartilage proteoglycan degradation in the rabbit knee. *Skeletal Radiology*, 1(1991), pp.31–36.
- Pepin, S.R. et al., 2009. A comparative analysis of 7.0-Tesla magnetic resonance imaging and histology measurements of knee articular cartilage in a canine posterolateral knee injury model: a preliminary analysis. *The American Journal of Sports Medicine*, 37(1), p.119S–124S.
- Peterfy, C.G. et al., 2006. MRI protocols for whole-organ assessment of the knee in osteoarthritis. *Osteoarthritis and Cartilage*, 14, pp.95–111.

- Podadera, J., Bell, R. & Dart, A., 2010. Using magnetic resonance imaging to diagnose non-displaced fractures of the second phalanx in horses. *Australian Veterinary Journal*, 88(11), pp.439–442.
- Pool, R.R. & Meagher, D.M., 1990. Pathologic findings and pathogenesis of racetrack injuries. *The Veterinary Clinics of North America: Equine Practice*, 6(1), pp.1–30.
- Recht, P. & Resnick, D., 1994. MR imaging of articular future directions cartilage: current status and future directions. *American Journal of Roentgenology*, 163, pp.283–290.
- Recht, M.P. et al., 2005. MRI of articular cartilage: Revisiting current status and future directions. *American Journal of Roentgenology*, 185(4), pp.899–914.
- Reddy, R. et al., 1997. In vivo sodium multiple quantum spectroscopy of human articular cartilage. *Magnetic Resonance in Medicine*, 38(2), pp.207–214.
- Reddy, R. et al., 1998. Sodium MRI of human articular cartilage in vivo. *Magnetic Resonance in Medicine*, 39(5), pp.697–701.
- Regatte, R. & Schweitzer, M.E., 2008. Novel contrast mechanisms at 3 Tesla and 7 Tesla. *Seminars in Musculoskeletal Radiology*, 12(3), pp.266–280.
- Regatte, R.R. et al., 2003. In vivo proton MR three-dimensional T1rho mapping of human articular cartilage: Initial experience. *Radiology*, 229(1), pp.269–274.
- Regatte, R.R. & Schweitzer, M.E., 2007. Ultra-high-field MRI of the musculoskeletal system at 7.0T. *Journal of Magnetic Resonance Imaging*, 25(2), pp.262–269.
- Rodgers, D.H. & Spirito, M.A., 2001. Repair of collateral ligament instability in 2 foals by using suture anchors. *Canadian Veterinary Journal*, 42(7), pp.557–560.
- Rogers, J., Jain, W. & Paul, D., 1990. Comparison of visual and radiographic detection of bony changes at the knee joint. *British Medical Journal*, 300(6721), pp.367–368.
- Rossdale, P.D. et al., 1985. Epidemiological study of wastage among racehorses 1982 and 1983. *The Veterinary Record*, 116(3), pp.66–69.
- Rothschild, P.A., Crooks, L.E. & Margulis, A.R., 1990. Direction of MR imaging. *Investigative Radiology*, 25(3), pp.275–281.
- Roughley, P. & Lee, E., 1994. Cartilage proteoglycans: Structure and potential functions. *Microscopy Research & Technique*, 28(5), pp.385–397.
- Rydell, N.W., Butler, J. & Balazs, E.A., 1970. Hyaluronic acid in synovial fluid. VI. Effect of intra-articular injection of hyaluronic acid on the clinical symptoms of arthritis in track horses. *Veterinaria Scandinavica*, 11, pp.139–155.
- Sarzi-Puttini, P. et al., 2005. Osteoarthritis: An overview of the disease and its treatment strategies. *Seminars in Arthritis and Rheumatism*, 35(Suppl 1), pp.1–10.
- Saveraid, T. & Judy, C., 2012. Use of intravenous gadolinium contrast in equine magnetic resonance imaging. *Veterinary Clinics of North America - Equine Practice*, 28(3), pp.617–636.
- Shapiro, E. et al., 2000a. Sodium visibility and quantitation in intact bovine articular cartilage using high field (²³Na) MRI and MRS. *Journal of Magnetic Resonance*, 142(1), pp.24–31.
- Shapiro, E. et al., 2000b. Sodium visibility and quantitation in intact bovine articular cartilage using high field Na-23 MRI and MRS. *Journal of Magnetic Resonance*, 142(1), pp.24–31.
- Shapiro, E.M. et al., 2002. ²³Na MRI accurately measures fixed charge density in articular cartilage. *Magnetic Resonance in Medicine*, 47(2), pp.284–291.

- Sittek, H. et al., 1996. Assessment of normal patellar cartilage volume and thickness using MRI: an analysis of currently available pulse sequences. *Skeletal Radiology*, 25(1), pp.55–62.
- Smith, M.A, Dyson, S.J. & Murray, R.C., 2012. Reliability of high- and low-field magnetic resonance imaging systems for detection of cartilage and bone lesions in the equine cadaver fetlock. *Equine Veterinary Journal*, 44(6), pp.684–691.
- Smith, M., Dyson, S. & Murray, R., 2011. The appearance of the equine metacarpophalangeal region on high-field vs. standing low-field magnetic resonance imaging. *Veterinary Radiology & Ultrasound*, 52(1), pp.61–70.
- Stammberger, T. et al., 1999. Determination of 3D cartilage thickness data from MR imaging: computational method and reproducibility in the living. *Magnetic Resonance in Medicine*, 41(3), pp.529–36.
- Staroswiecki, E. et al., 2010. In vivo sodium imaging of human patellar cartilage with a 3D cones sequence at 3 T and 7 T. *Journal of Magnetic Resonance Imaging*, 32(2), pp.446–451.
- Steidle, G., Graf, H. & Schick, F., 2004. Sodium 3-D MRI of the human torso using a volume coil. *Magnetic Resonance Imaging*, 22, pp.171–180.
- Stevens, R.L. et al., 1982. Biological changes in the annulus fibrosus in patients with low-back pain. *Spine*, 7(3), pp.223–233.
- Surowiec, R.K., Lucas, E.P. & Ho, C.P., 2014. Quantitative MRI in the evaluation of articular cartilage health: Reproducibility and variability with a focus on T2 mapping. *Knee Surgery, Sports Traumatology, Arthroscopy*, 22(6), pp.1385–1395.
- Taylor, C. et al., 2009. Comparison of quantitative imaging of cartilage for osteoarthritis: T2, T1rho, dGEMRIC and contrast-enhanced computed tomography. *Magnetic Resonance Imaging*, 27(6), pp.779–784.
- Tiderius, C.J. et al., 2004. dGEMRIC (delayed gadolinium-enhanced MRI of cartilage) indicates adaptive capacity of human knee cartilage. *Magnetic Resonance in Medicine*, 51, pp.286–290.
- Tiderius, C. et al., 2006. dGEMRIC as a function of BMI. *Osteoarthritis and Cartilage*, 14(11), pp.1091–1097.
- Tietje, S. et al., 2001. Computed tomographic evaluation of the distal aspect of the deep digital flexor tendon (DDFT) in horses. *Pferdeheilkunde*, 17(1), pp.21–29.
- Trattng, S. et al., 2007. Three-dimensional delayed gadolinium-enhanced MRI of cartilage (dGEMRIC) for in vivo evaluation of reparative cartilage after matrix-associated autologous chondrocyte transplantation at 3.0T: Preliminary results. *Journal of Magnetic Resonance Imaging*, 26(4), pp.974–82.
- Trattng, S. et al., 2010. ²³Na MR imaging at 7 T after knee matrix-associated autologous chondrocyte transplantation: Preliminary results. *Radiology*, 257(1), pp.175–184.
- Venn, M. & Maroudas, A., 1977. Chemical composition and swelling of normal and osteoarthrotic femoral head cartilage. I. Chemical composition. *Annals of the Rheumatic Diseases*, 36(2), pp.121–9.
- Verheyen, K.L.R. & Wood, J.L.N., 2004. Descriptive epidemiology of fractures occurring in British Thoroughbred racehorses in training. *Equine Veterinary Journal*, 36(2), pp.167–73.

- Wang, J. et al., 1990. The influence of walking mechanics and time on the results of proximal tibial osteotomy. *The Journal of Bone and Joint Surgery*, 72(6), pp.905–909.
- Wang, L. et al., 2009. Rapid isotropic 3D-sodium MRI of the knee joint in vivo at 7T. *Journal of Magnetic Resonance Imaging*, 30(3), pp.606–614.
- Watanabe, A. et al., 2009. Ability of dGEMRIC and T2 mapping to evaluate cartilage repair after microfracture: A goat study. *Osteoarthritis and Cartilage*, 17(10), pp.1341–9.
- Wayne, J.S. et al., 2003. MR imaging of normal and matrix-depleted cartilage: correlation with biomechanical function and biochemical composition. *Radiology*, 228(2), pp.493–499.
- Van Weeren, P.R. et al., 2008. Early exercise advances the maturation of glycosaminoglycans and collagen in the extracellular matrix of articular cartilage in the horse. *Equine Veterinary Journal*, 40(2), pp.128–135.
- Welker, K.M. et al., 2001. Radio-frequency coil selection for MR imaging of the brain and skull base. *Radiology*, 221(1), pp.11–25.
- Welsch, G.H. et al., 2008. In vivo biochemical 7.0 Tesla magnetic resonance: preliminary results of dGEMRIC, zonal T2, and T2* mapping of articular cartilage. *Investigative Radiology*, 43(9), pp.619–26.
- Welsch, G.H. et al., 2012. Magnetic resonance imaging of the knee at 3 and 7 Tesla: A comparison using dedicated multi-channel coils and optimised 2D and 3D protocols. *European Radiology*, 22(9), pp.1852–1859.
- Werpy, N.M., 2004. Magnetic resonance imaging for diagnosis of soft tissue and osseous injuries in the horse. *Clinical Techniques in Equine Practice*, 3(4), pp.389–398.
- Werpy, N.M., 2007. Magnetic resonance imaging of the equine patient: A comparison of high- and low-field systems. *Clinical Techniques in Equine Practice*, 6(1), pp.37–45.
- Wetterling, F. et al., 2012. The design of a double-tuned two-port surface resonator and its application to in vivo hydrogen- and sodium-MRI. *Journal of Magnetic Resonance*, 217, pp.10–8.
- Wheaton, A.J. et al., 2004a. Proteoglycan loss in human knee cartilage: quantitation with sodium MR imaging-feasibility study. *Radiology*, 231(3), pp.900–905.
- Wheaton, A.J. et al., 2004b. Correlation of T1rho with fixed charge density in cartilage. *Journal of Magnetic Resonance Imaging*, 20(3), pp.519–25.
- Whitton, R.C. et al., 1998. The Diagnosis of lameness associated with distal limb pathology in a horse: A comparison of radiography, computed tomography and magnetic resonance imaging. *The Veterinary Journal*, 155, pp.223–229.
- Wiener, E. et al., 2007. Contrast enhanced cartilage imaging: Comparison of ionic and non-ionic contrast agents. *European Journal of Radiology*, 63(1), pp.110–119.
- Williams, A. et al., 2005. Delayed gadolinium-enhanced magnetic resonance imaging of cartilage in knee osteoarthritis: Findings at different radiographic stages of disease and relationship to malalignment. *Arthritis & Rheumatism*, 52(11), pp.3528–3535.

- Wucherer, K.L., Ober, C.P. & Conzemius, M.G., 2012. The use of delayed gadolinium enhanced magnetic resonance imaging of cartilage and T2 mapping to evaluate articular cartilage in the normal canine elbow. *Veterinary Radiology and Ultrasound*, 53, pp.57–63.
- Xia, Y., Zheng, S. & Bidthanapally, A., 2008. Depth-dependent profiles of glycosaminoglycans in articular cartilage by microMRI and histochemistry. *Journal of Magnetic Resonance Imaging*, 28(1), pp.151–7.
- Yushmanov, V.E. et al., 2013. Correlated sodium and potassium imbalances within the ischemic core in experimental stroke: A ^{23}Na MRI and histochemical imaging study. *Brain Research*, 1527, pp.199–208.
- Yushmanov, V.E. et al., 2009. Sodium mapping in focal cerebral ischemia in the rat by quantitative ^{23}Na MRI. *Journal of Magnetic Resonance Imaging*, 29(4), pp.962–966.
- Zbýň, Š. et al., 2012. Evaluation of native hyaline cartilage and repair tissue after two cartilage repair surgery techniques with ^{23}Na MR imaging at 7 T: Initial experience. *Osteoarthritis and Cartilage*, 20(8), pp.837–845.
- Zbýň, S. et al., 2014. Sodium MR imaging of articular cartilage pathologies. *Current Radiology Reports*, 2, pp.41–51.